Integrated Analytical Systems
Series Editor: Radislav A. Potyrailo

Philip Day
Andreas Manz
Yonghao Zhang *Editors*

Microdroplet Technology

Principles and Emerging Applications in Biology and Chemistry

Springer

Integrated Analytical Systems

Series Editor
Radislav A. Potyrailo
GE Global Research Center
Niskayuna, NY

For further volumes:
http://www.springer.com/series/7427

Philip Day · Andreas Manz · Yonghao Zhang
Editors

Microdroplet Technology

Principles and Emerging Applications in Biology and Chemistry

Springer

Editors
Philip Day
Manchester Institute of Biotechnology
University of Manchester
Manchester, UK,

Andreas Manz
KIST Europe
Saarbrucken, Germany

Yonghao Zhang
Department of Mechanical
and Aerospace Engineering
University of Strathclyde
Glasgow, UK

ISBN 978-1-4614-3264-7 ISBN 978-1-4614-3265-4 (eBook)
DOI 10.1007/978-1-4614-3265-4
Springer New York Heidelberg Dordrecht London

Library of Congress Control Number: 2012941616

Printed on acid-free paper

Springer is part of Springer Science+Business Media (www.springer.com)

Preface

Microdroplet technology has recently been exploited to provide new and diverse applications via microfluidic functionality, especially in the arenas of biology and chemistry. This book gives a timely overview on state of the art of droplet-based microfluidics. The disciplines related to microfluidics and microdroplet technology are diverse and where interdisciplinary cooperation is pivotal for the development of new and innovative technological platforms. The chapters are contributed by internationally leading researchers from physics, engineering, biology and chemistry to address: fundamental flow physics; methodology and components for flow control; and applications in biology and chemistry. They are followed by a chapter giving a perspective on the field. Therefore, this book is a key point of reference for academics and students wishing to better their understanding and facilitate optimal design and operation of new droplet-based microfluidic devices for more comprehensive analyte assessments.

The first part of this book (Chaps. 1, 2, 3, 4 and 5) focuses on fundamental flow physics, device design and operation, while the rest of the chapters (Chaps. 6, 7, 8, 9 and 10) deal with the wide range of applications of droplet-based microfluidics. It starts with the discussion of flow physics of microdroplets confined in lab-on-a-chip devices in Chap. 1, where Zhang and Liu emphasize the important dimensionless parameters relating to droplet dynamics. Meanwhile, droplet generation process is used as an example to illustrate the unique flow physics in comparison with conventional droplet dynamics in unconfined environments.

Chapter 2 deals with microfluidics droplet manipulations and applications, including droplet fusion, droplet fission, mixing in droplets and droplet sorting. By combining these operations, Simon and Lee demonstrate how to execute chemical reactions and biological assays at the microscale. Using the flow rates, applied pressures and flow rate ratios in a closed feedback system, the active control of droplet size during formation process in microfluidics is addressed in Chap. 3 by Nguyen and Tan.

In Chap. 4, Barber and Emerson discuss the fundamental droplet handling operations and the recent advances in electrowetting microdroplet technologies and their applications in biological and chemical processes. Kaminski, Churski

and Garstecki review the recent advances in building modules for automation of handling of droplets in microfluidic channels, in Chap. 5, including the modules for generation of droplets on demand, aspiration of samples onto chips, splitting and merging of droplets, incubation of the content of the drops and sorting.

From Chap. 6, the book shifts its focus on the applications of microdroplet technology. In Chap. 6, Philip Day and Ehsan Karimiani discuss dropletisation of bio-reactions. The use of large-scale microdroplet production is described for profiling single cells from complex tissues and assists with the production of quantitative data for input into systems modelling of disease.

Droplet-based microfluidics as a biomimetic principle in diagnostic and biomolecular information handling are highlighted in Chap. 7 by Köhler. This chapter also addresses the potential of applying segmented fluid technique to answer to the challenges of information extraction from cellular and biomolecular systems. In Chap. 8, Carroll et al. focus on droplet microreactors for materials synthesis, with a brief description of microfluidics for droplet generation as well as fabrication technology. In addition, a detailed study of transport in microchannels and droplet microfluidics for mesoporous particle synthesis is included.

In Chap. 9, Zagnoni and Cooper demonstrate the use of on-chip biocompatible microdroplets both as a carrier to transport encapsulated particles and cells, and as microreactors to perform parallel single-cell analysis in tens of milliseconds. Finally, trends and perspectives are provided by Neužil, Xu and Manz to discuss challenges in fundamental research and technological development of droplet-based microfluidics.

This book is intended for established academics, researchers and postgraduate students at the frontier of fundamental microfluidic research, system design and applications (particularly bio/chemical applications) of microfluidic droplet technology. It can mainly be used as a reference book for the basic principles, components and applications of microdroplet-based microfluidic systems. Those postgraduates and researchers whose study is related to microfluidics will benefit from closely engaging the emerging droplet-based microfluidics comprehensively covered in this book. Furthermore, the publication will serve as a text or reference book for academic courses teaching advanced analytical technologies, medical devices, fluid engineering, etc. Potential markets for researchers include in sectors related to medical devices, fluid dynamics, engineering, analytical chemistry and biotechnology.

Manchester, UK — Philip Day
Saarbrucken, Germany — Andreas Manz
Glasgow, UK — Yonghao Zhang

Contents

Contributors

Robert W. Barber STFC Daresbury Laboratory, Warrington, UK

Nick J. Carroll Department of Chemical and Nuclear Engineering, University of New Mexico, NM, USA

Suk Tai Chang School of Chemical Engineering and Materials Science, Chung-Ang University, Seoul, South Korea

Krzysztof Churski Institute of Physical Chemistry, Polish Academy of Sciences, Warsaw, Poland

Jonathan M. Cooper School of Engineering, University of Glasgow, Glasgow, UK

Philip Day Manchester Institute of Biotechnology, University of Manchester, Manchester, UK

David R. Emerson STFC Daresbury Laboratory, Warrington, UK

Piotr Garstecki Institute of Physical Chemistry, Polish Academy of Sciences, Warsaw, Poland

Tomasz S. Kaminski Institute of Physical Chemistry, Polish Academy of Sciences, Warsaw, Poland

Ehsan Karimiani Manchester Institute of Biotechnology University of Manchester, Manchester, UK

J. Michael Köhler Manchester Interdisciplinary Biocentre University of Manchester, Manchester, UK

Abraham Lee Department of Biomedical Engineering University of California-Irvine, Irvine, CA, USA

Haihu Liu Department of Aerospace Engineering, University of Strathclyde, Glasgow, UK

Andreas Manz Korea Institute for Science and Technology Europe, Saarbrucken, Germany

Amelia Markey Manchester Institute of Biotechnology, University of Manchester, Manchester, UK

Pavel Neužil Korean Institute for Science and Technology Europe, Saarbrucken, Germany

Nam-Trung Nguyen School of Mechanical and Aerospace Engineering, Nanyang Technological University, Singapore, Singapore

Dimiter N. Petsev Department of Chemical and Nuclear Engineering, University of New Mexico, NM, USA

Melinda G. Simon Department of Biomedical Engineering, University of California-Irvine, Irvine, CA, USA

Say-Hwa Tan School of Mechanical and Aerospace Engineering, Nanyang Technological University, Singapore, Singapore

Orlin D. Velev Department of Chemical & Biochemical Engineering, North Carolina State University, Raleigh, NC, USA

Ying Xu YingWin Consulting, Oakland, NJ, USA

Michele Zagnoni Centre for Microsystems and Photonics, University of Strathclyde, Glasgow, UK

Yonghao Zhang Department of Mechanical & Aerospace Engineering, University of Strathclyde, Glasgow, UK

Chapter 1
Physics of Multiphase Microflows and Microdroplets

Yonghao Zhang and Haihu Liu

Multiphase microfluidic applications are very broad, ranging from DNA analysis such as PCR in droplets to chemical synthesis [19]. Optimal design and operation of such systems need insightful understanding of fundamental multiphase flow physics at microscale. In this chapter, we discuss some basic flow physics of multiphase microdroplets. The important dimensionless parameters relating to droplet dynamics are elaborated. We use droplet generation processes as examples to explain rich flow physics involved in microdroplet dynamics.

1.1 Surface Tension

In comparison with single phase microfluidic flows, surface tension (also called interfacial tension) plays a central role in dynamical behaviour of multiphase microdroplets. Over two centuries ago, Benjamin Franklin experimentally studied the effect of an insoluble fatty acid oil on the surface of water [11], which probably is the first time that the phenomenon of surface tension was given a scientific explanation.

For simplicity, we first consider a droplet in a carrier gas phase to explain surface tension. A liquid/gas interface is presented in Fig. 1.1, where fluid molecules interact with each other. A molecule in the bulk liquid is attracted by all neighbouring molecules from all directions, so any attraction by another molecule from one direction is always balanced by another molecule from the opposite direction. Meanwhile, a molecule at the interface is in a different situation. It is attracted inward and to the side but no sufficient outward attraction to balance the inward

Y. Zhang (✉) • H. Liu
Department of Mechanical and Aerospace Engineering, University of Strathclyde, Glasgow G1 1XJ, UK
e-mail: yonghao.zhang@strath.ac.uk

P. Day et al. (eds.), *Microdroplet Technology: Principles and Emerging Applications in Biology and Chemistry*, Integrated Analytical Systems,
DOI 10.1007/978-1-4614-3265-4_1,

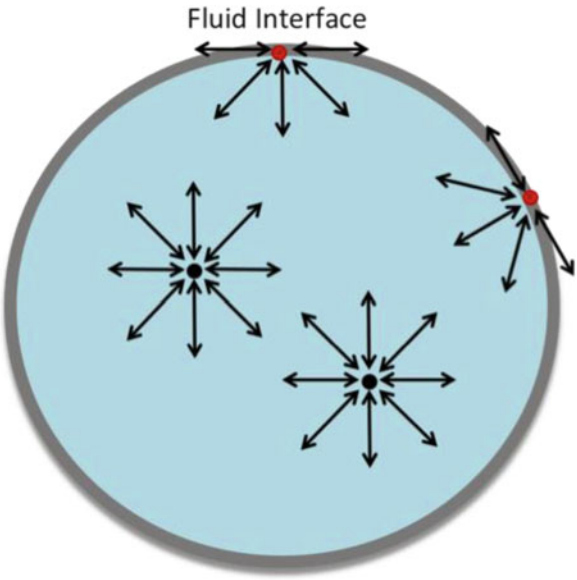

Fig. 1.1 Illustration of inter-molecule interactions in the bulk and interface for a liquid droplet in gas

attraction due to smaller amount of molecules outside in the gas. The consequence is that the attraction on an interface molecule is not balanced that induces the surface to contract and leads to surface tension.

The term surface tension can also be used interchangeably with surface free energy. Since the energy of a molecule at surface is higher than that of a molecule in bulk liquid, work needs to be done to move a molecule to surface from bulk liquid. The free energy of the system therefore increases. According to the thermodynamic principle, the free energy of the system always tends to a minimum. Therefore, the interface surface will tend to contract, forming least possible surface area.

The surface tension, represented by the symbol σ, can therefore be defined as a force per unit length or a surface free energy per unit area. Typical values at 20°C for water–air, ethanol–air, and mercury–air are 72.94, 22.27, and 487 mN/m, respectively. Surface tension depends on temperature, and usually decreases as the liquid temperature increases. It can also be altered by surface-active materials, i.e., surfactants, which form a monolayer at the interface. Due to large surface-to-volume ratio of microdroplets, surface tension often plays a dominant role in the determination of droplet behaviour.

1.2 Young Laplace Equation

For a liquid droplet in another immiscible fluid, e.g. water droplet in air or oil, the pressure inside the droplet will normally be different from the outside pressure, because the surface tension leads to the so-called capillary pressure across

the interface. For a stationary droplet in a rest surrounding immiscible fluid, i.e. the tangential stress is absent, the capillary pressure can be described by the Young Laplace equation as

$$\Delta P = \sigma\left(\frac{1}{R_1} + \frac{1}{R_2}\right), \tag{1.1}$$

where ΔP is the capillary pressure, i.e. the pressure difference across the fluid interface, and R_1 and R_2 are the principal radii of curvature. The equation is named after Thomas Young (who first proposed the theory of surface tension in 1805) and Pierre-Simon Laplace (who gave the mathematical description in 1806). This Young Laplace equation has been widely used as a bench-mark test case for multiphase models.

1.3 Marangoni Effects

When local temperature, solvent concentration or electric potential is not uniform along the interface, the surface tension is not constant, i.e. there is surface tension gradient along the interface. Consequently, the gradients in surface tension lead to forces, which are called Marangoni stresses, which appear along the interface. The mass transfer along an interface between two fluids due to surface tension gradient is called Marangoni effects. If the phenomenon is temperature induced, it is often called thermo-capillary effects. Although this phenomenon was first identified by James Thomson in 1855, it is named after Carlo Marangoni because he studied this phenomenon in detail for his doctoral dissertation at the University of Pavia and published his results in 1865.

1.4 Navier–Stokes Equations and Surface Tension Model

The commonly used fluids in microfluidic applications are the Newtonian fluids, i.e. the shear stress of the fluid is linearly proportional to the applied shear rate. For a Newtonian fluid not far away from thermodynamically equilibrium, the Navier–Stokes equations can describe fluid dynamical behaviour. The continuum equation which considers the conservation of mass is given by

$$\frac{\partial \rho}{\partial t} + \nabla \cdot (\rho \boldsymbol{u}) = 0, \tag{1.2}$$

where ρ is the fluid density, $\boldsymbol{u}$ is the velocity, t is time. As fluids usually move at low speed in microfluidic applications (a typical velocity is up to 1 cm/s), flow

can be considered as incompressible. The above continuum equation can be reduced to

$$\nabla \cdot \boldsymbol{u} = 0. \tag{1.3}$$

Note: incompressible flow does not necessarily mean that fluid density is constant, which only holds for steady flow where flow fields do not evolve in time. The momentum equation which considers the momentum conservation is described by:

$$\rho \frac{D\boldsymbol{u}}{Dt} = -\nabla p + \eta \nabla^2 \boldsymbol{u} + \rho g, \tag{1.4}$$

where p is static pressure, η is fluid viscosity, and g is gravity.

The above continuum and momentum equations are called the Navier–Stokes equations for single phase fluid. When an interface is presented in two immiscible Newtonian fluids, the interface, separating these two fluids, can be treated as a boundary condition which imposes an additional interface stress on fluids. Therefore, to consider the effect of interfacial stress, the above momentum equation becomes

$$\rho \frac{Du}{Dt} = -\nabla p + \eta \nabla^2 u - F_{\mathrm{s}} + \rho g, \tag{1.5}$$

where F_{s} is the interfacial stress forcing term. A commonly used model is the Brackbill's continuum surface force (CSF) model where this surface forcing term is treated as a body force [3], i.e.

$$F_{\mathrm{s}} = \sigma \kappa \nabla C, \tag{1.6}$$

where C is the volume fraction of the fluids at the interface and κ is the curvature of the local interface.

1.5 Numerical Methods

Experimentally, it is often difficult to measure local flow field including velocity, pressure, and temperature at microscale. Modelling and simulation offer an important complimentary means to understand droplet dynamics and optimize device design and operation. Several numerical methods have been developed to describe the complex evolution process of a multiphase system. These methods can be classified into two major categories: the interface tracking and the interface capturing [1, 17, 26, 33]. The interface tracking method is a sharp interface approach, in which the interfaces are assumed to be infinitely thin, i.e. zero thickness. A set of governing equations are applied to each phase or component, and the interfacial conditions are used as boundary conditions. Through iterations,

the velocity of the interface is determined, and the interface then moves to a new location ready for the next time step. In this manner, the computations continue, and the interface is exactly tracked. This approach can provide very accurate results for cases without severe topological changes, and it forms the foundation of the front tracking methods (see [35]). However, such an approach encounters singularity problems when significant topological changes (e.g., breakup and coalescence of droplets) occur. In these situations, artificial treatments or ad hoc criteria are required. In addition, this approach requires a large number of grid points on the interface in order to accurately represent large deformation, so dynamical local mesh refinements are essential to improve computational efficiency. However, significant research effort is required to overcome the computational difficulties associated with dynamic re-meshing and parallel computing.

Contrary to the interface-tracking approach, the interface-capturing method uses a continuous function (to be called 'indicator function' thereafter) to distinguish different phases. This type of approach is able to deal with topological changes in a natural way. The indicator function is generally chosen as the volume fraction of one of the two phases/components, as in the volume of fluid (VOF) method [17], the signed distance to the interface, as in the level-set method [26], or the density/mass fraction of one phase or component (also called order parameter), as in the phase-field models [1]. In this class of approach, the same set of governing equations (1.2 and 1.5) is used for fluid flows. The fixed Eulerian grids are usually used for simulation domains and the interfaces are implicitly captured by the indicator function (known as 'interface capturing'). Since the interface capturing methods have been widely used for multiphase microfluidic flow simulations, we briefly discuss these methods below.

1.5.1 Volume of Fluid Method

The VOF method uses the volume fraction of one fluid phase or component (denoted as C) to characterize the interfaces (here, we refer to two immiscible fluids). In the bulk phase (i.e. a pure fluid), C is equal to zero or unity; in multi-fluid computational cells, $0 < C < 1$. In general, the VOF method consists of three major steps: the interface reconstruction algorithm, which provides an explicit description of the interface in each multi-fluid cell based on the volume fractions at this time step; the advection algorithm, which calculates the distribution of C at the next time step by solving an advection equation (1.7) using the reconstructed interface and the solved velocity field at the previous time step; and the interfacial tension force model, which takes account of interfacial tension effects at the interface. Two widely used interface reconstruction methods are simple line interface calculation (SLIC) [17] and the piecewise linear interface calculation (PLIC) [15]. In the SLIC method, the VOF in each cell is treated as if its local interface is either a vertical or horizontal line. In the PLIC method, the local phase interface is determined by fitting a straight line in the cell that satisfies the VOF criteria, and the

orientation of the straight line is decided by the distribution of one of the fluids in the neighbouring cells. In addition to these geometrical re-construction schemes, there are some other numerical schemes to solve the transport equation of indicator function. For example, Yabe and Xiao [39] used a smooth function to transform C to avoid rapid change of C at the interface, which does not need a computationally costly interface re-construction step.

The volume fraction function is purely advected by the velocity field, i.e., it obeys the transport equation:

$$\frac{\partial C}{\partial t} + \boldsymbol{u} \cdot \nabla C = 0. \tag{1.7}$$

Generally, the effect of interfacial tension force is incorporated into the momentum equation (1.5) using the continuum surface force (CSF) model of Brackbill et al. [3]. The normal vector and the curvature of the interface are calculated from derivatives of this volume fraction function. The interfacial tension force is applied using these two computed quantities, and its magnitude is proportional to the interfacial tension σ (see 1.6). Therefore, in addition to be an indicator, the volume fraction function plays an important role in the enforcement of the interfacial tension effect. This method is so far most likely to be found in commercially available computational fluid dynamics (CFD) software.

1.5.2 Level Set Method

The level set method was first introduced by Osher and Seithian [26]. The basic idea was to use a smooth function (level set function, φ) defined in the whole solution domain to represent the interface. It is defined as a signed distance to the interface and is purely a geometrical variable. The advantage is that the level set function varies smoothly across the interface, which eliminates the discontinuity problem that occurs in the VOF method. The CSF model for interface tension force is also used in the level set method. Similar to the volume fraction function in the VOF method, the level set function used in the level set method is purely transported by the flow velocity field as

$$\frac{\partial \varphi}{\partial t} + \boldsymbol{u} \cdot \nabla \varphi = 0. \tag{1.8}$$

In contrast to the volume fraction, it is just an indicator that has no physical meaning. Therefore, the level set function does not need to satisfy the conservation law. It only needs to consider differentiation of the convection term. However, the level set method requires a re-initialization procedure to restore the signed distance property when large topological changes occur around the interface [29]. This may violate the mass conservation for each phase or component.

1.5.3 Phase-Field Method

Phase-field method originates from the theory for near-critical fluids, in which the fluid system is fundamentally viewed as a whole and the indicator function (i.e. order parameter θ) is associated with the free energy of the system based on the Cahn–Hilliard theory [4]. The order parameter is a conserved variable that varies continuously over thin interfacial layers and is mostly uniform in the bulk phases. In phase-field method, the interfacial region has its own physics. As the interface thickness becomes smaller and smaller in comparison with the droplet size, it can be mathematically proved that phase-field model approaches the original sharp interface equations [1, 21]. The equation of fluid motion which is modified to account for the presence of thin layer of interface can be applied over the entire flow domain. For example, the Navier–Stokes equations can be modified to include a pressure tensor accounting for the interfacial tension. The pressure tensor can be derived by the use of reversible thermodynamic arguments. The interfacial tension can be given in terms of the excess free energy which is distributed through a three-dimensional layer rather than being defined on a two-dimensional surface.

The order parameter is evolved by the Cahn–Hilliard equation,

$$\frac{\partial \theta}{\partial t} + \boldsymbol{u} \cdot \nabla \theta = \nabla \cdot (M \nabla \phi), \tag{1.9}$$

where M is mobility and ϕ is the chemical potential. In the phase-field method, the interface sharpness is automatically maintained by the anti-diffusive term without losing the continuity. The interface structure is preserved as the interface evolves, so that the method does not require additional efforts for interface reconstruction and re-initialization step as in the VOF and level set methods [9, 10]. In addition, the smooth representation of the interface as a region with the finite thickness prevents the numerical difficulties caused by the interface singularities. Detailed discussion on some important numerical issues related to phase-field method can be found in Jacqmin [20]. Since the phase-field method resolves the interface structure, and the thermodynamics is built into the model, it includes rich physics which is not available in the VOF and level set methods. Consequently, it has some distinctive advantages, e.g. dynamic contact angle becomes a part of solution rather than a prescribed value.

1.6 Flow Physics Clarification: Important Dimensionless Parameters

As flow physics at microscale can be very different from the conventional scales, it is important to clarify physical phenomena occurring at small scales. Dimensionless numbers which evaluate the importance of these phenomena are useful for us to

understand the underlying flow mechanisms of a flow system. Therefore, we discuss some important dimensionless numbers in this chapter.

1.6.1 Reynolds Number

For fluid dynamics, the most widely used important dimensionless number is Reynolds number, *Re*, which compares inertial forces to viscous forces, i.e.

$$\mathrm{Re} = \frac{\rho u L}{\eta}, \tag{1.10}$$

where L is the characteristic length of the flow system. Usually, *Re* is used to judge whether flow is laminar or turbulent. However, for microflows, the characteristic length is usually small, so the Reynolds number is small. This indicates that the inertial forces are relatively not important compared with the viscous forces. Typically, microfluidic devices use aqueous solutions which move at a speed between 1 μm/s and 1 cm/s. And the typical microchannels have height of 1–100 μm. Therefore, the Reynolds number is typically in the range of orders of 10^{-6} and 1. So the flows are laminar and the inertial forces may be neglected. The conventional Navier–Stokes equation can therefore reduce to the Stokes equation, which is given by

$$\rho \frac{\partial \boldsymbol{u}}{\partial t} = -\nabla p + \eta \nabla^2 \boldsymbol{u} + \rho g. \tag{1.11}$$

Comparing with the Navier–Stokes equation, the nonlinear term $\rho \boldsymbol{u} \cdot \nabla \boldsymbol{u}$ is gone in the right hand side of the equation. Note: as conventional flow devices are usually operated at higher *Re*, the counter-part microfluidic devices should not be simply designed by scaling down the conventional devices.

1.6.2 Capillary Number

While the most important dimensionless number for fluid dynamics, *Re*, is least interesting for microfluidics, the usually ignored interfacial tension in conventional free surface/interfacial flows becomes essential for micorfluidics. The corresponding dimensionless number is capillary number which compares surface tension forces with viscous forces.

$$Ca = \frac{\eta \boldsymbol{u}}{\sigma}, \tag{1.12}$$

where the viscosity of continuum phase is usually used.

1.6.3 Bond Number and Weber Number

The Bond number (Bo) (also known as Eötvös number (Eo)) is to evaluate buoyancy force against surface tension force,

$$Bo = \frac{\Delta\rho g L^2}{\sigma}, \tag{1.13}$$

where $\Delta\rho$ is the density difference between two phases. It is an important parameter for describing droplet dynamical behaviour when the continuum carrier phase is gas. If we consider typical microfluidic water droplet in oil or oil droplet in water, the Bo number may not be essential as density difference between the immiscible liquid phases is small.

The Weber number (We), named after Moritz Weber (1871–1951), is regarded as a measure of the relative importance of the fluid's inertia in comparison with its surface tension,

$$We = \frac{\rho u^2 L}{\sigma}. \tag{1.14}$$

It is not an independent parameter which can be determined by Re and Ca, i.e. $We = Re \times Ca$. Weber number is usually not important for usually low speed microfluidic microdroplet applications.

1.7 Droplet Generation in Microfluidic Devices

Generating uniform droplets is one important step of achieving microdroplet functionalities. Using pressure as driving force to generate droplets is one of the fastest and commonly used methods. Many microfluidic devices have been designed to apply pressure to generate uniform droplets, including geometry-dominated devices [28, 40], flow-focusing devices [2, 6, 12, 13, 30]; T-junctions [5, 7, 14, 16, 24, 31, 37] and co-flowing devices [18, 34]. For device design optimization and operation, it is important to understand the underlying mechanisms of droplet generation processes in microchannels. In comparison with unbounded flows, the two-phase flow characteristics in microchannels is determined by not only flow conditions and fluids properties but also channel geometry. Here, we select two most popular device configurations—T-junctions and cross-junctions—and discuss droplet generation mechanisms in details.

1.7.1 Droplet Generation at T-Junctions

T-junctions are one of the most frequently used microfluidic geometries to produce immiscible fluid segments (plugs) and droplets. Although this approach has been

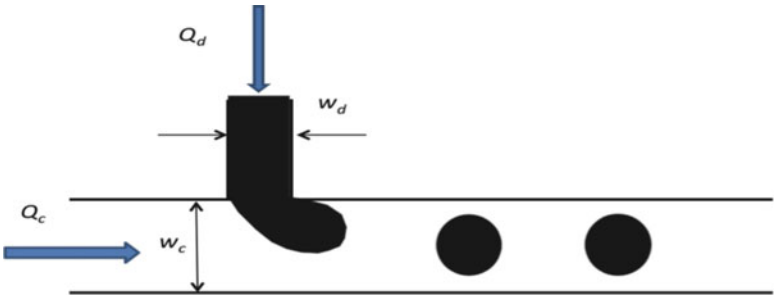

Fig. 1.2 Droplet generation in a microfluidic T-junction with the disperse phase injected through the side channel and the carrier phase injected through the main channel. Q_c and Q_d are volume flow rate of the carrier and disperse phases, respectively, while w_c and w_d are the width of the main and side channels

widely used, the currently available information is still fragmented due to differences in channel dimensions, flow rates, fluid properties and surface materials. The research challenge still remains to fully understand underlying mechanisms of droplet formation processes that are influenced by capillary number, flow rate ratio, viscosity ratio, contact angle and channel geometrical configurations. Meanwhile, some important advances have been recently made in experimental and numerical studies. For example, a squeezing mechanism due to confined geometry in droplet formation process, which does not exist in an unbounded flow condition, has been identified by Garstecki et al. [13]. In the following sections, we discuss state of the art of this research topic. The configuration of a typical T-junction is illustrated in Fig. 1.2.

1.7.1.1 The Flow Regimes

De Menech et al. [7] identified three distinctive flow regimes: squeezing, dripping and jetting. As jetting occurs at very high flow rates or capillary number, this regime is not often utilized in microfluidic applications. The authors found in their computational study that in the squeezing regime, droplets (plugs) are generated in a way very different from unconfined cases. The breakup process is dominated by the buildup pressure in the upstream of an emerging droplet which blocks or partially blocks the main flow channel. Meanwhile, in the dripping regime, both buildup pressure and shear stress are important. This finding has been experimentally observed (e.g. [8, 24, 25]). Figure 1.3 shows that plug fully blocks the main channel so that the buildup pressure will pinch off the plug. The breakup point of plug is at the junction corner and capillary number is very small. Figure 1.4 shows that with larger capillary number, the droplet emerges out of the side channel will experience shear force from the carrier fluid and buildup pressure due to partial blockage of the main channel. The breakup point in this dripping regime is at the downstream of the main channel.

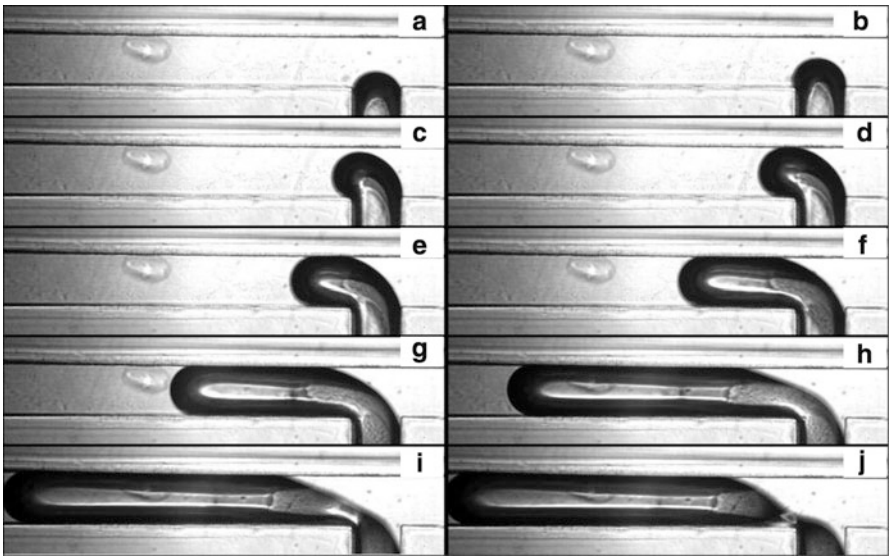

Fig. 1.3 The droplet generation in the squeezing regime (**a** to **j**) with $Ca = 0.0036$ and $Q = 1.2$, where Ca is defined as (1.15) and Q is the flow rate ratio (Q_d/Q_c)

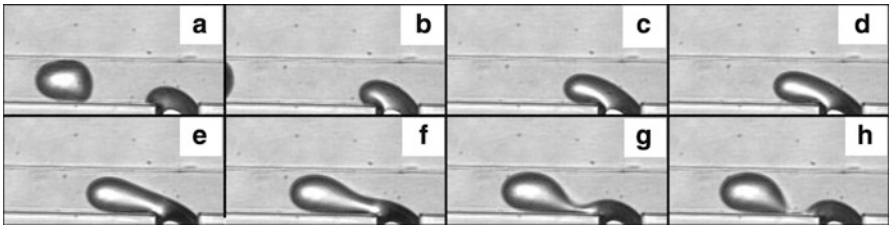

Fig. 1.4 The droplet generation in the dripping regime (**a** to **h**) with $Ca = 0.036$ and $Q = 1.2$, where Ca is defined as (1.15) and Q is the flow rate ratio (Q_d/Q_c)

Here, we focus on droplet generation processes in the squeezing and dripping regimes. Flow behaviour in a microfluidic T-junction can be classified by a group of dimensionless parameters, which are commonly defined by the experimentally measurable variables, e.g. the interfacial tension, the inlet volumetric flow rates (Q_c and Q_d) and viscosities (η_c and η_d) of the two fluids. For a typical microfluidic system, the Reynolds number is so small that the inertial effect can be neglected. The Bond number is also negligibly small due to the small density difference between two immiscible liquids. In contrast, the capillary number is the most important parameter in droplet generation processes, which can be defined by the average inlet velocity u_c and the viscosity η_c of the continuous phase, and the interfacial tension σ as

$$Ca = \frac{\eta_c u_c}{\sigma}. \tag{1.15}$$

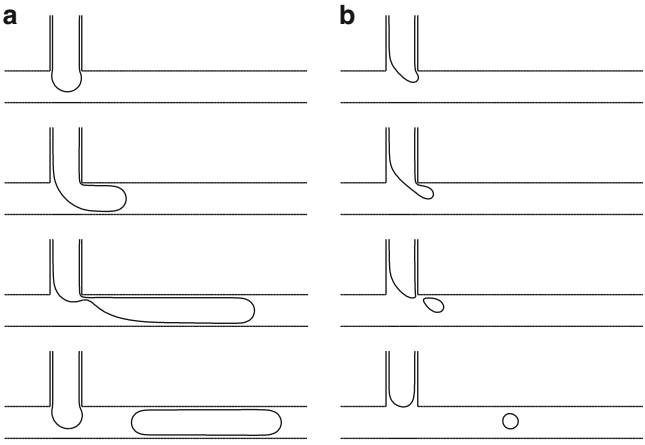

Fig. 1.5 An illustration of droplet generation flow regimes in T-junction (**a**) squeezing regime; (**b**) dripping regime. Reprinted with permission from Liu and Zhang [22], Journal of Applied Physics, 106, 034906, 2009. Copyright 2009, American Institute of Physics

1.7.1.2 Influence of the Capillary Number

Figure 1.5 illustrates droplet formation process in the T-junction in the squeezing regime (a) and the dripping regime (b). The droplet emerges from the side channel and deforms before detachment, and the necking of the dispersed phase is initiated once the continuous phase fluid intrudes into the upstream side of the side channel. The intrusion of the continuous phase accentuates the influence of the contact line dynamics, which is thought to be indispensable for the droplet detachment. Figure 1.5 shows that the necking occurs right after the dispersed phase moves into the main channel when Ca is large (the dripping regime), while the plugs are formed when Ca is small (the squeezing regime). This is both confirmed in experimental and numerical studies (e.g. [8, 22, 24, 25]).

Liu and Zhang [22] showed that when the capillary number is low, i.e. $Ca = 0.006$ in Fig. 1.6a, the incoming dispersed phase fluid tends to occupy the full width of the main channel, and the breakup occurs at the downstream side of T-junction corner. When the capillary number increases, i.e. $Ca = 0.032$ and 0.056 in Fig. 1.6 b,c, the dispersed phase fluid occupies only part of the main channel, and smaller droplets are formed. According to Ca, two distinctive droplet generation regimes, i.e. the squeezing and dripping regimes are identified. In the squeezing regime when Ca is small, the buildup of pressure at the upstream due to the obstruction of the main channel by the emerging droplet is responsible for the droplet 'pinching off', while the viscous shear force becomes increasingly important in the dripping regime when Ca increases.

In both experimental and numerical studies, [36, 37] found that the final droplet volume is a consequence of a two-stage droplet growth. Initially, the droplet grows to a critical volume V_c until the forces exerted on the interface become balanced.

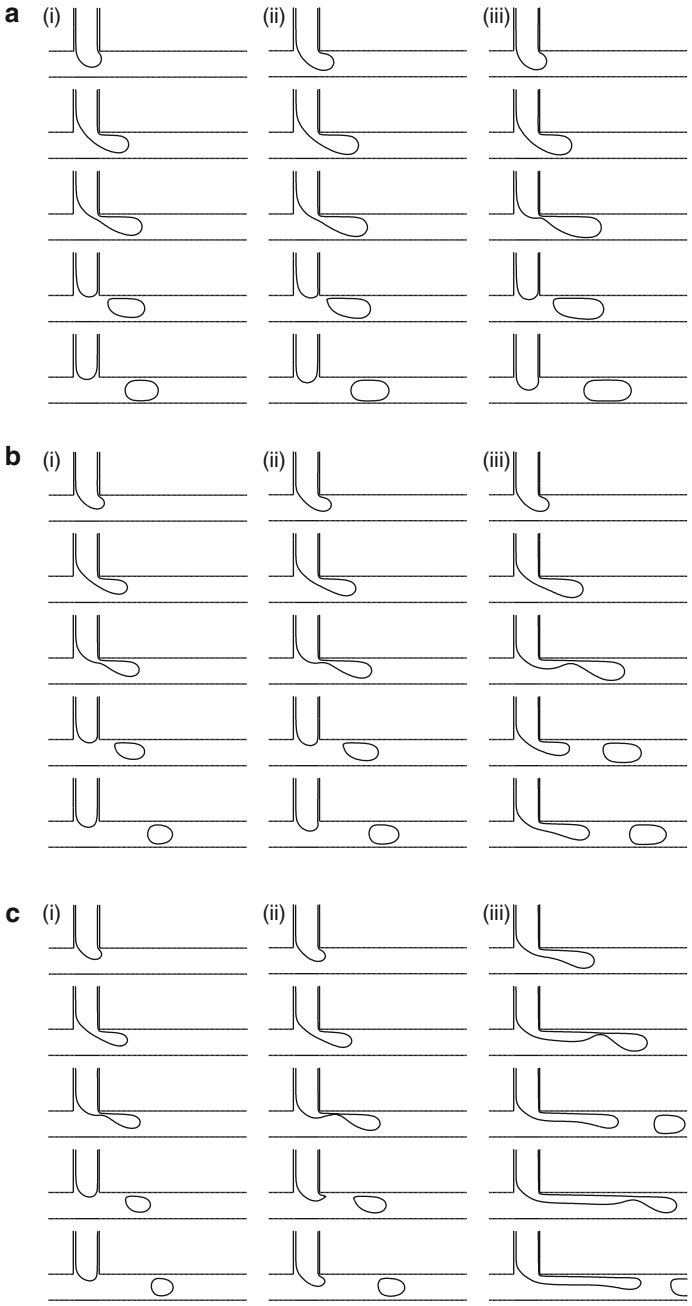

Fig. 1.6 The effect of capillary number and flow rate ratio in droplet generation process, where *Ca* is (**a**) 0.06, (**b**) 0.032 and (**c**) 0.056; the flow rate ratio *Q* is (i) 1/8, (ii) 1/4 and (iii) 1/2. Reprinted with permission from Liu and Zhang [22], Journal of Applied Physics, 106, 034906, 2009. Copyright 2009, American Institute of Physics

Subsequently, the droplet continues to grow for a time t_n for necking due to the continuous injection of the dispersed phase fluid. And the final droplet volume V can be predicted by the scaling law below (van der Graaf et al. [36]):

$$V = V_c + t_n Q_d, \tag{1.17}$$

where V_c depends only on Ca and the duration of necking t_n and decreases as Ca increases. An empirical correction was proposed to improve the prediction of the droplet volume by van der Graaf et al. [37]:

$$V = V_{c,ref} Ca^m + t_{n,ref} Ca^n Q_d, \tag{1.18}$$

where $V_{c,ref}$ and $t_{n,ref}$ are the reference values at $Ca = 1$ where the droplet detachment process is very fast, i.e. $t_n \to 0$; the exponents m and n depend on the device geometry, which were reported to be –0.75 [37].

1.7.1.3 Influence of the Flow Rate Ratio

Apart from capillary number, flow rate ratio Q ($Q = Q_d/Q_c$) plays an essential role in droplet generation processes. For small Q, the droplets are pinched off at the T-junction corner regardless of the capillary number. However, for larger Q, increasing Ca will force the detachment point to move from the corner to the downstream. Liu and Zhang [22] showed in Fig. 1.6 that when Ca is fixed at 0.006, varying Q from 1/8 to 1/2 does not change the detachment point of the droplet. When Ca is increased to 0.032 and 0.056, the detachment point will move from the T-junction corner to the downstream as Q increases. In addition, the droplet detachment point gradually moves downstream until a stable jet is formed when Ca and Q increase, which was also observed both numerically [7, 22] and experimentally [5].

The droplet grows as the flow rate ratio increases but becomes smaller as the capillary number increases. In addition to the capillary number, flow rate ratio will affect the formed droplet size significantly. Figure 1.6a shows that, in the squeezing regime, the flow rate ratio has significant effect on the droplet size. In the dripping regime as Ca increases, the effect of the flow rate ratio interestingly diminishes, which was also recently reported by De Menech et al. [7].

Many experimental studies were carried out in the squeezing regime so that the droplets filled the main channel and formed “plug-like” or “slug-like” shapes [14, 32, 42], where the viscous shear force may be ignored and the dominant force responsible for droplet breakup is the squeezing pressure caused by the channel obstruction. Garstecki et al. [14] argued that the detachment begins once the emerging droplet fills the main channel and the droplet continues to grow during this time due to continuous injection of the dispersed phase fluid. Assuming that the neck squeezes at a rate proportional to the average velocity of the continuous phase

fluid, and the plug fills at a rate proportional to Q_d, a scaling law for the final plug length was proposed:

$$l/w_c = 1 + \alpha\, Q, \tag{1.19}$$

where α is a constant of order one, whose value depends on the widths of both channels. It clearly shows the plug length depends only on Q. However, Liu and Zhang [22] suggested that the droplet size also strongly depends on Ca in the squeezing regime, which is consistent with the experimental observations (e.g. [5]). Therefore, the role of capillary number needs to be reflected in the scaling law. Although the scaling law (1.19) does not capture the capillary number dependency, it can predict the droplet size under various flow rate ratios when Ca is fixed in the squeezing regime. When Ca is taken into account, the scaling law given by (1.18) should be used.

1.7.1.4 Influence of Viscosity Ratio and Contact Angle

As shown in Fig. 1.7, in the squeezing regime, the predicted droplet diameter is nearly independent of the viscosity ratio, λ ($\lambda = \eta_d/\eta_c$), where the droplet formation is completely controlled by the capillary force and the squeezing pressure. In the dripping regime, the influence of viscosity ratio becomes more pronounced as Ca increases, where the large viscosity ratio leads to smaller droplet [7, 22]. However, it also shows that the influence of the viscosity ratio on the generated droplet diameter is not as significant as in the unbounded flow [34], where the breakup of droplets is controlled by a competition between the viscous shear force and the capillary force. This indicates that the squeezing pressure caused by the confinement of geometry of a T-junction has to be taken into account even in the dripping regime.

Due to large surface to volume ratio, fluid/surface interaction will significantly affect the droplet dynamics in microchannels. The contact angle influences droplet shape, generation frequency, and detachment point. Liu and Zhang [22] showed that the generated droplets become smaller when the contact angle increases. Interestingly, they also found that negligible viscosity ratio effect in the squeezing regime is only valid for more hydrophobic wetting conditions.

1.7.1.5 Regime Change: Critical Capillary Number

Three flow regimes for droplet generation in T-junction i.e. squeezing, dripping and jetting have been identified. It is important to understand the factors that control regime transition especially squeezing-to-dripping transition which is most relevant to microfluidic microdroplet applications. The recent work has suggested that transition from squeezing to dripping regime depends on a critical capillary number. For example, De Menech et al. [7], using the Navier–Stokes solver with a phase-field model, reported a critical capillary number of 0.015. However, the recent experimental study by Christopher et al. [5] did not observe the critical

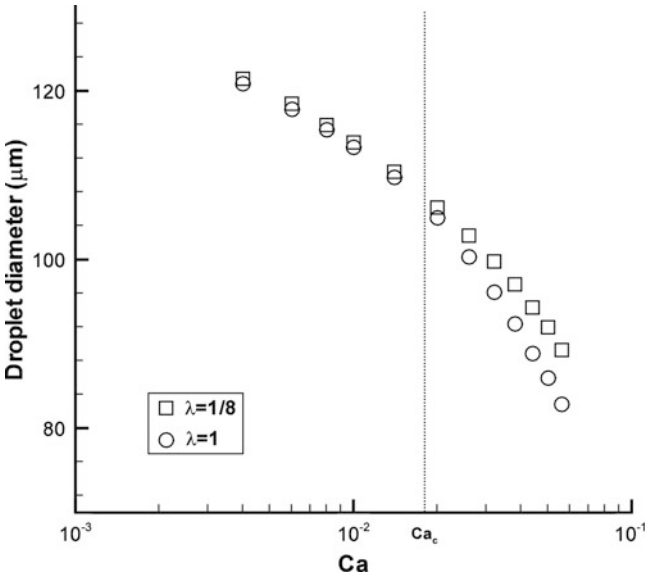

Fig. 1.7 Influence of viscosity ratio on droplet size. Reprinted with permission from Liu and Zhang [22], Journal of Applied Physics, 106, 034906, 2009. Copyright 2009, American Institute of Physics

capillary number during the squeezing-to-dripping transition. Liu and Zhang [22] noticed that the two regimes become difficult to distinguish as Q decreases because the droplet detachment point is always close to the downstream corner of the T-junction at small Q. This may explain why Christopher et al. [5] did not observe the critical Ca during the squeezing-to-dripping transition because they performed experiments at small viscosity ratio of 0.01, where the droplet breakup always occurs at the downstream corner of the T-junction. According to Liu and Zhang [22], there is a critical capillary number (see Fig. 1.8, $Ca_c = 0.018$), which distinguishes the squeezing and dripping regimes. Furthermore, they showed that this critical capillary number is independent of the flow rate ratio, the viscosity ratio and contact angle. However, their work is based on 2D simulation results, whether there is the critical capillary number remains to be investigated. Indeed, our recent experimental data suggests that squeezing-to-dripping transition depends on Ca, Q and channel geometries for the deep channels [41].

1.7.2 Droplet Generation in Cross-Junctions

In comparison with droplet generation at T-junctions, droplet generation in a confined cross-junction is quite similar. The coupled factors which affect the droplet formation process at T-junction are also important, i.e. interfacial tension, wetting properties and confinement of flow channels, fluid flow rates and

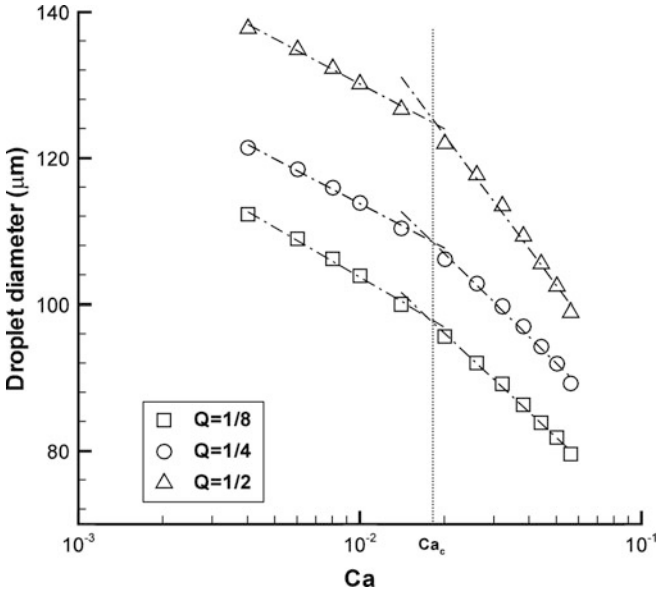

Fig. 1.8 Squeezing-to-dripping flow regime transition. Reprinted with permission from Liu and Zhang [22], Journal of Applied Physics, 106, 034906, 2009. Copyright 2009, American Institute of Physics

viscosities. In this section, we highlight the difference between the droplet generation processes of cross and T-shaped junctions.

1.7.2.1 Cross-Junction Flow Patterns

Similar to T-junctions as experimentally observed by Guillot and Colin [16], there are also three typical flow patterns in droplet generation at low capillary number: the droplets are formed at the cross-junction (DCJ); at downstream of the cross-junction (DC), forming a thread that becomes unstable after a distance of laminar flow; the stable parallel flows (PF), where the three incoming streams co-flow in parallel to the downstream without pinching. The flow pattern transition will be affected by capillary number and flow rate ratio (see Figs. 1.9 and 1.10).

1.7.2.2 Scaling Laws for Droplet Size

On the basis of the experimental observation of plug formation at microfluidic T-junctions, Garstecki et al. [14] argued that at low *Ca* the final length of a plug is contributed by two steps. First, the thread of the dispersed phase grows until it blocks the continuous phase liquid. At this moment the 'blocking length' of the plug is equal to w_c. Then the increased pressure in the continuous phase liquid begins to

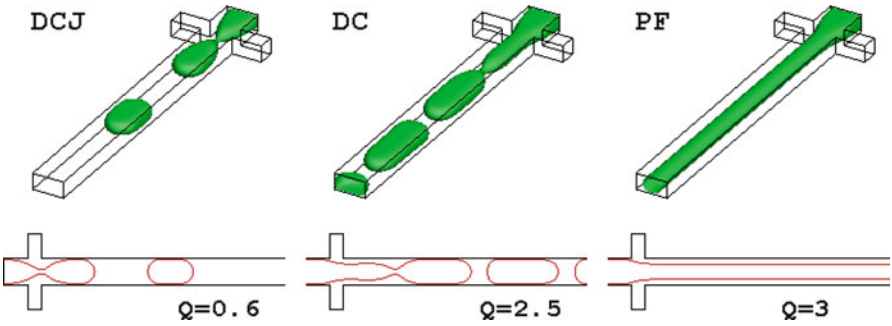

Fig. 1.9 Typical three flow patterns at $Ca = 0.004$ and $Q = 0.6$(DCJ), 2.5(DC) and 3(PF). Reprinted with permission from Liu and Zhang [23], Physics of Fluids, 23, 082101, 2011. Copyright 2011, American Institute of Physics

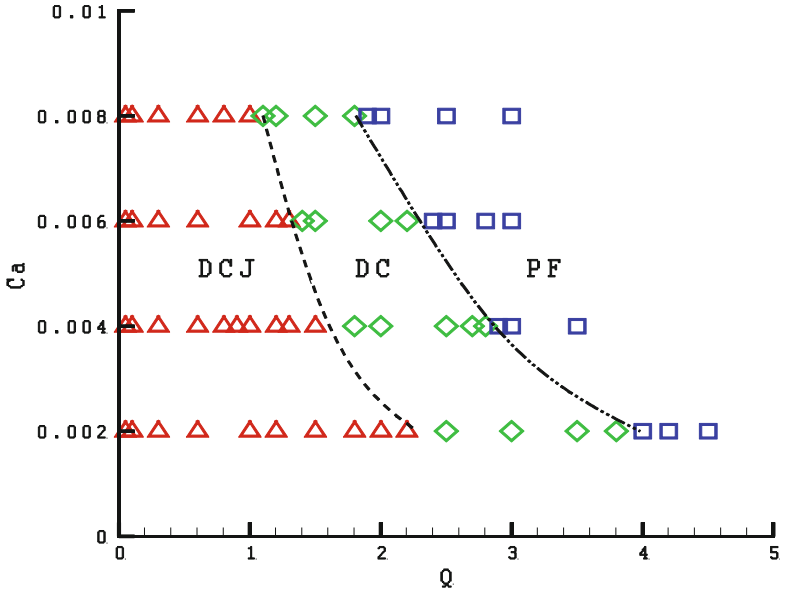

Fig. 1.10 Droplet flow patterns as a function of flow rate ratio Q and capillary number (the geometry configuration and viscosity ratio may also alter the flow pattern transition). Reprinted with permission from Liu and Zhang [23], Physics of Fluids, 23, 082101, 2011. Copyright 2011, American Institute of Physics

'squeeze' the neck of dispersed thread. They proposed a scaling law to predict droplet size as given by (1.19). Recently, Xu et al. [38] compared the experimental data from different authors and found that the 'blocking length' is not always equal to w_c, but is also dependent on the channel geometry. Therefore, the scaling law given by (1.19), is modified as

$$\frac{L}{w_c} = \varepsilon + \omega Q, \tag{1.20}$$

where ε and ω are fitting constants that are mainly dependent on the channel geometry. Experimentally, in the DCJ, Tan et al. [30] observed that the non-dimensional length of plugs (L/w_c) exhibits a power-law dependence on the capillary number, i.e. $L/w_c = kCa^m$, which is independent of the flow rate ratio Q. Considering the influence of capillary number and flow rate ratio, Liu and Zhang [23] proposed that the generated plug length (droplet diameter) can be predicted by

$$\frac{L}{w_c} = (\varepsilon + \omega Q)Ca^m, \tag{1.21}$$

where ε, ω and m are the fitting parameters that vary with the channel geometry. Based on their simulation results, Liu and Zhang [23] confirm this scaling law and determine the coefficients ($\varepsilon = 0.551$, $\omega = 0.277$ and $m = -0.292$). This is broadly consistent with the two-step model proposed by van der Graaf et al. [36], which was general enough to describe the T-junction droplet formation [27].

1.8 Conclusion

We do not aim to summarize complex multi-scale multi-physical droplet dynamics in a single chapter. Instead, we select the basic multiphase flow physics and pick droplet generation processes in microfluidic channels as examples to determine uniqueness of droplet dynamical behaviour in confined microchannels. We hope this chapter can be useful for readers new to flow physics which underpins microfluidic microdroplet technologies.

References

1. Anderson DM, McFadden GB (1998) Diffuse-interface methods in fluid mechanics. Annu Rev Fluid Mech 30:139–165
2. Anna SL, Bontoux N, Stone HA (2003) Formation of dispersions using "flow focusing" in microchannels. Appl Phys Lett 82:364–366
3. Brackbill JU, Kothe DB, Zemach C (1992) A continuum method for modelling surface tension. J Comput Phys 100(2):335–354
4. Cahn JW, Hilliard JE (1958) Free energy of a nonuniform system. I. Interfacial free energy. J Chem Phys 28(2):258–267
5. Christopher GF, Noharuddin NN, Taylor JA, Anna SL (2008) Experimental observations of the squeezing-to-dripping transition in T-shaped microfluidic junctions. Phys Rev E 78:036317
6. Cubaud T, Tatineni M, Zhong X, Ho C-M (2005) Bubble dispenser in microfluidic devices. Phys Rev E 72:037302
7. De Menech M, Garstecki P, Jousse F, Stone HA (2008) Transition from squeezing to dripping in a microfluidic T-shaped junction. J Fluid Mech 595:141–161

8. England P, Liu HH, Zhang YH, Mohr S, Goddard N, Fielden P, Wang CH (2010) Experimental study of droplet formation at microfluidic T-junctions. In: Proceedings of the second European conference on microfluidics—microfluidics 2010, Toulouse, 8–10 Dec 2010, paper No. 187
9. Enright D, Marschner S, Fedkiw R (2002) Animation and rendering of complex water surfaces. ACM Trans Graph 21(3):736–744
10. Enright D, Losasso F, Fedkiw R (2005) A fast and accurate semi-lagrangian particle level set method. Comput Struct 83(6–7):479–490
11. Franklin B, Brownrigg W, Farish J (1774) Of the stilling of waves by means of oil. Philos Tans Roy Soc Lond 64:445–460
12. Fu T, Ma Y, Funfschilling D, Li HZ (2009) Bubble formation and breakup mechanism in a microfluidic flow-focusing device. Chem Eng Sci 64(10):2392–2400
13. Garstecki P, Stone HA, Whitesides GM (2005) Mechanism for flow-rate controlled breakup in confined geometries: a route to monodisperse emulsions. Phys Rev Lett 94:164501
14. Garstecki P, Fuerstman MJ, Stone HA, Whitesides GM (2006) Formation of droplets and bubbles in a microfluidic T-junction–scaling and mechanism of break-up. Lab Chip 6:437–446
15. Gueyffier D, Li J, Nadim A, Scardovelli R, Zaleski S (1999) Volume-of-fluid interface tracking with smoothed surface stress methods for three-dimensional flows. J Comput Phys 152(2):423–456
16. Guillot P, Colin A (2005) Stability of parallel flows in a micro channel after a T junction. Phys Rev E 72:066301
17. Hirt C, Nichols B (1981) Volume of fluid (VOF) method for the dynamics of free boundaries. J Comput Phys 39:201–225
18. Hua J, Zhang B, Lou J (2007) Numerical simulation of microdroplet formation in coflowing immiscible liquids. AIChE J 53:2534–2548
19. Huebner A, Sharma S, Srisa-Art M, Hollfelder F, Edel JB, De Mello AJ (2008) Microdroplets: a sea of applications? Lab Chip 8:1244–1254
20. Jacqmin D (1999) Calculation of two-phase Navier-Stokes flows using phase-field modeling. J Comput Phys 155:96–127
21. Liu C, Shen J (2003) A phase field model for the mixture of two incompressible fluids and its approximation by a fourier-spectral method. Physica D 179(3–4):211–228
22. Liu HH, Zhang YH (2009) Droplet formation in a T-shaped microfluidic junction. J Appl Phys 106:034906
23. Liu HH, Zhang YH (2011) The mechanism of droplet formation in the squeezing regime in microfluidic cross-junction. Phys Fluids 23:082101
24. Nisisako T, Torii T, Higuchi T (2002) Droplet formation in a microchannel network. Lab Chip 2:24–26
25. Nisisako T, Torii T, Higuchi T (2004) Novel microreactors for functional polymer beads. Chem Eng J 101:23–29
26. Osher S, Sethian JA (1988) Fronts propagating with curvature-dependent speed: algorithms based on hamilton-jacobi formulations. J Comput Phys 79(1):12–49
27. Steegmans M, Schron C, Boom R (2009) Generalised insights in droplet formation at T-junctions through statistical analysis. Chem Eng Sci 64(13):3042–3050
28. Sugiura S, Nakajima M, Seki M (2004) Prediction of droplet diameter for microchannel emulsification: prediction model for complicated microchannel geometries. Ind Eng Chem Res 43:8233–8238
29. Sussman M, Fatemi E (1999) An efficient, interface-preserving level set redistancing algorithm and its application to interfacial incompressible fluid flow. SIAM J Sci Comput 20(4):1165–1191
30. Tan J, Xu J, Li S, Luo G (2008) Drop dispenser in a cross-junction microfluidic device: scaling and mechanism of break-up. Chem Eng J 136:306–311
31. Thorsen T, Roberts RW, Arnold FH, Quake SR (2001) Dynamic pattern formation in a vesicle-generating microfluidic device. Phys Rev Lett 86:4163–4166

32. Tice JD, Song H, Lyon AD, Ismagilov RF (2003) Formation of droplets and mixing in multiphase microfluidics at low values of the Reynolds and the Capillary numbers. Langmuir 19:9127–9133
33. Tryggvason G, Bunner B, Esmaeeli A, Juric D, Al-Rawahi N, Tauber W, Han J, Nas S, Jan Y-J (2001) A front-tracking method for the computations of multiphase flow. J Comput Phys 169 (2):708–759
34. Umbanhowar PB, Prasad V, Weitz DA (2000) Monodisperse emulsion generation via drop break off in a coflowing stream. Langmuir 16:347–351
35. Unverdi SO, Tryggvason G (1992) A front tracking method for viscous incompressible flows. J Comput Phys 100:25–37
36. van der Graaf T, Steegmans, MLJ, van der Sman RGM, Schroën CGPH, Boom RM (2005) Droplet formation in a T-shaped microchannel junction: a model system for membrane emulsification. Colloids Surf. A 266:106–116
37. van der Graaf T, Nisisako CGPH, Schroën RGM, van der Sman RM (2006) Boom, Lattice Boltzmann simulations of droplet formation in a T-shaped microchannel. Langmuir 22:4144–4152
38. Xu J, Li S, Tan J, Luo G (2008) Correlations of droplet formation in T junction microfluidic devices: from squeezing to dripping. Micro fluid Nanofluid 5:711–717
39. Yabe T, Xiao F (1995) Description of complex and sharp interface with fixed grids incompressible and compressible fluid. Computers Math Applic 29(1):15–25
40. Yasuno M, Sugiura S, Iwamoto S, Nakajima M, Shono A, Satoh K (2004) Monodispersed microbubble formation using microchannel technique. AIChE J 50:3227–3233
41. Zhang YH (2011) Dynamics of droplets in microfluidic devices. Bubble Tech to Bio App-Lab-on-a-Chip, October 17–18, KIST Europe, Saarbrucken, Germany
42. Zheng B, Tice JD, Roach LS, Ismagilov RF (2004) A droplet-based, composite PDMS/glass capillary microfluidic system for evaluating protein crystallization conditions by microbatch and vapor-diffusion methods with on-chip x-ray diffraction. Angew Chem Int Ed 43:2508–2511

Chapter 2
Microfluidic Droplet Manipulations and Their Applications

Melinda G. Simon and Abraham P. Lee

2.1 Introduction

"Droplet microfluidics" enables the manipulation of discrete fluid packets in the form of microdroplets that provide numerous benefits for conducting biological and chemical assays. Among these benefits are a large reduction in the volume of reagent required for assays, the size of sample required, and the size of the equipment itself. Such technology also enhances the speed of biological and chemical assays by reducing the volumes over which processes such as heating, diffusion, and convective mixing occur. Once the droplets are generated, carefully designed droplet operations allow for the multiplexing of a large number of droplets to enable large-scale complex biological and chemical assays. In this chapter, four major unit operations in droplets are discussed: droplet fusion, droplet fission, mixing in droplets, and droplet sorting. Combined, these operations allow for much complexity in executing chemical reactions and biological assays at the microscale. A broad overview of potential applications for such technology is provided throughout. While much research effort has been focused on the development of these individual devices, far fewer attempts to integrate these components have been undertaken. A review of many microfluidic unit operation devices is provided here, along with the advantages and disadvantages of each approach for various applications.

M.G. Simon • A.P. Lee (✉)
Department of Biomedical Engineering, University of California-Irvine, Irvine, CA, USA
e-mail: aplee@uci.edu

P. Day et al. (eds.), *Microdroplet Technology: Principles and Emerging Applications in Biology and Chemistry*, Integrated Analytical Systems,
DOI 10.1007/978-1-4614-3265-4_2,

2.2 Droplet Fusion

2.2.1 Theory

Droplet fusion is a critical operation for droplet manipulation, since it allows for the combination of different reagents and for the initiation of chemical and biological reactions in microfluidic devices. Contrary to intuition, simply initiating droplet collisions does not frequently result in fusion between the droplets. In fact, a systematic study of a passive droplet fusion technique revealed that it is the separation process of closely spaced microdroplets, rather than their collision, which results in coalescence of the droplets [1]. Bibette et al. provide a set of equations for predicting coalescence. For coalescence of droplets to occur, the continuous phase separating the two droplets must first be drained, bringing the droplets into close contact. Then, the droplets must be kept in close contact for a critical minimum amount of time, in order for fusion to occur. Fusion occurs due to fluctuations in the surface tension on the surface of droplets, which cause destabilization of the interface between the oil and water phases [2].

Although the fusion of droplets may seem straightforward, there are several key challenges involved in this process. In order for droplets to fuse, they must achieve temporal and spatial synchronization. Several creative strategies have been employed to synchronize droplets prior to fusion, both for passive and active droplet fusion systems. Still, with the development of more complex microfluidic systems with a large number of inputs, new strategies for the synchronization of droplets are being sought. The addition of surfactant to either the continuous or dispersed phases of a droplet microfluidic device is a common practice to stabilize the droplets; however, the presence of surfactant makes droplet fusion much more difficult. Other important considerations for any droplet fusion mechanism are its throughput and efficiency. While some methods presented below demonstrate a very high efficiency of fusion, with the vast majority of droplet pairs undergoing fusion, the throughput of such systems may be much lower than a system where the efficiency of fusion is not quite as high. While both high fusion efficiency and high throughput are desirable, it may be necessary to compromise one or the other of these qualities in order to satisfy the demands of the intended application. Due to the fact that fusion involves the coming together of contents from different droplets, inter-droplet contamination is also a concern. Additionally, preservation of the viability of biological material may be a concern in active fusion methods where electricity is used to fuse droplets. While passive fusion methods often carry a lower risk of contamination and are more biocompatible, they generally have a much lower throughput than active fusion methods. As a result, a variety of both passive and active methods for inducing the fusion of droplets have been developed. While each design has its strengths and shortcomings, a suitable method for inducing droplet fusion may certainly be found for a variety of applications.

2.2.2 *Passive Fusion Methods*

Passive droplet fusion mechanisms are those which do not require active control or electricity. These designs are often simpler than active fusion mechanisms, which may require complicated circuitry and control systems. One advantage of most passive droplet fusion techniques is that the possibility of inter-droplet contamination is lower than for active droplet fusion techniques. However, passive droplet fusion techniques are limited by the rate at which natural phenomena, such as surface tension fluctuations occur, and are therefore often slower than most active droplet fusion techniques.

2.2.2.1 Geometry-Mediated Passive Fusion

Among the earliest and simplest designs for passive fusion of microdroplets employs a section of widened channel, termed an "expansion volume." By controlling the continuous phase velocity and the dimensions of the expansion volume, consecutive droplets can be induced to fuse in this region. The expansion volume enables fusion by draining the continuous phase that separates one or more consecutive droplets in a channel. Upon entering the expansion volume, the continuous phase fluid spreads around the droplets to fill the increased volume, while droplets remain in the center of the channel. This removal of spacing between droplets allows interaction between the surfaces of adjacent droplets and induces fusion of the droplets as a result of minute disturbances in surface tension. Either a gradually tapering channel [3] or a wider section of the channel [4, 5] may be employed as an expansion volume (Fig. 2.1). Careful control of the frequencies of droplet generation from each droplet source is necessary for reliable fusion when using an expansion volume [6]. Another early method for passively inducing the fusion of consecutive droplets involved active drainage of the continuous phase between droplets, known as a flow-rectifying design. In this design, the droplet stream would flow past a junction with channels perpendicular to the direction of droplet transport. Through these perpendicular channels, continuous phase could be actively removed using an off-chip syringe pump, which induced droplet fusion by bringing consecutive droplets close together [4, 7, 8]. Alternatively, a 3D expansion volume can be used to fuse droplets. In this design, droplets carried along a microchannel "track" are carried through a chamber of larger width and height than the track. A control line adds continuous phase at a prescribed rate to control the number of fusion events that occur in the chamber. By controlling the flow rate of continuous phase from this line, researchers were able to perform arithmetic operations with the droplets, similar to the operation of an abacus [9].

Using an expansion volume, droplets from two different inlets have been fused in a tapering region of a microfluidic device. In this device, alternating droplets from two different inlets were produced. The droplet pairs fuse downstream in a tapering region of the channel to yield CdS nanoparticles within the

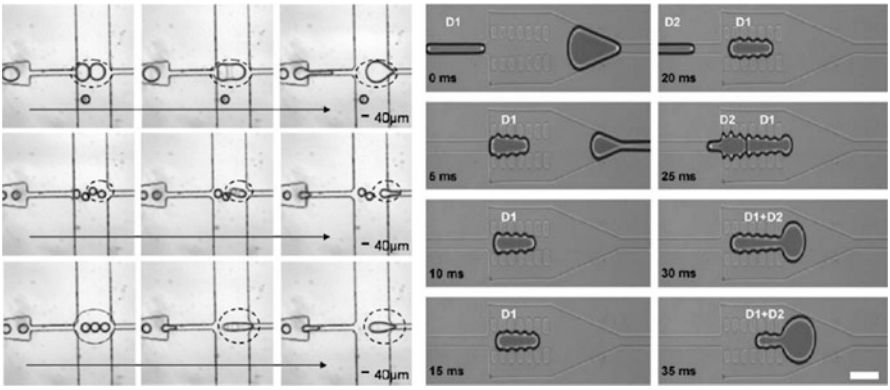

Fig. 2.1 *Left*: As droplets enter an expansion of the main fluidic chamber, the continuous phase is drained from between them and droplet fusion occurs (Reproduced from Tan et al. [4], by permission of the Royal Society of Chemistry, http://dx.doi.org/10.1039/b403280m) (*right*) Niu et al. used a pillar array to slow and trap a droplet entering an expansion of the main fluidic channel. The first droplet remains in the trap until a second droplet enters. After continuous phase drains from between them, the two droplets fuse, and hydrodynamic pressure from the entering second droplet pushes the fused droplet out of the trap and downstream (Reproduced from Niu et al. [10], by permission of the Royal Society of Chemistry, http://dx.doi.org/10.1039/b813325e)

fused droplets [3]. This development enabled the execution of simple chemical reactions, comprising a single mixing step, on a chip. The microfluidic platform enables synthesis of very small volumes of product, useful in situations where the reactants are expensive, hazardous, or simply limited.

While an expansion volume provides a way to fuse droplets passively, there are several limitations to this design. With the expansion volume approach, only consecutive droplets in a channel can fuse. This restriction requires that the order of droplets in a microchannel be carefully controlled, in order to achieve the desired fusion. In addition, an expansion volume is only able to fuse droplets that have a relatively small and uniform inter-droplet spacing. In order to enable more complex applications involving droplet fusion, several devices have been developed which overcome the problem of inter-droplet spacing, to ensure reliable droplet fusion. Building from the expansion volume concept for droplet fusion, Niu et al. designed an expansion volume containing two sets of tapering pillars in its center (Fig. 2.1). As a droplet enters the expansion volume, it is squeezed between the sets of pillars. Once the droplet has completely entered the expansion volume, continuous phase behind the droplet is allowed to drain around the droplet into the widened channel. The droplet is stopped in the pillar array due to the increase in surface tension it experiences. As the pillars narrow, the radius at the front of the droplet becomes smaller than the radius at the back of the droplet, which produces a net surface tension pressure that counters the hydrostatic pressure induced by the continuous phase. In this device, a droplet can be held indefinitely until the next droplet in the line approaches—this feature allows for droplet fusion to occur even if inter-droplet spacing does not remain constant. In addition, by changing the size of the expansion

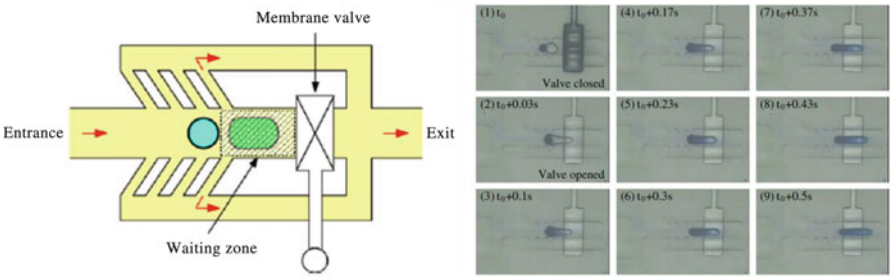

Fig. 2.2 A membrane valve and continuous phase drainage channels allow the first droplet to slow and become trapped. As a second droplet approaches the first and slows, the valve is released and the two droplets are fused as they leave the trap (Reproduced from Lin and Su [12], with permission from IOP Publishing, Ltd.)

chamber and the size of the droplets, multiple droplets can be induced to fuse in the pillar array [10]. In another design, droplets from one inlet become trapped in a narrowing channel, due to the increase in surface tension they experience as the radius of the front of the droplet decreases. Once a droplet is trapped, it is held in place indefinitely by surface tension forces. A bypass channel allows continuous phase and other droplets to continue to flow around the trapped droplet. Another droplet inlet, perpendicular to the first inlet, joins a fusion chamber at the location where a droplet is trapped. As a droplet from this second inlet approaches the fusion chamber, the second droplet fuses with the trapped droplet as it passes by. Due to the ability of this device to trap the first droplet and hold it indefinitely, droplets from separate inlets, and generated at different respective frequencies, can be fused. In addition, the inter-droplet spacing need not be uniform or short, for fusion to occur [11].

Instead of using surface tension forces to trap droplets before fusing, a membrane valve has also been used (Fig. 2.2). For fusion to occur, a membrane that occludes most of the width of an expansion volume is depressed. Droplets are constrained to the center of the expansion volume by a set of pillars as the membrane is depressed, while continuous phase is allowed to flow around the pillars and the depressed membrane. Once the desired number of droplets has been trapped in the expansion volume, the membrane valve is opened [12]. Droplets fuse as they are pulled away from one another out of the expansion volume. This is in accordance with recent theory and characterization describing how droplets are observed to merge as they are moving away from one another, instead of when they are pushed together [1].

2.2.2.2 Passive Fusion Induced by Physical and Chemical Phenomena

In addition to the above methods for passive droplet fusion, several designs which exploit physical or chemical phenomena have been developed. For instance,

droplets of different sizes or of different viscosity travel at different speeds within microfluidic channels. If a small droplet is introduced to the channel after a larger droplet, the small droplet will travel faster in the channel than the larger droplet, which decreases the inter-droplet spacing and allows fusion to occur at an expansion volume. As the viscosity of the dispersed phase is increased, the droplets travel with slower velocity. Hence, a droplet of lower viscosity will travel faster through a microchannel than a droplet of higher viscosity, allowing the lower viscosity droplet to "catch up" to a higher viscosity droplet. Droplets paired in this way can then become merged when they enter an expansion volume. One advantage to this technique is that droplets can self-synchronize if conditions are right, eliminating the need for an active mechanism of pairing droplets [13].

Surfactants are often added to a microdroplet emulsion to stabilize the droplets and prevent unwanted fusion events. One group has exploited the readiness with which surfactant-free droplets fuse to reliably fuse two populations of droplets one-to-one. A population of droplets with a surfactant concentration of 2.8% was generated and injected into a chip, where each surfactant-stabilized droplet was paired with a surfactant-free droplet. Upon entering a microchannel with 117° bends, the droplet pairs readily fused. Fusion occurs as a result of the geometric constraints imposed by the zigzag channel as well as the partial instability of the surfactant-free droplets. Since the droplets were paired one-to-one, secondary fusion of droplets was avoided, as fused droplets all contained surfactant and were thus stabilized against further fusion. Although useful for one-to-one fusion of two different droplet populations, this technique requires careful consideration of the chemistry of the system. Furthermore, the relatively high surfactant concentration required for the surfactant-stabilized population of droplets may be incompatible with some chemical or biological assays [14].

Another method which does not require synchronization of droplets for fusion relies on a hydrophilic patch inside a microchannel to trap droplets before fusion. A photomask is used to allow selective polymerization of acrylic acid on a PDMS device, using UV light. Areas exposed to the UV light are patterned with polyacrylic acid, rendering these areas hydrophilic. The rest of the PDMS device retains its native hydrophobicity. When a hydrophilic droplet approaches the hydrophilic patch in the channel, the droplet is slowed and stopped over the patch. Additional droplets gather behind the first droplet near the patch, until the viscous drag force generated by their presence is enough to overcome the interfacial forces holding the first droplet to the patch. At this point, the first droplet begins to move downstream, and the trapped droplets all fuse. Since this device functions by balancing the interfacial interaction force between the droplets and the patch, and the viscous drag force imposed by the continuous phase, the number of droplets to be trapped and fuse can be tuned by changing the continuous phase flow rate, which changes the viscous drag force on the droplets [15]. Although this fusion mechanism requires no special geometry and could potentially be incorporated into any straight microchannel, the possibility for contamination between droplets exists, due to the requisite interaction of droplets with the polyacrylic acid patch in the channel.

A unique approach to droplet fusion using a laser has been attempted in recent years. By carefully directing an Argon ion laser in a microchannel, localized heating is induced in the channel which can induce fusion between two droplets. Droplet fusion is induced when the laser is directed to the interface between the two droplets. Heat applied at this location leads to disturbances in the surface tension which result in destabilization of the droplet interfaces and eventually fusion. The laser is also capable of stopping droplets in a channel, potentially allowing for trapping a given number of droplets and fusing them together, using only a laser. Although this design minimizes the chance of inter-droplet contamination, due to the fact that droplets are not physically constrained on a surface, the throughput of this approach may be lower due to the need to precisely control the timing and location of laser heating [16].

2.2.2.3 Adding Reagents into Passing Droplets

An alternative to passive droplet fusion schemes that generate two droplets and then fuse them together is a technique where reagent is metered into a passing droplet from a microchannel intersecting the main channel. This strategy accomplishes the same goal of droplet fusion and precludes the need to generate many different populations of droplets. This technique has been used to produce nanoparticles in microdevices that are more monodispersed than nanoparticles produced in a benchtop process [17]. One drawback to this technique is that the possibility for contamination is more significant, since passing droplets come into direct contact with the second reagent stream. To overcome this issue, a device has been introduced more recently that uses several narrow hydrophilic channels to introduce the second reagent (Fig. 2.3). This reduction in the dimension of the injection channel raises the dimensionless Peclet number in this design, meaning that addition of reagent to passing droplets is due more to convection than diffusion. The authors postulate that the smaller injection channel dimension minimizes the effect of diffusion, which causes contamination between droplets due to the chaotic mixing it introduces. Although temporal synchronization of the release of the second reagent was a problem in the earlier designs, the technique employing several narrow channels can avoid the problem of extra droplet formation by carefully selecting the volumetric flow rate of the continuous and dispersed phases [18]. One disadvantage to this approach is less control over the specific amount of reagent that is added to a passing droplet. In systems where two separate droplets are generated and then brought together, the calculation of the specific volume of added reagent is more straightforward.

2.2.3 Active Fusion Methods

In addition to the passive fusion techniques discussed above, other fusion methods employing active controls, such as electrocoalescence, dielectrophoresis,

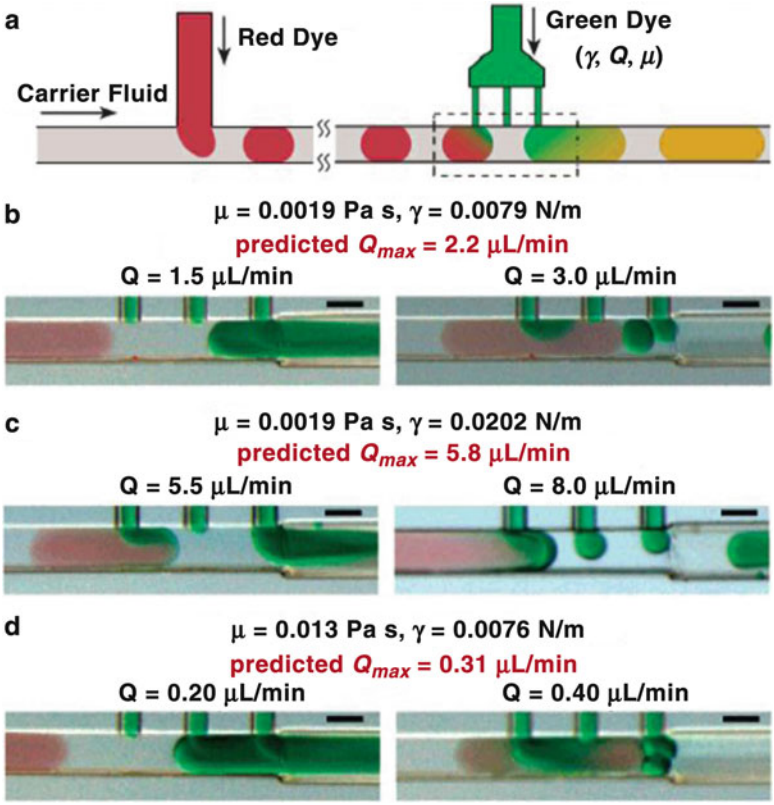

Fig. 2.3 As an alternative to fusing droplets, reagent may be metered into passing droplets from several narrow side channels. Successful injection of substrate requires a careful balance of the volumetric flow rates of the continuous and dispersed phases (Reproduced with permission from Li et al. [18])

and optical tweezers have also been developed. Such methods are inherently more complex than many passive droplet fusion schemes, since many require fabrication of electrodes and precise timing of electrical signals in order to fuse droplets. With the use of electricity come concerns of contamination between droplets, if some of the droplet contents become deposited on an electrode, as well as biocompatibility of electrical signals on biological molecules, such as DNA or proteins. The advantage to such systems is that the use of electricity can hasten the development of instabilities in the surface tension between droplets [19], initiating fusion more quickly and increasing the throughput capabilities of the device.

While several research groups have developed devices to fuse microdroplets using electrodes, the size and positioning of the electrodes in these devices is diverse, with each design presenting its own strengths for particular applications. In one design with applications for studying chemical kinetics, the electrodes comprise a platinum wire that is positioned inside the main microfluidic channel

where continuous phase flows, and an indium tin oxide ground electrode on the base of the microfluidic device. Perpendicular to this main channel, two dispersed phase streams enter near the wire and form droplets through a simple T-junction configuration. When voltage is applied across the electrodes, fusion of one droplet entering from each of the dispersed phase channels occurs at the tip of the wire. The application of voltage in this nonuniform electric field induces a positive dielectrophoretic (DEP) force on the droplets, which pulls them toward the wire. Once both droplets have been pulled close to the wire, the layer of continuous phase separating them becomes thin, and instabilities in the surface tension between the droplets result in fusion. Using this device, the progress of a chemical reaction can be tracked optically in the droplets, which each act as individual microreactors. Since the rate of droplet formation in the device is constant, the droplets produced display the progress of the chemical reaction at discrete time points, providing a simple means of studying the kinetics of a reaction [20]. While well suited for this purpose, this device is limiting in that the contents of all the fused droplets are exactly the same. For many applications, the production of many droplets with diverse contents is necessary.

For more complicated reactions or assays, the fusion of multiple droplets may be desired or needed. In 2009, Tan et al. developed a round microfluidic chamber in which a variable number of droplets could be fused. The chamber is designed to slow entering droplets, to give them more time for fusion, and helps to position the droplets parallel to the electric field. This orientation minimizes the electric field strength needed for droplet fusion, which occurs when the electric field disrupts surfactant molecules on the surface of the droplets. The fusion chamber is also designed large enough that droplets do not contact the electrodes during the fusion process, which decreases the risk of droplet-to-droplet contamination that may occur in devices where droplets come into contact with the electrodes. For fusion of two droplets, only the electric field is necessary both to align the droplets correctly and to fuse them. To fuse several droplets, however, laser tweezers were employed to position all of the droplets in a line parallel to the electrical field. The disadvantage to this technique is its low throughput. Five 10 μs pulses of DC voltage, space 0.2 s apart, were required for a single fusion event [21]. Due to the spaces between pulses, the maximum rate of fusion would be less than one event per second, which is much slower than most other droplet fusion mechanisms.

Another device traps passing droplets on the electrode surface to induce the fusion of multiple droplets. As the droplet slows and becomes trapped, it deforms and spreads on the electrode surface, which provides space allowing continuous phase to flow around the droplet. The next droplets carried through the channel also become trapped on top of the electrodes and fuse with previously trapped droplets (Fig. 2.4). The ability of the electrodes to trap and hold the droplets on their surface is a balance achieved between the DEP force imposed by the electrodes and the hydrodynamic force imposed by the flow of the continuous phase in the channel. Eventually, as multiple droplets become trapped on the electrodes, the hydrodynamic force on the droplets overcomes the DEP force from the electrodes, and the fused droplet is released from the electrode surface. The number of droplets to

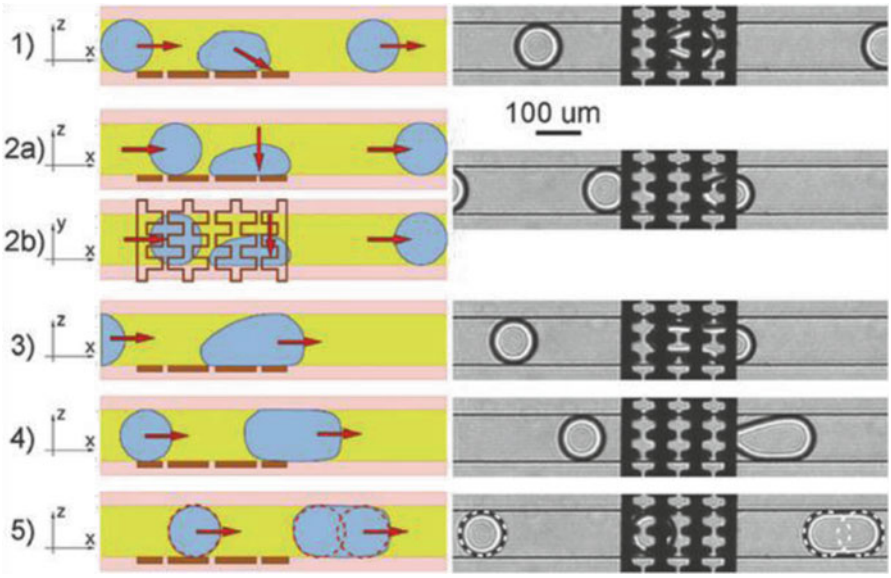

Fig. 2.4 Electrodes are used to slow and trap a droplet. Deformation of the droplet onto the electrodes allows continuous phase to pass around the droplet. As a second droplet approaches, it fuses with the first, and the blockage of continuous phase flow produces force that pushes the fused droplet off of the electrodes (Reproduced from Zagnoni and Cooper [19], by permission of The Royal Society of Chemistry, http://dx.doi.org/10.1039/b906298j)

be fused on the electrodes can thus be controlled by careful selection of the DEP force and hydrodynamic pressure applied to the system. Fusion rates of 50 per second were routinely demonstrated with this device. Higher rates of up to 100 fusions per second were achieved, but at high voltage levels, which could provide problems for biological assays and can also induce hydrolysis of water in the droplets. In addition, the reliance of this technique on droplet contact with the electrodes could mean that contamination from droplet-to-droplet is likely. One advantage to this technique is that no synchronization system is required. The first trapped droplet can wait indefinitely on the electrode surface until subsequent droplets arrive [19].

A common shortcoming in active fusion designs is their incompatibility to accommodate biological solutions, owing to the high voltages applied to induce droplet fusion. To address this problem, Priest et al. demonstrated a device that requires only a 1 V DC pulse to fuse droplets—a considerably lower voltage than many other systems. Lower voltages are required in this system due to the proximity of the droplets to the electrodes. While other designs used an expansion chamber to fuse their droplets, necessitating high voltage values to span a larger area [21], these design droplets are tightly packed as they flow past the electrodes. Even with tightly packed droplets, isolated fusion events between adjacent droplets can occur, as long as the droplet interface where fusion takes place is parallel to the electrodes.

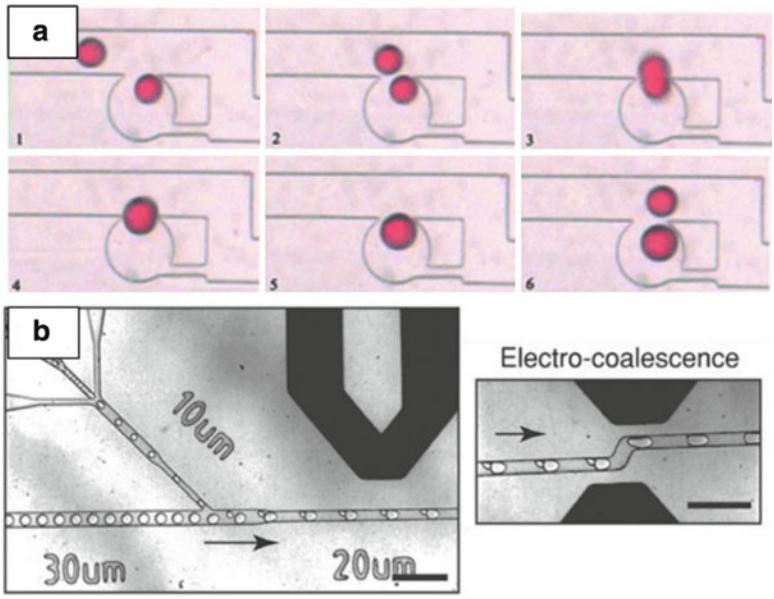

Fig. 2.5 (**a**) Droplets may be stored and fused in the same device by applying a DC voltage across the fluidic channel. Here, fused droplets may be removed from the array by increasing the continuous phase flow rate (Reproduced from Wang et al. [23], by permission of The Royal Society of Chemistry, http://dx.doi.org/10.1039/b903468d). (**b**) Droplets are paired and fused by an AC field (Reproduced from Mazutis et al. [29], by permission of The Royal Society of Chemistry, http://dx.doi.org/10.1039/b907753g)

For different types of droplet packing, different electrode orientations could be used to achieve this purpose. Fusion rates of around 10 per second can be obtained using this technique. In addition to the increased biocompatibility of this approach, an insulating layer of Poly(methyl methacrylate) coats the electrodes in the device, which reduces the chance of contamination, another significant concern for active fusion devices [22].

One unique approach to active droplet fusion allows for the trapping and storage of an array of fused droplets, in order to observe a reaction or the behavior of a cell over time. The first droplet is trapped in a side compartment adjoining the main fluidic channel when a DC voltage is applied (Fig. 2.5a). Voltage, applied across the channel, induces a DEP force on the droplet that causes it to move in one direction or another, depending on the type of DEP force applied. Using the DC voltage again, this trapped droplet can be induced to move toward the main channel, where it can contact and fuse with a passing droplet. Once fused, the droplet returns to the side compartment as the DC voltage is switched off, and the droplet may be observed indefinitely in the side compartment. These structures are designed to keep the fused droplet trapped at lower continuous phase flow rates, but allow the compartments to be cleared when the continuous phase flow rate is increased [23].

Instead of using electrodes to induce coalescence at the point of droplet contact, an alternative design imposes an opposite electrical charge on different populations of droplets, which then become fused together in the presence of an electrical field. As droplets are generated, either a positive or negative charge is imposed on them, such that droplets from one inlet become positively charged, while droplets from a second inlet become negatively charged. A potential disadvantage to this approach is that fused droplets become electrically neutral. In order to perform more than one fusion step, droplets would need to undergo charging after each fusion event [24].

Expanding upon a concept used to fuse droplets passively, one active fusion scheme induces pairing of droplets prior to fusion by generating droplets of different sizes. Smaller droplets move more rapidly through microfluidic channels, which cause them to catch up to and pair with larger droplets. Once paired, the droplets are fused controllably by a pair of electrodes across the microfluidic channel [25].

Electrowetting is another approach that has been used to manipulate droplets, inducing droplet formation as well as fusion. In this approach, droplets are positioned atop an array of individually addressable electrodes, and deform over the electrode when a voltage is applied, due to a minimum in the electric field that is induced over the electrode. Using computer software, the electrodes can be activated in a certain order to induce movement of the droplet. To fuse droplets using this technique, two droplets need only to be brought into close proximity using the electrode array. Although this technique offers very precise control over the movement of droplets, inter-droplet contamination is a concern, since the droplets wet the surface of the electrodes when they are trapped [26].

For most applications, droplet fusion is desired to initiate a chemical reaction; however, it may be necessary for some applications to convert information contained in individual droplets into a continuous stream for the purpose of analysis of droplet contents. For this purpose, Fidalgo et al. designed a device whereby selected droplets in a stream of oil could be induced to merge with an adjacent aqueous stream. If a droplet is selected to merge with the aqueous stream, an electric field is applied, inducing a DEP force on the droplet which causes it to move into the aqueous stream [27].

One particularly exciting application for droplet fusion technology is the ability to fuse liposomes or cells. Using a device with embedded electrodes, liposomes and prokaryotic cells were fused using a device which applied alternately AC and DC voltages. First, AC voltage is applied to align the liposomes or cells for fusion. This alignment is followed by the application of a DC voltage which fuses the liposomes or cells. Although this technique could find wide application in a wide variety of studies on cellular gene regulation, the fusion rate is relatively low at 75%, and the throughput of the technique is also very low, requiring 5 s alone to position liposomes close together, and another full second for the fusion event to occur [28].

Recently, electrofusion has also been used to combine reagents for the study of the kinetics of a biological reaction, such as the activity of the translated protein of the cotA laccase gene. Using electrodes on either side of the microfluidic channel, AC voltage was applied at a frequency of 30 kHz. Fusion events occurred at a rate

of 3,000 per second, and a high fusion efficiency of 90% was achieved (Fig. 2.5b). This high fusion rate provided by this active droplet fusion scheme allows a more precise study of the kinetics of the reaction, since more samples are produced with a shorter time step between them than could be achieved using a passive droplet fusion device [29].

Electrical fields may also be used to introduce reagent into passing droplets, as demonstrated by Abate et al. A series of fluid-dispensing channels were oriented perpendicular to a main microfluidic channel, and each dispensing channel contained a set of electrodes. By momentarily applying an electrical field across a set of electrodes, reagent could be dispensed from that channel into droplets in the main microfluidic channel without the use of valves. The application of an electrical field also destabilizes the interface between phases, leading to fusion of the passing droplet with the injected reagent. The amount of fluid injected into passing droplets may be tuned by adjusting the pressure in the dispensing channel as well as the velocity of the passing droplets. Using this device, researchers were able to add reagent selectively into passing droplets at a rate of 10,000 droplets per second [30].

2.3 Droplet Fission

The fusion or combining of the contents of different droplets has obvious importance for the execution of chemical reactions in droplet microfluidic systems; however, the ability to divide droplets is also a necessary operation for the execution of assays and the production of sample replicates. A simple way to introduce multiple sample types into a microfluidic device involves the consecutive aspiration of a large plug of fluid from a number of microtiter plate wells. In these devices, droplet fission is used to divide the plug into many smaller volume droplets, which allow individual droplets to be paired and mixed with different reagents [31], and also provide a smaller volume container, which allows for rapid mixing and reduces the reaction time in the droplet [32]. Droplet fission designs also provide the potential to increase the throughput of droplet production, and to digitize biological assays, increasing their sensitivity. Like droplet fusion, both passive, geometry-mediated droplet fission schemes have been developed, along with active droplet fission schemes, which employ the use of electricity or localized heating to split droplets.

2.3.1 Geometry-Mediated Splitting

Link et al. developed two simple methods to induce droplet fission, using only the geometry of the microchannels. In one device, a simple bifurcation of the main microfluidic channel is introduced in order to split droplets. Through experimentation, it was determined that droplet fission would occur at this bifurcation if the droplet is plug-like: that is, when the length of the droplet in the microchannel is

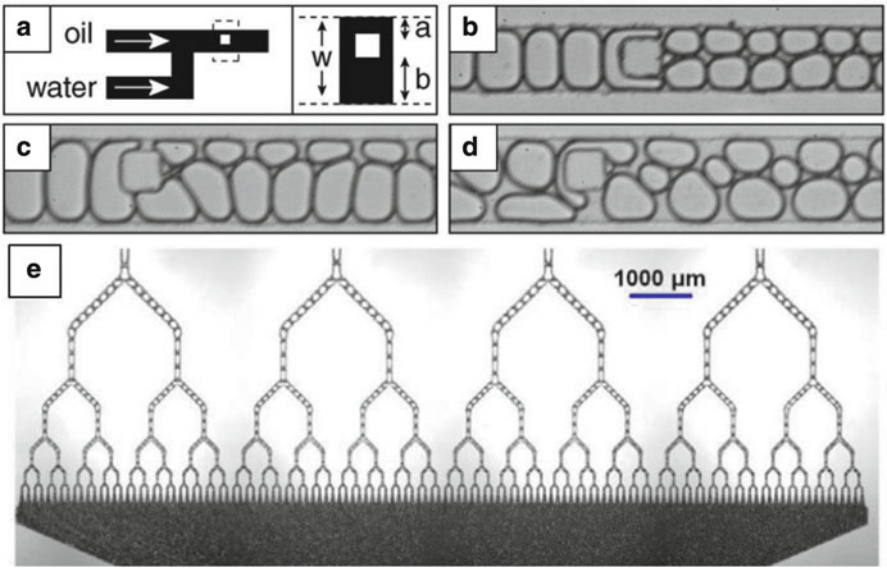

Fig. 2.6 (**a**–**d**) A large post structure in a microchannel packed with droplets mediates droplet splitting (**b**) symmetrically and (**c**, **d**) asymmetrically, depending on the placement of the post (Reproduced from Link et al. [33], Copyright 2004 by the American Physical Society, http://prl.aps.org/abstract/PRL/v92/i5/e054503). (**e**) Repeated fission is induced by 45° bifurcation junctions (Reproduced with permission from Hsieh, et al. [35])

greater than the circumference on the edge of the droplet. The droplet splits evenly if the resistances of the two daughter channels—downstream of the bifurcation—have the same fluidic resistance. Since fluidic resistance is proportional to microchannel length, according to the Hagen–Poiseuille equation, changing the length of one of the two daughter channels allows droplets to split unevenly. In this way, the volume ratio of the daughter droplets produced by the fission can be changed. Another design proposed by the group employed a large post near the middle of a microfluidic channel to induce droplet fission (Fig. 2.6a–d). By adjusting the position of this large post in the microchannel, the ratio of sizes of daughter droplets can be changed [33].

Building on this technology, another group used a repeating bifurcation structure to split a single parent droplet into 8 or 16 daughter droplets of nanoliter volumes. The bifurcation structure consists of a T-shaped junction, where the parent microfluidic channel meets the daughter microfluidic channels at an angle of 90°. This group observed asymmetric splitting of droplets despite symmetric channel designs, in devices containing consecutive bifurcations. It was hypothesized that asymmetric droplet breakup was due to a high surface tension pressure relative to the pressure drop in the microchannel. They determined that asymmetric splitting in bifurcating junctions can be minimized by keeping the surface tension low, for example, by adding surfactants to the system, or increasing the flow rate through the device [34].

Utilizing a different bifurcation design, a single droplet was split into 128 monodispersed droplets. In this design, the parent microfluidic channel splits into daughter channels at an angle of 45° forming a Y-shaped bifurcation junction (Fig. 2.6e). Hsieh et al. found that using a bifurcation channel angle of 45° reduced the asymmetric breakage of droplets, when compared to a design using an angle of 90°. In addition, the use of droplet fission for a new application—the production of a large number of PEG microspheres—was demonstrated [35].

Another approach to combating the problem of asymmetric droplet splitting involved the use of syringe pumps to withdraw fluid evenly from multiple outlets. In a device that split a single droplet into 8, fluid was withdrawn from 7 of the 8 outlets at 1/8 the rate of the inlet flow. The eighth outlet of the device was left open to remove any excess fluid from the device. This technique minimized the pressure differences between the outlet channels and as a result, the device produced droplets with a size coefficient of variation of 9.38% [31].

Finally, a liquid sample can be split into nanoliter volume plugs by feeding the liquid into a main channel that splits into several smaller, daughter channels. The liquid fills each smaller channel until it reaches a valve. Mielnik et al. used a hydrophobic valve to arrest the flow of fluid into each daughter channel, while a waste channel was placed downstream of the daughter channels to drain excess fluid [36]. Once filled, each daughter channel contains 335 nL of fluid that can be metered out of each channel for further processing. The series of daughter channels effectively splits a single sample plug into eight smaller plugs. Using this technique, a single nucleic acid sample from a patient was split into ten smaller plugs, and each plug could be screened against a different reagent, allowing simultaneous screening for multiple viruses [37].

2.3.2 Droplet Splitting Using Electrical Fields, Heat and Lasers

While the aforementioned devices have the ability to split a droplet reliably into daughter droplets, the fission product volumes are constrained by the fixed geometry of these devices. Thus, several devices employing electrical fields, heat, and lasers have been developed to achieve more control over the droplet fission process and allow for dynamic adjustment of the daughter droplet volumes. In addition, such methods have the ability to "switch" droplets completely to one outlet or another, in lieu of executing droplet fission, so that only selected droplets may be divided if necessary. These additional functionalities come at the cost of a more complex device, but may be desirable or necessary, depending on the system's application.

The throughput of droplet fission can be raised dramatically through the use of electric fields to split droplets. Link et al. used a device similar in geometry to the previously developed passive devices with bifurcating junctions, but added electrodes to charge and induce droplet splitting. Electrodes are placed under the two daughter channels after the bifurcation junction, and an electrical field

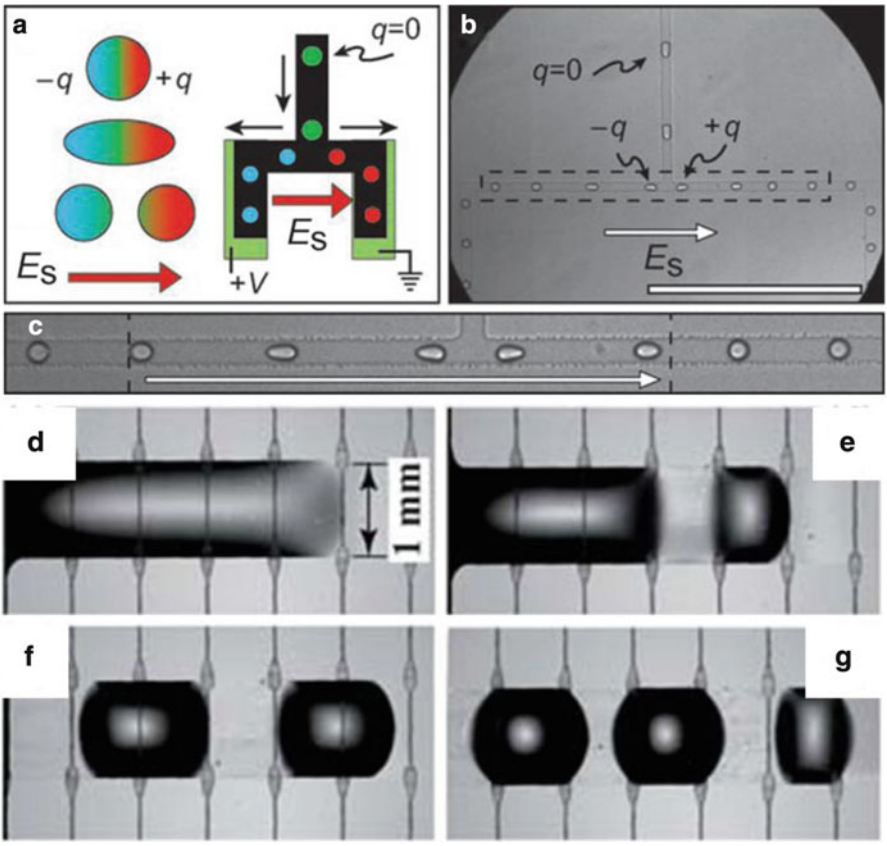

Fig. 2.7 (**a**–**c**) Droplet splitting induced by an electric field (Reproduced from Link et al. [24], Copyright Wiley-VCH Verlag GmbH & Co. KGaA. Reproduced with permission.). (**d**–**g**) Thermocapillary actuation, combined with chemical patterning of the device surface, was used to induce droplet fission through selective heating of the device surface (Reproduced from Darhuber et al. [41], by permission of The Royal Society of Chemistry, http://dx.doi.org/10.1039/b921759b)

is established between them. Uncharged droplets enter the bifurcation junction and the electrical field. The droplets polarize in the field and divide at the bifurcation (Fig. 2.7a–c). Simultaneously, opposite charges are induced on the two daughter droplets. Additionally, the authors noticed that at higher electrical fields, no droplet splitting occurred and the entire parent droplet was diverted to one of the daughter channels. Such a phenomenon could be used to remove erroneous droplets, or control the number of volume of daughter droplets produced in a bifurcating design. While this technique allows high throughput of up to 100,000 Hz, the use of electrical fields may preclude the use of this technique for some applications where reagents may be damaged by electrical fields [24].

Droplets may also be divided using a technique known as electrowetting-on-dielectric (EWOD). In this technique, electrical potentials are applied to specific points on a dielectric surface in order to induce movement of droplets by changing the wetting ability and contact angle of the fluid. Numerous groups have demonstrated the use of EWOD for droplet splitting [38, 39], however, the detailed mechanism and use of this technique is beyond the scope of this text.

One unique method for inducing droplet splitting involves the use of a laser. To use this technique, a microfluidic channel containing a post near the middle of the channel is used. In the absence of the laser, droplets split evenly around the post and form two daughter droplets of equal volume. However, when the laser is applied to one side of the post, the droplet is induced to split asymmetrically. Heat from the laser causes a local increase in the surface tension on the droplet, which prevents forward movement of the droplet past the laser [40]. The laser acts to block the droplet, and can affect the volume of the daughter droplets produced based on the length of time that the laser is applied in this position. As with the electrical fields, a droplet can be "switched" into a single channel instead of divided, by increasing the laser power used [16]. Although novel, this technique may not deliver as high a throughput as the technique in which electrical fields were used to split droplets, and may suffer from the same biocompatibility issue as well. However, the use of a laser provides even greater control over the volume of daughter droplets produced and may prove useful in devices where very precise manipulation of droplets is required.

Finally, microheaters integrated into microfluidic chips have been used to control droplet splitting and "switch" droplets to one of multiple downstream channels. In a technique similar to EWOD, Darhuber et al. used a technique called thermocapillary actuation, combined with chemical patterning of the surface of the device, to induce droplet splitting (Fig. 2.7d–g). The technique consists of stretching a fluid over a set of microheaters, activating the heaters sequentially to draw the fluid out, and then selectively turning off microheaters to induce splitting of the fluid [41]. Another group used an integrated microheater, positioned beneath one of the daughter channels (downstream of a bifurcation junction) to provide control over the volume of daughter droplets produced, as well as to allow switching of the droplet from one daughter channel to another. When the heater is turned on, a viscosity gradient is created and the viscosity of continuous phase in the heated daughter channel decreases. The fluidic resistance in the heated daughter channel is decreased owing to this decrease in viscosity. When a droplet reaches the bifurcation junction, a larger daughter droplet is produced in the heated daughter channel due to the difference in viscosity and interfacial tension between the two branches. By adjusting the temperature of the heater, different daughter droplet volumes can be produced. In addition, the use of an integrated microheater does not preclude the use of biological materials, since the heater works sufficiently for dividing droplets at 36°C. At slightly higher temperatures, the droplet does not split at the junction, but the entire droplet is carried or switched to the daughter branch containing the heater, providing a simple sorting mechanism [42].

2.4 Droplet Mixing

One advantage to digital or droplet microfluidics over other types of microfluidic platforms is that droplets serve to contain the contents of a reaction. Owing to their small volumes (in the nanoliter or picoliter range) droplet contents mix more rapidly than the contents of a microtiter plate well, due to the decrease in diffusion distance alone. The advantages of rapid mixing in droplet microfluidics systems have motivated new methods for directly observing the kinetics of reactions with millisecond resolution [43], and will allow for higher throughput testing for many different types of applications.

When the droplet diameter is greater than the width of the channel and the droplet forms a plug, mixing within the droplet is enhanced by the contact of the droplet with the device wall. This contact induces the formation of a double recirculating flow pattern within the droplet, which increases the rate of mixing due to advection. This double recirculation flow has been observed optically [44] and measured, using particle image velocimetry [45]. Although the rate of mixing in such small volumes is relatively fast, high-throughput applications may demand even faster mixing. Several microfluidic devices to further enhance the mixing speed in droplets are discussed below.

Mixing in droplets is aided by recirculating flow inside the droplets, which is induced by shear forces from either the continuous phase fluid or the channel wall. However, the recirculation flow alone limits the ability of droplets to mix, since a double recirculating flow pattern does not allow for rapid movement of droplet contents across the centerline of the droplet. To overcome this limitation, winding channels have been implemented into microfluidic devices. As a droplet enters a winding channel, the shear forces experienced on either side of a droplet become uneven, and the droplet contents undergo a phenomenon known as "stretching and folding," in which the recirculation patterns begin to cross the center of the droplet (Fig. 2.8a–c). The result of this folding action is that the distance over which diffusion must occur is shortened, thereby accelerating mixing of droplet contents. In addition, increasing the velocity of the droplets exaggerates the difference in shear force on either side of the droplet, and further increases the rate of mixing within the droplet [44, 45]. A mixing time of 2 ms was achieved using such a device. Another group studied the effect of the angle of the winding channels on droplet mixing, and concluded that a 45° winding channel provided faster mixing than either 90 or 135° bends [46]. The theory of mixing in droplets using these techniques is developed further elsewhere [47, 48].

To improve mixing further, several research groups have added bumps onto the edges of the winding channel design [49, 50]. This feature further enhances the asymmetry of shear forces on either side of the droplet as it traverses the winding channels, which aids mixing (Fig. 2.8d). In this design, one research group observed sticking of protein solution from droplets on the microchannel walls, but this problem was addressed by selecting a perfluorinated chemical as the continuous phase around the droplets [50]. Such a device was used for the detection of DNA in

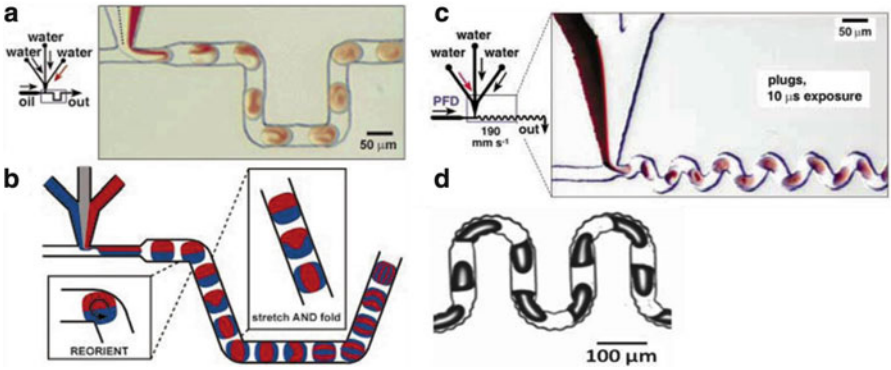

Fig. 2.8 (**a**–**c**) Mixing within droplets is enhanced by winding channels, which fold the fluid and decrease the diffusion distance within the droplet (**a**, **b**, Reprinted with permission from reference [47], Copyright 2003, American Institute of Physics. (**c**) Reprinted from reference [44], Copyright Wiley-VCH Verlag GmbH & Co. KGaA. Reproduced with permission). (**d**) Further agitation within droplets is induced by adding bumps to the edges of the winding channels (Reproduced from Fig. 2.3b of Hsieh et al. [49], with kind permission from Springer Science + Business Media BV)

droplets using molecular beacons, and allowed for monitoring of the hybridization reaction in real time [49].

An alternative to the geometry-mediated methods of droplet mixing presented above is active mixing in droplet aided by lasers. By pulsing two lasers at high frequencies in a time-varying pattern, asymmetric mixing could be induced in droplets. The laser locally heats fluid inside the droplet and induces flow toward this heated spot. While novel, this technique may have limited applicability to microfluidic systems requiring high throughput, since droplets must be stopped in order for the mixing to occur. Hence, the maximum processing rate of droplets for mixing has been 1 per second. The advantage is that such a technique offers control over the duration and intensity of mixing [51].

2.5 Droplet Sorting

2.5.1 Passive (Hydrodynamic)

The simplest droplet sorting techniques require no detection or switching mechanisms, but instead rely on creative device geometry that allows the separation of droplets by size. By simply creating a bifurcating junction geometry in which the daughter channels had different widths, droplets were induced to sort into one of the channels (Fig. 2.9). For droplets within a certain size range, all of the droplets in a stream will sort into the daughter channel with a smaller width, since the shear is higher in this direction than the channel with a larger width [4]. A similar geometry

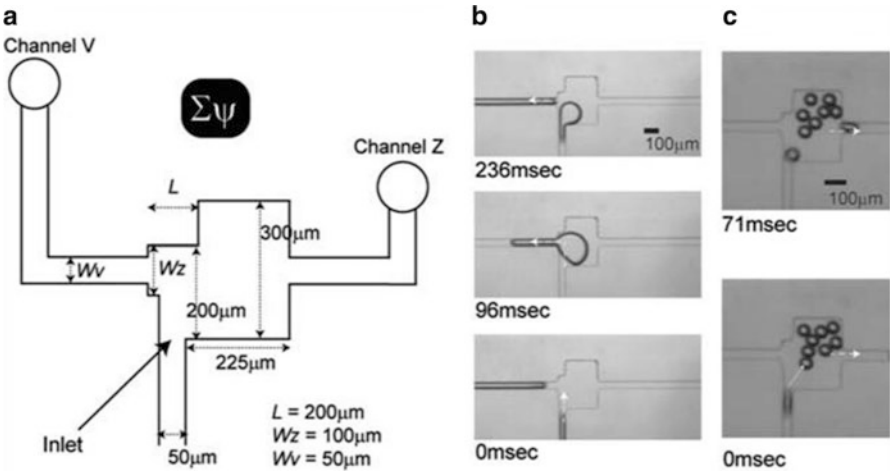

Fig. 2.9 (**a**) Schematic of a microfluidic device for passive sorting of droplets by size. (**b**) *Large droplets* sort to the left due to higher shear on this side while (**c**) *smaller droplets* sort to the *right* due to a lower fluidic resistance in the shorter channel (Reproduced from Fig. 2.4a–c of Hsieh et al. [53], with kind permission from Springer Science + Business Media BV)

to exploit the streaming patterns of differently sized droplets was used to remove droplets much smaller than the desired size (termed "satellite droplets") [52]. Building on the idea that large droplets could be diverted to a stream with higher shear, an asymmetrical bifurcating junction was created to separate large and small droplets based on two principles. The daughter channels from the bifurcating junction were designed with different widths as well as different channel lengths, to induce sorting based on both the shear at the bifurcating junction as well as the flow rate difference created by the difference in resistance due to channel length. While larger droplets were induced to sort into the narrower daughter channel, due to higher shear at that point, smaller droplets were sorted into the other channel [53]. Although simple to implement, the limitations of this technology are due in part to its fixed geometry. Only a certain range of droplet sizes and speeds are amenable to sorting using a given device with fixed dimensions. However, given a stable method of droplet generation, the size variation in produced droplets should not preclude the use of such a device to obtain monodispersed droplets after sorting.

One group used the principle of hydrodynamic sorting to sort droplets containing cells from those without cells. A hydrodynamic, flow focusing geometry was used to generate droplets from a stream containing cells in solution. Since the droplet generator was operated in the jetting regime, the droplets generated from the cell solution were normally small. However, when a cell approached the droplet generation junction, jetting was disrupted, and a larger than normal droplet was created. By applying uneven flow rates of continuous phase on either side of the cell solution phase, smaller droplets were directed toward the channel wall while larger droplets containing cells remained in the center of the channel. Then, the droplets containing cells were separated from those without cells downstream by dividing

the main channel into several outlet channels. Such a device was able to process up to 160 cells per second, and the sorted droplet population was 99% pure. The device was later used to separate rare cells from whole blood, since T-lymphocytes, indicative of disease, are larger than red blood cells [54]. Hydrodynamic flow has also been combined with gravity-induced sedimentation in a device for the separation of polydispersed perfluorocarbon droplets into more monodispersed populations [55].

2.5.2 Magnetic

Just as magnetic particles have been used to tag and separate cell populations of interest, this technique can also be used to separate droplets containing magnetic particles from those which do not contain the particles. In 2004, a research group showed that such technology could be used to move aqueous droplets in air over a surface using a magnetic field. The aqueous droplets contained iron oxide nanoparticles, encased in silicon particles, which enabled control over the direction of the droplets [56]. Although efficient, the throughput of this approach was limited. Several years later, another group incorporated this concept into a microfluidic device to enable continuous sorting of droplets in this manner. Superparamagnetic magnetite nanoparticles were produced and incorporated into droplets, which could then be deflected into different channels by the targeted application of a perpendicular magnetic field (Fig. 2.10). To change the destination of the droplets and switch them to different outlets, the magnets were moved to different locations parallel to the main channel flow. This technique allowed separation of droplets at a rate of 10 per second. The use of such small magnetic particles ensures that they retain no magnetic "memory", reducing the possibility of aggregation of the particles, and increasing their biocompatibility. Indeed, similar particles have been used safely in several types of biological assays [57].

2.5.3 Dielectrophoresis

Just as dielectrophoresis has been used to facilitate the fission of droplets, it has also been used to sort droplets for further processing. The application of a nonuniform electric field exerts a force on droplets that can be used to direct droplets into one of several outlets of a device. In a device by Ahn et al., droplets flowed into the lower resistance outlet in the absence of DEP force. With the application of this force, however, the droplets were directed to a higher resistance outlet of the device (Fig. 2.11a–d). Sorting could occur at rates of up to 4,000 droplets per second using this approach [58]. For more precise manipulation of droplets, an array of 128×256 individually addressable electrodes was designed and used to move droplets. Droplets could be moved over the surface of this array at speeds of up to

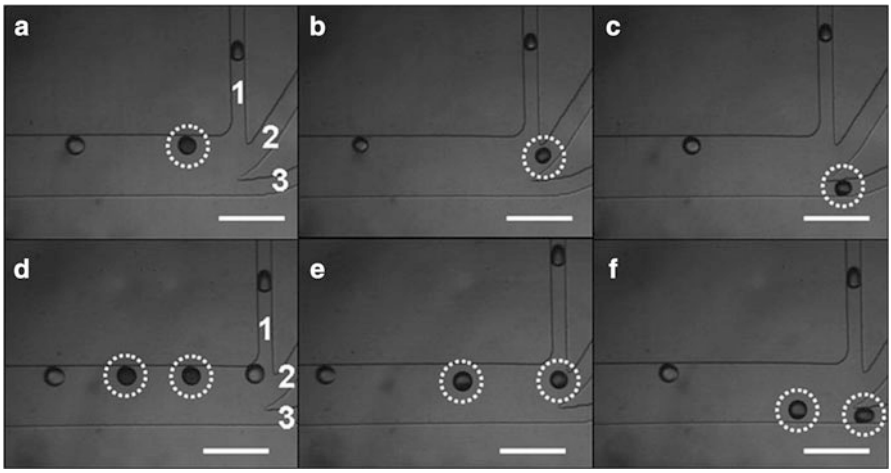

Fig. 2.10 (**a–c**) Droplets loaded with magnetic nanoparticles are sorted into different outlet channels by positioning a magnet at different locations near the sorting region. (**d–f**) Consecutive droplets containing magnetic nanoparticles can be deflected in similar to the single droplets in panes (**a–c**) (Reproduced from Zhang et al. [57], by permission of The Royal Society of Chemistry, http://dx.doi.org/10.1039/b906229g)

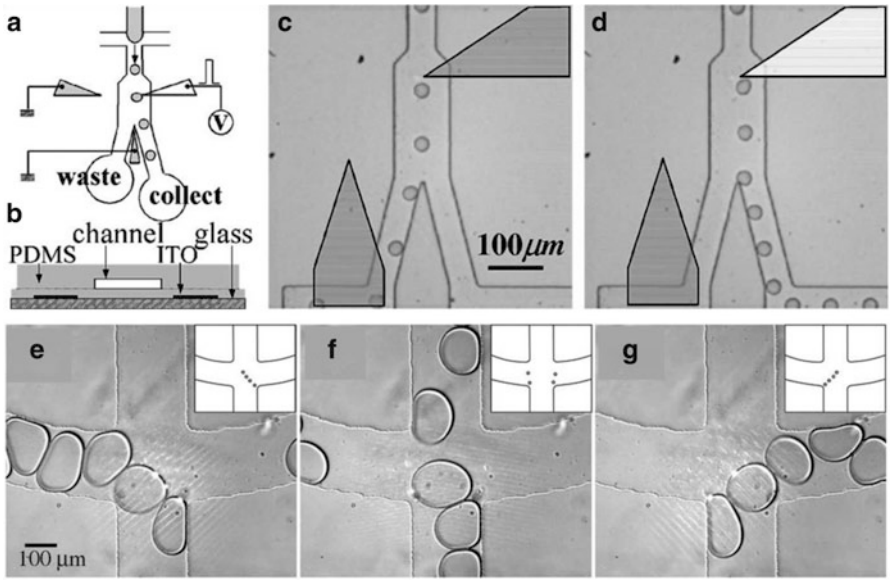

Fig. 2.11 (**a–d**) Droplets are sorted by dielectrophoretic force, imposed by application of potential across the two electrodes (Reprinted with permission from Ahn et al. [58], Copyright 2006, American Institute of Physics). (**e–g**) Patterned laser light is used to deflect droplets toward the desired outlet (Reprinted with permission from Cordero et al. [65], Copyright 2008, American Institute of Physics)

30 μm per second by selectively activating electrodes. A lubrication layer of oil separate from the continuous phase surrounding the droplets facilitates movement of the droplets. This layer also prevents contamination between droplets during sorting. In addition, the application of DEP is made biocompatible by the application of an AC field, which is not as harmful to cells as DC fields [59, 60]. Several other devices employing dielectrophoresis with different electrode designs have been used for the separation of cells or beads [61–63].

In much the same manner as fluorescent cells can be sorted by a technique known as fluorescence-activated cell sorting (FACS), droplets containing fluorescent contents have been separated using dielectrophoresis. Such a device, termed a fluorescence-activated droplet sorter (FADS) detects passing fluorescent droplets and applies an AC field to direct fluorescent droplets to an alternate outlet channel. In the absence of the AC field, droplets are carried to the lower resistance outlet by default. A device by Baret et al. was able to achieve a sorting speed of up to 2,000 droplets per second, with a false sorting rate of 1 in 10,000 droplets, under optimal conditions for speed and accuracy, respectively. The FADS device was used to sort cells encapsulated in the droplets, and successfully distinguished between droplets with an active enzyme (which fluoresced) and those without the active enzyme (which did not fluoresce) [64].

2.5.4 Optical

For precise manipulation of droplets, focused laser light can also be used. In a device fabricated with a post structure in the middle of a microfluidic channel, a laser can be focused to one side of the post to prevent the droplet from passing the post on that side. After a droplet passes the post on the other side, hydrodynamic flow will direct the droplet into the corresponding branch of a bifurcation that follows the post structure in the channel. In this way, by positioning the laser on either side of the post, droplets can be sorted into one of two daughter channels. Although not addressed directly in the paper, the comparatively low throughput of the system as well as the biocompatibility of a laser could be issues [40]. To sort droplets into more than two daughter channels, a pattern of laser light spots has been used to direct droplets into one of three outlets (Fig. 2.11e–g). The sorting speed using a laser light pattern was between 30 and 60 droplets per second [65]. In a more complex approach, Kovac et al. enabled phenotype sorting of cells using an infrared laser—however, the technique could presumably be applied to sorting of cells encapsulated in droplets. Cells were first allowed to settle onto an array inside a microfluidic device, and cells of interest were identified manually by observation. Selected cells were lifted from the array using an infrared laser, into the flow through the device, and collected at the outlet. This approach avoids the manufacture and control issues associated with making an array of individually addressable electrodes. In addition, a low divergence laser beam was used in this method, which provided a large enough working distance to move the cells to the

desired area, while operating at a lower intensity than optical tweezers to avoid damaging the cells. One disadvantage to this approach is its low throughput—between 18 and 45 s were needed to sort a single cell [66]. Despite a lower throughput, these approaches offer a greater degree of precision in the sorting of droplets and may prove valuable for an application where the purity of the sorted population must be very high. Several other optical sorting approaches, including the use of optical tweezers and handles have been used for sorting particles or cells, and the technology could potentially be applied to droplet sorting as well [67].

2.5.5 Other

A handful of other techniques have been used to sort droplets, using electrical phenomena, fluid pressure induced by mechanical actuation, heat, surface acoustic waves (SAW), and others. An electric field imposed at a bifurcating junction has been shown in a device to induce sorting of droplets into one daughter channel or the other, depending on the direction in which the field is applied [24]. In another technique employing use of an electric field, selected droplets could be pushed into a separate stream by applying an electric field. Once selected, droplets were pushed into an aqueous stream flowing adjacent to the continuous phase flow, and the sorted aqueous droplets were absorbed into the continuous aqueous flow stream. Such a technique could be useful for downstream processing and enable droplets to be characterized using techniques that rely on analog, rather than digital flow, such as chromatography [27].

A unique approach to droplet sorting induced by mechanical actuation is the use of piezoelectric materials to produce a cross flow across the main channel of a microfluidic device containing droplets. To sort a droplet or train of droplets, a piezoelectric material is actuated, which depresses a PDMS membrane above a reservoir of continuous phase fluid. Depression of this membrane induces a flow of the continuous phase fluid in a channel perpendicular to the main channel flow. When streamlines from this side channel occupy at least 50% of the cross-sectional area of the main fluidic channel, droplets are diverted into a secondary outlet. Depending on the type of detector used to identify droplets for sorting, droplets could be sorted based on their volume or fluorescence [68]. Using similar device geometry, another group enabled droplet sorting by inducing electrokinetic crossflow in a device. In contrast to the device enabling crossflow using a piezoelectric actuator, fluid movement can be induced instantaneously upon activation of the electrodes which induce the electrokinetic flow. The disadvantage to this approach is that electrokinetic flow can only occur in a continuous phase where ions are present—thus the technique would not work well in a system where the droplets comprise the aqueous phase and the continuous phase is hydrophobic oil. Nevertheless, this sorting approach may be useful for some applications and was demonstrated successfully for the sorting of fluorescent beads from a stream of water [69], as well as cell sorting [70]. Franke et al. also demonstrated success in

droplet sorting using a piezoelectric actuator. In the absence of actuation, droplets in the main channel sort into the device outlet with lower resistance. For sorting, the piezoelectric material is actuated, which creates SAW that induces acoustic streaming to move droplets in the main channel. In this manner, droplets may be sorted into the higher resistance outlet, simply by actuating the piezoelectric material [71].

As mentioned earlier, passive sorting designs employ asymmetric bifurcation junction geometries to induce sorting based on flow rates and hydrodynamic resistance. Using a similar approach, Yap et al. induced droplet sorting by designing a device in which the fluidic resistance of the bifurcation junction daughter channels could be changed. A microheater, integrated into the microfluidic device, allowed switching of droplets into the higher resistance daughter channel following a bifurcation by heating the fluid in that channel. This heat reduced the hydrodynamic resistance in that daughter channel, which caused droplets to sort into the heated channel [42].

2.6 Conclusion

Although many varied and creative strategies have been devised for the manipulation of droplets—including the combination, separation, mixing, and sorting of these droplets—the potential for integration of these techniques into a complete processing device is what would eventually revolutionize the field and change the paradigm of how biological and chemical assays are carried out. Attempts to combine several droplet manipulation steps on chip have been successful for the execution of biological assays, but these techniques often depend on off-chip equipment for sample preparation or droplet storage [29]. The transition of microfluidic devices from a pursuit largely backed by academic labs to one endorsed and supported by industry will rely on the continued integration of multiple droplet processing steps in a single device. With the continued development of integrated microfluidic devices for droplet processing will come a reduction in processing time due to automation, a decrease in contamination potential by reducing manual handling steps, and a reduction of the cost of assays and reactions, due to a minimal consumption of all reagents involved.

References

1. Bremond N, Thiam A, Bibette J (2008) Decompressing emulsion droplets favors coalescence. Phys Rev Lett 100:24501
2. Bibette J, Calderon F, Poulin P (1999) Emulsions: basic principles. Rep Prog Phys 62:969–1033
3. Hung L, Choi K, Tseng W, Tan Y, Shea K, Lee A (2006) Alternating droplet generation and controlled dynamic droplet fusion in microfluidic device for CdS nanoparticle synthesis. Lab Chip 6:174–178

4. Tan Y, Fisher J, Lee A, Cristini V, Lee A (2004) Design of microfluidic channel geometries for the control of droplet volume, chemical concentration, and sorting. Lab Chip 4:292–298
5. Liu K, Ding H, Chen Y, Zhao X (2007) Droplet-based synthetic method using microflow focusing and droplet fusion. Microfluidics Nanofluidics 3:239–243
6. Sivasamy J, Chim Y, Wong T, Nguyen N, Yobas L (2010) Reliable addition of reagents into microfluidic droplets. Microfluid Nanofluidics 8:409–416
7. Köhler J, Henkel T, Grodrian A, Kirner T, Roth M, Martin K, Metze J (2004) Digital reaction technology by micro segmented flow— components, concepts and applications. Chem Eng J 101:201–216
8. Tan Y, Ho Y, Lee A (2007) Droplet coalescence by geometrically mediated flow in microfluidic channels. Microfluid Nanofluidics 3:495–499
9. Um E, Park J (2009) A microfluidic abacus channel for controlling the addition of droplets. Lab Chip 9:207–212
10. Niu X, Gulati S, Edel J, deMello A (2008) Pillar-induced droplet merging in microfluidic circuits. Lab Chip 8:1837–1841
11. Simon MG, Lin R, Fisher JS, Lee AP (2012) A Laplace pressure based microfluidic trap for passive droplet trapping and controlled release. Biomicrofluidics 6(2):024103
12. Lin B, Su Y (2008) On-demand liquid-in-liquid droplet metering and fusion utilizing pneumatically actuated membrane valves. J Micromech Microeng 18:115005
13. Jin B, Kim Y, Lee Y, Yoo J (2010) Droplet merging in a straight microchannel using droplet size or viscosity difference. J Micromech Microeng 20:035003
14. Mazutis L, Baret J, Griffiths A (2009) A fast and efficient microfluidic system for highly selective one-to-one droplet fusion. Lab Chip 9:2665–2672
15. Fidalgo L, Abell C, Huck W (2007) Surface-induced droplet fusion in microfluidic devices. Lab Chip 7:984
16. Baroud C, Vincent M, Delville J (2007) An optical toolbox for total control of droplet microfluidics. Lab Chip 7:1029–1033
17. Shestopalov I, Tice J, Ismagilov R (2004) Multi-step synthesis of nanoparticles performed on millisecond time scale in a microfluidic droplet-based system. Lab Chip 4:316–321
18. Li L, Boedicker J, Ismagilov R (2007) Using a multijunction microfluidic device to inject substrate into an array of preformed plugs without cross-contamination: comparing theory and experiments. Anal Chem 79:2756–2761
19. Zagnoni M, Cooper J (2009) On-chip electrocoalescence of microdroplets as a function of voltage, frequency and droplet size. Lab Chip 9:2652–2658
20. Wang W, Yang C, Li C (2009) Efficient on-demand compound droplet formation: from microfluidics to microdroplets as miniaturized laboratories. Small 5:1149–1152
21. Tan W, Takeuchi S (2006) Timing controllable electrofusion device for aqueous droplet-based microreactors. Lab Chip 6:757–763
22. Priest C, Herminghaus S, Seemann R (2006) Controlled electrocoalescence in microfluidics: targeting a single lamella. Appl Phys Lett 89:134101
23. Wang W, Yang C, Li C (2009) On-demand microfluidic droplet trapping and fusion for on-chip static droplet assays. Lab Chip 9:1504–1506
24. Link D, Grasland Mongrain E, Duri A, Sarrazin F, Cheng Z, Cristobal G, Marquez M, Weitz D (2006) Electric control of droplets in microfluidic devices. Angew Chem Int Ed Engl 118:2618–2622
25. Ahn K, Agresti J, Chong H, Marquez M, Weitz D (2006) Electrocoalescence of drops synchronized by size-dependent flow in microfluidic channels. Appl Phys Lett 88:264105
26. Schwartz J, Vykoukal J, Gascoyne P (2004) Droplet-based chemistry on a programmable micro-chip. Lab Chip 4:11–17
27. Fidalgo L, Whyte G, Bratton D, Kaminski C, Abell C, Huck W (2008) From microdroplets to microfluidics: selective emulsion separation in microfluidic devices. Angew Chem Int Ed Engl 120:2072–2075

28. Tresset G, Takeuchi S (2004) A microfluidic device for electrofusion of biological vesicles. Biomed Microdevices 6:213–218
29. Mazutis L, Baret J, Treacy P, Skhiri Y, Araghi A, Ryckelynck M, Taly V, Griffiths A (2009) Multi-step microfluidic droplet processing: kinetic analysis of an in vitro translated enzyme. Lab Chip 9:2902–2908
30. Abate A, Hung T, Mary P, Agresti J, Weitz D (2010) High-throughput injection with microfluidics using picoinjectors. Proc Natl Acad Sci U S A 107:19163
31. Clausell-Tormos J, Griffiths A, Merten C (2010) An automated two-phase microfluidic system for kinetic analyses and the screening of compound libraries. Lab Chip 10:1302–1307
32. Hsieh A, Hori N, Massoudi R, Pan P, Sasaki H, Lin Y, Lee A (2009) Nonviral gene vector formation in monodispersed picolitre incubator for consistent gene delivery. Lab Chip 9:2638–2643
33. Link D, Anna S, Weitz D, Stone H (2004) Geometrically mediated breakup of drops in microfluidic devices. Phys Rev Lett 92:54503
34. Adamson D, Mustafi D, Zhang J, Zheng B, Ismagilov R (2006) Production of arrays of chemically distinct nanolitre plugs via repeated splitting in microfluidic devices. Lab Chip 6:1178–1186
35. Hsieh AT-H, Pan J-H, Pinasco PG, Fisher JS, Hung LH, Lee AP (2007) Polymer microsphere mass production using 128-channel digital fluidic chip. In: The Eleventh international conference on miniaturized systems for chemistry and life sciences (uTAS 2007), Paris, France, pp. 346–348
36. Mielnik MM, Voitel J, Solli LA, Furuberg L (2007) Sample metering and parallel liquid plug actuation for multiple biochemical assays. In: Eleventh international conference on miniaturized systems for chemistry and life sciences, Paris, France, pp. 1513–1515
37. Furuberg L, Mielnik M, Gulliksen A, Solli L, Johansen I, Voitel J, Baier T, Riegger L, Karlsen F (2008) RNA amplification chip with parallel microchannels and droplet positioning using capillary valves. Microsys Technol 14:673–681
38. Cho S, Moon H, Kim C (2003) Creating, transporting, cutting, and merging liquid droplets by electrowetting-based actuation for digital microfluidic circuits. J Microelectromech Syst 12:70–80
39. Fan S, Hsieh T, Lin D (2009) General digital microfluidic platform manipulating dielectric and conductive droplets by dielectrophoresis and electrowetting. Lab Chip 9:1236–1242
40. Baroud C, Delville J, Gallaire F, Wunenburger R (2007) Thermocapillary valve for droplet production and sorting. Phys Rev E Stat Nonlin Soft Matter Phys 75:46302
41. Darhuber AA, Valentino JP, Troian SM (2010) Planar digital nanoliter dispensing system based on thermocapillary actuation. Lab Chip 10:1061–1071
42. Yap Y, Tan S, Nguyen N, Murshed S, Wong T, Yobas L (2009) Thermally mediated control of liquid microdroplets at a bifurcation. J Phys D: Appl Phys 42:065503
43. Song H, Ismagilov R (2003) Millisecond kinetics on a microfluidic chip using nanoliters of reagents. J Am Chem Soc 125:14613–14619
44. Song H, Tice J, Ismagilov R (2003) A microfluidic system for controlling reaction networks in time. Angew Chem Int Ed 42:768–772
45. Wang C, Nguyen N, Wong T (2007) Optical measurement of flow field and concentration field inside a moving nanoliter droplet. Sensors Actuators A: Physical 133:317–322
46. Sarrazin F, Prat L, Di Miceli N, Cristobal G, Link D, Weitz D (2007) Mixing characterization inside microdroplets engineered on a microcoalescer. Chem Eng Sci 62:1042–1048
47. Song H, Bringer M, Tice J, Gerdts C, Ismagilov R (2003) Experimental test of scaling of mixing by chaotic advection in droplets moving through microfluidic channels. Appl Phys Lett 83:4664–4666
48. Bringer M, Gerdts C, Song H, Tice J, Ismagilov R (2004) Microfluidic systems for chemical kinetics that rely on chaotic mixing in droplets. Philos Transact A Math Phys Eng Sci 362:1087
49. Hsieh A, Pan P, Lee A (2009) Rapid label-free DNA analysis in picoliter microfluidic droplets using FRET probes. Microfluid Nanofluidics 6:391–401

50. Liau A, Karnik R, Majumdar A, Cate J (2005) Mixing crowded biological solutions in milliseconds. Anal Chem 77:7618–7625
51. Cordero M, Rolfsnes H, Burnham D, Campbell P, McGloin D, Baroud C (2009) Mixing via thermocapillary generation of flow patterns inside a microfluidic drop. New J Phys 11:075033
52. Tan Y, Lee A (2005) Microfluidic separation of satellite droplets as the basis of a monodispersed micron and submicron emulsification system. Lab Chip 5:1178–1183
53. Tan Y, Ho Y, Lee A (2008) Microfluidic sorting of droplets by size. Microfluid Nanofluidics 4:343–348
54. Chabert M, Viovy J (2008) Microfluidic high-throughput encapsulation and hydrodynamic self-sorting of single cells. Proc Natl Acad Sci 105:3191
55. Huh D, Bahng J, Ling Y, Wei H, Kripfgans O, Fowlkes J, Grotberg J, Takayama S (2007) Gravity-driven microfluidic particle sorting device with hydrodynamic separation amplification. Anal Chem 79:1369–1376
56. Dorvee J, Derfus A, Bhatia S, Sailor M (2004) Manipulation of liquid droplets using amphiphilic, magnetic one-dimensional photonic crystal chaperones. Nat Mater 3:896–899
57. Zhang K, Liang Q, Ma S, Mu X, Hu P, Wang Y, Luo G (2009) On-chip manipulation of continuous picoliter-volume superparamagnetic droplets using a magnetic force. Lab Chip 9:2992–2999
58. Ahn K, Kerbage C, Hunt T, Westervelt R, Link D, Weitz D (2006) Dielectrophoretic manipulation of drops for high-speed microfluidic sorting devices. Appl Phys Lett 88:024104
59. Hunt T, Lee H, Westervelt R (2004) Addressable micropost array for the dielectrophoretic manipulation of particles in fluid. Appl Phys Lett 85:6421–6423
60. Hunt T, Issadore D, Westervelt R (2008) Integrated circuit/microfluidic chip to programmably trap and move cells and droplets with dielectrophoresis. Lab Chip 8:81–87
61. Choi S, Park J (2005) Microfluidic system for dielectrophoretic separation based on a trapezoidal electrode array. Lab Chip 5:1161–1167
62. Wang L, Flanagan L, Jeon N, Monuki E, Lee A (2007) Dielectrophoresis switching with vertical sidewall electrodes for microfluidic flow cytometry. Lab Chip 7:1114–1120
63. Li Y, Dalton C, Crabtree H, Nilsson G, Kaler K (2007) Continuous dielectrophoretic cell separation microfluidic device. Lab Chip 7:239–248
64. Baret J, Miller O, Taly V, Ryckelynck M, El-Harrak A, Frenz L, Rick C, Samuels M, Hutchison J, Agresti J (2009) Fluorescence-activated droplet sorting (FADS): efficient microfluidic cell sorting based on enzymatic activity. Lab Chip 9:1850–1858
65. Cordero M, Burnham D, Baroud C, McGloin D (2008) Thermocapillary manipulation of droplets using holographic beam shaping: Microfluidic pin ball. Appl Phys Lett 93:034107
66. Kovac J, Voldman J (2007) Intuitive, image-based cell sorting using optofluidic cell sorting. Anal Chem 79:9321–9330
67. Ozkan M, Wang M, Ozkan C, Flynn R, Esener S (2003) Optical manipulation of objects and biological cells in microfluidic devices. Biomed Microdevices 5:61–67
68. Shemesh J, Bransky A, Khoury M, Levenberg S (2010) Advanced microfluidic droplet manipulation based on piezoelectric actuation. Biomed Microdevices 12(5):907–914
69. Dittrich P, Schwille P (2003) An integrated microfluidic system for reaction, high-sensitivity detection, and sorting of fluorescent cells and particles. Anal Chem 75:5767–5774
70. Fu A, Chou H, Spence C, Arnold F, Quake S (2002) An integrated microfabricated cell sorter. Anal Chem 74:2451–2457
71. Franke T, Abate A, Weitz D, Wixforth A (2009) Surface acoustic wave (SAW) directed droplet flow in microfluidics for PDMS devices. Lab Chip 9:2625–2627

Chapter 3
Active Control of Droplet Formation Process in Microfluidics

Nam-Trung Nguyen and Say-Hwa Tan

3.1 Introduction

Droplet-based microfluidics involves the generation and manipulation of droplets. Highly monodispersed droplets of diameter ranging from nanometers to micrometers can be produced at a frequency of up to 20,000 per second [1]. The compartmentalization of liquid within a droplet is useful as the droplet interface acts as a barrier confining its content thus limiting contamination. Droplets can be transported, mixed, and analyzed [2]. The high surface area to volume ratio in microscale results in improved heat and mass transfer. Droplet-based microfluidics has been used in a number of biological and chemical applications such as polymerase chain reaction [3–5], protein crystallization [6], DNA/blood analysis [7, 8], enzyme kinetics studies [9], and synthesizing uniform nanoparticles [10].

Droplets are formed in a system of immiscible liquids such as water and oil. In general, both water in oil (W/O) and oil in water (O/W) droplets can be formed [13]. The determination of which liquid is inside the droplet depends on the wetting property of the channel wall. On the one hand, if the aqueous liquid is used as the dispersed phase and oil as the continuous phase in a channel with hydrophobic walls, water in oil (W/O) droplets are formed as oil can wet the channel walls. On the other hand, if the channel wall is hydrophilic, oil in water (O/W) droplets are formed when aqueous liquid and oil work as the continuous phase and the dispersed phase, respectively. Multiphase emulsions such as water-in-oil-in-water system can also be formed using encapsulation in a two-step process [11, 12]. The surface wettability can be altered using different methods. For instance, SDS can be added into water when used as the continuous fluid to make partially hydrophilic polymethylmethacrylate (PMMA) hydrophobic [20]. The surface properties of polydimethylsiloxane (PDMS) can be modified using different methods such as

N.-T. Nguyen (✉) • S.-H. Tan
Nanyang Technological University, 50 Nanyang Avenue, 639798, Singapore
e-mail: mntnguyen@ntu.edu.sg

P. Day et al. (eds.), *Microdroplet Technology: Principles and Emerging Applications in Biology and Chemistry*, Integrated Analytical Systems,
DOI 10.1007/978-1-4614-3265-4_3,

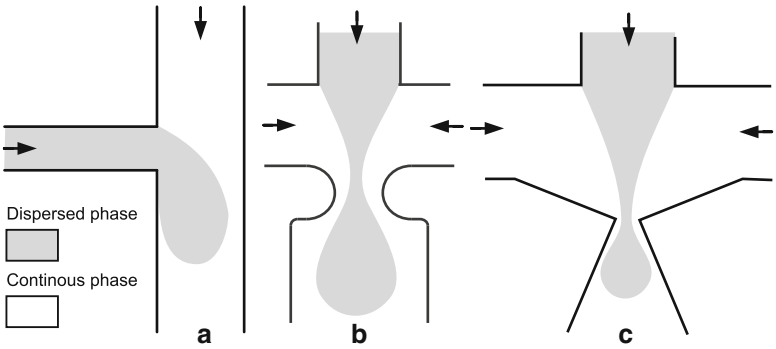

Fig. 3.1 Two main droplet formation configurations: (**a**) T-Junction; (**b**) cross junction; and (**c**) cross junction with diffuser for improved velocity gradient

coating of the inner walls [14], attachment of active groups [15], plasma oxidation [16], and thermal aging [17].

In droplet-based microfluidics, droplets are formed mainly by hydrodynamic means, which are categorized here as passive methods. A passive formation process relies on the flow field to deform the interface and to promote the growth of interfacial instabilities. Passive droplet formation can be achieved with a T-junction (Fig. 3.1a) and cross-junction (Fig. 3.1b). Further design optimization such as using a nozzle structure at the junction can improve the breakup process of the droplets, Fig. 3.1c. In a passive formation process, two immiscible liquids are driven into separate microchannels by external pumps or pressure sources. Either the volumetric flow rates or the pressures are fixed. The immiscible liquids meet at the junction and the dispersed phase liquid extends to form a "finger," while the continuous phase liquid acts to deform the interface. A droplet is formed when the dispersed phase "finger" is pinched off due to the instability of the interface. The geometry and depth of the microchannels, flow rates, applied pressures, and fluid properties determine the local flow field which act to deform the interface and thus the formation process.

As a variety of physical phenomena occur in microfluidic devices, their relative significance is judged against competing phenomena by dimensionless numbers. Dimensionless numbers expressing the ratio of these phenomena can represent the operation regimes in the space of fluidic parameters [18]. For instance, the Reynolds number indicates the relative importance of inertia compared to viscous stress:

$$Re = \frac{\text{Inertial force}}{\text{Viscous force}} = \frac{\rho U D_{\text{h}}}{\mu}, \tag{3.1}$$

where D_{h} is the hydraulic diameter of the microchannel, ρ and μ are the density and the dynamic viscosity of the fluid, and U is the mean flow velocity. If the

microchannel has a rectangular cross section of width w and height h, the Reynolds number is calculated as:

$$Re = \frac{2\rho Q}{\mu(w+h)}, \tag{3.2}$$

where Q is the volumetric flow rate.

In a droplet formation process, capillary number is used to describe the ratio between viscous stress and surface tension:

$$\mathrm{Ca} = \frac{\text{Viscous stress}}{\text{Surface tension}} = \frac{\mu_c U_c}{\sigma}, \tag{3.3}$$

where μ_c is the dynamic viscosity of the continuous phase and σ is the interfacial tension between the immiscible liquids. For the case of a rectangular channel, the capillary number is calculated as $\mathrm{Ca} = \mu_c \mathrm{Q}/(\sigma \mathrm{wh})$.

The T-junction is probably one of the most common microfluidic configuration for generating droplets. This configuration is popular as droplets can be formed easily at high monodispersity over a wide range of flow rates and at a relatively high frequency. The dispersity is defined as the standard deviation of the droplet size relative to the average droplet size. Thorsen et al. [22] demonstrated stable droplet formation in microfluidic devices using pressure controlled flows. The devices were fabricated using acrylated urethane molded from a silicon master. The device consists of a tapered channel at the junction where water and oil/surfactant mixture meet. The tapered channel increases the local shear stress gradient and promotes the formation of the droplets. In their experiment, Thorsen et al. demonstrated that stable droplet formation is achieved when the imposed pressure of both water and oil/surfactant mixture are comparable. The size of the water droplet increases when the driving pressure for water increases. The size of the droplet can be estimated by balancing the capillary stress and viscous stress leading to the correlation between the droplet radius and the capillary number of $R \propto \mathrm{Ca}^{-1}$. Nisisako et al. [19] used another T-junction fabricated on PMMA to generate water in oil droplets. Sunflower oil was used as the continuous phase and water as the dispersed phase. Uniform droplets were generated at a rate of up to 250 per second. The results also showed the correlation of $R \propto \mathrm{Ca}^{-1}$ as proposed by Thorsen et al.

In other experiments with different devices fabricated in PMMA and glass, Nisisako et al. [19] also showed that surface properties of channel walls also determine the formation of either O/W or W/O droplets. Uniform W/O droplets can only be generated using the PMMA device and O/W droplets in the device fabricated out of glass. This work indicated that low interfacial tension between the continuous phase and channel surface, and a high interfacial tension between the dispersed phase and channel wall are needed to generate monodispersed droplets. In addition, the channel width for the continuous phase affects the size of the formed droplets. A narrower channel causes a greater shearing force and consequently smaller droplet size.

Xu et al. used a quartz capillary embedded in PMMA to form the T-junction for generating O/W droplets [20, 21]. N-Octane was used as the dispersed phase and water with different concentration of sodium dodecyl sulfate (SDS) as the continuous phase. The results showed that the surfactant concentration affects the interfacial tension and the wetting ability of the fluid. The formation of disordered and ordered two-phase flow pattern depends on the surfactant concentration. When the surfactant concentration is below the critical micelle concentration (CMC), disordered flow pattern formed as the water partially adheres to the channel walls. Ordered flow pattern can only be formed when the concentration is greater than the CMC as the surfactant makes the channel wall hydrophilic. The diameter of the formed droplet was found to be smaller than the height of the microchannel. The correlation of $R \propto \mathrm{Ca}^{-1}$ agrees reasonably well with the experimental data. However, when the diameter of the droplet formed was greater than the channel height, the dependency of the droplet diameter with the Ca number was much weaker. If the droplet is small, the hydrodynamic forces exerted by the channel walls are not important, and hence the droplet breakup fully relies on the shear stresses imposed by the flow. If the droplet is big, the wall effects become dominant over the shearing stresses and hence the dependency of the droplet sizes on the continuous flow rate is weaker. The average droplet size decreases with increasing continuous phase viscosity and depends weakly on the dispersed phase. Increasing the viscosity of the continuous phase increases the shearing stress leading to the formation of smaller droplets.

The results of Xu et al. [20] showed that the proposed correlation by Thorsen et al. [22] may not be suitable for all cases of droplet formation in a T-junction. When the droplet formed is much bigger than the channel height, additional forces seem to affect the dynamics of the droplet formation. Garstecki et al. suggested that when the Ca number is low ($\mathrm{Ca} < 0.01$), interfacial force dominates the shear stress [23]. In this regime, the dynamics of droplet breakup should be dominated by the pressure drop across the droplet as it is forming. At a low capillary number, the droplet grows into a plug which obstructs the continuous phase channel. This obstruction increases the upstream pressure in the continuous phase and results in an addition force exerted on the interface that promotes the breakup. The added force scales with the gap d between the emerging droplet and the outer channel wall as:

$$F_\mathrm{p} = \frac{\mu_\mathrm{c} Q_\mathrm{c} w_\mathrm{c}}{h^2 d^3}. \tag{3.4}$$

The droplet formation process at low capillary number is called the squeezing regime. In this regime, the size of the droplets is solely determined by the ratio of the volumetric flow of the two immiscible fluids. Garstecki et al. [23] proposed the following scaling law for the size of the droplets:

$$\frac{L}{w} = 1 + \alpha \frac{Q_\mathrm{d}}{Q_\mathrm{c}}, \tag{3.5}$$

where L is the length of the immiscible plug, w is the width of the continuous phase channel, Q_d and Q_c are the volumetric flow rates of the continuous and dispersed phases, and α is a constant on the order of unity. The above equation clearly shows that the plug lengths formed do not depend on the capillary number and the properties of the fluids. The measured plug lengths agree well with the above scaling law when α is unity.

To operate in the squeezing regime, the T-junction should fulfill two conditions: (a) the width of the main channel should be greater than the channel height, and (b) the width of the inlet channel should be at least equal to half the width of the main channel. De Menech et al. used a diffuse interface method to numerically simulate the droplet breakup in a T-junction with a square cross section. Three distinct droplet formation regimes were identified: squeezing, dripping, and jetting [24]. A critical capillary number of $Ca_{cr} \approx 0.015$ was also identified to distinguish between the squeezing and dripping regime. In the squeezing regime $Ca < Ca_{cr}$, the tip of the dispersed fluid almost blocks the entire continuous phase channel. The obstruction created by the dispersed fluid led to an increase of pressure in the upstream which starts to squeeze the neck of the dispersed fluid. The squeezing time is defined as the time between the continuous phase fluids beginning to squeeze the neck of the dispersed fluid to until breakup. De Menech et al. argued that as the squeezing time mainly depends on the velocity of the fluids, the size of the formed droplets is independent of capillary number and the viscosity ratio of the fluids. As the capillary number increases to $Ca = 0.5$, the dripping regime gives way to the jetting regime. The droplet formed in this regime is mainly caused by the Plateau–Rayleigh instability. In this regime, the droplet detachment point moves gradually downstream with increasing flow rate.

An alternative to the T-junction configuration described above is the cross-junction, Fig. 3.1b, c. Droplets can be formed via shearing elongational flows through an orifice. This flow focusing approach was first implemented by Anna et al. to form water droplets [25]. In this configuration, the dispersed fluid (DI Water) flows in the middle stream and the continuous fluid (oil) flows in the two side channels. The two immiscible liquids are then forced to flow through the orifice which is located downstream. In the experiments, two different droplet formation regimes were observed. The first regime forms droplets that are comparable to the size of the orifice. The second regime generates droplets that are much smaller than the orifice, and the droplet size is mainly determined by the diameter of the thin "focused" thread.

Anna et al. later observed four different droplet formation regimes using the same device [26]. The four main droplet formation modes identified are geometry controlled, thread formation, dripping, and jetting. In addition, each droplet regime is a function of both the capillary number Ca and flow rate ratio. In the geometry controlled regime, the droplet sizes are roughly equal to the orifice size. The generated droplets are also highly monodisperse. Increasing the capillary number by increasing in the flow rate leads to the thread formation regime. In this regime, very thin threads are formed after the breakup of the droplets. Several tiny discrete droplets are formed. The droplet generation is not monodisperse and the size of the

tiny discrete droplets varies. The dripping regime is formed when the capillary number increases further. In this regime, the tip does not retract but remain at a fixed position in the orifice. The droplets formed are smaller than the previous two modes. The dripping regime gives way to the jetting regime as the capillary number Ca continues to increase. In this case, the tip will extend beyond the orifice and resembles a long viscous jet. The droplets formed are bigger than the dripping regime but has a higher polydispersity.

Wacker et al. used a glass-based flow focusing device to study the influence of viscosity and different oil types [27]. The experimental results showed that the oil type has a bigger influence on the droplet size than the viscosity of the oil. Results from the passive formation process at a T-junction or at a cross-junction indicate that if the flow rates are fixed, controlling the pressure in squeezing or geometry-controlled regime and controlling the capillary number would allow controlling the size of the formed droplets. Changing these parameters involves external physical fields such as temperature field and magnetic field. In the following sections, active control of droplet formation by using these external fields is discussed. The control schemes are categorized according to the actuation concepts. The different schemes either change the hydrodynamic properties of the liquids and consequently the capillary number or induce additional forces that support or act against the capillary pressure of the droplet.

3.2 Thermal Control

3.2.1 Thermal Control at T-Junction

As elaborated in the introduction of this chapter, the capillary number can be used to control the droplet formation process. If the flow rates are fixed, the capillary number is determined only by the interfacial tension and the dynamic viscosity. Therefore, the temperature dependence of both dynamic viscosity and interfacial tension can be used to control and manipulate the size of the droplets formed.

Figure 3.2 shows the characteristic temperature dependency of the viscosity of a mineral oil (Sigma M5904, mixed with 2% w/w Span 80 surfactant Sigma S6760) and the interfacial tension between this oil and water. The interfacial tension was measured with a commercial tensiometer (FTA 200, USA) and viscosity was measured with a low-shear rheometer (LS 40, Switzerland). Both viscosities and interfacial tensions are normalized by their nominal values at 25°C. At 25°C, viscosities of mineral oil is 26.4 mPa/s. The interfacial tension between water and mineral oil is 27.35 mN/m. The two empirical correlations for the interfacial tension and the viscosity at different temperatures are $\sigma = \sigma_0 \exp[-0.0144(T - T_0)]$ and $\mu = \mu_0 \exp[-0.0344(T - T_0)]$, where $\mu_0 = 23.8 \times 10^{-3}$Pa.s, $\sigma_0 = 3.65 \times 10^{-3}$ Nm^{-1} and $T_0 = 25$°C [39].

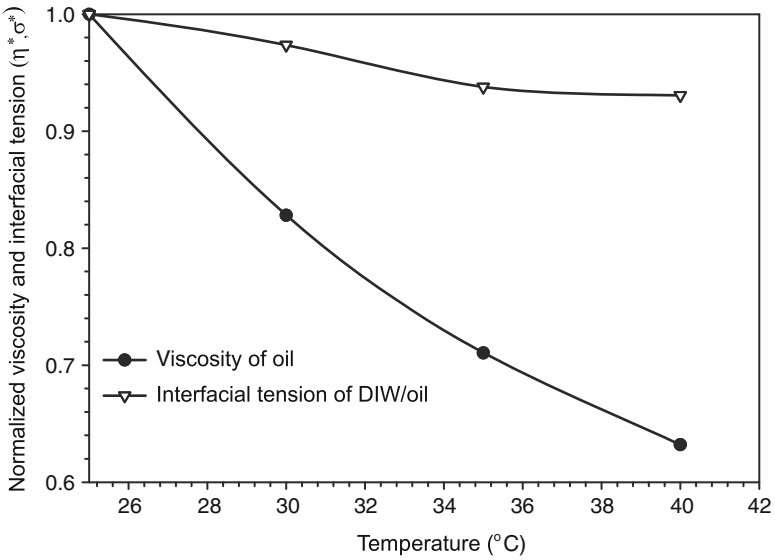

Fig. 3.2 Characteristic temperature dependency of viscosity of a mineral oil and of the interfacial tension between this oil and water

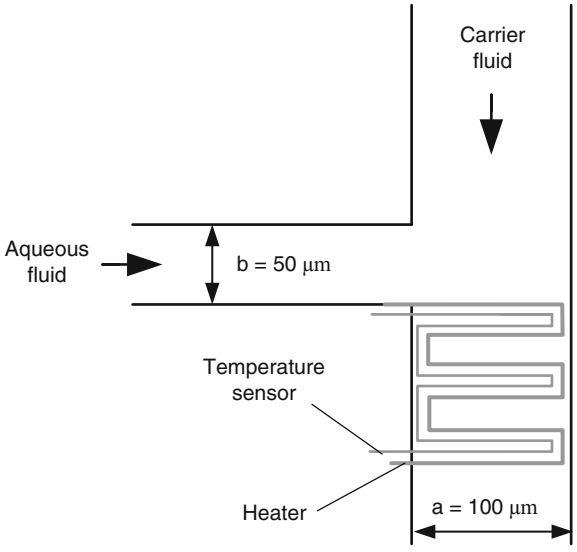

Fig. 3.3 A T-junction with integrated heater and temperature sensor

The T-junction device with the integrated micro heater and sensors as shown in Fig. 3.3 were fabricated using molding PDMS on a SU-8 template and lift-off technique. The widths of the channels for the dispersed and continuous phases are 100 μm and 50 μm, respectively. Devices with channel depth of 30 or 300 μm were used to investigate the effect of heating in channels with different depths.

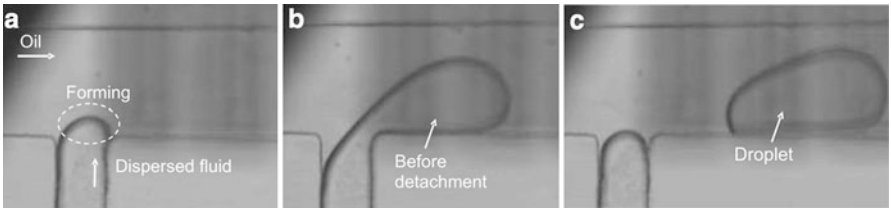

Fig. 3.4 Droplet formation process at a T-junction, the flow rates of the dispersed phase and continuous phase are 6 μl/h and 12 μl/h, respectively

The fluids are driven separately into the device using two syringe pumps (KDS 200 Two-Syringe Infusion Pump). A DC power source (Instek GPS-3030D) was used to supply current to the device via the wires connected to the contact pads. The temperature was varied by changing the magnitude of the supply current. A digital multimeter (Fluke 8808A) measured the resistances of the temperature sensor. The resistance was subsequently used for calculating the temperature of the heated junction. Since the droplet diameter is larger than the channel height and has a disc shape, the equivalent diameter of a spherical droplet with the same volume is calculated as [28]:

$$D_{\mathrm{eq}} = 2\left(\frac{1}{16}\right)^{\frac{1}{3}}\left[2D^3 - (D-h)^2(2D+h)\right]. \tag{3.6}$$

Figure 3.4 shows the typical droplet formation process achieved with the device. At the initial stage, the dispersed phase extrudes into the main channel (channel for continuous fluid) and forms a half disk as shown in Fig. 3.4a. As the flows proceed, the extruded dispersed phase starts to grow and gains more volume. The continuous phase continues to flow in the main stream and deforms the extruded dispersed phase. Figure 3.4b shows the moment right before the detachment of the droplet and form into a droplet. The characteristic necking was also clearly observed as shown in Fig. 3.4b. The breakup process confirms that droplet size is primarily controlled by local shear stress, Fig. 3.4c.

If the heater is located at one side of the channel, the channel depth will affect the temperature distribution at the junction and consequently the formation process. A channel with a smaller depth has a larger temperature gradient as compared to a channel with a larger depth. As mentioned above, the effect of channel depth on the droplet formation process was investigated using two T-junction devices with different depths (30 and 300 μm) and keeping both the flow rate ratio and average flow velocity constant. The experiment was first conducted using the device with a channel depth of 30 μm. The flow rates of both the dispersed phase (DI water) and continuous phase (Mineral oil with surfactant) were kept constant at 6 μl/h and 12 μl/h, respectively. The droplets formed at different temperature were then recorded and evaluated. Next, flow rates of 60 and 120 μl/h were used for the channel with a depth a 300 μm. The flow rate increased by ten times to keep

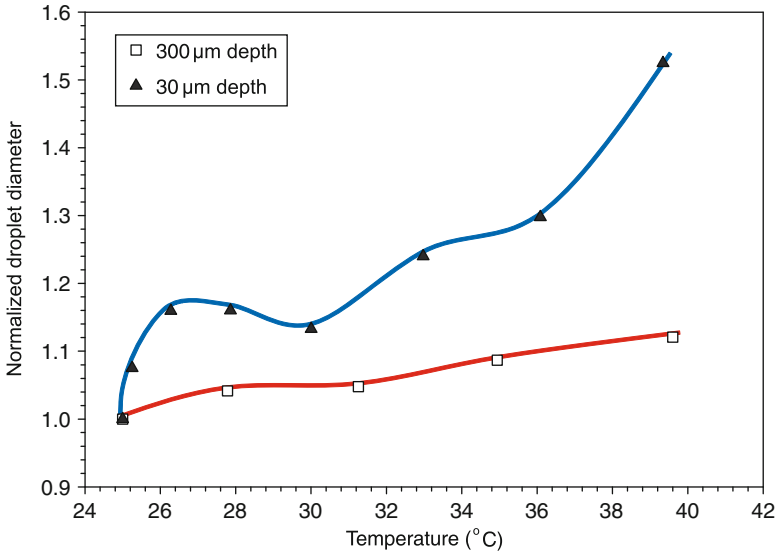

Fig. 3.5 Droplet size as function of temperature at T-junctions with different depths

the mean velocity constant as the depth increased by the same amount. The same mean velocity is needed for both experiments to maintain the same condition for heat convection and shear stress. Figure 3.5 shows the normalized diameters as a function of temperature. The diameters are normalized by the values at 25°C. The droplet sizes formed at the T-junctions of 300 µm and 30 µm channel depths are 334 µm and 85 µm, respectively. Experimental results show that the droplet size increases with temperature in both channel depths. However, for the channel with 300 µm depth, overall droplets size increased only by 14% as the temperature increases from 25°C to 39°C. The increase is 86% for the channel with a depth of 30 µm.

3.2.2 Thermal Control at Cross Junction

To investigate the concept of thermal control at a cross junction, a microfluidic device was fabricated in PDMS. Similar to the T-junction device, the cross-junction device was equipped with integrated micro heater and temperature sensor, Fig. 3.6. The junction is designed as a nozzle to increase the velocity gradient. A higher velocity gradient means a higher shear stress and easier droplet breakup. The heating effect on the droplet formation regimes at constant flow rates was studied and the transition capillary numbers Ca at different temperatures were identified.

As mentioned in the introduction of this chapter, the capillary number Ca is often used in droplet-based microfluidics to estimate the size of formed droplets and to

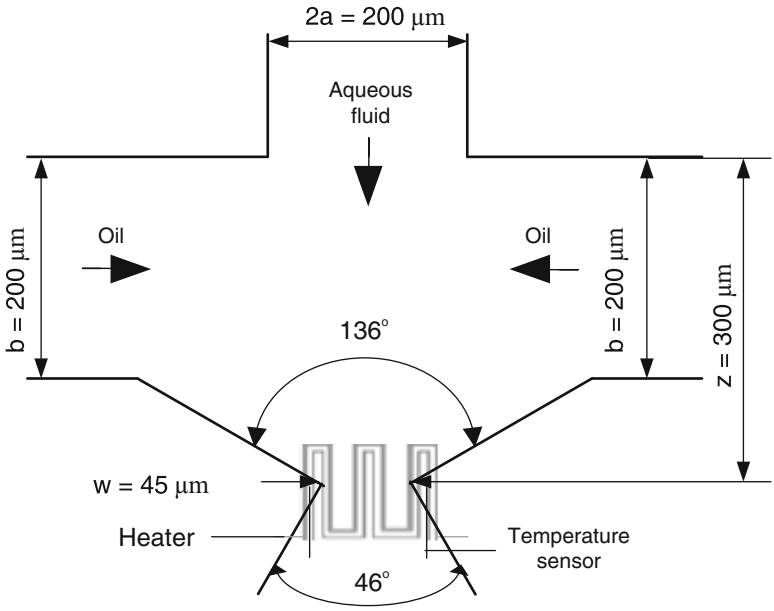

Fig. 3.6 Cross junction device with integrated heater and temperature sensor

determine the droplet formation regimes. For the flow focusing geometry, the capillary number Ca and the effective shear rate G can be determined as [25]:

$$\mathrm{Ca} = \frac{\mu_\mathrm{c} a Q_\mathrm{c}}{\sigma h}\left[\frac{1}{wz} - \frac{1}{b^2}\right], \tag{3.7}$$

where μ_c and Q_c are the dynamic viscosity and the total volumetric flow rate of the continuous phase, σ is the interfacial tension between the two fluids, a is the half-width of the dispersed phase channel, h is the channel depth, w is the width of the orifice entrance, z is the distance between the dispersed phase channel and the orifice, and b is the width of the channel for the continuous phase.

DI water with 0.05% w/w fluorescence dye (Sigma F6377) and mineral oil (Sigma M5904) with 2% w/w of surfactants (Span 80) worked as the dispersed phase and the continuous phase, respectively. With the empirical temperature-dependent functions of the viscosity and the interfacial tension, the capillary number Ca can be expressed as a function of temperature:

$$\mathrm{Ca}(T) = \frac{\mu_0 a Q_\mathrm{c}}{\sigma_0 h}\left[\frac{1}{wz} - \frac{1}{b^2}\right]\exp(-0.02\Delta T). \tag{3.8}$$

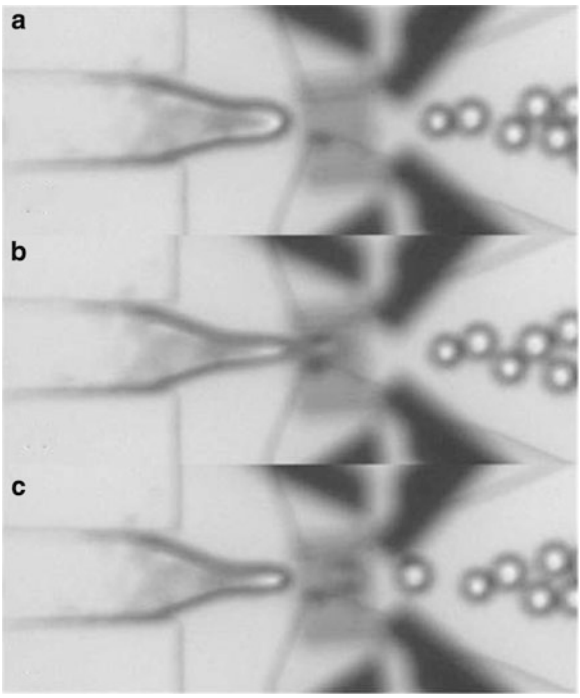

Fig. 3.7 Dripping regime encountered at room temperature of 25°C

Thus, the expected relationship between the droplet diameter and the temperature is:

$$D \propto \mathrm{Ca}(T)^{-1} = \left[\frac{\mu_0 a Q_c}{\sigma_0 h}\left(\frac{1}{wz} - \frac{1}{b^2}\right)\right]^{-1} \exp(0.02\Delta T). \tag{3.9}$$

As shown in the above equations, temperature can be used to control the capillary number and consequently the formation regimes and the droplet size. An increase in temperature reduces the capillary numbers as viscosity decreases more than the interfacial tension over the same temperature change, Fig. 3.2. Thus the temperature also changes the droplet formation regimes leading to an increase in size of the formed droplets.

The same experimental setup described in Sect. 3.2.1 was used. The flow rates of the dispersed phase (DI water) and the continuous phase (mineral oil with 2% w/w surfactant) were first kept constant at 5 µl/h and 30 µl/h, respectively. As the temperature increases from 25°C to 45°C, three different droplet formation regimes were observed.

At room temperature (25°C), the size of the formed droplets was smaller than the width of the constriction (Fig. 3.7). This formation regime was similar to the dripping regime reported by Anna et al. [26]. In this regime, the tip of the dispersed phase is fixed and oscillates around the constriction, and the neck does not block the

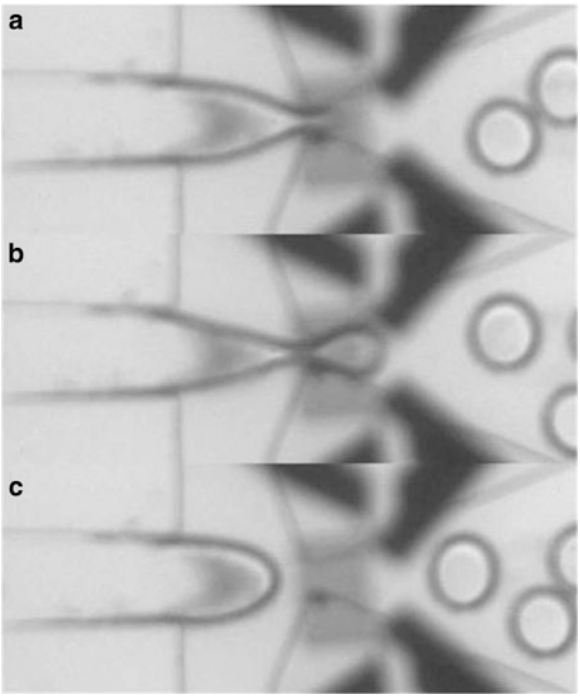

Fig. 3.8 Squeezing regime A encountered at a temperature of 35°C

constriction, Fig. 3.7b. The breakups are observed at a fixed point at the orifice due to the focused velocity gradient created by the nozzle geometry. As a droplet breaks free, the tip never retracts from the constriction and immediately starts forming a new droplet, Fig. 3.7c. The formed droplets were smaller than the width of the orifice.

As the temperature increased to 35°C, the formation process started to change. A second formation regime similar to the squeezing regime described by Anna et al. [26] was observed. In this regime, the tip of water is some distance away upstream of the constriction. The tip gradually narrows down as it extends toward the constriction, Fig. 3.8. The tip then penetrates into the constriction and grows into a bulb behind the constriction until it breaks off, Fig. 3.8b. After the breakup, the tip retracts back upstream, Fig. 3.8c. The formed droplets in this case were significantly larger than the width of the orifice. In order to distinguish between the different modes of squeezing, this mode is called squeezing regime A.

At a temperature of around 45°C, a third droplet formation regime was observed. This droplet formation mechanism is similar to the squeezing regime mentioned above. However, the water tip grows into a bulb with a large radius of curvature, Fig. 3.9a. In contrast, in the previous regime, the tip is pointed toward the constriction and has a smaller radius. There is also a slight difference after the droplets were formed. In this regime, the tip retracts further away from the constriction as compared to the previous regime, Fig. 3.9c.

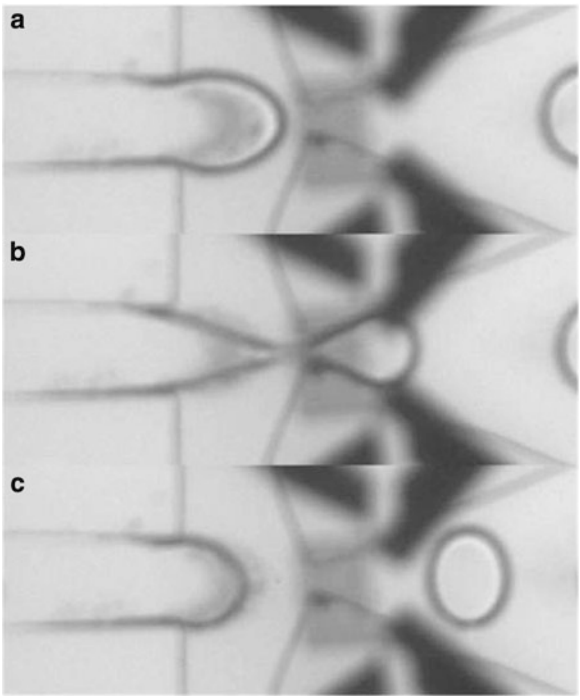

Fig. 3.9 Squeezing regime B encountered at a temperature of 45°C

In the water/oil system tested above, an increase in temperature results in the decrease in capillary number due to the temperature dependency of viscosity and interfacial tension, Fig. 3.10. The dripping regime was observed from 25°C to 30°C in the capillary number range of $0.018 > Ca > 0.016$. In the temperature range of 30°C to 42°C, the squeezing A regime was observed in the capillary number range of $0.016 > Ca > 0.013$. Lastly, at temperature greater than 42°C, squeezing regime B was observed in the capillary number range of $Ca < 0.013$. Figure 3.11 shows the change of droplet diameters in the different regimes over the investigated temperature range.

3.3 Magnetic Control

If the fluids in the formation process can respond to an external field other than temperature field, this field can also be used for controlling the droplet formation process. For the case of a magnetic field, the fluid needs to be magnetic. Ferrofluid is a class of smart fluids [29] that have been extensively used in many engineering applications. They are colloidal suspension of single domain magnetic nanoparticles coated by a layer of surfactants in a carrier liquid such as water or oil [30]. The surfactants provide a short range steric repulsion between particles and

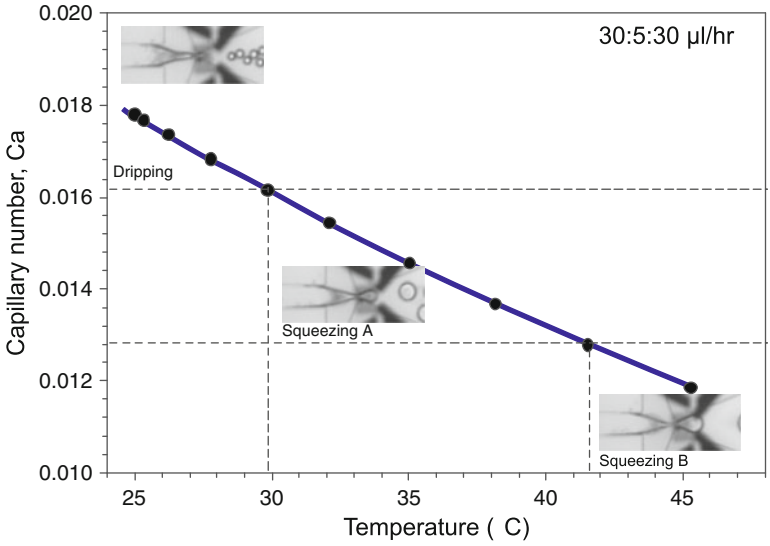

Fig. 3.10 Ca number and droplet formation regimes at different temperature

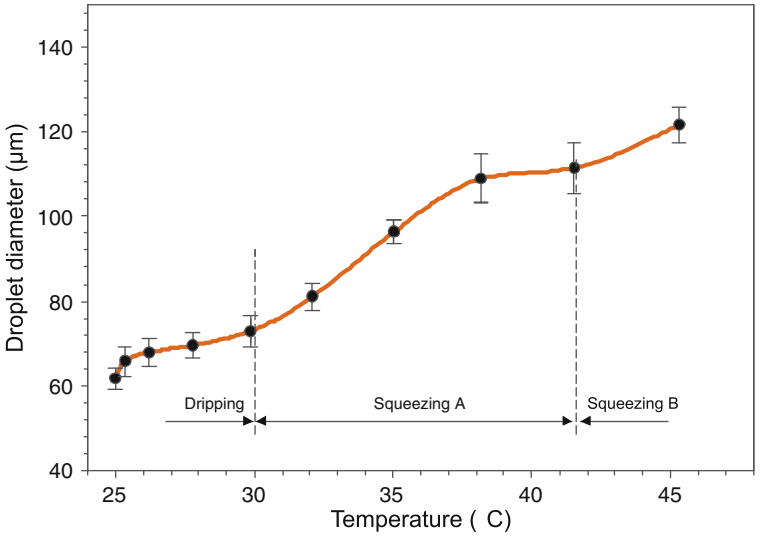

Fig. 3.11 Droplet diameter as function of temperature

prevent particle agglomeration in the presence of a magnetic field [31]. Brownian motion keeps the magnetite (Fe_3O_4) from settling under gravity [35]. Ferrofluids have superparamagnetic properties, because the magnetic domains have the same size as the particles [32]. Unlike magnetorheological fluids (MRF) which may behave like a solid in the presence of a strong magnetic field, ferrofluids keeps its

fluidity even when subjected to a strong magnetic field [33]. As the typical size of the commercial ferromagnetic particles is around 10 nm, only very weak magnetoviscous effects are present [34].

In the absence of a magnetic field, the magnetic nanoparticles are randomly distributed and thus the ferrofluid has no net magnetization. The size of each ferrofluid droplet is determined by the geometry, flow rates, and capillary number, i.e., the balance of viscous forces and capillary pressure. In contrast, when a magnetic field is applied to the ferrofluid, the ferro-particles will automatically orient themselves in neat alignment along the magnetic field. The magnetization of the ferrofluid responds quickly to any changes in the applied magnetic field and the moments randomize rapidly when the applied field is removed. In a gradient field, the forces acting on the magnetic fluid are proportional to the gradient of the external field and the magnetization value of the fluid. The magnetic force density [35] acting on an incompressible ferrofluid can be described as

$$F_{\mathrm{m}} = \mu_0 M \nabla H, \tag{3.10}$$

where μ_0 is the dynamic viscosity of the fluid, M is the magnetization of the ferrofluid, and ∇H is the gradient of the external magnetic field. This means that the induced magnetic forces can be used to manipulate and to control the size of the ferrofluid droplets formed in a microchannel. The magnitude and direction of the magnetic force can also be manipulated by changing the location of the magnet and the gradient of the external magnetic field.

3.3.1 Magnetic Control at a T-Junction

In the absence of a magnetic field, the size of the formed ferrofluid droplets decreases linearly with the increase of the continuous phase flow rate. In the presence of a magnetic field, the size of ferrofluid droplets was controlled and manipulated using a disk-shaped permanent magnet. A nonuniform magnetic field with different strengths at the junction was generated by placing the magnet at different locations relative to the junction. This induced attractive magnetic force affects the droplet formation process leading to the change in the size of the droplets. In addition, experimental results show that relative change in the size of the droplets depends on the continuous flow rates.

The T-junction devices used in the experiments were fabricated using the same soft lithography method mentioned in Sect. 3.2. However, the PDMS microchannel was now bonded to a flat piece of glass with thickness of about 100 μm. The glass substrate provides a rigid support which enables the magnet to be placed easily at the desired location. The inlet widths of the dispersed and continuous phase channels are 50 μm and 300 μm, respectively. A small circular permanent magnet of 3-mm diameter and 2-mm thickness was integrated to provide the external magnetic field. The magnetic field strength was varied by placing the magnet at

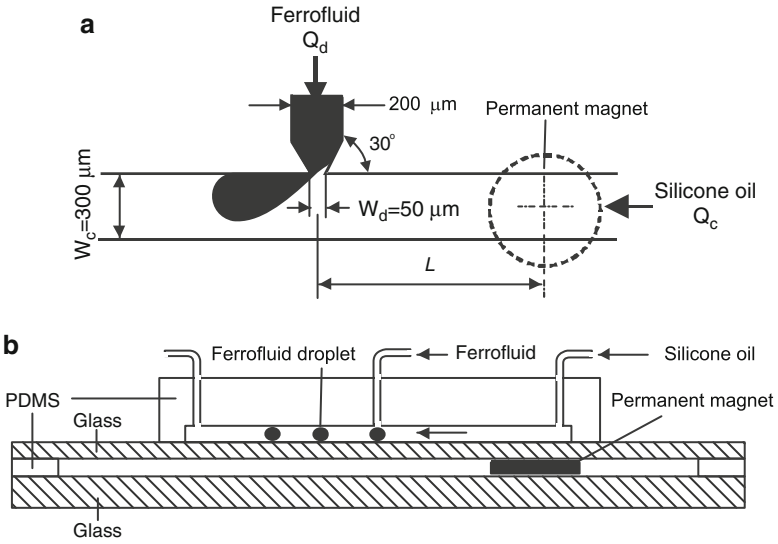

Fig. 3.12 Schematics of the experimental setup (not to scale): (**a**) the microfluidic network; (**b**) the setup with the permanent magnet

different locations relative to the junction. The droplet diameters and evolving shapes were evaluated by a customized MATLAB program. Figure 3.12 shows the geometry of the T-junction and the experimental setup.

Water-based ferrofluid (Ferrotech, EMG 807) was used in the experiment as the dispersed phase fluid. The dynamic viscosity and density of the ferrofluid at 27°C are $\mu = 2$ mPa.s and $\rho = 1{,}100$ kg/m^3, respectively. The saturation magnetization of this ferrofluid is 10 mT. The initial susceptibility of this ferrofluid is $\chi = 0.39$. Silicone oil (Sigma Aldrich) was used as the continuous phase fluid. The kinematic viscosity and density are $\mu = 100$ mPa.s and $\rho = 960$ kg/m^3. The interfacial tension between the ferrofluid and silicone oil of approximately $\sigma = 21.07$ mN/m was measured using a commercial tensiometer (TVT-2, Lauda, Germany).

In order to understand the formation of ferrofluid droplets in the absence of a magnetic field and to investigate the effect of the continuous flow on the formation of ferrofluid droplets, the experiment was first carried out by fixing the flow rate of the dispersed phase Q_d at 10 μl/h and varying the flow rate of the continuous phase from $Q_c = 50$ μl/h to 150 μl/h. Figure 3.13 shows the diameter of the formed ferrofluid droplet as a function of the flow rate of the continuous phase as well as of the capillary number. This result shows that as the continuous flow Q_c increases, the diameter of the droplets decreases linearly. The capillary number ranges from approximately 0.002 to 0.006 and is in the transition between squeezing and dripping regimes. In this transition regime, the droplet formation process is dominated by both the viscous shear stress and squeezing pressure [36]. Figure 3.14 compares the droplet formation process at different continuous flow rates ($Q_c = 50$μl/h and $Q_c = 100$μl/h). The dispersed flow rate is fixed at 10 μl/h. The time

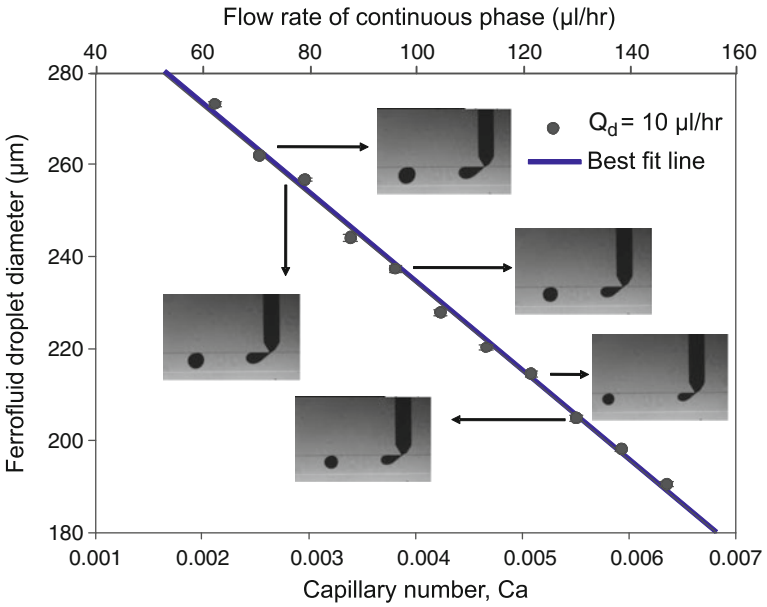

Fig. 3.13 Ferrofluid droplet diameters as a function of continuous flow rate

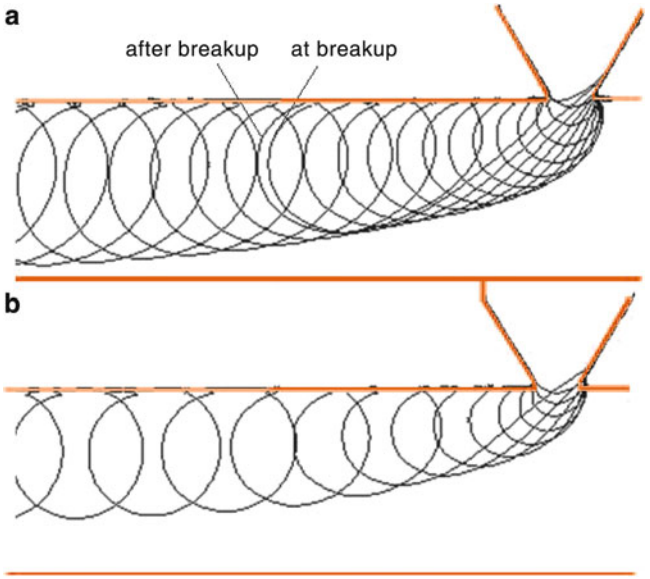

Fig. 3.14 Measured formation process of ferrofluid in the absence of an external magnetic field: (**a**) $Q_c = 50$ μl/h; (**b**) $Q_c = 100$ μl/h

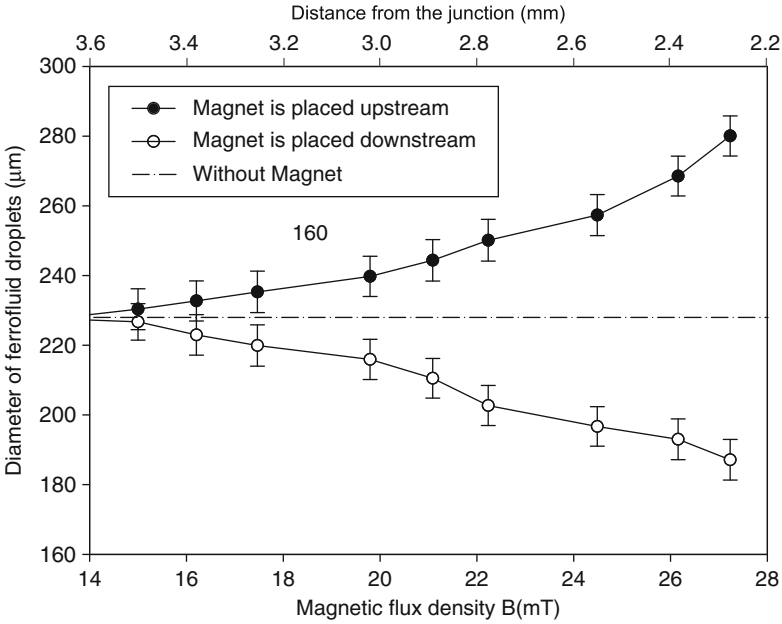

Fig. 3.15 Measured magnetic flux density as a function of distance

evolving images are generated using a customized MATLAB program whereby the interfaces between the ferrofluid and silicone oil are detected. The overlapping images of the droplet clearly show that when the continuous flow increases, the interface radius of curvature becomes steeper and the distance between the emerging fluid and the channel wall also decreases.

In order to investigate the effect of magnetic field during droplet formation, a permanent magnet is placed upstream and downstream of the junction. The magnet was placed at a distance to the junction ranging from 2,300 to 3,800 μm. Fixed flow rates of $Q_d = 10$ μl/h and $Q_c = 100$ μl/h were used throughout the experiments. Magnetic flux density of the permanent magnet was measured using a commercial gaussmeter with accuracy level of $\pm$ 1% (Hirst, GM05, UK). A micropositioner was used to align and adjust the distance between the magnet and the probe. Figure 3.15 depicts the droplet size as function of both distance and magnetic flux density. The results show that when the magnet is placed upstream of the junction, the size of the formed droplets is larger than in the case without an external magnet. However, as the magnet is shifted further upstream, the size of the droplets decreases and approaches that without the magnetic field. The difference in droplet size becomes insignificant when the magnet is placed at a distance greater than 3,000 μm. Conversely, when the magnet is placed at the downstream of the continuous phase channel, the size of the droplets decreases as compared to the droplets formed without an external magnet. The difference in the droplets size becomes insignificant when the distance is greater than 3,000 μm.

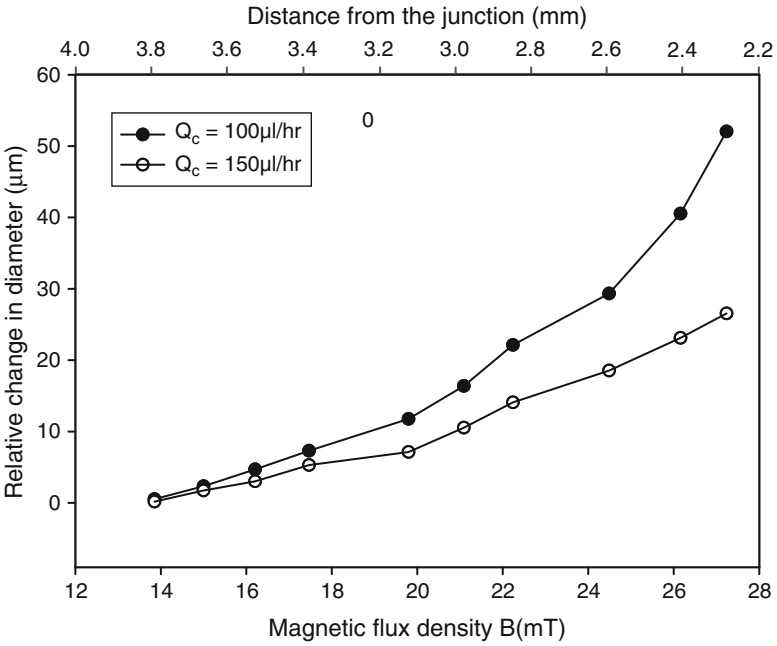

Fig. 3.16 Droplet diameters as a function of Ca number

Magnetic force acting on the ferrofluids depends on both the magnetic field strength and the relative location of the permanent magnet. When the distance between the ferrofluids and the magnet increases, a relatively smaller magnetic force acts on the ferrofluid. Thus, a smaller difference in the droplet size can be expected. The location of the magnet also plays an important part in influencing the size of the formed droplets. When placed upstream of the junction, a pulling magnetic force retards the droplet breakup process. This pulling force allows more dispersed fluid to emerge and flow into the continuous phase channel. This force holds and supports the ferrofluid leading in a larger formed droplet. When the magnet is placed a downstream of the junction, a pushing force acts on the emerging ferrofluids. However, in this case, the pushing magnetic force accelerates the droplet breakup process. The particles in the ferrofluid align and move toward the magnet due to the magnetic attraction. This phenomenon results in forming smaller droplets as less ferrofluid emerges into the continuous phase channel prior to breakup.

In the absence of a magnetic field, the flow rate of the continuous phase affects the size of the formed droplet significantly. The induced shear stress allows the droplet to break up more easily. Thus, increasing flow rate reduces the diameter of the formed droplet. In order to investigate the role of the flow rate of the continuous phase in the presence of a magnetic field, the experiment was repeated using another set of flow rates of $Q_d = 10\mu l/h$ and $Q_c = 150\mu l/h$. Figure 3.16 shows the

relative change in droplet diameter versus magnet position and flux density at the two different flow rates. At a lower flow rate, the formation results in a larger change in droplet diameter. The curve of $Q_c = 100\mu l/h$ has higher gradient. This phenomenon can be explained by the nature of the magnetic force as a volume force. The magnetic force acting on the ferrofluid is proportional to its volume emerging into the continuous phase. At a higher flow rate of $Q_c = 150\mu l/h$, the volume of the ferrofluid in the continuous phase is smaller leading to a decrease of magnetic force. The less significant magnetic force leads to a smaller change in droplet size at the higher flow rate.

3.3.2 Magnetic Control at Cross Junction

In a nonuniform magnetic field, the magnetic body force is generated toward the direction of the highest magnetic flux. This induced force as described in the previous section manipulates the size of ferrofluid droplets formed at a T-junction. However in a uniform magnetic field, the nanoparticles in the ferrofluid aligns with the magnetic field and results in magnetization of the fluid. For instance, a spherical ferrofluid droplet elongates along the field direction with maximum magnetization at both of its poles. The coupling of magnetic field results in a singular normal force acting on the interface between the droplet and the surrounding medium. This magnetic interfacial force has a similar effect as the interfacial tension. Under a uniform magnetic field, this force can be used to control the size of a ferrofluid droplet during the formation process.

A cross-junction device was fabricated using standard soft lithography as described previously. However, the PDMS microchannels were now bonded to a spin coated layer of PDMS of thickness 200 μm, to ensure uniform surface properties of the microchannels. The device was aligned and placed on a glass slide. The rectangular channel has a uniform height of 100 μm. The inlet widths of the continuous and dispersed phase fluids are fixed at 100 μm. Figure 3.17 and 3.18 shows the schematic sketch of the flow focusing device and the experimental setup. To generate a uniform magnetic field, an electromagnet [37] with 350 turns around a C-shape soft-magnetic core (Fig. 3.17). The air gap for the uniform magnetic field measures 26 mm. A DC power source (Instek, GPS-3030DD) was used to control the magnitude of the magnetic field strength, which is calibrated using a commercial gaussmeter (Hirst, GM05, UK).

Figure 3.19 shows the normalized diameters of the droplets formed as a function of both current and magnetic field strength. The diameter at 0 A is about 115 μm. The normalized diameter is calculated using $d* = d_i/d_0$, where d_0 refers to the diameter of the formed droplet in the absence of the magnetic field and d_i is the diameter at the respective field strengths. At fixed flow rates, the size of the ferrofluid droplets increases with the increase of the magnetic field strength, Fig. 3.19. Figure 3.19 compares the effect of the flow rates on the dependence of the droplet size on the magnetic field strength. Keeping the flow rate ratio between

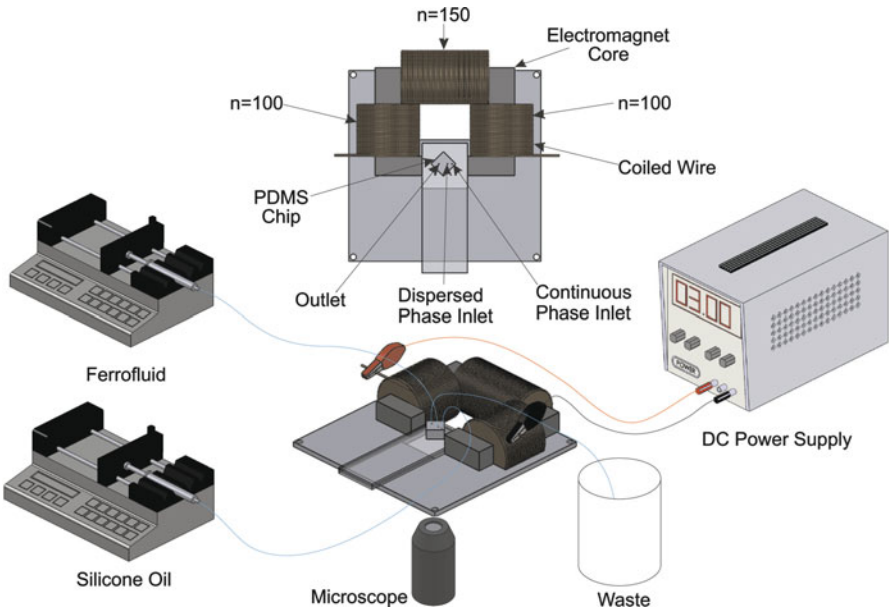

Fig. 3.17 Schematic sketch of the experimental setup for the formation of ferrofluid droplets under a uniform magnetic field

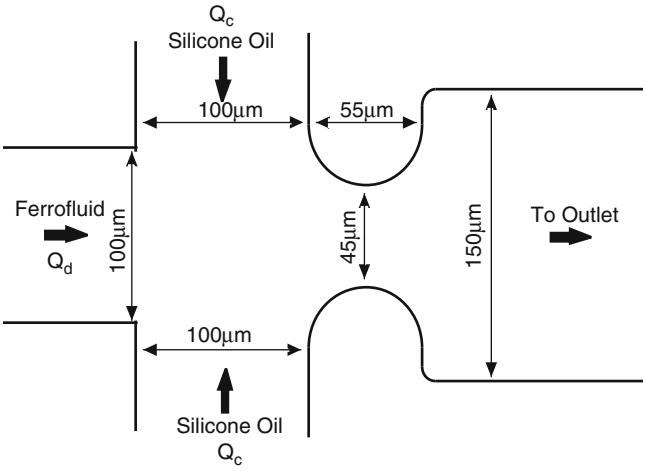

Fig. 3.18 The microfluidic flow focusing geometry used in the experiment

the dispersed phase and the continuous phase as 1:8, flow rates combinations of $Q_d = 6$, $Q_c = 24$ µl/h and $Q_d = 5$, $Q_c = 20$ µl/h were used to investigate the effect of flow rates. Similar to the case of a T-junction, lower flow rates lead to a larger dependence of the droplet size on the magnetic field strength.

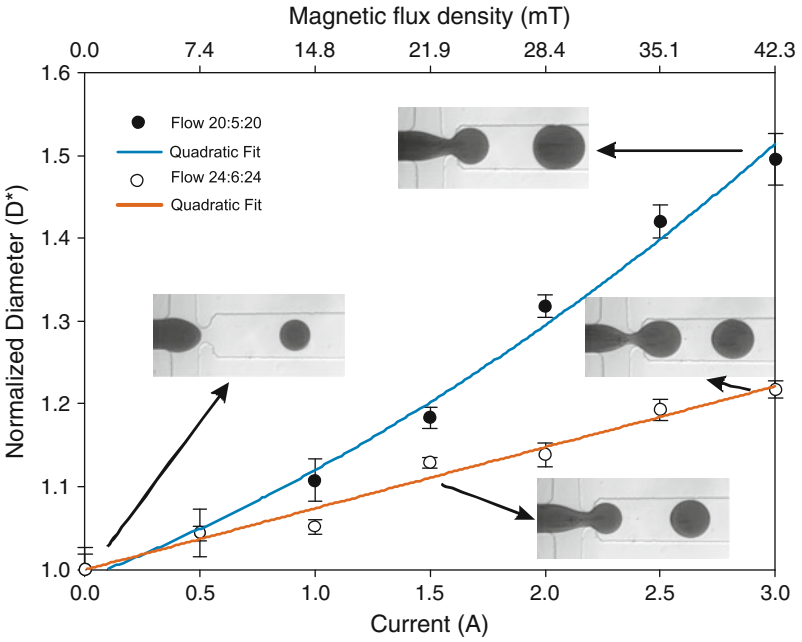

Fig. 3.19 Normalized diameters as a function of both current and magnetic field strength

Figure 3.20 visualizes the formation process of a ferrofluid droplet in the absence (Fig. 3.20a) and presence (Fig. 3.20b) of a magnetic field. In the absence of a magnetic field, the droplets were formed in the "squeezing" regime described by Garstecki et al. [38]. In the presence of a uniform magnetic field, the magnetic interfacial force allows more dispersed fluid to flow into the orifice by virtually "holding" onto the forming droplet. The size of the droplets thus increases in the process. The time taken for the droplet to form in the absence of the magnetic field is about 0.592 s. In the presence of the magnetic field ($B = 42.3$ mT), the time taken for the droplet to form is about 1.016 s. The droplet formation period almost doubled in the presence of the magnetic field.

3.4 Conclusions

The temperature dependence of droplet formation at both T-junction and cross-junction devices was investigated. An integrated micro heater and a temperature sensor was used to control the temperature. In the experiments reported in this chapter, the droplet sizes increases with increasing temperature due to the dominance of temperature dependency of viscosity. The smaller the depth of the channel, the larger is the increase of droplet size with temperature. At constant flow rates, three different droplet formation regimes were observed at a cross

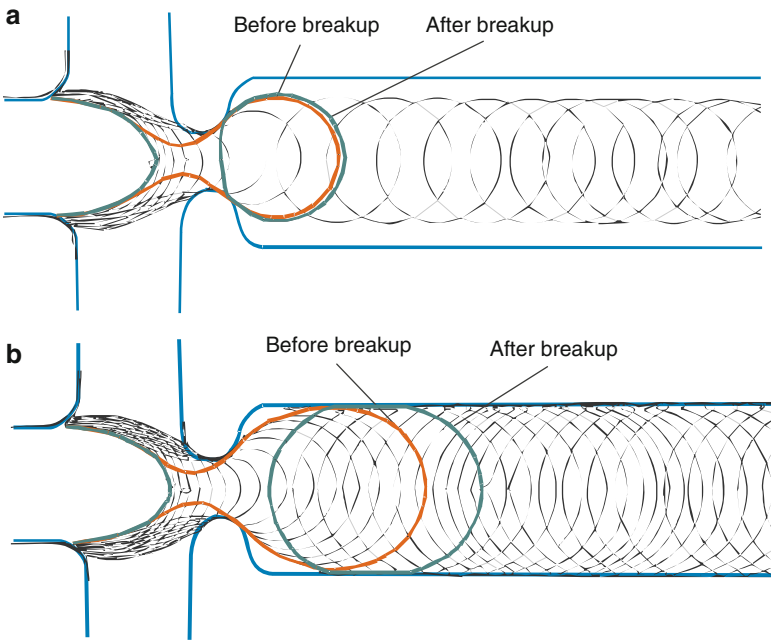

Fig. 3.20 Normalized diameters as a function of both current and magnetic field strength

junction and when the temperature increases. The formation and manipulation of ferrofluid droplets at a T-junction and a cross-junction were investigated using a permanent magnet and an electromagnet. In the presence of a magnetic field, the size of the droplets depends on the magnetic field strength and the location of the permanent magnet. The induced magnetic force may accelerate or decelerate the droplet formation process depending on both the magnetic field strength and location of the magnet. An electromagnet was used to control and manipulate ferrofluid droplets formed in a cross-junction device. The stronger the applied uniform magnetic field, the larger are the formed droplets. For both permanent magnet and electromagnet, the dependence on the magnetic field strength increases with decreasing flow rates.

References

1. Kobayashi I et al (2007) Formulation of monodisperse emulsions using submicron-channel arrays. Colloid Surface Physicochem Eng Aspect 296:285–289
2. Teh SY et al (2008) Droplet microfluidics. Lab Chip 8:198–220
3. Sun Y et al (2009) Rapid amplification of genetically modified organisms using a circular ferrofluid-driven PCR microchip. Anal Bioanal Chem 394:1505–1508
4. Sun Y et al (2008) High-throughput polymerase chain reaction in parallel circular loops using magnetic actuation. Anal Chem 80:6127–6130

5. Wang W et al (2005) Droplet-based micro oscillating-flow PCR chip. J Micromech Microeng 15:1369–1377
6. Zheng B et al (2004) Formation of droplets of alternating composition in microfluidic channels and applications to indexing of concentrations in droplet-based assays. Anal Chem 76:4977–4982
7. Song H et al (2006) Reactions in droplets in microfluidic channels. Angew Chem Int Ed 45:7336–7356
8. Li L et al (2007) Using a multijunction microfluidic device to inject substrate into an array of preformed plugs without cross-contamination: comparing theory and experiments. Anal Chem 79:2756–2761
9. Song H, Ismagilov RF (2003) Millisecond kinetics on a microfluidic chip using nanoliters of reagents. J Am Chem Soc 125:14613–14619
10. Shestopalov I et al (2004) Multi-step synthesis of nanoparticles performed on millisecond time scale in a microfluidic droplet-based system. Lab Chip 4:316–321
11. Nisisako T et al (2005) Controlled formulation of monodisperse double emulsions in a multiple-phase microfluidic system. Soft Matter 1:23–27
12. Okushima S et al (2004) Controlled production of monodisperse double emulsions by two-step droplet breakup in microfluidic devices. Langmuir 20:9905–9908
13. Xu JH et al (2006) Controllable preparation of monodisperse O/W and W/O emulsions in the same microfluidic device. Langmuir 22:7943–7946
14. Dou YH et al (2002) A dynamically modified microfluidic poly(dimethylsiloxane) chip with electrochemical detection for biological analysis. Electrophoresis 23:3558–3566
15. Alcantar NA et al (2000) Polyethylene glycol-coated biocompatible surfaces. J Biomed Mater Res 51:343–351
16. Tan et al (2010) Oxygen plasma treatment for reducing hydrophobicity of a seal polydimethylsiloxane microchannel. Biommicrofluidics 4:032204
17. Eddington DT et al (2006) Thermal aging and reduced hydrophobic recovery of polydimethylsiloxane. Sensor Actuator B Chem 114:170–172
18. Squires TM, Quake SR (2005) Microfluidics: fluid physics at the nanoliter scale. Rev Mod Phys 77:977–1026
19. Nisisako T et al (2002) Droplet formation in a microchannel network. Lab Chip 2:24–26
20. Xu JH et al (2006) Shear force induced monodisperse droplet formation in a microfluidic device by controlling wetting properties. Lab Chip 6:131–136
21. Xu JH et al (2006) Preparation of highly monodisperse droplet in a T-junction microfluidic device. AIChE J 52:3005–3010
22. Thorsen T et al (2001) Dynamic pattern formation in a vesicle-generating microfluidic device. Phys Rev Lett 86:4163–4166
23. Garstecki P et al (2006) Formation of droplets and bubbles in a microfluidic T-junction-scaling and mechanism of break-up. Lab Chip 6:437–446
24. De Menech M et al (2008) Transition from squeezing to dripping in a microfluidic T-shaped junction. J Fluid Mech 595:141–161
25. Anna SL et al (2003) Formation of dispersions using "flow focusing" in microchannels. Appl Phys Lett 82:364–366
26. Anna SL, Mayer HC (2006) Microscale tipstreaming in a microfluidic flow focusing device. Phys Fluid 18:121512
27. Wacker J et al (2009) Influence of oil type and viscosity on droplet size in a flow focusing microfluidic device. Procedia Chem 1:1083–1086
28. Nie Z et al (2008) Emulsification in a microfluidic flow-focusing device: effect of the viscosities of the liquids. Microfluid Nanofluid 5:585–594
29. Nair SS et al (2008) An optical limiter based on ferrofluids. Appl Phys Lett 92:171908
30. Chen CY et al (2009) Experiments on breakups of a magnetic fluid drop through a micro-orifice. J Magn Magn Mater 321:3520–3525

31. Zahn M (2001) Magnetic fluid and nanoparticle applications to nanotechnology. J Nanopart Res 3:73–78
32. Berger P et al (1999) Preparation and properties of an aqueous ferrofluid. J Chem Educ 76:943–948
33. Scherer C, Neto AMF (2005) Ferrofluids: properties and applications. Braz J Phys 35:718–727
34. Odenbach S (2003) Ferrofluids - magnetically controlled suspensions. Colloid Surface Physicochem Eng Aspect 217:171–178
35. Rinaldi C et al (2005) Magnetic fluid rheology and flows. Curr Opin Colloid Interface Sci 10:141–157
36. Christopher GF et al (2008) Experimental observations of the squeezing-to-dripping transition in T-shaped microfluidic junctions. Phys Rev E Stat Nonlinear Soft Matter Phys 78:036317
37. Ogawa C et al (2001) Domain structure and MR effect of ferrofluid emulsion. Int J Mod Phys B 15:859–863
38. Garstecki P et al (2005) Formation of bubbles and droplets in microfluidic systems. Bull Pol Acad Sci Tech Sci 53:361–372
39. Nguyen et al (2007) Thermally mediated droplet formation in microchannel. Appl Phys Lett 91:084102

Chapter 4
Recent Advances in Electrowetting Microdroplet Technologies

Robert W. Barber and David R. Emerson

4.1 Introduction

The ability to handle small volumes of liquid, typically from a few picolitres (pL) to a few microlitres (μL), has the potential to improve the performance of complex chemical and biological assays [1–6]. The benefits of miniaturisation are well documented [7–9] and include smaller sample requirements, reduced reagent consumption, decreased analysis time, lower power consumption, lower costs per assay and higher levels of throughput and automation. In addition, miniaturisation may offer enhanced functionality that cannot be achieved in conventional macroscale devices, such as the ability to combine sample collection, analyte extraction, preconcentration, filtration and sample analysis onto a single microfluidic chip [10]. Microfluidics-based lab-on-a-chip devices have received considerable attention in recent years, and are expected to revolutionise clinical diagnostics, DNA and protein analysis and many other laboratory procedures involving molecular biology [11–13]. Currently, most lab-on-a-chip devices employ continuous fluid flow through closed microchannels. However, an alternative approach, which is rapidly gaining popularity, is to manipulate the liquid in the form of discrete, unit-sized microdroplets—an approach which is often referred to as *digital microfluidics* [14–18]. The use of droplet-based microfluidics offers many benefits over continuous flow systems; one of the main advantages is that the reaction or assay can be performed sequentially in a similar manner to traditional (macroscale) laboratory techniques. Consequently, a wide range of established chemical and biological protocols can be transferred to the micro-scale without the need to establish continuous flow protocols for the same reaction. In addition, droplet-based systems avoid many of the problems associated with single-phase microfluidics such as sample cross-contamination and diffusional dilution.

R.W. Barber (✉) • D.R. Emerson
Centre for Microfluidics and Microsystems Modelling, STFC Daresbury Laboratory, Warrington WA4 4AD, UK
e-mail: robert.barber@stfc.ac.uk

P. Day et al. (eds.), *Microdroplet Technology: Principles and Emerging Applications in Biology and Chemistry*, Integrated Analytical Systems,
DOI 10.1007/978-1-4614-3265-4_4,

One of the most important consequences of miniaturisation is the increase in the surface-to-volume ratio of the fluid. For example, the surface-to-volume ratio for a device with a characteristic length of 1 m is of order 1 m^{-1} whilst the surface-to-volume ratio for a microfluidic device having a characteristic length of 1 μm will increase to 10^6 m^{-1}. In other words, the surface-to-volume ratio of the fluid scales according to the inverse of the characteristic length [8]. Consequently, as devices are reduced in size, inertial forces will decrease while viscous effects and surface energies will become increasingly important. In the case of submillimetre-sized liquid droplets, capillary forces dominate the motion [19]. Under these circumstances, the control of the surface energy provides a useful tool for manipulating droplets [20–23]. Although chemical and topographical patterning of substrates has received considerable attention in recent years [24–26], the static nature of these surface treatments prevents the *active* control of droplets, as required in a fully-controllable digital microfluidic system. As a consequence, considerable work has been dedicated to the development of techniques that allow the wettability of the substrate to be varied both spatially and temporally. The most promising droplet actuation technique for digital microfluidic applications appears to be electrowetting [27–32], although other mechanisms have been demonstrated including dielectrophoresis [33–35], thermocapillary actuation [36–38] and optoelectrowetting [39–43]. In addition, other promising droplet handling techniques such as surface acoustic wave (SAW) actuation have been developed [44–47] although in this case, the droplet movement is achieved via the creation of acoustic waves rather than by changing the wettability of the surface. Furthermore, electrowetting can be combined with electrophoresis/dielectrophoresis, to provide a method for particle separation or sample enrichment [48–51], or can be used to collect or separate magnetic particles [52–54].

Over the last few years, electrowetting has become an increasingly important technology for droplet manipulation. Electrowetting can commonly achieve contact angle variations of more than 40° and the switching cycles can be performed hundreds of thousands of times without any detrimental effects to either the fluid or the chip. The switching response time for millimetre-sized droplets is relatively fast (typically several milliseconds) and is only limited by the inertia of the droplet rather than the switching time of the equilibrium contact angle [31]. Within just a few years, a rapidly expanding community of researchers has taken the concept of electrowetting from the initial research stage into fully-integrated digital microfluidic devices that are capable of complex chemical and biological assays [55–57].

4.2 Theory of Electrowetting

The phenomenon of electrocapillarity (or electrowetting) was first described by Lippmann [58] in 1875 when he showed that the capillary depression of mercury in contact with an electrolyte solution could be controlled by the application of a voltage.

As well as formulating the basic theory for electrocapillarity, he also proposed several practical devices that made use of the phenomenon, including a very sensitive electrometer which was later used to record the world's first electrocardiogram (ECG). Unfortunately, the application of electrowetting to aqueous electrolytes is severely restricted due to the electrolytic decomposition of water beyond a few hundred millivolts. In the 1990s, however, Berge [59] and Vallet et al. [60] realised that the problem of electrolysis could be overcome by the introduction of a thin insulating layer to separate the conductive liquid from the metal electrode. This concept is nowadays referred to as electrowetting-on-dielectric (EWOD) [61] or electrowetting-on-insulator-coated-electrodes (EICE) [28] and involves applying a voltage to modify the wetting behaviour of a conductive liquid in contact with a hydrophobic, insulated electrode. Thorough descriptions of electrowetting have been published by Mugele and Baret [31], Berthier [62] and Berthier and Silberzan [63] whilst investigations into the types of liquids that can be transported by EWOD have been conducted by Pollack [64], Srinivasan [65] and Chatterjee et al. [66].

In most practical electrowetting applications, the droplets reside on a horizontal planar substrate and are usually composed of aqueous solutions with a typical droplet diameter of 1 mm or less. The medium surrounding the droplet can either be air or another immiscible liquid such as silicone oil. However, recent work by Brassard et al. [67] has shown that it is possible to use an alternative mode of operation where the aqueous droplet is enclosed in a thin layer of oil which in turn is surrounded by air; this technique is referred to as *water-oil core-shell* droplets.

The relative importance of the gravitational force to the surface tension force can be expressed by the Bond number [62], $Bo = \Delta\rho g R^2/\sigma_{\mathrm{lv}}$ where $\Delta\rho$ is the difference in density between the droplet and the surrounding medium, g is the acceleration due to gravity, R is the radius of curvature of the droplet, and σ_{lv} is the *liquid-vapour* surface tension. (The Bond number is sometimes referred to as the Eötvös number, *Eo*.) In most electrowetting applications, the Bond number is usually less than unity [62], implying that gravitational forces are small in comparison to the surface tension force; it is therefore appropriate to ignore gravity in electrowetting applications [31].

In the absence of an external electric field, the shape of the droplet is determined solely by the surface tension, according to standard equilibrium theory (Young's equation) [62]. As shown in Fig. 4.1a, a surface tension (a force per unit length or an energy per unit area) is associated with the interface between each of the three phases; the *solid* substrate (s), the *liquid* droplet (l) and the surrounding ambient phase, which for simplicity is often denoted as *vapour* (v). Each interface exerts a force on the three-phase contact line, and the balance between the interfacial surface tensions i.e. σ_{sv} (solid-vapour), σ_{sl} (solid–liquid) and σ_{lv} (liquid-vapour) must be in equilibrium:

$$\sigma_{\mathrm{sv}} - \sigma_{\mathrm{sl}} - \sigma_{\mathrm{lv}} \cos\theta_{\mathrm{eq}} = 0 \tag{4.1}$$

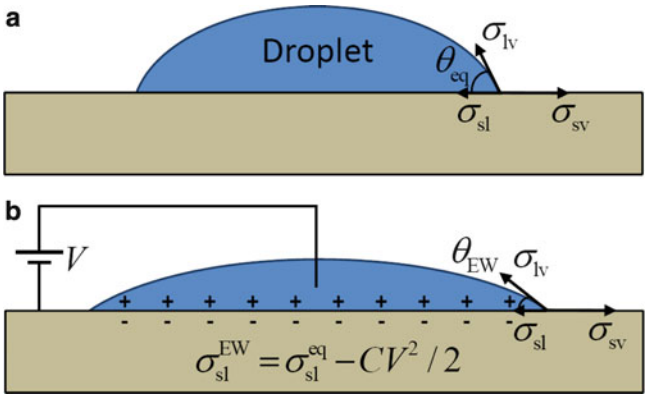

Fig. 4.1 A schematic diagram of wetting and electrowetting. (**a**) In the absence of an external electric field, the sum of the forces along the three-phase contact line must balance, leading to an equilibrium contact angle, θ_{eq}. (**b**) Application of a potential difference between the liquid and the substrate creates a capacitance, C, at the solid–liquid interface which causes the solid–liquid interfacial surface tension to be reduced by $CV^2/2$. This causes the droplet to spread and reduces the contact angle to θ_{EW}

where θ_{eq} is the *equilibrium* (or Young's) contact angle. Rearranging (4.1) yields the familiar form of Young's equation:

$$\cos\theta_{eq} = \frac{\sigma_{sv} - \sigma_{sl}}{\sigma_{lv}} \tag{4.2}$$

It should be noted that the vertical component of the surface tension force is balanced by normal stresses within the solid substrate [31].

Applying a potential difference, V, between the liquid and the substrate will change the shape of the droplet, as shown schematically in Fig. 4.1b. This is due to the fact that the solid–liquid interface effectively behaves as a parallel-plate capacitor, with a capacitance per unit area, C. The energy stored in the capacitor is $CV^2/2$ whilst the work done by the external supply voltage is $-CV^2$ and therefore the free energy of the droplet per unit interfacial area is reduced by $CV^2/2$. Application of the voltage therefore causes the solid–liquid interfacial surface tension to be reduced to $\sigma_{sl} - CV^2/2$ leading to a new force balance equation:

$$\sigma_{sv} - (\sigma_{sl} - CV^2/2) - \sigma_{lv}\cos\theta_{EW} = 0 \tag{4.3}$$

where θ_{EW} is the steady-state contact angle after the application of the *electrowetting* voltage. Combining (4.1) and (4.3) leads to the Lippmann-Young equation governing the contact angle of the droplet:

$$\cos\theta_{EW} = \cos\theta_{eq} + \frac{CV^2}{2\sigma_{lv}} \tag{4.4}$$

Equation (4.4) shows that the contact angle will decrease (i.e. the surface will become more hydrophilic) as the applied voltage increases.

Early electrowetting experiments were conducted with exposed metallic electrodes in direct contact with the conductive liquid or electrolyte. In this case, the potential difference between the liquid and electrode forms an electrical double layer at the solid–liquid interface. The specific capacitance (i.e. the capacitance per unit area) of the ionic double layer can be estimated by making the assumption that the counter-ions in the liquid are located at a fixed distance from the surface; this is sometimes referred to as the Helmholtz model [31, 62]. The specific capacitance of the electrical double layer is therefore given by

$$C_{\mathrm{H}} = \frac{\varepsilon_0 \varepsilon_{\mathrm{l}}}{\lambda_{\mathrm{D}}} \tag{4.5}$$

where ε_0 is the permittivity of free space ($\varepsilon_0 = 8.8541878 \times 10^{-12}$ F/m), ε_{l} is the relative permittivity of the conductive liquid and λ_{D} is the Debye screening length [68], typically in the nanometre range. Substituting (4.5) into the Lippmann-Young equation leads to

$$\cos\theta_{\mathrm{EW}} = \cos\theta_{\mathrm{eq}} + \frac{\varepsilon_0 \varepsilon_{\mathrm{l}} V^2}{2\lambda_{\mathrm{D}} \sigma_{\mathrm{lv}}} \tag{4.6}$$

As discussed by Mugele and Baret [31] and Berthier [62], it is sometimes necessary to modify the Lippmann-Young equation to account for the spontaneous charge which occurs when a conducting surface is immersed in an electrolyte:

$$\cos\theta_{\mathrm{EW}} = \cos\theta_{\mathrm{eq}} + \frac{\varepsilon_0 \varepsilon_{\mathrm{l}}}{2\lambda_{\mathrm{D}} \sigma_{\mathrm{lv}}} (V - V_{\mathrm{pzc}})^2 \tag{4.7}$$

where V_{pzc} is the potential difference at zero charge. Usually, the electrical double layer has a relatively high capacitance, and therefore large changes in contact angle can be achieved using relatively small applied voltages. Unfortunately, direct application of electrowetting using metallic electrodes is somewhat limited due to the electrolytic decomposition of the aqueous liquid above a certain voltage.

To overcome the problem of electrolysis, a thin dielectric layer can be used to insulate the conductive liquid from the electrode. The main advantage of EWOD over conventional electrowetting is that higher potential differences and, therefore, greater contact angle changes can be employed without any detrimental electrochemical reactions on the electrode. In addition, the surface of the microfluidic chip can be coated with highly hydrophobic compounds to enhance the contact angle changes due to electrowetting. A practical demonstration of EWOD-based actuation is shown in Fig. 4.2 [69] which illustrates the variation in the wettability of a water droplet on a Teflon surface.

With the introduction of a dielectric layer, the EWOD system is effectively composed of two capacitors in *series* with each other; namely, the capacitance due

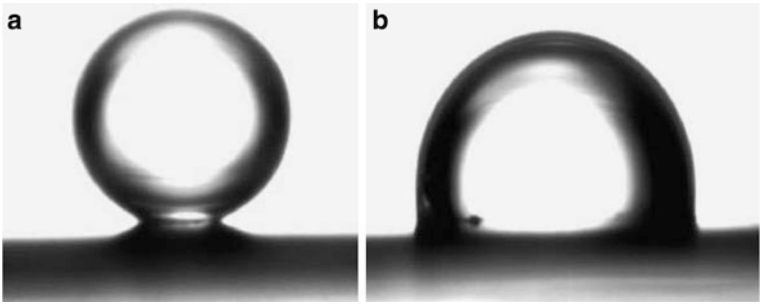

Fig. 4.2 Experimental visualisation of electrowetting clearly demonstrating the control of the contact angle: (**a**) in the absence of an external electric field, the water droplet exhibits a strong hydrophobic contact with the Teflon substrate (DuPont® AF 1600), (**b**) application of an electric potential of 80 V to the droplet causes a significant reduction in the contact angle. Reproduced from Berthier et al. [69] with kind permission from Elsevier

to the electrical double layer at the solid–liquid interface, C_H and the capacitance due to the dielectric layer, C_d which is given by

$$C_d = \frac{\varepsilon_0 \varepsilon_d}{d} \tag{4.8}$$

where ε_d is the relative permittivity of the dielectric layer and d is the thickness of the layer. Comparing (4.5) and (4.8) leads to

$$\frac{C_H}{C_d} = \frac{\varepsilon_l}{\varepsilon_d} \frac{d}{\lambda_D} \tag{4.9}$$

Since $d \gg \lambda_D$ and $\varepsilon_l > \varepsilon_d$ then $C_H \gg C_d$ i.e. the capacitance of the electrical double layer, C_H is usually much larger than the capacitance of the dielectric film, C_d. Since the capacitors are in series, the total specific capacitance, C, is given by

$$\frac{1}{C} = \frac{1}{C_H} + \frac{1}{C_d} \tag{4.10}$$

which can be approximated by $C \approx C_d$. Thus, for EWOD actuation, (4.6) is replaced by

$$\cos\theta_{EW} = \cos\theta_{eq} + \frac{\varepsilon_0 \varepsilon_d V^2}{2d\sigma_{lv}} \tag{4.11}$$

The last term on the right-hand side of (4.11) is sometimes referred to as the dimensionless electrowetting number, $\eta = \varepsilon_0 \varepsilon_d V^2/(2d\sigma_{lv}) = CV^2/(2\sigma_{lv})$ and is a measure of the relative importance of the electrostatic energy compared to the surface tension [31]. One of the disadvantages of EWOD is that the lower specific

capacitance of the dielectric layer requires significantly larger potentials to achieve a given reduction in contact angle. For example, considering a 1 μm thick dielectric layer composed of Teflon AF 1600 ($\varepsilon_d = 1.93$) with water as the conductive liquid ($\sigma_{lv} = 0.072\ \mathrm{N/m}$), gives a dimensionless electrowetting number of approximately $10^{-4}V^2$. This implies that external voltages of between 30 and 80 V [62] are required to create substantial reductions in the contact angle. One of the other disadvantages of using a dielectric layer is the fact that biomolecules can sometimes bind nonspecifically to the hydrophobic surface. Yoon and Garrell [70] have shown that biomolecular adsorption can be controlled by minimising the time during which the electrodes are switched off and also by carefully choosing the pH of the solution and the polarity of the electrodes. In addition, Luk et al. [71] have shown that low concentrations of Pluronic F127 can limit the extent of protein adsorption.

In practical EWOD applications, the substrate usually comprises of a metallic electrode, a dielectric layer (Parylene, SiO_2 or Si_3N_4) and a hydrophobic layer (spin-coated Teflon or plasma deposited SiOC). In some cases, the situation is further complicated by the fact that the dielectric layer is formed from a sandwich structure composed of $SiO_2/Si_3N_4/SiO_2$. The effective capacitance of the combined substrate (formed from n parallel layers) can be determined from the usual law for capacitors in series:

$$\frac{1}{C} = \sum_{i=1}^{n} \frac{1}{C_i} \tag{4.12}$$

The capacitance of the electrical double layer at the solid–liquid interface is usually neglected. However, direct calculation of the capacitance of the dielectric layer can sometimes be avoided by fitting the Lippmann-Young equation to experimental data of contact angle vs. applied voltage. This is usually done by plotting $(\cos\theta_{EW} - \cos\theta_{eq})$ against V^2. The gradient of the fitted line is equal to $C/(2\sigma_{lv})$ and therefore knowledge of the liquid-vapour surface tension, σ_{lv} leads to an estimate of the capacitance, C. This technique is sometimes preferred to direct computation, due to uncertainties in estimating the thickness and relative permittivities of the deposited layers.

A significant advantage of controlling the variation in the wetting angle via electrowetting, rather than by thermocapillary effects, is the speed with which the contact angle can be modified. Mugele and Baret [31] indicate switching times of typically several milliseconds, and this makes the technique potentially fast enough to be used in video display screens [72]. The manipulation and transport of droplets above a solid surface are equally as fast; velocities of between 1 and 100 mm/s have been reported [27, 29, 73, 74] while droplets have been shown to be split in less than 1 s [74]. Other potential applications for electrowetting include variable focal length liquid micro-lenses [75–77], dynamically tuneable fibre-optic devices which act as switches and waveguides [78, 79] and adaptive cooling of integrated circuits [80].

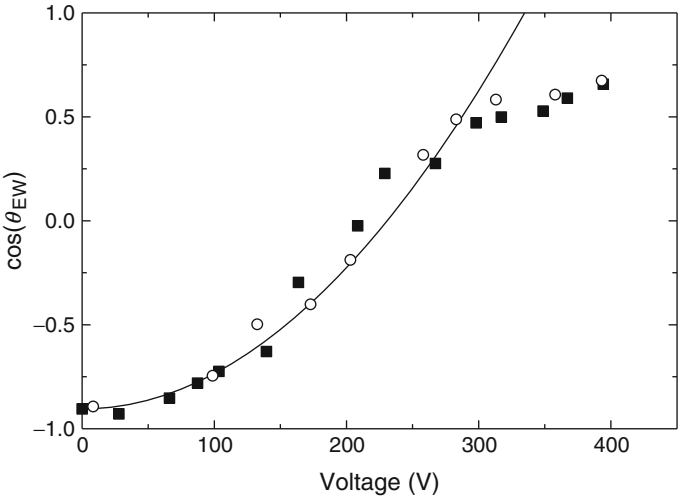

Fig. 4.3 Variation of measured contact angle vs. applied voltage for a glycerol-NaCl water droplet with silicone oil as the ambient medium and a 5 μm thick layer of Teflon AF 1601 as the dielectric. The *filled symbols* denote increasing voltage and the *open symbols* denote decreasing voltage. The *solid line* denotes the fitted parabolic variation in the value of $\cos\theta_{EW}$ as predicted by the Lippmann-Young law—(4.11). Adapted from Mugele and Baret [31] with permission from IOPscience 2005

4.2.1 Contact Angle Saturation and Dielectric Breakdown

An important observation that is common to all EWOD studies is that the contact angle variation in the Lippmann-Young equation is only valid below a critical threshold voltage, after which the electrowetting process *saturates* and the contact angle becomes independent of the applied voltage [81–84]. The essential features of contact angle saturation are illustrated in Fig. 4.3 which indicates that there is an effective upper limit to the electrowetting force, implying that it is impossible to achieve perfect wetting of $\theta_{EW} = 0$ ($\cos\theta_{EW} = 1$). However, Krupenkin et al. [85] have shown that it is possible to achieve complete wetting at voltages as low as 22 V, by using superhydrophobic nanostructured surfaces.

Although contact angle saturation is well documented [86, 87], the physical explanation for the saturation limit is not fully understood [62] and a number of different (and sometimes conflicting) theories have been developed to explain the phenomenon. Verheijen and Prins [88] have proposed that the injection of charges into the insulating layer at higher voltages causes a screening, or trapping effect, which reduces the density of the charges at the solid–liquid interface thereby weakening the electrowetting force. On the other hand, Vallet et al. [86] have explained the phenomenon by the ionisation of the air in the vicinity of the contact line. This reduces the electric charge density and prevents the electrowetting force increasing with applied voltage. However, Vallet et al.'s explanation assumes that

the droplet is surrounded by air and therefore cannot explain the occurrence of contact angle saturation when the droplet is surrounded by another liquid, such as silicone oil. Other researchers, such as Papathanasiou and Boudouvis [83], have explained the phenomenon by the presence of 'fringe' effects at the contact line. These fringe effects can increase the electric field strength in the dielectric by an order of magnitude, or more, causing breakdown in the dielectric, and leakage of electrical charge.

4.2.1.1 Modified Lippmann-Young Equation

Despite the lack of consensus as to the physical explanation for contact angle saturation, it is possible to derive a constitutive relationship for the contact angle variation in terms of the *saturation* contact angle, θ_s. At low voltages, the Lippmann-Young equation (4.4) indicates that there is a linear relationship between $\cos\theta_{EW}$ and V^2 whilst at large voltages, the contact angle asymptotes to a fixed value, θ_s. This situation is analogous to paramagnetism where the induced magnetic moment is a linear function of the magnetic field at small field strengths and asymptotes to the saturation limit at large field strengths. The work on paramagnetism was pioneered by Langevin in the early twentieth century and led directly to the so-called Langevin (or sometimes, Langevin-Debye) function, L, defined by

$$L(x) = \coth(3x) - \frac{1}{3x} \tag{4.13}$$

Berthier et al. [62, 63, 69] have shown that the Langevin function can be used to modify the standard Lippmann-Young equation to account for contact angle saturation. Firstly, the Lippmann-Young formula (4.4) is written in the following form:

$$\frac{\cos\theta_{EW} - \cos\theta_{eq}}{\cos\theta_s - \cos\theta_{eq}} = \frac{CV^2}{2\sigma_{lv}(\cos\theta_s - \cos\theta_{eq})} \tag{4.14}$$

The *modified* Lippmann-Young equation, accounting for contact angle saturation, can then be obtained by introducing the Langevin function into the right-hand side of (4.14) to give:

$$\frac{\cos\theta_{EW} - \cos\theta_{eq}}{\cos\theta_s - \cos\theta_{eq}} = L\left(\frac{CV^2}{2\sigma_{lv}(\cos\theta_s - \cos\theta_{eq})}\right) \tag{4.15}$$

Experimental evidence [69] suggests that the Langevin approximation provides a fairly accurate constitutive law for the variation of contact angle with applied electrical potential.

4.2.1.2 Dielectric Breakdown

If the electric field strength exceeds a critical value, denoted as E_{BD}, the dielectric will suddenly break down resulting in an electrically-conductive pathway through the material which degrades or even destroys the insulating properties of the dielectric layer. It is therefore necessary to ensure that the operating conditions within the EWOD system are below the critical value of the electric field strength. For a dielectric layer of thickness, d, the breakdown voltage, V_{BD} is related to the critical electric field strength, E_{BD} by

$$V_{BD} = E_{BD} d \tag{4.16}$$

Taking Teflon as an example insulator, the critical electric field strength is 60 V/μm. Thus, a 1.5 μm thick layer of Teflon should be able to withstand an applied voltage of just under 90 V. However, dielectric breakdowns are sometimes observed at voltages lower than theory would suggest; these are thought to be caused by defects in the dielectric layer or in the underlying substrate. In addition, anomalous dielectric breakdowns can occur when cells or proteins adhere to the dielectric layer [63]. In this case, geometrical inhomogeneities in the relative permittivity are thought to increase the local electric field strength causing dielectric breakdown.

The choice of dielectric thickness is crucial to the design of any EWOD system since the thickness not only affects the breakdown voltage but also the capacitance of the dielectric layer which in turn affects the dimensionless electrowetting number, η. Increasing the thickness of the dielectric layer reduces the electrowetting number which leads to larger electric potentials to achieve a given reduction in contact angle. A criterion for the dielectric thickness can be obtained by rearranging the Lippmann-Young relationship (4.11) in the following form:

$$V = \sqrt{\frac{2d\sigma_{lv}}{\varepsilon_0 \varepsilon_d}(\cos\theta_{EW} - \cos\theta_{eq})} \tag{4.17}$$

For a fixed reduction in the contact angle, it can be seen that the externally applied voltage, V, varies according to the square root of the dielectric thickness, d. However, to prevent dielectric breakdown, the thickness of the layer also needs to satisfy (4.16). Combining (4.16) and (4.17) then leads to a minimum dielectric thickness [62]:

$$d_{min} = \frac{2\sigma_{lv}}{\varepsilon_0 \varepsilon_d E_{BD}^2}(\cos\theta_{EW} - \cos\theta_{eq}) \tag{4.18}$$

If the dielectric layer is thinner than this limit, the voltage required to create the desired contact angle of θ_{EW} will cause the dielectric to break down.

4.2.2 Contact Angle Hysteresis

Experimental evidence indicates that electrowetting and thermocapillary processes exhibit dynamic hysteresis whenever the three-phase contact line is in motion [31, 62, 89, 90]. This is due to the different contact angles at the advancing and receding menisci. Increasing the applied voltage on a droplet reduces the solid–liquid interfacial surface tension, σ_{sl}, causing the droplet to spread; this situation gives rise to an *advancing* contact line. Conversely, when the voltage is decreased, the droplet will revert to its original (equilibrium) shape creating a *receding* contact line. Experimental observations indicate that, for a given electrowetting voltage, the advancing contact angle is always larger than the receding contact angle. The change in the contact angle away from the equilibrium (static) value can be defined as the *electrowetting hysteresis angle*, α. In the case of de-ionised water surrounded by silicone oil on an SiOC substrate, the hysteresis angle is typically between 1.5 and 2°. However, de-ionised water surrounded by air on a Teflon substrate has a much larger electrowetting hysteresis angle of between 7 and 9° [90]. Contact angle hysteresis can therefore have an important effect on EWOD-based droplet manipulation [91].

4.2.2.1 Minimum Actuation Potential

Contact angle hysteresis is responsible for the minimum or threshold potential that has frequently been observed when transporting droplets between different control electrodes [90]. It is informative to consider the motion of a droplet straddling two adjacent control electrodes, as shown schematically in Fig. 4.4. One of the control electrodes is assumed to be actuated whereas the other electrode is switched off. In the absence of contact angle hysteresis (i.e. $\alpha = 0$), the droplet would be able to move under the smallest of applied voltages. However, experimental evidence indicates that, in practice, the droplet will not begin to move until the electrical potential exceeds a certain threshold, $V_{\min}$. At the onset of droplet motion, the contact angle above the actuated electrode will be $\theta_{EW} + \alpha$ (i.e. an advancing contact line) whereas the contact angle above the non-actuated electrode will be $\theta_{eq} - \alpha$ (a receding contact line). The potential at the threshold of droplet motion can then be determined from the requirement that there must be a net positive electrowetting force towards the activated electrode, i.e.

$$\theta_{EW} + \alpha \leq \theta_{eq} - \alpha \Rightarrow \cos(\theta_{EW} + \alpha) \geq \cos(\theta_{eq} - \alpha) \tag{4.19}$$

This expression can be combined with the Lippmann-Young formula (4.4) to determine the minimum actuation potential, $V_{\min}$. It can readily be shown that

$$\frac{C}{2\sigma_{lv}} V_{\min}^2 = \tan\alpha[\sin\theta_{EW}(V_{\min}) + \sin\theta_{eq}] \tag{4.20}$$

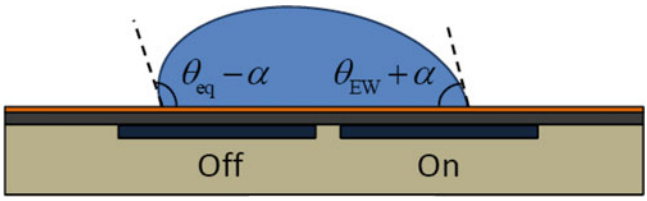

Fig. 4.4 Schematic diagram of the advancing and receding contact angles at the onset of droplet motion. Due to contact angle hysteresis, the contact angle above the actuated electrode is $\theta_{EW} + \alpha$ whilst the contact angle above the non-actuated electrode is $\theta_{eq} - \alpha$. For the droplet to move, $\theta_{EW} + \alpha < \theta_{eq} - \alpha$

Assuming V_{min} and α are small, then $\theta_{EW}(V_{min}) \rightarrow \theta_{eq}$ and (4.20) can be simplified to

$$V_{min} \approx 2\sqrt{\frac{\sigma_{lv}\alpha \sin\theta_{eq}}{C}} \tag{4.21}$$

where α is expressed in radians. It can be seen that a large dielectric capacitance, C, a large equilibrium contact angle, θ_{eq}, (i.e. a very hydrophobic surface), a small hysteresis angle, α, and a low surface tension, σ_{lv}, are desirable in order to minimise the actuation potential of the droplets.

4.2.3 AC Actuation

The theoretical descriptions of electrowetting discussed so far are applicable to the *static* conditions that occur in DC actuation. In the case of a very slowly varying AC voltage, the contact angle will follow the instantaneous value predicted by the Lippmann-Young equation. However, if the frequency of the applied AC voltage exceeds the hydrodynamic response frequency of the droplet, then the liquid will have insufficient time to adjust to the voltage variations, and the response then depends on the *time-averaged* voltage on the control electrode. (In EWOD applications involving millimetre-sized droplets, this will typically occur when the AC frequency exceeds approximately 100–200 Hz). Thus, in the case of AC droplet actuation, the voltage in the Lippmann-Young equation has to be replaced by the RMS (root-mean-square) value. As discussed by Mugele and Baret [31], the use of the Lippmann-Young equation for AC conditions is appropriate as long as the basic assumptions used to derive the equation are still valid. One of the most important assumptions is that the liquid can be treated as a perfect conductor. This is valid at low and moderate frequencies but above a critical frequency, ω_c, the liquid will start to behave as a dielectric, and the Lippmann-Young equation will begin to break down. The value of ω_c for a 10^{-4} M aqueous solution of NaCl is

of order 10^8 s^{-1} but demineralised water, for example, has a much lower value of $\omega_c \approx 4 \times 10^3$ s^{-1} [31].

AC actuation is often preferred for transporting solvents such as acetone, chloroform, dimethylformamide, ethanol, etc. since it has been found difficult or impossible to transport these liquids with DC voltages [64]. In addition, AC actuation has a number of other advantages including reduced dielectric hysteresis of the capacitance-voltage characteristics, and increased reliability by avoiding the build up of charges on the insulators. As a consequence, AC actuation has become the favoured method in most EWOD applications [14]. Actuation using a square wave is also considered a useful transport option in EWOD systems [92].

Section 4.2 has presented a brief overview of the theoretical considerations behind electro-wetting-on-dielectric actuation. In the interests of brevity, the descriptions of the underlying theory and the mathematical derivations have been kept as concise as possible. However, it is hoped that the reader will have obtained an increased awareness of the many subtleties that underpin electrowetting theory. For a more detailed description of the fundamentals of electrowetting, the reader is referred to the comprehensive review article by Mugele and Baret [31], and the appropriate chapters in Berthier [62] and Berthier and Silberzan [63]. In addition, there is now a growing volume of literature on the modelling and simulation of droplet-based electrowetting, with important work reported by Shapiro et al. [93], Zeng and Korsmeyer [94], Zeng [95], Lienemann et al. [96], Walker and Shapiro [97], Berthier et al. [69, 90], Lu et al. [98], Song et al. [99] and Clime et al. [100]. The main goal of the present chapter is to focus on the progress that has been made in the development of droplet-based electrowetting technologies for chemical and biological applications. The next section therefore discusses the various types of EWOD systems that are currently used in digital lab-on-a-chip applications.

4.3 Implementation of EWOD-Based Digital Microfluidics

EWOD-based microfluidic systems can be divided into two distinct categories depending on whether the system is open to the atmosphere or is covered. In open EWOD systems, the droplets are manipulated on a horizontal solid substrate which is exposed to the atmosphere, whereas in covered EWOD systems, the droplets are confined between two horizontal parallel plates, typically separated by a distance of between 50 and 200 μm. Each of these approaches has advantages and disadvantages. For example, it has been found that dispensing, transporting and splitting of droplets are best performed in covered EWOD systems, whereas droplet mixing and evaporation (so as to increase the concentration of the sample) are best performed in open EWOD systems [62].

Figure 4.5 illustrates a typical cross-section through a covered EWOD microfluidic chip. The lower plate of the chip contains the individual addressable electrodes and is usually fabricated from silicon or glass. The electrodes are then

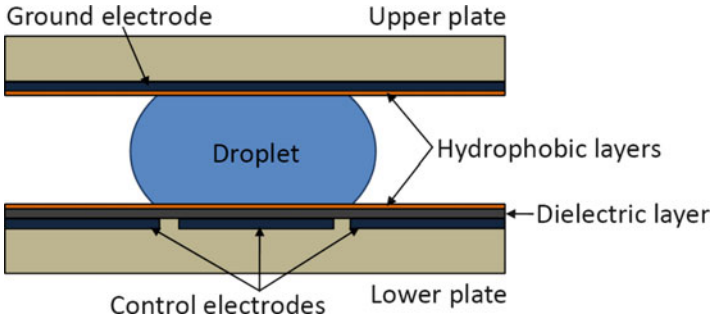

Fig. 4.5 A typical cross-section through a covered EWOD microfluidic chip

covered with a thin dielectric layer (Parylene, SiO_2 or Si_3N_4), typically about 1 μm in thickness, and finally the surface is coated with a highly hydrophobic layer (spin-coated Teflon or plasma deposited SiOC) to achieve an equilibrium contact angle larger than 90°. In closed EWOD systems, the upper confining plate usually contains a continuous electrode. Alternatively, the upper plate can be fabricated from conductive ITO (indium tin oxide) glass to provide the necessary electrical contact to the droplets. The upper plate is usually treated with the same hydrophobic coating as the lower plate, and the gap between the plates is generally filled with a silicone oil to prevent droplet evaporation and reduce surface contamination. In the case of open EWOD systems, the electrical contact to the droplets is achieved either through the use of a network of conducting wire electrodes (*catenae*) located a suitable distance above the surface of the chip [62, 69] or via the use of a *co-planar* design in which the lower plate contains both the buried activation electrodes and the contact electrodes [14, 101]. Co-planar designs have also been used successfully with closed EWOD systems; in this case, the upper conducting plate is simply replaced by a passive confining plate.

The basic concept of EWOD microfluidics is illustrated conceptually in Fig. 4.6. The chip is arranged with an array of equispaced control electrodes so that the droplets can be directed to various locations on the chip. In most applications, the electrodes are typically between 500 μm and 1 mm square, although considerable effort is currently being directed towards further miniaturisation of the technology. Sequential activation of the control electrodes creates zones of increased wettability which can be used to dispense, transport, split and merge the droplets in order to perform chemical and biological assays.

Many research groups have developed practical systems to implement EWOD-based droplet actuation. Some of the earliest demonstrations of EWOD microfluidic systems were presented by Pollack et al. [27, 29], Lee et al. [61], Moon et al. [102], Cho et al. [74], Paik et al. [103, 104] and Srinivasan et al. [105, 106]. Within a very short period of time, electrowetting technologies have developed to the point where it is now possible to conduct on-chip multiplexed assays to determine the concentration of target analytes. An example of a fully automated and integrated EWOD-based multiplexed lab-on-a-chip assay is shown in Fig. 4.7 which shows a pipelined glucose

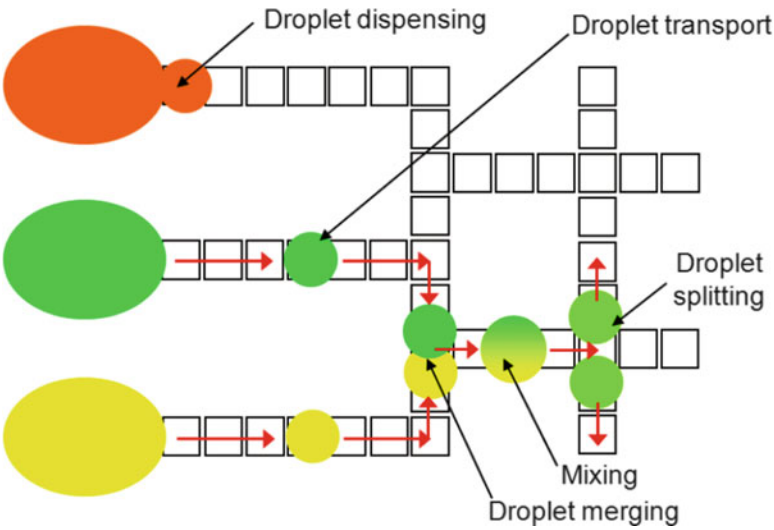

Fig. 4.6 Schematic representation of EWOD-based digital microfluidics showing each of the four main droplet handling operations: droplet dispensing, droplet transport, droplet merging and droplet splitting

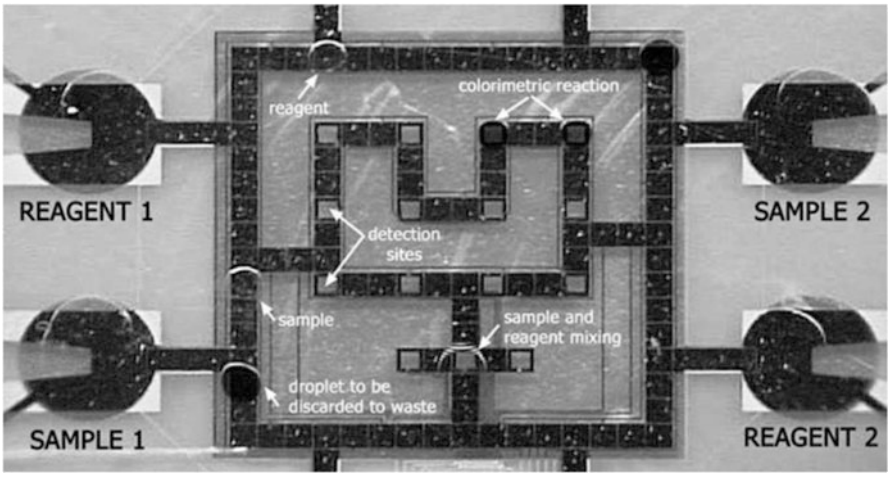

Fig. 4.7 Example of a fully automated and integrated EWOD-based system for conducting multiplexed lab-on-a-chip glucose assays. Reproduced from Srinivasan et al. [105] by permission of the Royal Society of Chemistry

assay developed by Srinivasan et al. [105]. In addition, Srinivasan et al. [107], Wheeler et al. [108] and Moon et al. [109] have demonstrated the use of EWOD-based systems for multiplexed proteomic sample preparation for high-throughput MALDI-MS (matrix assisted laser desorption/ionisation mass spectrometry).

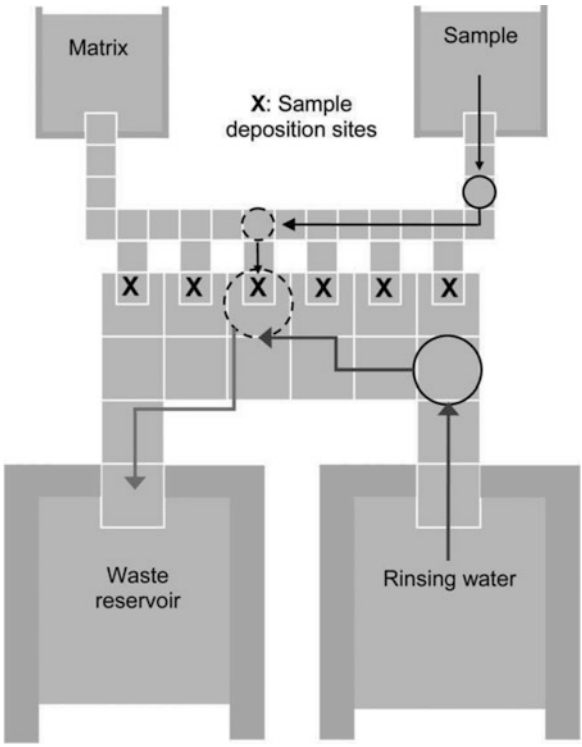

Fig. 4.8 Schematic view of an EWOD-based system for multiplexed sample preparation for MALDI-MS. Reproduced from Moon et al. [109] by permission of the Royal Society of Chemistry

Figure 4.8 shows a conceptual representation of the sample pre-treatment developed by Moon et al. [109] which consists of seven individual stages. Initially, droplets of the sample are dispensed from the sample reservoir and transported to the deposition sites where they are dried under vacuum for between 1 and 2 min. A series of water droplets are then dispensed from the rinsing water reservoir and moved over the protein deposition sites in order to remove any impurities from the samples; the rinsing droplets being discarded in the waste reservoir. Finally, droplets of 2,5-dihydroxybenzoic acid (DHB) are dispensed from the matrix reservoir and transported to the deposition sites where they are again dried under vacuum for between 1 and 2 min. After the drying stage is complete, the MALDI mass spectra can then be collected. The complex droplet handing protocols in this example serve to illustrate the huge potential of EWOD-based digital microfluidic systems for many laboratory procedures. However, one of the issues in developing fully-integrated digital microfluidic devices that can be used for chemical and biological assays is related to devising suitable protocols for the activation of the control electrodes. Some of the challenges of automating the droplet control operations in highly parallelised digital microfluidic chips have been addressed by Böhringer [110] and Griffith et al. [111].

One of the practical limitations of EWOD-based actuation is the requirement to fabricate a paved track of control electrodes beneath the surface of the microfluidic chip. In EWOD applications which require a large number of electrodes, it is

sometimes difficult to address each of the electrodes individually; this is especially the case if the electrical control circuitry is arranged on a single plane within the substrate of the chip. An elegant solution to the problem is the use of *multiplexing*, where groups of electrodes are attached to the same electrical control line. Multiplexing is particularly efficient for high-throughput parallel applications where the same droplet manipulation sequence is simultaneously performed on a large number of droplets. However, in some EWOD applications, there may be specific requirements to address all the electrodes separately. In this case, the control circuits need to use multiple conducting layers as found in IC (integrated-circuit) technologies. Gascoyne et al. [112] demonstrated the feasibility of individually addressing a large number of electrodes with a 32×32 programmable element dielectrophoresis chip based on CMOS (complementary metal-oxide-semiconductor) technology. More recently, Li et al. [113] have reported the integration of EWOD actuation on a standard CMOS chip. In addition, Gong and Kim [114] have investigated the use of EWOD-based systems fabricated from low-cost multilayer PCB (printed circuit board) substrates. Four different PCB post-processing methods were investigated, resulting in PCB-EWOD devices with varying degrees of performance and fabrication cost. The droplet handling operations on the best performing PCB substrate were found to be comparable to those on polished glass or silicon, making the PCB-EWOD approach valid for low-cost/disposable applications. A number of highly innovative, low-cost microfabrication approaches have also been developed by Abdelgawad and Wheeler [115, 116]. These enable EWOD systems to be manufactured without the use of specialist photolithographic and vapour deposition equipment, thus increasing the accessibility of EWOD technologies.

One of the most important parameters in EWOD devices is the voltage required to manipulate the droplets. Early EWOD applications typically required control voltages in the region of 80–100 V. However, by carefully selecting a dielectric material with a high relative permittivity, ε_d (both barium strontium titanate or bismuth zinc niobate appear to be very promising materials in this respect), and by carefully controlling the thickness of the dielectric layer, control voltages can be substantially reduced. This is enormously beneficial in EWOD applications due to the difficulties of implementing high-voltage CMOS technologies. The use of better dielectric materials has enabled EWOD-based droplet actuation to be reduced below 15 V in some applications [113].

Considerable effort is currently being directed towards improving the properties of the hydrophobic layer in order to create as large an equilibrium contact angle as possible. One of the most promising techniques for creating superhydrophobic surfaces is to pattern the substrate with nanostructured pillars [117]. Verplanck et al. [118] have studied a variety of wettability switching technologies for superhydrophobic surfaces, and have concluded that electrowetting droplet actuation is still the most promising approach compared to other control techniques such as optical, mechanical or thermal switching. However, electrowetting on superhydrophobic surfaces is still in its infancy and there are a number of problems to be overcome associated with the non-reversibility of the EWOD effect [62]. Another promising area for EWOD-based digital microfluidics is the development

of *all-terrain droplet actuation* (ATDA) [119] which removes the requirement to perform the droplet manipulation on a single horizontal plane. ATDA has been demonstrated for a wide range of non-planar geometries including inclined, vertical, twisted and upside-down surfaces and is a powerful technique that will enable the development of three-dimensional EWOD microfluidic systems, by stacking multiple layers on top of each other. In addition, ATDA should allow EWOD-based devices to be readily integrated into other microfluidic technologies. For example, Abdelgawad et al. [120] have recently demonstrated a hybrid device that integrates digital microfluidics and microchannels on the same substrate. This is an important step towards fully-integrated lab-on-a-chip systems for automatic sample processing and separation. Furthermore, Fan et al. [121] have demonstrated that ATDA technologies can be used to manipulate droplets against gravity around a flexible 8-in. (203 mm) long curved pathway, opening up the possibility of EWOD-based 'droplet-on-a-wristband' technologies for point-of-care applications.

4.4 Droplet Manipulation Using EWOD

The success of any microfluidic assay employing EWOD actuation relies crucially on the accuracy of the on-chip droplet handling operations which need to be precise, in terms of the volumes of the droplets produced, and repeatable over many operating cycles. It is therefore informative to consider each of the fundamental unit droplet operations in detail. However, before discussing the underlying theory and practical issues related to droplet manipulation, it is useful to assess the relative importance of the various forces that affect the droplets in EWOD devices.

4.4.1 Dimensional Considerations

In Sect. 4.2, the relative importance of the gravitational force to the surface tension force was shown to be expressed by the Bond number, Bo. In most electrowetting applications, the Bond number is usually less than unity, implying that gravitational forces are small in comparison to the surface tension forces. However, when dealing with droplets in motion, it is necessary to consider additional forces acting on the droplet, including the electrowetting, viscous and inertial forces. As previously discussed in Sect. 4.2, the strength of the electrowetting effect can be expressed by the dimensionless electrowetting number, $\eta = CV^2/(2\sigma_{\mathrm{lv}})$. In addition, the ratio between the viscous force and the inertial and surface tension forces in a droplet can be expressed by the non-dimensional Ohnesorge number, Oh [69]:

$$Oh = \frac{\mu}{\sqrt{\rho l \sigma_{\mathrm{lv}}}} \tag{4.22}$$

where μ is the dynamic viscosity of the liquid and l is the characteristic dimension of the droplet. Above a critical Ohnesorge number, $Oh_{\text{crit}} \approx 0.03$ [62], viscosity is found to play an important role in droplet handling operations. Considering a typical EWOD application using millimetre-sized droplets of water gives $\mu = 10^{-3}$ Ns/m^2, $\rho = 1,000$ kg/m^3, $l = 0.001$ m and $\sigma_{\text{lv}} = 0.072$ N/m—yielding an Ohnesorge number, $Oh \approx 4 \times 10^{-3}$ which is an order of magnitude less than the critical value of 0.03. This indicates that the effects of the viscosity of the liquid are generally quite small in most EWOD applications. However, it should be noted that in certain applications, involving highly viscous ionic liquids, the Ohnesorge number may exceed the critical value and the resulting droplet motion will then be significantly damped by the viscous forces.

It is also necessary to consider the ratio between the inertial and surface tension forces which can be determined from the non-dimensional Weber number, We [69]:

$$We = \frac{\rho v^2 l}{\sigma_{\text{lv}}} \tag{4.23}$$

where v is the velocity of the droplet. Above a critical Weber number, $We_{\text{crit}} \approx 1.1$ [62] the droplet will start to become distorted by the inertial forces and droplet break-up is a strong possibility [122]. Again, it is useful to consider the Weber number for typical EWOD applications involving millimetre-sized droplets. Experimental evidence indicates that droplet transport is relatively fast with typical transit times of order 20 ms to move a droplet between two adjacent electrodes spaced 800 μm apart [69]. This gives a characteristic velocity of approximately 0.04 m/s and leads to a Weber number (for a 1 mm diameter droplet) of $We = 0.022$ which is well below the critical value. Inertial effects are therefore relatively unimportant in most EWOD systems. However, in certain applications, surfactants are added to the liquid in order to allow easier spreading and splitting of the droplets. The addition of a surfactant reduces the liquid-vapour interfacial surface tension [123] and therefore increases the Weber number, making droplet distortion more likely.

The analysis of droplet motion often makes use of two further dimensionless numbers; the capillary number, Ca and the Reynolds number, Re. The capillary number expresses the ratio between the viscous and surface tension forces and is defined as

$$Ca = \frac{\mu v}{\sigma_{\text{lv}}} \tag{4.24}$$

However, the capillary number can be written in terms of the Ohnesorge and Weber numbers: $Ca = Oh\sqrt{We}$ and therefore the capillary number is not strictly an independent dimensionless parameter. Similarly, the Reynolds number expresses the ratio between the inertial and viscous forces and is defined as

$$Re = \frac{\rho v l}{\mu} \tag{4.25}$$

The Reynolds number can be also written in terms of the Ohnesorge and Weber numbers using the relationship: $Re = \sqrt{We}/Oh$. Consequently, EWOD-induced droplet handling is usually classified in terms of the Ohnesorge and Weber numbers.

4.4.2 Droplet Transport

Droplet motion in EWOD systems is carried out by sequentially activating the buried control electrodes one-at-a-time in order to set up suitable surface tension gradients on the surface of the microfluidic chip. This causes the droplets to move incrementally between neighbouring electrodes in accordance to changes in the electrowetting force. Since the Weber number in most EWOD applications is relatively low, the inertial forces acting on the droplets are generally small. Thus, the droplets will respond quickly to any changes in the electrowetting force and will rapidly accelerate up to a steady velocity before finally decelerating again once the droplets reach the target electrode. However, as discussed in Sect. 4.2.2.1, droplet motion can only be induced once the applied voltage exceeds a certain threshold voltage, $V_{\min}$, due to contact angle hysteresis. In practice, the threshold voltage can be reduced by immersing the droplets in silicone oil although the magnitude of the reduction in the threshold voltage has been found to depend on both the viscosity of the silicone oil as well as the viscosity of the liquid in the droplets [64]. Alternatively, simply exposing the surface of the chip to silicone oil and then drying has also been found to be effective at reducing the threshold voltage [64].

The droplet transport velocity is found to depend on the magnitude of the applied electrowetting force, as well as many other factors including the viscosity of the liquid, the electrowetting hysteresis angle and, in the case of covered EWOD systems, the separation distance between the upper and lower plates of the chip. An estimate of the maximum (steady-state) velocity of the droplet can be obtained by considering a simple force balance between the electrowetting force causing the motion and the viscous damping force due to the shear stress along the surface of the chip. In the case of covered EWOD systems, Berthier [62] has shown that the droplet velocity can be approximated by

$$v \approx \frac{h\sigma_{\mathrm{lv}}}{6\pi\mu r}\left(\cos\theta_{\mathrm{a}} - \cos\theta_{\mathrm{r}}\right) \tag{4.26}$$

where h is the separation between the upper and lower plates, r is the radius of the droplet in the horizontal plane, and θ_{a} and θ_{r} are the contact angles at the advancing and receding contact lines, given by $\theta_{\mathrm{a}} = \theta_{\mathrm{EW}} + \alpha$ and $\theta_{\mathrm{r}} = \theta_{\mathrm{eq}} - \alpha$, respectively. If the actuation voltage is less than the saturation voltage, and assuming that contact

angle hysteresis is small, then the Lippmann-Young equation can be substituted into (4.26) to obtain

$$v \approx \frac{h}{12\pi\mu r} CV^2 \tag{4.27}$$

indicating that the droplet velocity varies with the square of the applied voltage. Repeating the analysis using the modified Lippmann-Young equation (4.15) which accounts for contact angle saturation, leads to

$$v \approx \frac{h\sigma_{\mathrm{lv}}}{6\pi\mu r}(\cos\theta_{\mathrm{s}} - \cos\theta_{\mathrm{eq}})L\left(\frac{CV^2}{2\sigma_{\mathrm{lv}}(\cos\theta_{\mathrm{s}} - \cos\theta_{\mathrm{eq}})}\right) \tag{4.28}$$

where L is the Langevin function. Similar expressions to (4.26) and (4.27) can be derived for open EWOD systems, giving [62]:

$$v \approx \frac{4H\sigma_{\mathrm{lv}}}{5\pi\mu r}(\cos\theta_{\mathrm{a}} - \cos\theta_{\mathrm{r}}) = \frac{2H}{5\pi\mu r} CV^2 \tag{4.29}$$

where H is the maximum height of the droplet above the surface of the chip. The dynamics of EWOD-based droplet transport have been considered by a number of investigators including Ren et al. [124], Bahadur and Garimella [125], Chakraborty and Mittal [126], Baird et al. [127], Bavière et al. [128], Ahmadi et al. [129], Chatterjee et al. [130] and Song et al. [99].

4.4.2.1 Geometry of the Electrodes

Section 4.4.2 has shown how droplets can be transported across the substrate of a microfluidic chip using an incremental displacement from one electrode to the next. Ideally, the control electrodes should be placed as close as possible to each other in order to minimise the gap between the electrodes. Unfortunately, the method of fabrication often places a restriction on the proximity of the electrodes which usually have to be separated by a gap of between 10 and 30 μm, depending on the precision of the manufacturing process. The separation gap effectively creates a permanent hydrophobic halo around each electrode which can cause difficulties when trying to move a droplet to an adjacent electrode. This is especially the case in covered EWOD systems where the droplets are usually similar in size to the control electrodes. If a droplet comes to rest entirely within the perimeter of a single electrode, it becomes impossible to transport it any further, and the droplet is left permanently stranded or 'pinned' at the location.

An ingenious solution to the problem of droplet pinning is to incorporate jagged or crenellated edges around each of the electrodes, as shown in Fig. 4.9. The use of crenellated or inter-digitated electrodes ensures that at least part of the droplet

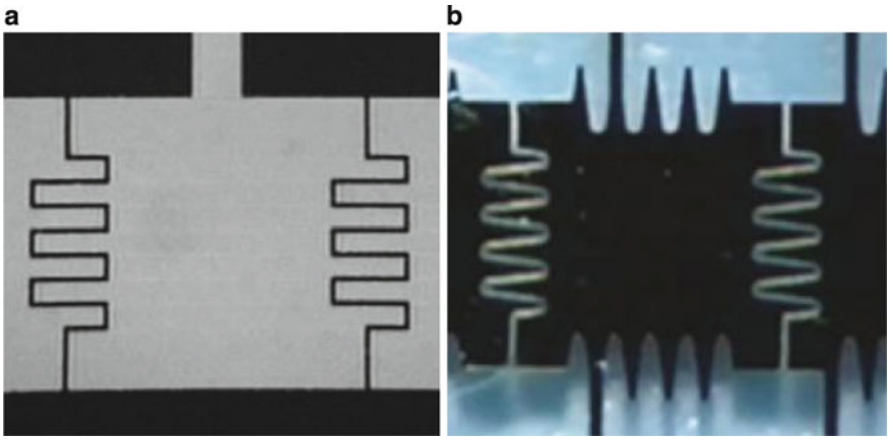

Fig. 4.9 Examples of crenellated and jagged electrode design. Reproduced from (**a**) Moon and Kim [132] with permission from Elsevier and (**b**) Pollack et al. [29] with permission from the Royal Society of Chemistry

extends onto the neighbouring electrode, thereby avoiding the problem of droplets becoming stranded. Clearly, the use of crenellations introduces additional complexity into the fabrication process but experimental evidence has shown that it is a very effective design strategy for aiding droplet motion. However, for the technique to be effective, the geometry and dimensions of the indentations have to be carefully selected. Berthier and Peponnet [131] have developed a detailed mathematical criterion that can be used to assess the effectiveness of the indentations, using the assumption that the crenellated edge can be approximated by a sinusoidal boundary. The effectiveness of the indentations can be found from the value of the function, G:

$$G(\lambda, e, \delta, n) = \frac{\lambda/e}{\delta/e + [\theta_1/\theta_2 - 1]/\pi n} \tag{4.30}$$

where λ is the size of the indentations, e is the width of the electrode, δ is the separation gap between the electrodes, n is the total number of indentations along one side of an electrode and θ_1 and θ_2 are the contact angles on the non-activated and activated electrodes, respectively. It should be noted, however, that not all EWOD applications make use of inter-digitated electrodes; a simple alternative is to ensure that the droplets are sufficiently large so that they always extend onto the adjacent electrodes.

4.4.3 Droplet Splitting and Merging

Splitting and merging are important droplet handling operations that are found in almost all EWOD applications. The basic principle of droplet splitting is illustrated

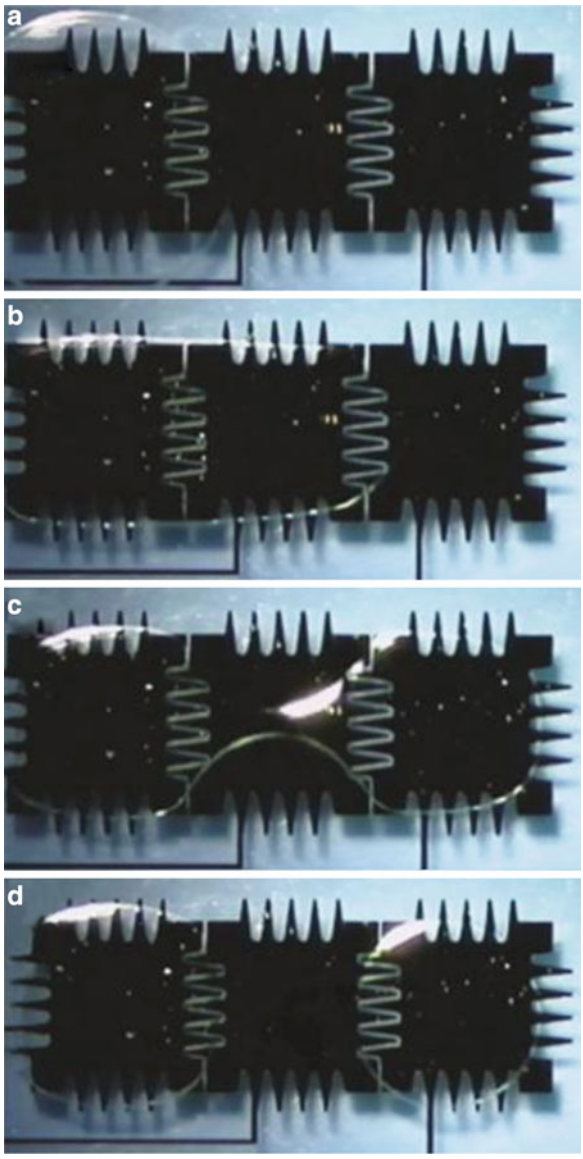

Fig. 4.10 Time-lapse sequence of images showing the successful splitting of a 900 nL droplet of 0.1 M KCl into two equal-sized daughter droplets in a covered EWOD system. Initially, only the left-hand electrode is energised (**a**). The middle electrode is then activated (**b**) and, after a short time delay, the voltage is switched from the middle to the right-hand electrode (**c**) resulting in division of the droplet (**d**). The electrodes are spaced at a pitch of 1.5 mm and the plate separation distance is 300 μm. The droplet is surrounded by 1 cSt silicone oil. Reproduced from Pollack et al. [29] by permission of the Royal Society of Chemistry

in Fig. 4.10 and involves three electrodes as described by Pollack et al. [29]. During the splitting process, the outermost electrodes are activated which reduces the contact angle. This creates two hydrophilic zones that stretch the droplet in the longitudinal direction. At the same time, the non-actuated central electrode is a hydrophobic region which tends to exert a 'pinching' force on the droplet which causes the neck of the droplet to split. In practice, splitting is very difficult to achieve in open EWOD systems since the droplet tends to 'escape' to one of the

hydrophilic electrodes. However, droplet splitting is feasible in covered EWOD systems, provided the plate separation distance is sufficiently small. By considering the pressure difference inside the droplet due to the different surface curvatures above the hydrophilic and hydrophobic electrodes, it is possible to show that for a square electrode of dimension, e, an approximate criterion for the maximum plate separation is given by [69]:

$$\frac{h_{\max}}{e} = -\cos\theta_{\text{eq}} \tag{4.31}$$

where it is assumed that the equilibrium contact angle, θ_{eq}, is larger than 90° so that $\cos\theta_{\text{eq}}$ is negative. Taking a typical EWOD system with a hydrophobic contact angle of $\theta_{\text{eq}} = 110°$ and 1 mm^2 electrodes, implies that the vertical separation of the plates should not exceed 340 μm. In practice, however, the plate separation is usually between 50 and 150 μm for 1 mm^2 electrodes.

A criterion for droplet splitting has been developed by Cho et al. [74] using Laplace's theorem [19, 31] to estimate the pressure within the droplet. Assuming that the principal radii of curvature of the droplet above the hydrophobic and hydrophilic electrodes are R_1 and R_2, respectively, then it can be shown that droplet splitting will occur when

$$\frac{R_2}{R_1} = 1 - \frac{R_2}{h}(\cos\theta_2 - \cos\theta_1) \tag{4.32}$$

where θ_1 and θ_2 are the contact angles on the non-activated (hydrophobic) and activated (hydrophilic) electrodes, respectively. The cutting operation is initiated by a pinching process in the middle of the droplet, yielding a concave contact line and a negative value of R_1. This condition can be achieved either by having a large value of $(\cos\theta_2 - \cos\theta_1)$ due to the electrowetting process, or by employing a small plate separation distance, h. It is interesting to note that the contact angle along the upper plate of the EWOD system does not affect the droplet splitting process. Neglecting contact angle hysteresis, then $\theta_1 = \theta_{\text{eq}}$ and $\theta_2 = \theta_{\text{EW}}$. The droplet splitting criterion can be then found by substituting the Lippmann-Young expression (4.11) into (4.32) to yield:

$$\frac{R_2}{R_1} = 1 - \frac{R_2}{h}\frac{\varepsilon_0\varepsilon_{\text{d}}V^2}{2d\sigma_{\text{lv}}} \tag{4.33}$$

The radius of curvature above the hydrophilic electrode, R_2, can be approximated from the size of the control electrode, e. At the point of droplet splitting $|R_1|$ is usually much larger than $|R_2|$ and hence the voltage required to split the droplet can be determined from (4.33). Recently, Song et al. [99] have presented a more detailed criterion for droplet splitting, based on the critical capillary number for droplet break-up, $Ca_{\text{crit}} \approx 10^{-3}$. In practice, the voltage required to split a droplet can also be determined by CFD (computational fluid dynamics) simulations.

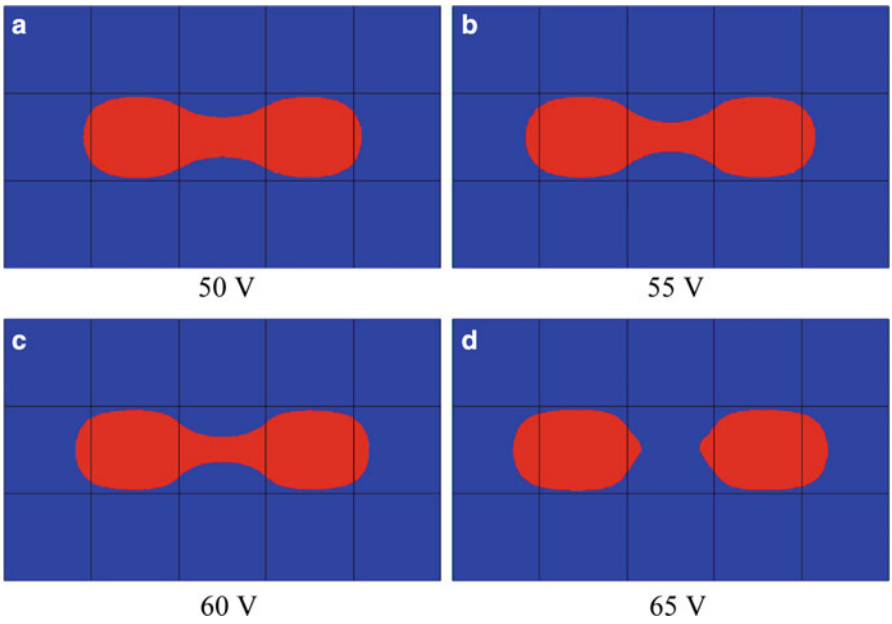

Fig. 4.11 Simulation of droplet splitting in a covered EWOD system using the commercial computational fluid dynamics (CFD) solver, CFD-ACE+ [133]. The images show the maximum elongation of the droplet as a function of applied voltage: (**a**) 50 V, (**b**) 55 V, (**c**) 60 V, (**d**) 65 V. Below a critical threshold voltage, the droplet fails to split

As an example, Fig. 4.11 shows the results of a simulation using the commercial CFD software tool, CFD-ACE+ [133]. The simulations allow the determination of the minimum actuation voltage for droplet splitting.

The merging of droplets in EWOD systems is an important handling operation since it enables the dilution of samples/reagents. For example, merging a sample droplet of concentration, C, with a buffer droplet of equal volume results in a droplet of twice the volume but with a concentration of $C/2$. Splitting this droplet then yields two droplets of concentration, $C/2$. By repeating this process of merging and then splitting the diluted droplets yields an exponential dilution of 2^N after N steps. Fortunately, the merging of droplets is relatively straightforward in EWOD systems and simply involves displacing the two droplets using electrowetting onto a common electrode. For applications involving aqueous liquids, the droplets generally coalesce very quickly due to the relatively high surface tension of water. However, the speed of coalescence is found to be reduced at higher Ohnesorge numbers.

One of the most challenging aspects when merging droplets is to ensure that the combined droplet is adequately mixed afterwards. This is especially important if the merging operation is part of a dilution assay. Droplet mixing is best performed in open EWOD systems since the presence of the confining plate in covered EWOD devices tends to suppress the natural droplet oscillations during the

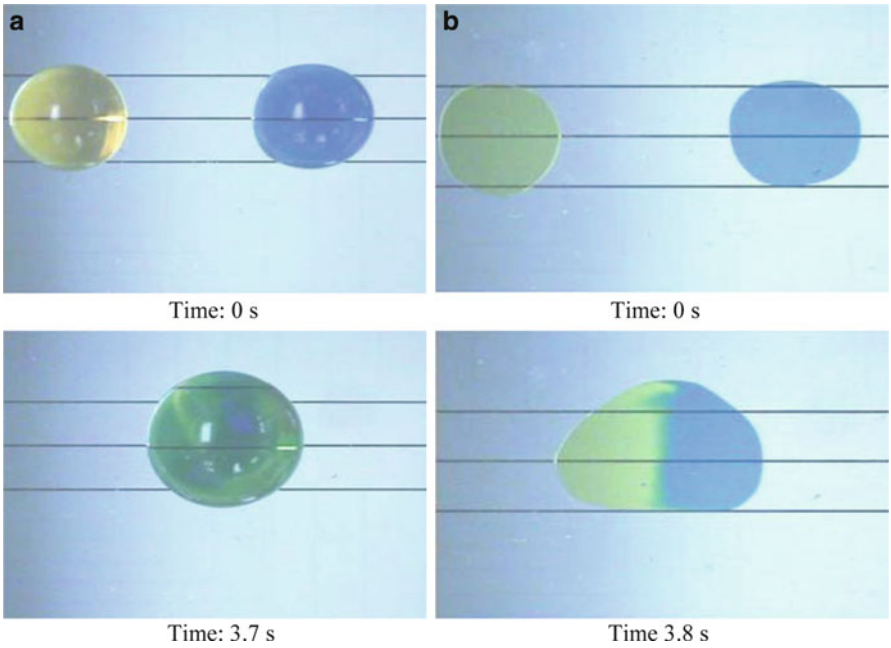

Fig. 4.12 Comparison of the mixing behaviour of two identically-sized droplets in an open EWOD system (**a**) and a covered EWOD system (**b**). Reproduced from Cooney et al. [134] with kind permission of Springer Science and Business Media

coalescence stage, thereby slowing the mixing processes [134]. The relatively poor mixing behaviour in covered EWOD systems is demonstrated in Fig. 4.12 which shows an experimental visualisation of the mixing following two identical droplet merging operations using an open and a covered EWOD system. Paik et al. [103, 104] have investigated a number of strategies to overcome the lack of mixing in covered EWOD systems. One possible remedy is to 'shuttle' the merged droplet backwards and forwards several times along a row of electrodes; the repeated changes in direction tend to increase the level of mixing inside the droplet. Alternatively, successive merging and splitting of the same droplet is also found to aid the mixing process. Another mixing strategy that is sometimes favoured is to transport the droplet in a looped motion, around a 2×2 or 2×4 array of electrodes, to promote a simultaneous stretching and folding motion in the liquid [104].

The success of any dilution study using repeated merging and splitting depends crucially on the reproducibility of the droplet volumes. The conventional 'three electrode splitting procedure', as described by Cho et al. [74], can lead to relatively large errors in the volumes of the individual droplets [14]. This in turn leads to significant errors in the accuracy of the dilution assay. To enhance the uniformity of the droplet splitting procedure, Ren [135] developed a novel electrode design which automatically aligns the droplet at the centre of the electrode. The design replaces

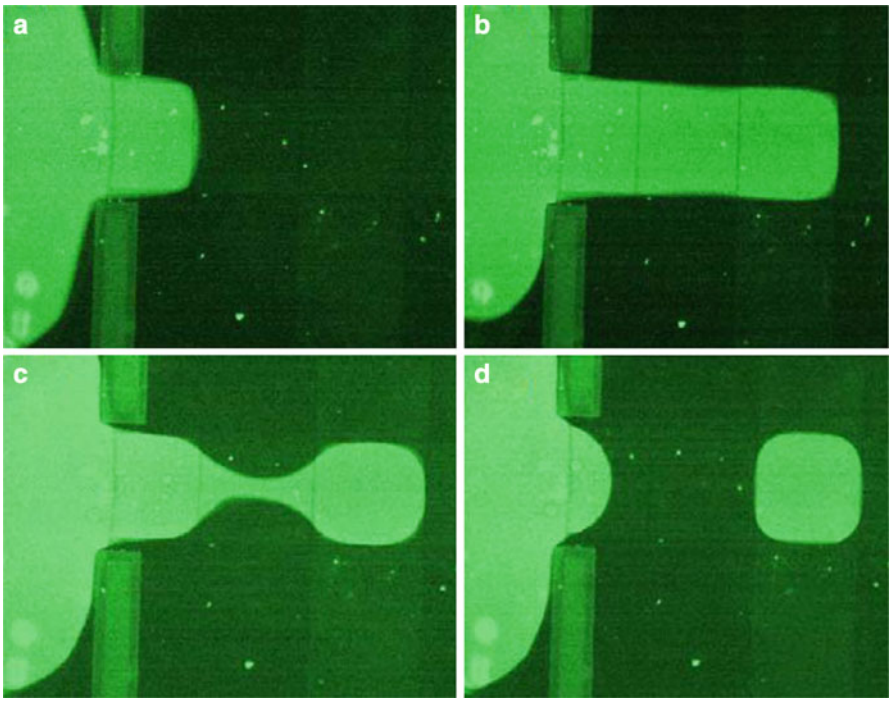

Fig. 4.13 Visualisation of droplet dispensing from a reservoir. The time-lapse sequence shows fluid being drawn out of the reservoir by activating the control electrodes immediately adjacent to the reservoir (**a, b**), the deactivation of the voltage on the 'cutting' electrode (**c**) and the 'back-pumping' stage (**d**). Reproduced from Berthier et al. [69] with kind permission from Elsevier

the single central electrode by three specially-shaped electrodes [14] that help guide the droplet into the correct symmetrical position. After droplet alignment, conventional side electrodes are then activated to complete the splitting process.

4.4.4 Droplet Dispensing

Droplet dispensing or droplet creation is the process of dividing a larger volume of liquid into smaller droplets that are suitable for manipulation within the EWOD system. As pointed out by Fair [14], droplet dispensing is one of the most crucial procedures in EWOD applications because it represents the interface from the macroscopic outside world to the microfluidic world within the chip. A typical droplet dispensing procedure is illustrated in Fig. 4.13 and is usually composed of three individual steps. Initially, the liquid is extruded from the reservoir by activating a number of electrodes to create a hydrophilic region that draws fluid out of the reservoir (see Fig. 4.13a, b). The extrusion of liquid is assisted by switching off the electrode(s) under the reservoir, creating a hydrophobic region

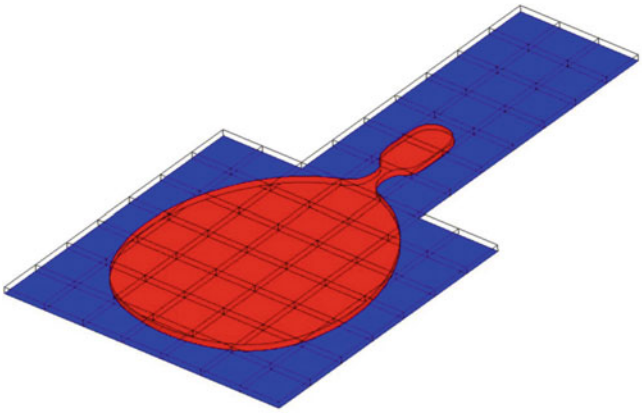

Fig. 4.14 Simulation of droplet dispensing from a reservoir using the commercial CFD solver, CFD-ACE+ [133]. The image shows the 'back-pumping' stage when the control electrode under the reservoir has been reactivated to reduce the pressure in the droplet in order to aid the cutting process

that tends to push fluid out of the reservoir. Once the extruded 'finger' of liquid has reached the electrode where the droplet is to be created, the voltage is deactivated on the 'cutting' electrode, causing a pinching effect as illustrated in Fig. 4.13c. In some applications, this pinching step is sufficient to create the droplet. However, a 'back-pumping' stage [62, 69] is sometimes used to assist the droplet formation process; this consists of reactivating the control electrode(s) under the reservoir to create either a hydrophilic ($\theta_{EW}<90°$) or a neutral ($90°<\theta_{EW}<95°$) contact angle. This reduces the pressure within the liquid which enhances the pinching effect, causing the droplet to detach from the main body of liquid. A detailed mathematical analysis of the criterion required for droplet detachment has been presented by Fair [14] and Song et al. [99]. Alternatively, the voltage required to draw liquid out of the reservoir and the voltage required for the back-pumping stage can be determined from CFD simulations. As an example, Fig. 4.14 shows the results of a numerical simulation using CFD-ACE+ [133] for determining the contact angle (and hence the required voltage) in the reservoir during the back-pumping stage. Experimental evidence and numerical simulations show that the magnitude of the surface tension, σ_{lv}, has very little effect on the droplet dispensing process [62, 69]. Instead, the main factor affecting the successful creation of droplets is the aspect ratio of the electrode size to plate separation distance, e/h. Droplet dispensing becomes easier as the value of e/h increases and it has been found that droplets can be created using a single cutting electrode when the ratio is larger than about six [14]. In some applications, the dispensing process can be assisted by incorporating a plastic wall to separate the reservoir from the main part of the fluidic chip [62, 69], as shown in Fig. 4.13.

EWOD microfluidic chips generally have a minimum of three reservoirs; one containing the sample, one for the reagent and the third for collecting the waste droplets once they have been analysed. In some applications, additional reservoirs

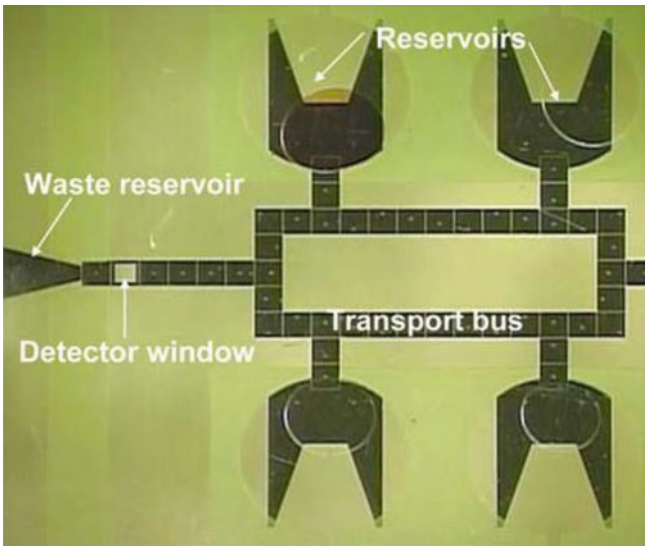

Fig. 4.15 An example of an EWOD multiplexed assay chip developed by Srinivasan [65] which contains one sample reservoir, one waste reservoir and three reagent reservoirs. Reproduced from Fair [14] with kind permission of Springer Science and Business Media

are needed to store a range of calibration solutions. An example of the layout of reservoirs on a typical EWOD system is shown in Fig. 4.15. One of the critical parameters affecting the overall reliability of EWOD systems is the shape of the electrode under the reservoir. This is important because the volume of liquid in the reservoir progressively decreases each time a droplet is dispensed. It is essential to ensure that the droplet in the reservoir is always in contact with the first working electrode along the dispensing track, otherwise the droplet creation mechanism will fail. One of the most popular designs for the reservoir electrode involves a tapered shape, as shown in Fig. 4.15. The tapered geometry is able to guide the droplet automatically into the correct position at the start of the dispensing track. In other applications, star-shaped electrodes have been found to be particularly effective at centralising the reservoir droplet at a predetermined location on the chip [69].

Section 4.4 has reviewed the fundamental EWOD droplet handling operations that are used in digital microfluidic systems. The final section of this chapter discusses how these individual operations can be integrated together to enable complex biological and chemical assays to be performed.

4.5 Chemical and Biological Applications of EWOD

One of the most common application areas for digital EWOD-based microfluidics is determining the concentration of target analytes in multiplexed assays, where multiple analytes are detected in a single sample. The fluidic steps usually involve

the following operations: (1) loading of the sample and reagents into the reservoirs, (2) dispensing droplets of the sample and reagent, (3) transport of the droplets to other parts of the chip, (4) mixing the sample and reagent droplets together, and (5) detection of the reaction products, either in-situ or remotely. In some applications, sample dilution, sample purification and particle separation may also be required. In most EWOD systems, the droplets containing the sample and the reagents, by necessity, have to be transported along the same fluidic tracks and consequently, there is potential for cross-contamination of the droplets. Experience has shown that non-biological electrolytes can be transported relatively easily, in both air and silicone oil, without cross-contamination being a major issue. However, the transport of droplets containing proteins, enzymes or human physiological fluids is more problematic due to the fact that biomolecules can sometimes bind nonspecifically to the hydrophobic layer, thus contaminating the surface of the chip. To avoid bio-fouling, silicone oil is normally used to isolate the droplet from the surface of the chip. In addition, proteins such as bovine serum albumin or casein are sometimes added to biological samples to reduce the level of nonspecific binding [62] while biocompatible surfactants such as Pluronic F127 can also be used to the limit the extent of protein adsorption [71]. Furthermore, experience suggests that the voltages required to perform the fundamental EWOD droplet handling operations are generally higher when the droplets contain biological macromolecules, proteins, cells or whole blood [62]. Despite these difficulties, a wide range of EWOD-based technologies have been developed. This section attempts to highlight some of the possible application areas in chemistry and biology.

4.5.1 EWOD-Based Glucose Assay

One of the first successful EWOD-based lab-on-a-chip devices for performing multiplexed assays was developed by Srinivasan et al. [105, 106] for determining the concentration of glucose in human physiological fluids. The device has already been illustrated in Fig. 4.7 of Sect. 4.3, and is based on a colorimetric enzyme-kinetic method based on Trinder's reaction [136]. The microfluidic device consists of fluid injection ports, reservoirs for the sample and reagents, fluidic tracks for droplet transport, an area for droplet mixing, and optical detection sites which use light-emitting-diodes (LEDs) and photodiodes to measure the absorbance of the sample. The glucose assay is performed as follows: droplets of the sample and reagent are dispensed from the appropriate reservoirs and then merged and mixed by shuttling the combined droplet across three electrodes for 15 s at a frequency of 8 Hz. After mixing, the droplet is then transported to the detection site where a photodiode measures the absorbance of the droplet at a wavelength of 545 nm for 30 s. The device is thus able to measure the concentration of glucose in less than 60 s and repeated measurements on the same sample concentration reveals changes in the measured concentration of less than 2%, indicating minimal variation in the

volumes of the droplets. Cross-contamination was avoided by filling the chip with silicone oil which effectively isolates the droplets from the Teflon AF hydrophobic layer.

4.5.2 EWOD-Based TNT Assay

Pamula et al. [137] have demonstrated the use of EWOD-based microfluidics for detecting nitroaromatic compounds such as commercial-grade 2,4,6-trinitrotoluene (TNT) or 2,4-dinitrotoluene (DNT). The most widely-accepted solvents for performing TNT analyses include acetone, acetonitrile or methanol. Unfortunately, none of these solvents are compatible with oil-based EWOD systems since they are miscible with silicone oil. To overcome this difficulty, Pamula et al. used dimethyl sulfoxide (DMSO) as the solvent since this dissolves nitroaromatic compounds whilst being immiscible with silicone oil. The basis of the assay involves reacting TNT or DNT with potassium hydroxide (KOH) to form coloured Jackson-Meisenheimer complexes [138] which can easily be detected on the chip using optical measurements in the UV and visible parts of the spectrum. Since the coloured complexes formed by reacting TNT and DNT with KOH are mutually independent, the assay is able to measure the concentration of TNT in the presence of DNT. The microfluidic chip developed by Pamula et al. was found to be capable of detecting TNT concentrations down to approximately 2.6 μg/mL.

4.5.3 EWOD-Based PCR Systems

The feasibility of EWOD-based polymerase chain reaction (PCR) devices was first demonstrated by Pollack et al. [139] for single-nucleotide polymorphisms (SNPs) and by Chang et al. [140] for a detection gene for the Dengue II virus. PCR involves the exponential amplification of fragments of DNA using a thermal cycling procedure which theoretically doubles the DNA concentration each cycle. At present, PCR is normally performed in large thermocycler systems that heat and cool 96-, 384- or 1536-well assay plates between three predetermined temperatures that are associated with the denaturation, annealing and extension phases of the DNA amplification process. One of the key advantages of being able to perform PCR in digital microfluidic systems is the ability to reduce the volume (and thereby cost) of the reagents and also to reduce the time taken to perform the thermal cycling due to the smaller thermal mass.

Pollack et al. [139] showed that the electrowetting actuation mechanism does not affect the PCR amplification process, thus demonstrating that EWOD can be used in PCR applications. In addition, they found that the higher ambient temperatures associated with PCR amplification tended to reduce the threshold voltage for droplet movement, enabling faster droplet transport. To date, most PCR-EWOD

systems apply the thermal cycling to the entire chip, allowing heating and cooling rates of between 1 and 2°C/s. However, alternative designs of EWOD chip are currently being investigated where the thermal regulation is performed on the chip itself to provide faster cycling times [62, 140]. One option is to use stationary droplets above a zone which is repeatedly heated and cooled while the other possibility is to transport the droplets between regions having different temperatures. A particularly promising technology for temperature regulation on EWOD chips is the use of mini-Peltier devices to cool (or heat) specific regions of the chip. However, there are a number of difficulties associated with PCR-EWOD systems. Firstly, the relatively high temperature of the denaturation stage (95°C) can lead to the formation of bubbles which disrupt the droplet transport mechanism and can also damage the dielectric layer. Rigorous de-gassing protocols are therefore essential in order to avoid problems with bubble formation. Evaporation is also a major issue at high temperatures and therefore it is essential that the droplets are surrounded by silicone oil. However, the main concern regarding EWOD-based PCR systems is the possibility of cross-contamination of DNA from one individual droplet to the next. Although cross-contamination can occur via the silicone oil, it is more likely to be caused by adsorption/desorption of the DNA on the hydrophobic layer of the chip. Pollack et al. [139] conducted experiments to ascertain the level of cross-contamination in a PCR-EWOD system, by repeatedly transporting DNA-containing and DNA-free droplets across a common electrode. After transporting the droplets for 45 min (and 75 thermal cycles), during which there were 15,000 separate opportunities for cross-contamination, little evidence was found for the transfer of DNA into the DNA-free droplets. Nevertheless, there are still some concerns regarding the problem of adsorption of DNA on to the surface of the chip, especially if the EWOD-chip is to be reused several times for different PCR assays.

4.5.4 EWOD-Based DNA Sequencing

Recent advances in digital microfluidics have opened up the possibility of performing DNA sequencing by synthesis. Figure 4.16 shows a prototype EWOD-based digital microfluidic device for DNA pyrosequencing that has been developed by *Advanced Liquid Logic* [14]. 'Sequencing-by-synthesis' involves taking the DNA strand of interest and synthesising its complementary strand enzymatically, one base pair at a time. The pyrosequencing method is based on detecting the activity of DNA polymerase (a DNA synthesising enzyme) using a chemiluminescent enzyme (luciferase). The assay is carried out by sequentially adding solutions of the four nucleotide bases—adenine (A), thymine (T), cytosine (C) and guanine (G) to the DNA sample of interest and detecting (by chemiluminescence) which of the nucleotides is added at each stage; this then allows the sequence of the unknown strand of DNA to be determined.

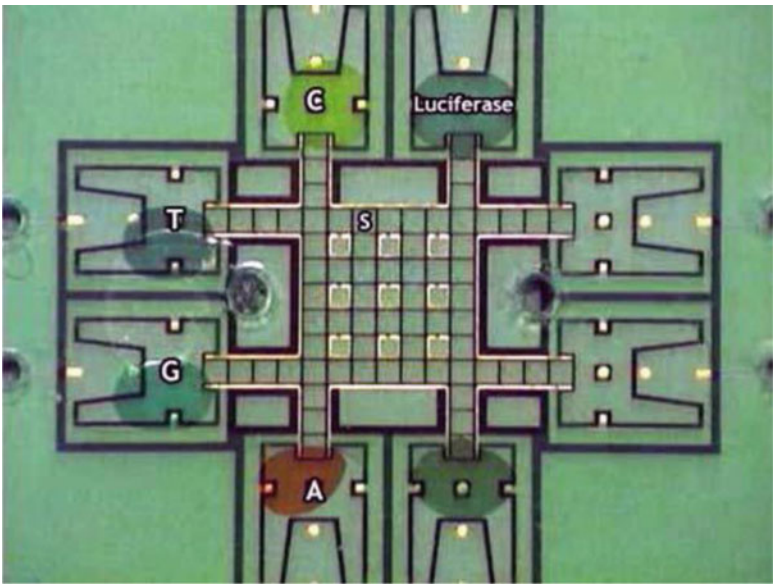

Fig. 4.16 Prototype DNA pyrosequencing chip developed by *Advanced Liquid Logic*. The chip contains reservoirs for dispensing solutions of A, T, C and G nucleotides and also a reservoir for the chemiluminescent enzyme (luciferase). The DNA is immobilised at location 'S'. Reproduced from Fair [14] with kind permission of Springer Science and Business Media

The operating sequence for the EWOD-based pyrosequencing chip involves dispensing a droplet containing one of the nucleotides (A, T, C or G) and transporting it to the site labelled 'S' containing the immobilised single-stranded DNA. The droplet is allowed to incubate at the site to allow time for polymerisation to take place, and is then transported away from the site and allowed to react with a droplet containing the chemiluminescent enzyme. After mixing, the combined droplet is transported to an optical sensor that detects chemiluminescent activity in the droplet. The system has no limitations on the number of bases than can be read since the synthesis and optical detection are physically separated on different parts of the chip. However, one of the practical difficulties appears to be the on-chip immobilisation of the DNA strand since the movement of the droplets over the site can cause the DNA molecules to be dislodged after many droplet operations. Nevertheless, the prototype EWOD-based pyrosequencing chip developed by *Advanced Liquid Logic* graphically demonstrates the power of digital microfluidic systems.

4.6 Future Trends and Concluding Remarks

Droplet handling technologies based on electrowetting have the potential to revolutionise many areas of analytical science by providing new functionalities and paradigms that are not possible in conventional laboratory procedures.

The recent developments in EWOD-based microfluidics have demonstrated that complex biological and chemical assays, including DNA and protein analyses, can be performed in digital microfluidic systems. EWOD-based microfluidic technologies are still very much in their infancy. However, the growing literature on EWOD droplet manipulation suggests that the technique will become an important technology in the development of the next generation of microfluidic devices.

Initial results have demonstrated that the use of digital microfluidics provides all the usual benefits associated with miniaturisation including smaller sample requirements, reduced reagent consumption, decreased analysis time, lower power consumption, lower costs per assay and higher levels of throughput and automation. However, the introduction of fully-controllable 'digital' microfluidic systems where the samples and reagents are manipulated using a standard set of droplet handling operations takes the technology beyond that which can be achieved using continuous flow microfluidics. The elegance of digital (droplet-based) microfluidics originates in the fact that the reactions or assays can be performed sequentially rather than as a continuous reaction, enabling complex chemical and biological protocols to be performed on a relatively simple microfluidic chip.

Undoubtedly, one of the factors that would make the use of electrowetting more attractive is further miniaturisation of the technology. The reduction in the volume of the droplets by scaling the control electrodes from the current dimensions (typically hundreds of microns) down to tens of microns, and the associated increase in the electrowetting switching speed will bring enormous benefits to EWOD-based applications. For example, miniaturisation of the technology would enable massively parallel DNA sequencing to be to be carried out, which would make sequencing a one million base-pair long genome feasible on a single microfluidic chip. Without doubt, further miniaturisation will be enormously challenging, not only due to the limitations and difficulties in device fabrication, but also due to fundamental issues associated with the fluid mechanics of micron-sized droplets. However, overcoming these challenges will enable EWOD-based digital microfluidic systems to play a major role in the next generation of microdroplet technologies.

References

1. Manz A, Becker H (1998) Microsystem technology in chemistry and life sciences: topics in current chemistry, vol 194. Springer, Berlin
2. Jakeway SC, de Mello AJ, Russell EL (2000) Miniaturized total analysis systems for biological analysis. Fresenius J Anal Chem 366:525–539
3. Squires TM, Quake SR (2005) Microfluidics: fluid physics at the nanoliter scale. Rev Mod Phys 77:977–1026
4. Whitesides GM (2006) The origins and the future of microfluidics. Nature 442:368–373
5. Tian W-C, Finehout E (2008) Microfluidics for biological applications. Springer, New York
6. Arora A, Simone G, Salieb-Beugelaar GB, Kim JT, Manz A (2010) Latest developments in micro total analysis systems. Anal Chem 82:4830–4847

7. Janasek D, Franzke J, Manz A (2006) Scaling and the design of miniaturized chemical-analysis systems. Nature 442:374–380
8. Karniadakis G, Beskok A, Aluru N (2005) Microflows and nanoflows: fundamentals and simulation. Springer, New York
9. Kockmann N (2008) Transport phenomena in micro process engineering. Springer, Berlin
10. de Mello AJ, Beard N (2003) Dealing with 'real' samples: sample pre-treatment in microfluidic systems. Lab Chip 3:11N–19N
11. Craighead H (2006) Future lab-on-a-chip technologies for interrogating individual molecules. Nature 442:387–393
12. Song H, Chen DL, Ismagilov RF (2006) Reactions in droplets in microfluidic channels. Angew Chem Int Ed 45:7336–7356
13. Haeberle S, Zengerle R (2007) Microfluidic platforms for lab-on-a-chip applications. Lab Chip 7:1094–1110
14. Fair RB (2007) Digital microfluidics: is a true lab-on-a-chip possible? Microfluid Nanofluid 3:245–281
15. Fair RB, Khlystov A, Tailor TD, Ivanov V, Evans RD, Srinivasan V, Pamula VK, Pollack MG, Griffin PB, Zhou J (2007) Chemical and biological applications of digital-microfluidic devices. IEEE Design Test Comput 24:10–24
16. Teh S-Y, Lin R, Hung L-H, Lee AP (2008) Droplet microfluidics. Lab Chip 8:198–220
17. Fouillet Y, Jary D, Chabrol C, Claustre P, Peponnet C (2008) Digital microfluidic design and optimization of classic and new fluidic functions for lab on a chip systems. Microfluid Nanofluid 4:159–165
18. Abdelgawad M, Wheeler AR (2009) The digital revolution: a new paradigm for microfluidics. Adv Mater 21:920–925
19. de Gennes P-G, Brochard-Wyart F, Quéré D (2004) Capillarity and wetting phenomena: drops, bubbles, pearls, waves. Springer, New York
20. Rosslee C, Abbott NL (2000) Active control of interfacial properties. Curr Opin Colloid Interface Sci 5:81–87
21. Lee J, Kim C-J (2000) Surface-tension-driven microactuation based on continuous electrowetting. J Microelectromech Syst 9:171–180
22. Darhuber AA, Troian SM (2005) Principles of microfluidic actuation by modulation of surface stresses. Annu Rev Fluid Mech 37:425–455
23. Gras SL, Mahmud T, Rosengarten G, Mitchell A, Kalantar-zadeh K (2007) Intelligent control of surface hydrophobicity. Chem Phys Chem 8:2036–2050
24. Lipowsky R (2001) Morphological wetting transitions at chemically structured surfaces. Curr Opin Colloid Interface Sci 6:40–48
25. Pfohl T, Mugele F, Seemann R, Herminghaus S (2003) Trends in microfluidics with complex fluids. Chem Phys Chem 4:1291–1298
26. Seemann R, Brinkmann M, Kramer EJ, Lange FF, Lipowsky R (2005) Wetting morphologies at microstructured surfaces. Proc Natl Acad Sci USA 102:1848–1852
27. Pollack MG, Fair RB, Shenderov AD (2000) Electrowetting-based actuation of liquid droplets for microfluidic applications. Appl Phys Lett 77:1725–1726
28. Quilliet C, Berge B (2001) Electrowetting: a recent outbreak. Curr Opin Colloid Interface Sci 6:34–39
29. Pollack MG, Shenderov AD, Fair RB (2002) Elecrowetting-based actuation of droplets for integrated microfluidics. Lab Chip 2:96–101
30. Mugele F, Klingner A, Buehrle J, Steinhauser D, Herminghaus S (2005) Electrowetting: a convenient way to switchable wettability patterns. J Phys Condens Matter 17:S559–S576
31. Mugele F, Baret J-C (2005) Electrowetting: from basics to applications. J Phys Condens Matter 17:R705–R774
32. Shamai R, Andelman D, Berge B, Hayes R (2008) Water, electricity, and between... On electrowetting and its applications. Soft Matter 4:38–45

33. Schwartz JA, Vykoukal JV, Gascoyne PRC (2004) Droplet-based chemistry on a programmable micro-chip. Lab Chip 4:11–17
34. Fan S-K, Hsieh T-H, Lin D-Y (2009) General digital microfluidic platform manipulating dielectric and conductive droplets by dielectrophoresis and electrowetting. Lab Chip 9:1236–1242
35. Wang K-L, Jones TB, Raisanen A (2009) DEP actuated nanoliter droplet dispensing using feedback control. Lab Chip 9:901–909
36. Darhuber AA, Valentino JP, Troian SM, Wagner S (2003) Thermocapillary actuation of droplets on chemically patterned surfaces by programmable microheater arrays. J Microelectromech Syst 12:873–879
37. Darhuber AA, Chen JZ, Davis JM, Troian SM (2004) A study of mixing in thermocapillary flows on micropatterned surfaces. Philos Trans R Soc Lond A 362:1037–1058
38. Darhuber AA, Valentino JP, Troian SM (2010) Planar digital nanoliter dispensing system based on thermocapillary actuation. Lab Chip 10:1061–1071
39. Chiou PY, Moon H, Toshiyoshi H, Kim C-J, Wu MC (2003) Light actuation of liquid by optoelectrowetting. Sens Actuators A 104:222–228
40. Chuang H-S, Kumar A, Wereley ST (2008) Open optoelectrowetting droplet actuation. Appl Phys Lett 93:064104
41. Chiou PY, Park S-Y, Wu MC (2008) Continuous optoelectrowetting for picoliter droplet manipulation. Appl Phys Lett 93:221110
42. Krogmann F, Qu H, Mönch W, Zappe H (2008) Push/pull actuation using optoelectrowetting. Sens Actuators A 141:499–505
43. Chiou PY, Chang Z, Wu MC (2008) Droplet manipulation with light on optoelectrowetting device. J Microelectromech Syst 17:133–138
44. Guttenberg Z, Müller H, Habermüller H, Geisbauer A, Pipper J, Felbel J, Kielpinski M, Scriba J, Wixforth A (2005) Planar chip device for PCR and hybridization with surface acoustic wave pump. Lab Chip 5:308–317
45. Beyssen D, Le Brizoual L, Elmazria O, Alnot P (2006) Microfluidic device based on surface acoustic wave. Sens Actuators B 118:380–385
46. Luo JK, Fu YQ, Li Y, Du XY, Flewitt AJ, Walton AJ, Milne WI (2009) Moving-part-free microfluidic systems for lab-on-a-chip. J Micromech Microeng 19:054001
47. Fu YQ, Luo JK, Du XY, Flewitt AJ, Li Y, Markx GH, Walton AJ, Milne WI (2010) Recent developments on ZnO films for acoustic wave based bio-sensing and microfluidic applications: a review. Sens Actuators B 143:606–619
48. Cho SK, Kim C-J (2003) Particle separation and concentration control for digital microfluidic systems. In: 16th IEEE annual international conference on MEMS, Kyoto, Japan, pp 686–689
49. Zhao Y, Yi U-C, Cho SK (2007) Microparticle concentration and separation by traveling-wave dielectrophoresis (twDEP) for digital microfluidics. J Microelectromech Syst 16:1472–1481
50. Cho SK, Zhao Y, Kim C-J (2007) Concentration and binary separation of microparticles for droplet-based digital microfluidics. Lab Chip 7:490–498
51. Fan S-K, Huang P-W, Wang T-T, Peng Y-H (2008) Cross-scale electric manipulations of cells and droplets by frequency-modulated dielectrophoresis and electrowetting. Lab Chip 8:1325–1331
52. Wang Y, Zhao Y, Cho SK (2007) Efficient in-droplet separation of magnetic particles for digital microfluidics. J Micromech Microeng 17:2148–2156
53. Sista RS, Eckhardt AE, Srinivasan V, Pollack MG, Palanki S, Pamula VK (2008) Heterogeneous immunoassays using magnetic beads on a digital microfluidic platform. Lab Chip 8:2188–2196
54. Shah GJ, Kim C-J (2009) Meniscus-assisted high-efficiency magnetic collection and separation for EWOD droplet microfluidics. J Microelectromech Syst 18:363–375

55. Nashida N, Satoh W, Fukuda J, Suzuki H (2007) Electrochemical immunoassay on a microfluidic device with sequential injection and flushing functions. Biosens Bioelectron 22:3167–3173
56. Sista R, Hua Z, Thwar P, Sudarsan A, Srinivasan V, Eckhardt A, Pollack M, Pamula V (2008) Development of a digital microfluidic platform for point of care testing. Lab Chip 8:2091–2104
57. Malic L, Brassard D, Veres T, Tabrizian M (2010) Integration and detection of biochemical assays in digital microfluidic LOC devices. Lab Chip 10:418–431
58. Lippmann G (1875) Relations entre les phénomènes électriques et capillaires. Ann Chim Phys 5:494–549
59. Berge B (1993) Electrocapillarity and wetting of insulator films by water. C R Acad Sci Paris, Série II 317:157–163
60. Vallet M, Berge B, Vovelle L (1996) Electrowetting of water and aqueous solutions on poly (ethylene terephthalate) insulating films. Polymer 37:2465–2470
61. Lee J, Moon H, Fowler J, Schoellhammer T, Kim C-J (2002) Electrowetting and electrowetting-on-dielectric for microscale liquid handling. Sens Actuators A 95:259–268
62. Berthier J (2008) Microdrops and digital microfluidics. William Andrew, Norwich, NY
63. Berthier J, Silberzan P (2010) Microfluidics for biotechnology, 2nd edn. Artech House, Boston
64. Pollack MG (2001) Electrowetting-based microactuation of droplets for digital microfluidics. PhD thesis, Duke University, USA
65. Srinivasan V (2005) A digital microfluidic lab-on-a-chip for clinical applications. PhD thesis, Duke University, USA
66. Chatterjee D, Hetayothin B, Wheeler AR, King DJ, Garrell RL (2006) Droplet-based microfluidics with nonaqueous solvents and solutions. Lab Chip 6:199–206
67. Brassard D, Malic L, Normandin F, Tabrizian M, Veres T (2008) Water–oil core-shell droplets for electrowetting-based digital microfluidic devices. Lab Chip 8:1342–1349
68. Probstein RF (1994) Physicochemical hydrodynamics: an introduction, 2nd edn. Wiley, New York
69. Berthier J, Clementz P, Raccurt O, Jary D, Claustre P, Peponnet C, Fouillet Y (2006) Computer aided design of an EWOD microdevice. Sens Actuators A 127:283–294
70. Yoon J-Y, Garrell RL (2003) Preventing biomolecular adsorption in electrowetting-based biofluidic chips. Anal Chem 75:5097–5102
71. Luk VN, Mo GCH, Wheeler AR (2008) Pluronic additives: a solution to sticky problems in digital microfluidics. Langmuir 24:6382–6389
72. Hayes RA, Feenstra BJ (2003) Video-speed electronic paper based on electrowetting. Nature 425:383–385
73. Washizu M (1998) Electrostatic actuation of liquid droplets for microreactor applications. IEEE Trans Ind Appl 34:732–737
74. Cho SK, Moon H, Kim C-J (2003) Creating, transporting, cutting, and merging liquid droplets by electrowetting-based actuation for digital microfluidic circuits. J Microelectromech Syst 12:70–80
75. Berge B, Peseux J (2000) Variable focal lens controlled by an external voltage: an application of electrowetting. Eur Phys J E 3:159–163
76. Kuiper S, Hendriks BHW (2004) Variable-focus liquid lens for miniature cameras. Appl Phys Lett 85:1128–1130
77. Dong L, Agarwal AK, Beebe DJ, Jiang H (2006) Adaptive liquid microlenses activated by stimuli-responsive hydrogels. Nature 442:551–554
78. Cattaneo F, Baldwin K, Yang S, Krupenkine T, Ramachandran S, Rogers JA (2003) Digitally tunable microfluidic optical fiber devices. J Microelectromech Syst 12:907–912
79. Levy U, Shamai R (2008) Tunable optofluidic devices. Microfluid Nanofluid 4:97–105
80. Chakrabarty K, Paik PY, Pamula VK (2007) Adaptive cooling of integrated circuits using digital microfluidics. Artech House, Boston

81. Peykov V, Quinn A, Ralston J (2000) Electrowetting: a model for contact-angle saturation. Colloid Polym Sci 278:789–793
82. Quinn A, Sedev R, Ralston J (2005) Contact angle saturation in electrowetting. J Phys Chem B 109:6268–6275
83. Papathanasiou AG, Boudouvis AG (2005) Manifestation of the connection between dielectric breakdown strength and contact angle saturation in electrowetting. Appl Phys Lett 86:164102
84. Mugele F (2009) Fundamental challenges in electrowetting: from equilibrium shapes to contact angle saturation and drop dynamics. Soft Matter 5:3377–3384
85. Krupenkin TN, Taylor JA, Schneider TM, Yang S (2004) From rolling ball to complete wetting: the dynamic tuning of liquids on nanostructured surfaces. Langmuir 20:3824–3827
86. Vallet M, Vallade M, Berge B (1999) Limiting phenomena for the spreading of water on polymer films by electrowetting. Eur Phys J B 11:583–591
87. Wang K-L, Jones TB (2005) Saturation effects in dynamic electrowetting. Appl Phys Lett 86:054104
88. Verheijen HJJ, Prins MWJ (1999) Reversible electrowetting and trapping of charge: model and experiments. Langmuir 15:6616–6620
89. Chen JZ, Troian SM, Darhuber AA, Wagner S (2005) Effect of contact angle hysteresis on thermocapillary droplet actuation. J Appl Phys 97:014906
90. Berthier J, Dubois P, Clementz P, Claustre P, Peponnet C, Fouillet Y (2007) Actuation potentials and capillary forces in electrowetting based microsystems. Sens Actuators A 134:471–479
91. Keshavarz-Motamed Z, Kadem L, Dolatabadi A (2010) Effects of dynamic contact angle on numerical modeling of electrowetting in parallel plate microchannels. Microfluid Nanofluid 8:47–56
92. Fan S-K, Yang H, Wang T-T, Hsu W (2007) Asymmetric electrowetting—moving droplets by a square wave. Lab Chip 7:1330–1335
93. Shapiro B, Moon H, Garrell RL, Kim C-J (2003) Equilibrium behavior of sessile drops under surface tension, applied external fields, and material variations. J Appl Phys 93:5794–5811
94. Zeng J, Korsmeyer T (2004) Principles of droplet electrohydrodynamics for lab-on-a-chip. Lab Chip 4:265–277
95. Zeng J (2006) Modeling and simulation of electrified droplets and its application to computer-aided design of digital microfluidics. IEEE Trans Comput Aid Des Integr Circ Syst 25:224–233
96. Lienemann J, Greiner A, Korvink JG (2006) Modeling, simulation, and optimization of electrowetting. IEEE Trans Comput Aid Des Integr Circ Syst 25:234–247
97. Walker SW, Shapiro B (2006) Modeling the fluid dynamics of electrowetting on dielectric (EWOD). J Microelectromech Syst 15:986–1000
98. Lu H-W, Glasner K, Bertozzi AL, Kim C-J (2007) A diffuse-interface model for electrowetting drops in a Hele-Shaw cell. J Fluid Mech 590:411–435
99. Song JH, Evans R, Lin Y-Y, Hsu BN, Fair RB (2009) A scaling model for electrowetting-on-dielectric microfluidic actuators. Microfluid Nanofluid 7:75–89
100. Clime L, Brassard D, Veres T (2010) Numerical modeling of electrowetting transport processes for digital microfluidics. Microfluid Nanofluid 8:599–608
101. Yi U-C, Kim C-J (2006) Characterization of electrowetting actuation on addressable single-sided coplanar electrodes. J Micromech Microeng 16:2053–2059
102. Moon H, Cho SK, Garrell RL, Kim C-J (2002) Low voltage electrowetting-on-dielectric. J Appl Phys 92:4080–4087
103. Paik P, Pamula VK, Pollack MG, Fair RB (2003) Electrowetting-based droplet mixers for microfluidic systems. Lab Chip 3:28–33
104. Paik P, Pamula VK, Fair RB (2003) Rapid droplet mixers for digital microfluidic systems. Lab Chip 3:253–259
105. Srinivasan V, Pamula VK, Fair RB (2004) An integrated digital microfluidic lab-on-a-chip for clinical diagnostics on human physiological fluids. Lab Chip 4:310–315

106. Srinivasan V, Pamula VK, Fair RB (2004) Droplet-based microfluidic lab-on-a-chip for glucose detection. Anal Chim Acta 507:145–150
107. Srinivasan V, Pamula V, Paik P, Fair R (2004) Protein stamping for MALDI mass spectrometry using an electrowetting-based microfluidic platform. In: Lab-on-a-chip: platforms, devices, and applications. Proceedings of SPIE, vol 5591, Philadelphia, Pennsylvania (PA), USA, pp 26–32
108. Wheeler AR, Moon H, Bird CA, Loo RRO, Kim C-J, Loo JA, Garrell RL (2005) Digital microfluidics with in-line sample purification for proteomics analyses with MALDI-MS. Anal Chem 77:534–540
109. Moon H, Wheeler AR, Garrell RL, Loo JA, Kim C-J (2006) An integrated digital microfluidic chip for multiplexed proteomic sample preparation and analysis by MALDI-MS. Lab Chip 6:1213–1219
110. Böhringer KF (2006) Modeling and controlling parallel tasks in droplet-based microfluidic systems. IEEE Trans Comput Aid Des Integr Circ Syst 25:334–344
111. Griffith EJ, Akella S, Goldberg MK (2006) Performance characterization of a reconfigurable planar-array digital microfluidic system. IEEE Trans Comput Aid Des Integr Circ Syst 25:345–357
112. Gascoyne PRC, Vykoukal JV, Schwartz JA, Anderson TJ, Vykoukal DM, Current KW, McConaghy C, Becker FF, Andrews C (2004) Dielectrophoresis-based programmable fluidic processors. Lab Chip 4:299–309
113. Li Y, Parkes W, Haworth LI, Stokes AA, Muir KR, Li P, Collin AJ, Hutcheon NG, Henderson R, Rae B, Walton AJ (2008) Anodic Ta_2O_5 for CMOS compatible low voltage electrowetting-on-dielectric device fabrication. Solid State Electron 52:1382–1387
114. Gong J, Kim C-J (2008) Direct-referencing two-dimensional-array digital microfluidics using multilayer printed circuit board. J Microelectromech Syst 17:257–264
115. Abdelgawad M, Wheeler AR (2007) Rapid prototyping in copper substrates for digital microfluidics. Adv Mater 19:133–137
116. Abdelgawad M, Wheeler AR (2008) Low-cost, rapid-prototyping of digital microfluidics devices. Microfluid Nanofluid 4:349–355
117. Herbertson DL, Evans CR, Shirtcliffe NJ, McHale G, Newton MI (2006) Electrowetting on superhydrophobic SU-8 patterned surfaces. Sens Actuators A 130–131:189–193
118. Verplanck N, Coffinier Y, Thomy V, Boukherroub R (2007) Wettability switching techniques on superhydrophobic surfaces. Nanoscale Res Lett 2:577–596
119. Abdelgawad M, Freire SLS, Yang H, Wheeler AR (2008) All-terrain droplet actuation. Lab Chip 8:672–677
120. Abdelgawad M, Watson MWL, Wheeler AR (2009) Hybrid microfluidics: a digital-to-channel interface for in-line sample processing and chemical separations. Lab Chip 9:1046–1051
121. Fan S-K, Yang H, Hsu W (2011) Droplet-on-a-wristband: chip-to-chip digital microfluidic interfaces between replaceable and flexible electrowetting modules. Lab Chip 11:343–347
122. Duan R-Q, Koshizuka S, Oka Y (2003) Two-dimensional simulation of drop deformation and breakup at around the critical Weber number. Nucl Eng Des 225:37–48
123. Raccurt O, Berthier J, Clementz P, Borella M, Plissonnier M (2007) On the influence of surfactants in electrowetting systems. J Micromech Microeng 17:2217–2223
124. Ren H, Fair RB, Pollack MG, Shaughnessy EJ (2002) Dynamics of electro-wetting droplet transport. Sens Actuators B 87:201–206
125. Bahadur V, Garimella SV (2006) An energy-based model for electrowetting-induced droplet actuation. J Micromech Microeng 16:1494–1503
126. Chakraborty S, Mittal R (2007) Droplet dynamics in a microchannel subjected to electrocapillary actuation. J Appl Phys 101:104901
127. Baird E, Young P, Mohseni K (2007) Electrostatic force calculation for an EWOD-actuated droplet. Microfluid Nanofluid 3:635–644

128. Bavière R, Boutet J, Fouillet Y (2008) Dynamics of droplet transport induced by electrowetting actuation. Microfluid Nanofluid 4:287–294
129. Ahmadi A, Najjaran H, Holzman JF, Hoorfar M (2009) Two-dimensional flow dynamics in digital microfluidic systems. J Micromech Microeng 19:065003
130. Chatterjee D, Shepherd H, Garrell RL (2009) Electromechanical model for actuating liquids in a two-plate droplet microfluidic device. Lab Chip 9:1219–1229
131. Berthier J, Peponnet C (2007) A model for the determination of the dimensions of dents for jagged electrodes in electrowetting on dielectric microsystems. Biomicrofluidics 1:014104
132. Moon I, Kim J (2006) Using EWOD (electrowetting-on-dielectric) actuation in a micro conveyor system. Sens Actuators A 130–131:537–544
133. CFD-ACE+ (2008) User manual: version 2008.2. ESI CFD, Inc., Huntsville, AL
134. Cooney CG, Chen C-Y, Emerling MR, Nadim A, Sterling JD (2006) Electrowetting droplet microfluidics on a single planar surface. Microfluid Nanofluid 2:435–446
135. Ren H (2004) Electrowetting-based sample preparation: an initial study for droplet transportation, creation and on-chip digital dilution. PhD thesis, Duke University, USA
136. Trinder P (1969) Determination of blood glucose using 4-amino phenazone as oxygen acceptor. J Clin Pathol 22:246
137. Pamula VK, Srinivasan V, Chakrapani H, Fair RB, Toone EJ (2005) A droplet-based lab-on-a-chip for colorimetric detection of nitroaromatic explosives. In: 18th IEEE international conference on MEMS, Miami Beach, FL, USA, pp 722–725
138. Terrier F (1982) Rate and equilibrium studies in Jackson-Meisenheimer complexes. Chem Rev 82:78–152
139. Pollack MG, Paik PY, Shenderov AD, Pamula VK, Dietrich FS, Fair RB (2003) Investigation of electrowetting-based microfluidics for real-time PCR applications. In: Seventh international conference on miniaturized chemical and biochemical analysis systems—proceedings of the 2003 MicroTAS conference, Squaw Valley, CA, pp 619–622
140. Chang Y-H, Lee G-B, Huang F-C, Chen Y-Y, Lin J-L (2006) Integrated polymerase chain reaction chips utilizing digital microfluidics. Biomed Microdevices 8:215–225

Chapter 5
Automated Droplet Microfluidic Chips for Biochemical Assays

Tomasz S. Kaminski, Krzysztof Churski, and Piotr Garstecki

5.1 Automation of Droplet Microfluidics: Opportunities and Challenges

After 20 years of research on microfluidic systems a vast expertise is available on automation of single phase flows through the use of mechanical actuation [1, 2] or through the use of electrokinetic effects [3, 4]. These systems are perfectly suited for a range of applications but are inherently inefficient in handling massively large numbers of processes due to correspondingly large number of input/output controls that at best scales logarithmically in the number of processes.

On the other hand, conducting reactions in thousands micro droplets embodies many of the acclaimed promises of microfluidics—ultra-miniaturization, speed, rapid mixing, and extensive control of physical conditions. Demonstrations of incubation of bacteria [5], in vitro translation [6, 7] and directed evolution [8, 9] confirm that these techniques can reduce the cost and time of existing processes by orders of magnitude. The critical opportunities and challenges in applications of the droplet microfluidic systems in biochemistry are in *automation* of these systems. Here we discuss the technical state of the art in building *modules* for automation of droplet microfluidic systems and the use of automated droplet chips in biochemistry.

Building on the original fabrication techniques and demand for portable analytical systems for defense [10], the science of controlling flow in microchannels progressed from the pressure driven [11] and electrokinetic [3] flow, onto more complicated configurations. There are a number of different schemes of driving the fluids through microchannels. The first demonstration [3] employed electrophoretic separation on chip. Electrokinetic systems that utilize both electrosmosis and

T.S. Kaminski • K. Churski • P. Garstecki (✉)
Institute of Physical Chemistry Polish Academy of Sciences, Kasprzaka 44/52, Warsaw 01-224, Poland
e-mail: garst@ichf.edu.pl

P. Day et al. (eds.), *Microdroplet Technology: Principles and Emerging Applications in Biology and Chemistry*, Integrated Analytical Systems,
DOI 10.1007/978-1-4614-3265-4_5,

electrophoresis to drive and separate the liquids and analytes are now among the more important classes of systems. Interesting modifications include the use of centrifugal force, mostly in systems designed for analytics purposes [12]. Other schemes are increasingly researched, as, e.g., recent advances in the use of patterned strips of paper to execute complicated assays with the flow forced solely by capillary forces [13]. The techniques of microfluidics and their use have been extensively reviewed, see, e.g., [14, 15].

A completely separate class of systems encompasses multiphase flows in which two (or more) immiscible liquids are driven through microchannels, and one (or more) of them is controllably dispersed in droplets. Droplet microfluidics started off in 2001 [16] progressively building fundamental understanding of the dynamics of formation and transport of droplets and the use of these as micro-reaction beakers. The techniques of formation of ultra small droplets (pL to μL in volume) at high rates (up to several kHz) opened up the possibility of conducting chemical and biochemical reactions inside droplets. The droplet microfluidic systems excel [17, 18] in many of the most important advantages of microfluidics: (1) ultra small volumes of reactions, (2) perfect control of reaction conditions (including temperature, rate of mixing, exposure to stimuli, titrations, kinetics), and (3) phenomenal statistics through the ease, speed, and low cost of running multiple repetitions of the same miniaturized experiments. These characteristics prompted a myriad of academic demonstrations of reactions in droplets, as diverse as, e.g., synthesis of monodisperse nanoparticles, [19, 20] crystallization of proteins [21–24] or incubation and detection of bacteria [25]. Important recent developments include performing directed evolution of enzymes [9] or screening of the activity of hormones [26] done at rates that are by far superior with respect to traditional apparatus and with a greatly smaller consumption of reagents. Advantages of conducting reactions within microdroplets and opportunity in automation prompt for further research that needs to be directed towards applications.

Still, the vision of applications of droplet microfluidic chips to perform a wide range of reactions is still outstanding. In order for the droplet microfluidic systems to realize their true potential to perform multiplexed reactions at high throughput, they need to be able to realize arbitrary, programmed, protocols for aspiration of samples, preparation of a range of compositions of reaction (or incubation) mixtures, sort the droplets, and recycle them on chip to avoid off-chip manipulations. All these operations require interfacing the chips with computer control. The use of constant rate of flow (or pressure) inputs enable only formation of thousands (or millions) of *identical* droplets. Programmable syringe pumps allow to scan the concentrations of a set of reagents inside the droplets but at rates that are much slower than the generation of droplets [21]. There are already a number of demonstrations of modules for automation of generation and trafficking of droplets, and we review them below. An interested reader should also consult other chapters in this book for a review of, e.g., the very attractive digital-microfluidic systems in which droplets travel on plates rather than in channels and are guided with the use of gradients of temperature [27] or gradients of intensity of electric field [28].

Here we review the recent advances in building modules for automation of handling of droplets in microfluidic channels. These include the modules for generation of droplets on demand, aspiration of samples onto chips, splitting and merging of droplets, incubation of the content of the drops, and sorting. There are a number of demonstrations of each of these operations and many (e.g., sorting [29]) are already well developed. As the whole field of microfluidics experiences a significant shift of interest from fundamental aspects to applications, we also review the existing demonstrations of use of automated droplet systems in biochemistry, diagnostics, and handling of living cells in microdroplets.

5.2 Modules

5.2.1 Formation of Droplets

The most important module in any droplet microfluidic system is the one for formation of droplets. Generation of monodisperse segments of liquids with the use of either constant pressure applied to the inlets of the device or with constant rates of flow of the liquids is relatively well studied. The common microfluidic geometries used for formation of droplets include the T-junction introduced by Thorsen et al., [16] and a flow-focusing junction introduced first in an axisymmetric version by Ganan-Calvo [30] and in the planar format that is relevant to lab on chip systems by Anna et al. [31] The mechanisms of formation of drops in the T-junction [32–35] and in the flow-focusing geometry [36–39] are qualitatively similar. At low values of capillary numbers ($Ca < 10^{-2}$), which are typical to use of these systems, generation of droplets is dominated by interfacial effects. The tip of the fluid-to-be-dispersed obstructs the cross section of the junction or orifice which leads to an effective blocking of the flow of the continuous liquid and to an increase of pressure upstream of this tip. The elevated pressure squeezes the neck between the inlet stream of the fluid-to-be-dispersed and the growing droplet at a rate that is proportional to the rate of flow of the continuous phase. [36] Within this regime the volume of the bubbles or droplets is a function solely of the ratio of the rates of flow of the two immiscible phases. [32, 36] At higher rates of flow the shear stresses exerted by the continuous fluid on the growing droplet introduce additional effects. This introduces a dependence of the volume of the generated droplets on the value of the capillary number. [34, 35] These mechanisms allow for formation of monodisperse droplets at rates up to several kHz. However, because fluids are supplied at constant rates of flow these systems do not provide for control of the volume of each individual droplet. Such control can be realized only within active (on-demand) systems that are controlled with a preprogrammed electronics.

Any active system for formation of droplets on demand must use a module for controlling the flow of at least one of the two immiscible liquids. Most of the research on development of droplet on demand systems concentrated on

construction of microvalves integrated with the chips. Several different strategies can be applied, and these include the use of thermocapillary, electrokinetic and acoustic effects and mechanical valving. Below we review the recent advances in formation of droplets on demand. We want to underline that by formation of droplets on demand we understand techniques for formation of droplets at an individually (i.e., independently for each droplet) prescribed time of emission and of an individually prescribed volume. The vast literature on modulating the frequency and volume of continuously produced droplets with the use of external fields does not fall into this category.

Formation of droplets at microscale allows for use of the interfacial tension to create a mechanism for blocking the flow of the liquid-to-be-dispersed. Prakash and Gershenfeld [40] constructed a system that used the thermo-capillary effect. The inlet channel for the discontinuous phase had a gradual narrowing immediately upstream of the flow-focusing junction. This narrowing induced an increasing curvature of the tip of the liquid-to-be-dispersed and the Laplace pressure blocked the flow. A thin film heater positioned underneath the converging nozzle served to increase the temperature and lower the interfacial tension to allow the stream of gas to enter the junction to create a single bubble. A similar concept was used by Attinger and colleagues [41]: a piezoelectric element increased the pressure in a reservoir of the liquid-to-be-dispersed and forced the tip of this phase into the flow focusing junction. This system generated uniform droplets of average volume of single nano-liters at few Hz. Bransky et al. [42] reported slightly faster generation of droplets in a similar system that had the piezoelectric actuator integrated in the polydimethylsiloxane (PDMS) device. The systems using the Laplace blockade to control the flow of the droplet phase are limited in the range of pressures that can be applied to the discontinuous phase as it cannot surpass the Laplace pressure (of the order of ~10 mbar).

Electrokinetic effects can be effectively used to form droplets on demand. Most common demonstrations of the use of electric field to generate droplets use dielectrophoresis and electrowetting. Jones et al. [43] reported a configuration of two parallel electrodes with a source of the liquid to be dispersed positioned between them. Application of pulses of alternating electric field dragged the dispersed phase into the space between the electrodes and allowed for formation of droplets [44]. Quite well developed are also the techniques within the digital microfluidics platform which use electrowetting to form single droplets. In these systems the dispersed phase is fed from reservoirs positioned at the edges of planar arrays of electrodes [45]. Application of current between selected electrodes drags the liquid to the regions of higher intensity of the electric field. The major drawback of this technique lies in typically extended times of generation of droplets and in incompatibility with the idea of massively high-throughput screening (operations on tens of thousands of droplets).

Conceptually most straightforward is the use of mechanical valves. These can be either integrated with the chips (microvalves) or external to the chip, providing for modularity. The most popular microfluidic microvalve was introduced by Quake and colleagues [1]. The valve is fully fabricated in PDMS—an elastic polymer and

comprises two perpendicular channels (a flow channel and a control channel) separated by a thin PDMS membrane. Application of high pressure to the control channel deflects the membrane and closes the cross section of the flow channel. This technique is widely used in microfluidics both in academia and in commercial applications (e.g., Fluidigm). Zeng et al. [46] reported the use of the multilayer PDMS microvalves for generation of sequences of droplets on demand. The droplets were drawn from four reservoirs containing different aqueous solutions. Galas et al. [47] situated the valve on top of the chip at the inlet port for the liquid to be dispersed. This solution simplifies fabrication of the chip. Hulme et al. [48] instead of controlling the valve with pressure of gas, constructed a system in which an electromagnetic actuator was situated directly over the PDMS membrane. Motion of the actuator opened and closed the microvalve. The main disadvantage of all these solutions dwells in the use of PDMS which is not compatible with a wide range of organic substances that induce swelling of this material [49].

An alternative is to use elastic membranes integrated into systems of channels fabricated in stiff materials, such as glass or stiff polymers. Grover et al. [2] described a microvalve that comprised two microstructured plates of glass separated with a PDMS membrane. The advantage of this design is that the membrane can be formed of a range of materials. Churski et al. [50] constructed a pneumatic microvalve in which the elastic (nitrile) membrane was stretched on a microfabricated chuck that could be simply pressed into microfluidic chip. This microvalve, positioned on the microchannel that supplied the liquid-to-be-dispersed, allowed for formation of droplets on demand both in the T-junction and flow-focusing systems, at rates up to 30 Hz.

The use of integrated microvalves is elegant but requires complicated microfabrication. Integrated microvalves are always more expensive (or more difficult to fabricate) than chips that posses solely the microchannels. Following the idea of modularity of microfluidic systems, Churski et al. [51] presented the use of standard electromagnetic valve that is external to the chip to control generation of droplets in microscale. The valve was modified by insertion of a long steel capillary at its outlet to minimize the dead volume. This allowed for on-demand generation of droplets as small as 70 nL in volume. Churski et al. [51] used the valves to control the flow of *both* of the immiscible phases. This in turn allowed them to form droplets on demand within an arbitrarily large range of volumes—a characteristic that is critical for implementation of the droplet on demand techniques, for example, screening of compositions of reaction mixtures [51]. The advantages of using external valves for formation of droplets on demand include (1) low cost of standard, reusable electromagnetic valves, (2) compatibility of the technique with chips fabricated in virtually any material providing for compatibility with different chemistries, (3) simple architecture of the chips providing for their disposability and (4) very small an on-chip footprint of less than 1 mm^2. These features should make the techniques of formation droplets on demand with the use of external valves particularly suitable for applications.

5.2.2 Preparation of Samples (Aspiration and Splitting)

One of the aims of microfluidic technology is to minimize the use of liquids and the volume of sample that is required to perform the analyses. In conventional microfluidics, although the volume of the actual reaction mixtures may be small, the dead volume of the fluidic connections, syringes, etc., can add up to several milliliters. Thus techniques for introduction of small volumes of samples onto the chips for their further manipulation are constantly being developed. One common solution is to use a tubing to first aspire small volumes of sample into a form of plugs and then to connect this tubing to the chip and purge the samples through the microchannels. For example, Adamson et al. [52] presented a system in which each plug of sample was separated with a bubble to prevent mixing and crosscontamination. Such prepared sequences of plugs were subsequently split into nL droplets on chip—in a microfluidic tree of bifurcating microchannels. Splitting at bifurcations [53] can be precisely controlled with pressure equalizing structures [54], that can be used to enforce either symmetric [54] or asymmetric [55] splitting. Active methods of controlling the ratio of volumes of daughter droplets can also be used. For example, Barouad used lasers to manipulate droplets at the junction [56]. Trivedi et al. [57] used flow-focusing to split large droplets from a tubing-cartridge into a large number of microdroplets.

Ideally, aspiration of samples should be automated. Sung et al. [58] presented an automated system in which the samples were drawn from test tubes. The chip possessed an open, sharply pointed port that could be inserted (by a robot) into the eppendorf tubes for aspiration of samples. Clausell-Tormos et al. [59] presented an automated system to aspire samples from a 96-well plate. The system utilized a multichannel valve, popular in chromatography. The samples were first aspired into a tubing and then split into small droplets with the use of geometry proposed by Adamson et al. [52].

Chen et al. [60] presented a very interesting device called “chemistrode” that enabled aspiration of liquid from a cell culture directly into micro-droplets. A modification of this system reported by Liu et al. [61] enables aspiration of samples from small reservoirs of samples.

Finally, Churski et al. [50] demonstrated a system in which the sample could be deposited on the chip in the form of small (tens of microliters in volume) droplets in a prefabricated well. This sample was then aspired directly into the droplet generating junctions to form droplets on demand.

5.2.3 Merging of Droplets

A very important aspect of droplet microfluidics is the stability of droplets against coalescence. In some applications (e.g., storing of large libraries of random mutations in pL droplets [9]) it is important to prevent coalescence. This can be achieved by an appropriate choice of surfactant added to the emulsion. On the

other hand, for preparation of reaction mixtures, coalescence (or merging) of droplets is required to mix solutions from two (or more) different droplets. There are a number of passive techniques that ensure merging of droplets. For example Bremond et al. [62] demonstrated a coalescence chamber that synchronizes two droplets and merges them. Similarly, Niu et al. [63] proposed a set of micropillars to hold a droplet until the next one collides with it. After merging, the droplet is large enough to be pushed out into a microchannel. Jin et al. [64] used the difference in speed of translation of droplets of higher and lower viscosity to synchronize and merge them.

In systems in which surfactant stabilizes droplets against coalescence, merging of droplets needs to be stimulated by an application of external fields. A common solution is to utilize the effect of electrocoalescence in alternating electric field [65]. Ahn et al. [66] proposed a system in which small droplets that did not fill the cross section of the channel flowed slower than large plugs. This effect brought two different droplets in contact and an application of electric field merged them. Similarly, Churski et al. [51] generated droplets on demand in three parallel T-junctions and merged them by applying alternating electric field across the chamber.

An alternative to application of oscillating electric field is to use electrophoretic effects. Link et al. [67] charged droplets positively and negatively already upon their formation. This approach proved to be efficient in subsequent synchronization and merging of pairs of positively and negatively charged droplets.

5.2.4 Detection

Automated systems must provide means for detection of the content of the droplets. Detection of the positions (presence at given spots on the chip) of droplets is also critical for feedback and synchronization. The simplest method for detection of both the presence and content (via colorimetry) of droplets is to use a CCD camera [68]. This system can distinguish the presence, size, and color of droplets. Interfacing the chips with spectrophotometers can yield higher resolution and sensitivity of detection. Lau et al. [69] used Raman spectroscopy to analyze composition of droplets. In high-throughput screening high rates of detection are needed. The custom built detectors of fluorescence can read the signal from droplets at high rates (up to several kHz) and can provide input to fast sorters of droplets [70]. Although optical detection is the method of choice in most demonstrations, other approaches are also used, as, e.g., detection of presence of droplets through a capacitive measurement [71].

5.2.5 Sorting

Sorting of droplets can be done in two conceptually and technically different frameworks. One (passive) sorts droplets through a physical mechanism that

distinguishes between varied properties of the droplets. In other words, the given property (e.g., size) of the droplet is used in a physical mechanism of sorting. In an alternative approach, sorting is done actively by application of an external field or mechanical forcing. These active sorters require detection of the presence and property of the droplets to trigger the state of the sorting machinery.

Passive sorters fractionate a mixture of droplets of different properties such as size or dielectrophoretic conductance in a continuous manner, always with the same criterion. For example, Tan et al. [72] demonstrated a microfluidic chip in which the geometry of the channel upstream of a bifurcation sorted droplets by size. Griffits and colleagues [73] also used a clever geometrical design of the channel that discriminated small droplets that traveled fast through the junction from large droplets that were slower. Maenaka et al. [74] used a system in which a side channel delivered additional continuous liquid to the main one. Small droplets flowing in the main channel followed the streamlines of the continuous liquid and translated closer to the wall of the main channel (opposite to the additional inlet). Large droplets, because of their size could not translate across the channel and could be effectively sorted out from the original mixture.

There are a number of strategies to realize active sorting. One is to use computer-controlled valves to close or open additional streams of continuous liquid to manipulate the trajectories of droplets. Shemesh et al. [68] demonstrated a system in which a CCD camera detected the color of the droplets inflowing into a bifurcation of channels. Using the signal from the camera a computer either opened or closed an additional inflow of continuous phase into the bifurcation which allowed the Authors to separate droplets by color into the left and right bifurcation. Another strategy is to actively change the resistance of one of the channels downstream of a bifurcation. Abate et al. [75] used a construct similar to the PDMS valve to actively modify the cross section of the channel at bifurcation and steer the droplets. Shirasaki et al. [76] used a thermo reversibly gelling polymer (TGP), which gels in contact with IR light.

Other active methods of sorting include the use of lasers [56, 69, 77], thermocapillary [78] and electrorheological [79] effects or acoustic waves [80] but the most efficient droplet sorters are the ones that use externally applied electric field. There are few different methods to use either electrophoretic or dielectrophoretic forces exerted on droplets. Niu et al. [71] proposed to charge the droplets electrically, and then to sort them at a bifurcation by changing the polarization of the electric field. Ahn et al. [81] reported a system, in which the electric field across the bifurcation was constant, but the droplets were on-demand charged either positively or negatively to be diverted to the desired channel. Baret et al. [82] used a system in which one of the arms had a smaller hydraulic resistance and without the application of electric field all droplets flew into this channel. When desired the application of an alternating electric field pulled the droplets into the second channel. The strategy that proved most useful in applications is the one that uses dielectrophoretic force in a symmetrical bifurcation. In such a system [9, 83] there are two active electrodes positioned on the sides of the bifurcation

and one, central, ground electrode. Application of alternating current between one of the side electrodes and the ground electrode sorts the droplets at rates in excess of 1 kHz.

5.2.6 Incubation

Preparation of thousands of microdroplets each containing a predesigned chemical content is one thing—another is their storage for incubation. Some reactions or processes (e.g., growth of crystals) may need prolonged time for incubation. Similarly, bacteria growing in droplets must be allowed time to grow to make it possible to observe differences in viability between populations incubated in different conditions. Thus, one of the problems that need clever solutions is incubation of large numbers of droplets. In some assays, in which each droplet contains a different and known chemical environment it is necessary that droplets are incubated without the loss of information on the identity of each of them.

For very fast reaction [84] the situation is simple—preparation of droplets and readout can be done within a few seconds of each other, all in situ within the chip. For longer incubation intervals large numbers of droplets can be stored in delay lines or wide reservoirs [85]. This solution, however, creates the problem of dispersion of time of residence in the delay line: droplets in the central part of the channel move faster than the droplets closer to the side walls of the channel. Frenz et al. [86] proposed a constriction that reduces the dispersion of incubation time in delay lines by stochastic redistribution. Another approach is the use of arrays of thousands of "dropspots," [87] i.e., chambers or hydrodynamic traps [88] for droplets. These systems make it possible to observe the droplets in time and to recover the drops after incubation. Bai et al. used a similar system to trap pairs of chemically distinct droplets to study the transport of small molecules across surfactant bilayers [89].

Still, for massive numbers of droplets, such as those used in, e.g., experiments on directed evolution, the only way to incubate tens of thousands of droplets is to store them off-chip in a tubing or syringe and to perform subsequent reinjection into chip for subsequent manipulations [90].

5.3 Applications

The modules for automation of microfluidic handling of droplets are constantly being developed. Progress on these techniques certainly requires further research. Currently, only the module for sorting [9, 83] awaited implementation in what seems a truly useful biochemical assay. Many techniques are promising, as, e.g., the ability to form droplets of well defined and individually controlled composition [51], yet many elementary automated protocols are yet to be realized, e.g., cycling

of large numbers of droplets on chip, dilution of the content of droplets, repetitive splitting and titrations, etc. We strongly believe that these modules will be developed in the near future and that they will lead to the development of useful tools for studies in biochemistry. Below we review the existing demonstrations of working droplet microfluidic systems and point to the problems that still need to be resolved.

5.3.1 High-Throughput Screening in Biochemistry

One of the first experiments that demonstrated the potential of droplet microfluidics as a tool for studying biochemistry was done by the Ismagilov group [84]. This work demonstrated that a droplet microfluidic system can be very useful for measurements of the kinetics of enzymatic reactions. Advantages such as fast mixing and lack of dispersion of time of residence of molecules undergoing reaction provide a possibility for studying the kinetics with millisecond resolution. The vision of industrial implementation of microfluidic systems into high-throughput screening of drugs or inhibitors acting on enzymes and cells seemed to be very close at that time.

Screening performed in microdroplets might be a very attractive alternative to classical high-throughput screening. For economical reasons primary screens in microtiter plates are usually performed with only one concentration of each compound. This can cause a significant fraction of false positives and false negatives [91]. The activity of particular compounds can strongly depend and locally change of their concentration. Testing multiple concentrations of each compound in standard microtiter plates is uneconomical even in the largest (1536-well) format. Another problem that traditional screening experiences is evaporation, especially, when the volume of individual reactions is decreased to single microliters [92]. Using droplet microfluidics can remedy both of these problems. It is possible to obtain dose–response profiles that provide reliable information on the activity of the tested compound. The volume of each reaction can be several orders of magnitude lower, so one can perform hundreds of repetitions and the overall cost and time will be still reduced with respect to traditional robotic stations. This point is very important in assays on cells [26] or proteins that are difficult to obtain.

Still, there are open challenges that need to be addressed in order for droplet microfluidic techniques to present a reliable and attractive alternative to traditional robotic high-throughput screening. For example, the conceptually simple task of interfacing the chip with libraries of chemicals remains an outstanding and difficult problem. Second challenge is associated with construction of chips capable of screening broad ranges of concentrations of every compound, e.g., for determination of characteristic parameters as IC_{50}, EC_{50} or K. So far only few reports showed this possibility [26, 59], but speed and simplicity of analysis are still not satisfactory in comparison to existing screening methods. Possibly, new approaches such as generating gradients by interfacing the chip with a chromatography column [93]

and automated systems for screening based on generation of droplets on demand [51, 94] will lead to new advances in this area.

One alternative to preparation of libraries on chip is to pregenerate stable (against coalescence) libraries of droplets, with every element of the library prepared independently. Then all subsets can be mixed together and driven through the microfluidic system. The limiting step is in the production of droplet libraries consisting of hundreds or thousands of different compounds. Still, once such libraries are prepared they can be used in multiple experiments. In an example reported by Brouzes et al. each type of elements of the library were coded by neutral fluorescent dies with different excitation/emission spectra. This technique was used to determine IC_{50} of drug mitomycin C acting on human cells [95]. In order to rate the activity of a given compound in toxological screening additional dyes for the live/dead assaying are needed [25, 95]. In another example Baret et al. [26] used cell-based reporter gene assay to quantitatively determine dose-dependence relationship of nuclear receptor agonist—20-hydroxyecdysone, acting on a single silkworm cell.

Droplet microfluidic systems promise advantages also in protein crystallization screening. This subject was extensively examined by the Ismagilov group [21–24]. Automated microfluidics can be especially useful here, as in applications large number of crystallization conditions must be tested: appropriate combination, concentration of different precipitants, ions, surfactants, and other chemicals are essential to obtain high-quality crystals.

The droplet microfluidic chips have an important potential also in a different area that can be relevant industrially: directed evolution of enzymes. In vitro compartmentalization in aqueous/oil emulsion invented by Tawfik and Griffiths [96] turned out to be a breakthrough. Compartmentalization of single copies of enzymes in microdroplets provide a vista for detectable linkage between phenotype and genotype, similar to other, earlier strategies such as ribosome-, phage- or yeast-displays. This creates immense possibilities in directed biochemical evolution. The use of microfluidic techniques for formation of monodisperse droplets circumvents the problem in classical emulsion compartmentalization that uses bulk emulsification and polydisperse droplets that bias the results. A range of biochemical applications of the droplet systems are now possible. Several researchers reported even in vitro translation in droplets; e.g., of a green fluorescent protein [97, 98]. Mazutis et al. [90] coupled in vitro translation of an enzyme with subsequent kinetic analysis. Two-phase microfluidic systems are also excellent tools for performing retroviral display of enzymes—droplets provide additional boundaries that confine fluorescent product to enable efficient selection [83]. All these advances were accumulated in a method proposed by Agresti et al. [9]—several aspects of this work make it a potential milestone in microfluidic research in the past few years. Briefly, yeast display, two rounds of error-prone off-chip PCR, and a very high-performance sorting resulted in a tenfold increase of catalytic activity of a horseradish peroxidase. The report confirms the potential of microfluidic techniques to reduce by several orders of magnitude the cost and time of existing processes. This work exhibits also the current limitations of droplet

microfluidics (1) significant labor needs to be performed off-chip (e.g., error-prone PCR and transformation of DNA libraries into the yeast cells), (2) lack of ability to test new mutant-enzymes in different chemical environments, and (3) sorting based on fluorescence detection which is limited only to small subpopulation of enzymes. We expect that in the coming years the automation of chips will progress to the level that will enable all the steps of in vitro evolution to be performed on chip. This will greatly speed up the processes and make them more practical.

5.3.2 Cell Assays

Droplet microfluidics opens new tools for quantitative studies of biology of cells at the single-cell level. Many different types of organism and cells have been shown to be cultivable in droplets, e.g., bacteria [99–101], yeast [87], mammalian cells [95, 102], and other types of cells [26]. Cultivation and analysis in different combinations of carrier fluids and surfactants is possible, but fluorinated oils seem to be the best existing choice, mostly due to chemical neutrality and high-oxygen permeability.

Studying single cells in very small volumes provide many advantages apart from the obvious minimization of consumption of reagents. It is widely known that response of single cell is often noise-dependent and bimodal (especially in simpler organisms such as bacteria) [103]. Successful observation of gene expression in single cells was done in tiny microfluidic chambers [104]. We believe that droplet technologies will provide further advances in, e.g., attempts to evaluate physiological and genetic features of complex and heterogeneous communities such as cancer tissue or bacterial environmental samples [5]. Confining single cells in tiny compartments can mimic high-density populations and allows for studies of quorum sensing and signal processing among bacterial communities [25]. Tight confinement facilitates also the detection of chemical signals produced by the organism. This feature can be used, e.g., for faster detection of pathogens [101].

Cultivation of single cells in droplets presents also challenges. For example, the rudimentary task of encapsulation single cells in every droplet is difficult. Division of a suspension into droplets results in a Poisson distribution of number of cells in compartments. Small concentrations of cells result in only a small fraction of droplets containing single cells. Large concentrations results in many droplets that contain multiple copies. This limits throughput and lowers the efficiency of the assay in terms of usage of cells. To increase throughput Chabert and Viovy [105] proposed to sort droplets and incubate only those containing cells. Edd et al. proposed a different solution in which the cells were preorganized before encapsulation so they entered the droplet generating junction at exactly the same frequency at which droplets were formed [106].

Another problem, and one that has not yet been solved, is the control and rapid screening of conditions of incubation—changing concentration of reagents such as drug, inhibitors, source of nutrients, ions, hormones, and other stimuli, both

between droplets, and within every droplet in time. The emerging solutions include, e.g., the use of varied in time ratio of rates of flow of liquids forming the droplets [21]. This solution, however, yields a narrow range of concentrations, is limited to a small number of components that cannot be tuned independently. Introduction of new techniques that can control composition of droplets is essential. We believe that further improvements of automated techniques recently developed in our group [51] may provide solutions to this problem. In a recent example we have demonstrated [94] rapid screening of compositions of cocktails of antibiotics, incubation, and readout of the viability of bacterial cells in an automated droplet microfluidic system.

There are several reports on advanced biochemical assays in single cells encapsulated in droplets. For example, in a pioneer work He et al. [102] encapsulated mouse mast cells in droplets and subsequently preformed on chip photolysis to release enzymes expressed inside the cell. Lysis is unnecessary when enzyme is expressed in periplasm (space between outer and inner membrane in bacteria). Huebner et al. [100] demonstrated overexpression of alkaline phosphatase in *Escherichia coli* cells with the enzymatic reaction taking place upon transfer of the enzyme into periplasm. Shim et al. reported simultaneous measurement of activity of expressed enzyme and fluorescent protein (mRFP1) serving as an internal standard [107]. This normalization removed the variance introduced by Poisson distribution of number of cells, unequal copy numbers of plasmid DNA, or different global expression levels. Joensson et al. [108] showed an interesting method for detecting antigens presented at low concentrations on the surface of cells. After biotin-coupled antibody binding to target biomarker and subsequent washing, complex of streptavidin conjugated with an enzyme (β-galactosidase) was added. Next, cells were loaded into droplet and fused with droplets containing fluorogenic substrate. This allowed for readout of fluorescence and for sorting. These methods discriminated cells with very low abundance of cell-surface biomarkers, a feature impossible with standard FACS, due to low fluorescence intensity of labeled antibodies.

5.3.3 Polymerase Chain Reaction

Several unique features decided that Polymerase Chain Reaction is probably the most successful application of droplet microfluidics. First, scaling down and compartmentalization enable isolation and amplification of single sequences. This has obvious advantages such as lack of competition or other interactions between replication processes of different amplicons yielding equal distribution of quantities of PCR products. Droplet microfluidics seems to be an ideal platform for high-throughput sequence enrichment for large scale sequencing [109].

Droplet PCR can be easily integrated within microfluidic devices. For thermocycling the entire chip can be heated and cooled by Peltier plates and amplification can be monitored in a real time with the use of fluorescent probes

and an XY stage [110, 111]. The throughput and speed of PCR processes can be improved by cycling the droplets between two or three sectors of different temperatures [112, 113]. Besides PCR, other amplification strategies were performed on a chip—e.g., isothermal amplification [114].

Another advantage of droplet microfluidics in conducting PCR is digitalization. The droplet techniques make it straightforward to compartmentalize the samples and primers into large numbers of partitions. Single partitions must consist zero or one molecule of DNA. After amplification, it is sufficient to count the compartments that contain amplified products to estimate the original concentration of nucleic acid. This technique—called digital PCR—was first described already in 1992 by Sykes et al. [115] but in spite of many advantages over classical quantitative PCR it awaited technical possibilities for compartmentalization and handling of large numbers of independent PCR processes. Droplet microfluidics provides perfect tools for these tasks: it is relatively easy to create very large numbers of monodisperse droplets at high-throughput and to perform single molecule amplification [112]. The only limitation is again associated with the Poisson's distribution of molecules of DNA in compartments. In order for the process to yield expected resolution and sensitivity, the solution of sample needs to be adequately diluted. Thus several off-chip dilution steps are required. Another challenge is multiplexing—it can be realized by droplet libraries [109], or by probes labeled with different fluorophores [116] but less expensive and less labor intensive methods are definitely needed. We envision that further progress in automation of droplet microfluidics will make it possible to perform multiplexed assays with all the necessary steps done on-chip.

5.4 Conclusions

Microfluidic systems promise a revolution in a range of disciplines such as point-of-care diagnostics and in-field analytics, bench-top apparatus for chemical and biochemical analyses, new tools for research and high-end high throughput stations for rapid screening in chemistry and biochemistry. These diverse applications impose an important classification of the technical requirements. For example, point-of-care diagnostics and in-field analyses require simplicity, portability, robustness, and specialization. The most promising vistas in this area comprise capillary-driven assays and electrokinetic chips. High-end, high-throughput stations require superior performance that often comes at the cost of specialization and smaller flexibility. Good examples of these include the commercialized apparatus for sequencing or high-throughput analyses. Bench top microfluidic analyzers require a combination of flexibility of protocols (programmability) and speed. At the moment, it seems that it is exactly this niche where the automated droplet microfluidic system will make the biggest impact in the coming years.

There are two major directions in using droplets as compartments for biochemical reactions. One takes advantage of compartmentalization itself. The sole ability

to split the reaction volume into tens of thousands of small and identical compartments makes it possible to perform polymerase chain reaction on single copies of target oligonucleotide, as in the diagnostic digital PCR commercialized by QuantaLife, or with a single pair of primers, as in the microfluidic machine for high-throughput sequence enrichment commercialized by Raindance Technologies. Coupling of compartmentalization with efficient sorting enables experiments on directed evolution.

The second, largely unexplored area of opportunities should take advantage of handling individual droplets and performing a set of different reactions in a predesigned manner (not, e.g., a set of reactions on a random library). Development of efficient microfluidic modules for cycling, splitting, merging, titrations of droplets, all done automatically on chip should enable construction of platforms that will be able to compete with the conventional platforms such as microtiter robotics.

References

1. Unger MA, Chou HP, Thorsen T, Scherer A, Quake SR (2000) Monolithic microfabricated valves and pumps by multilayer soft lithography. Science 288:113–116
2. Grover WH, Skelley AM, Liu CN, Lagally ET, Mathies RA (2003) Monolithic membrane valves and diaphragm pumps for practical large-scale integration into glass microfluidic devices. Sens Actuators B Chem 89:315–323
3. Harrison DJ, Fluri F, Seiler K, Fan Z, Effenhauser CS, Manz A (1993) Micromachining a miniaturized capillary electrophoresis based chemical analysis system on a chip. Science 261:895–897
4. Persat A, Santiago JG (2009) Electrokinetic control of sample splitting at a channel bifurcation using isotachophoresis. New J Phys 11:075026
5. Vincent ME, Liu WS, Haney EB, Ismagilov RF (2010) Microfluidic stochastic confinement enhances analysis of rare cells by isolating cells and creating high density environments for control of diffusible signals. Chem Soc Rev 39:974–984
6. Wu N, Zhu Y, Brown S, Oakeshott J, Peat TS, Surjadi R, Easton C, Leech PW, Sexton BA (2009) A PMMA microfluidic droplet platform for in vitro protein expression using crude E. coli S30 extract. Lab Chip 9:3391–3398
7. Zhu Y, Power BE (2008) Lab-on-a-chip in vitro compartmentalization technologies for protein studies. Adv Biochem Eng/Biotechnol 110:81–114
8. Miller OJ, Bernath K, Agresti JJ, Amitai G, Kelly BT, Mastrobattista E, Taly V, Magdassi S, Tawfik DS, Griffiths AD (2006) Directed evolution by in vitro compartmentalizaton. Nat Methods 3:561–570
9. Agresti JJ, Antipov E, Abate AR, Ahn K, Rowat AC, Baret JC, Marquez M, Klibanov AM, Griffiths AD, Weitz DA (2010) Ultrahigh-throughput screening in drop-based microfluidics for directed evolution (vol 170, pg 4004, 2010). Proc Natl Acad Sci U S A 107:6550
10. Whitesides GM (2006) The origins and the future of microfluidics. Nature 442:368–373
11. Kenis PJA, Ismagilov RF, Whitesides GM (1999) Microfabrication inside capillaries using multiphase laminar flow patterning. Science 285:83–85
12. Focke M, Stumpf F, Roth G, Zengerle R, von Stetten F (2010) Centrifugal microfluidic system for primary amplification and secondary real-time PCR. Lab Chip 10:3210–3212
13. Martinez AW, Philips ST, Whitesides GM, Carrilho E (2010) Diagnostic for the developing worlds: microfluidic paper-based analytical devices. Anal Chem 82:3–10

14. Squires TM, Quake SR (2005) Microfluidics: fluid physics at the nanoliter scale. Rev Mod Phys 77:977–1026
15. Arora A, Simone G, Salieb-Beugelaar GB, Kim JT, Manz A (2010) Latest developments in micro total analysis systems. Anal Chem 82:4830–4847
16. Thorsen T, Roberts RW, Arnold FH, Quake SR (2001) Dynamic pattern formation in a vesicle-generating microfluidic device. Phys Rev Lett 86:4163–4166
17. Song H, Chen DL, Ismagilov RF (2006) Reactions in droplets in microfluidic channels. Angew Chem Int Ed 45:7336–7356
18. Theberge AB, Courtois F, Schaerli Y, Fischlechner M, Abell C, Hollfelder F, Huck WTS (2010) Microdroplets in microfluidics: an evolving platform for discoveries in chemistry and biology. Angew Chem Int Ed 49:5846–5868
19. Gunther A, Jensen KF (2007) Multiphase microfluidics: from flow characteristics to chemical and materials synthesis (vol 6, pg 1487, 2006). Lab Chip 7:399
20. Shestopalov I, Tice JD, Ismagilov RF (2004) Multi-step synthesis of nanoparticles performed on millisecond time scale in a microfluidic droplet-based system. Lab Chip 4:316–321
21. Zheng B, Roach LS, Ismagilov RF (2003) Screening of protein crystallization conditions on a microfluidic chip using nanoliter-size droplets. J Am Chem Soc 125:11170–11171
22. Zheng B, Tice JD, Roach LS, Ismagilov RF (2004) A droplet-based, composite PDMS/glass capillary microfluidic system for evaluating protein crystallization conditions by microbatch and vapor-diffusion methods with on-chip X-ray diffraction. Angew Chem Int Ed 43:2508–2511
23. Gerdts CJ, Tereshko V, Yadav MK, Dementieva I, Collart F, Joachimiak A, Stevens RC, Kuhn P, Kossiakoff A, Ismagilov RF (2006) Time-controlled microfluidic seeding in nL-volume droplets to separate nucleation and growth stages of protein crystallization. Angew Chem Int Ed 45:8156–8160
24. Li L, Mustafi D, Fu Q, Tereshko V, Chen DLL, Tice JD, Ismagilov RF (2006) Nanoliter microfluidic hybrid method for simultaneous screening and optimization validated with crystallization of membrane proteins. Proc Natl Acad Sci U S A 103:19243–19248
25. Boedicker JQ, Vincent ME, Ismagilov RF (2009) Microfluidic confinement of single cells of bacteria in small volumes initiates high-density behavior of quorum sensing and growth and reveals its variability. Angew Chem Int Ed 48:5908–5911
26. Baret JC, Beck Y, Billas-Massobrio I, Moras D, Griffiths AD (2010) Quantitative cell-based reporter gene assays using droplet-based microfluidics. Chem Biol 17:528–536
27. Darhuber AA, Valentino JP, Troian SM (2010) Planar digital nanoliter dispensing system based on thermocapillary actuation. Lab Chip 10:1061–1071
28. Fair RB (2007) Digital microfluidics: is a true lab-on-a-chip possible? Microfluid Nanofluid 3:245–281
29. Baret JC, Tally V, Ryckelynck M, Merten CA, Griffiths AD (2009) Droplets and emulsions: very high-throughput screening in biology. Med Sci (Paris) 25:627–632
30. Ganan-Calvo AM (1998) Generation of steady liquid microthreads and micron-sized monodisperse sprays in gas streams. Phys Rev Lett 80:285–288
31. Anna SL, Bontoux N, Stone HA (2003) Formation of dispersions using "flow focusing" in microchannels. Appl Phys Lett 82:364–366
32. Garstecki P, Fuerstman MJ, Stone HA, Whitesides GM (2006) Formation of droplets and bubbles in a microfluidic T-junction—scaling and mechanism of break-up. Lab Chip 6:437–446
33. Guillot P, Colin A (2005) Stability of parallel flows in a microchannel after a T junction. Phys Rev E 72:066301
34. De Menech M, Garstecki P, Jousse F, Stone HA (2008) Transition from squeezing to dripping in a microfluidic T-shaped junction. J Fluid Mech 595:141–161
35. Christopher GF, Noharuddin NN, Taylor JA, Anna SL (2008) Experimental observations of the squeezing-to-dripping transition in T-shaped microfluidic junctions. Phys Rev E 78:036317

36. Garstecki P, Stone HA, Whitesides GM (2005) Mechanism for flow-rate controlled breakup in confined geometries: a route to monodisperse emulsions. Phys Rev Lett 94:164501
37. Dollet B, van Hoeve W, Raven JP, Marmottant P, Versluis M (2008) Role of the channel geometry on the bubble pinch-off in flow-focusing devices. Phys Rev Lett 100:034504
38. Nie ZH, Seo MS, Xu SQ, Lewis PC, Mok M, Kumacheva E, Whitesides GM, Garstecki P, Stone HA (2008) Emulsification in a microfluidic flow-focusing device: effect of the viscosities of the liquids. Microfluid Nanofluid 5:585–594
39. Lee W, Walker LM, Anna SL (2009) Role of geometry and fluid properties in droplet and thread formation processes in planar flow focusing. Phys Fluids 21:032103
40. Prakash M, Gershenfeld N (2007) Microfluidic bubble logic. Science 315:832–835
41. Xu J, Attinger D (2008) Drop on demand in a microfluidic chip. J Micromech Microeng 18:065020
42. Bransky A, Korin N, Khoury M, Levenberg S (2009) A microfluidic droplet generator based on a piezoelectric actuator. Lab Chip 9:516–520
43. Jones TB, Gunji M, Washizu M, Feldman MJ (2001) Dielectrophoretic liquid actuation and nanodroplet formation. J Appl Phys 89:1441–1448
44. Zeng J, Korsmeyer T (2004) Principles of droplet electrohydrodynamics for lab-on-a-chip. Lab Chip 4:265–277
45. Malloggi F, Gu H, Banpurkar AG, Vanapalli SA, Mugele F (2008) Electrowetting—a versatile tool for controlling microdrop generation. Eur Phys J E 26:91–96
46. Zeng S, Li B, Su X, Qin J, Lin BC (2009) Microvalve-actuated precise control of individual droplets in microfluidic devices. Lab Chip 9:3
47. Galas JC, Bartolo D, Studer V (2009) Active connectors for microfluidic drops on demand. New J Phys 11:075027
48. Hulme SE, Shevkoplyas SS, Whitesides GM (2009) Incorporation of prefabricated screw, pneumatic, and solenoid valves into microfluidic devices. Lab Chip 9:79–86
49. Lee JN, Park C, Whitesides GM (2003) Solvent compatibility of poly(dimethylsiloxane)-based microfluidic devices. Anal Chem 75:6544–6554
50. Churski K, Michalski J, Garstecki P (2010) Droplet on demand system utilizing a computer controlled microvalve integrated into a stiff polymeric microfluidic device. Lab Chip 10(4):512–518
51. Churski K, Korczyk P, Garstecki P (2010) High-throughput automated droplet microfluidic system for screening of reaction conditions. Lab Chip 10:816–818
52. Adamson DN, Mustafi D, Zhang JXJ, Zheng B, Ismagilov RF (2006) Production of arrays of chemically distinct nanolitre plugs via repeated splitting in microfluidic devices. Lab Chip 6:1178–1186
53. Link DR, Anna SL, Weitz DA, Stone HA (2004) Geometrically mediated breakup of drops in microfluidic devices. Phys Rev Lett 92:054503
54. Cristobal G, Benoit JP, Joanicot M, Ajdari A (2006) Microfluidic bypass for efficient passive regulation of droplet traffic at a junction. Appl Phys Lett 89:034104
55. Nie J, Kennedy RT (2010) Sampling from nanoliter plugs via asymmetrical splitting of segmented flow. Anal Chem 82:7852–7856
56. Baroud CN, de Saint Vincent MR, Delville JP (2007) An optical toolbox for total control of droplet microfluidics. Lab Chip 7:1029–1033
57. Trivedi V, Doshi A, Kurup GK, Ereifej E, Vandevord PJ, Basu AS (2010) A modular approach for the generation, storage, mixing, and detection of droplet libraries for high throughput screening. Lab Chip 10:2433–2442
58. Sung JH, Kam C, Shuler ML (2010) A microfluidic device for a pharmacokinetic-pharmacodynamic (PK-PD) model on a chip. Lab Chip 10:446–455
59. Clausell-Tormos J, Griffiths AD, Merten CA (2010) An automated two-phase microfluidic system for kinetic analyses and the screening of compound libraries. Lab Chip 10:1302–1307
60. Chen D, Du WB, Liu Y, Liu WS, Kuznetsov A, Mendez FE, Philipson LH, Ismagilov RF (2008) The chemistrode: a droplet-based microfluidic device for stimulation and recording

with high temporal, spatial, and chemical resolution. Proc Natl Acad Sci U S A 105:16843–16848
61. Liu WS, Kim HJ, Lucchetta EM, Du WB, Ismagilov RF (2009) Isolation, incubation, and parallel functional testing and identification by FISH of rare microbial single-copy cells from multi-species mixtures using the combination of chemistrode and stochastic confinement. Lab Chip 9:2153–2162
62. Bremond N, Thiam AR, Bibette J (2008) Decompressing emulsion droplets favors coalescence. Phys Rev Lett 100:024501
63. Niu X, Gulati S, Edel JB, deMello AJ (2008) Pillar-induced droplet merging in microfluidic circuits. Lab Chip 8:1837–1841
64. Jin BJ, Kim YW, Lee Y, Yoo JY (2010) Droplet merging in a straight microchannel using droplet size or viscosity difference. J Micromech Microeng 20:035003
65. Chabert M, Dorfman KD, Viovy JL (2005) Droplet fusion by alternating current (AC) field electrocoalescence in microchannels. Electrophoresis 26:3706–3715
66. Ahn K, Agresti J, Chong H, Marquez M, Weitz DA (2006) Electrocoalescence of drops synchronized by size-dependent flow in microfluidic channels. Appl Phys Lett 88:264105
67. Link DR, Grasland-Mongrain E, Duri A, Sarrazin F, Cheng ZD, Cristobal G, Marquez M, Weitz DA (2006) Electric control of droplets in microfluidic devices. Angew Chem Int Ed 45:2556–2560
68. Shemesh J, Bransky A, Khoury M, Levenberg S (2010) Advanced microfluidic droplet manipulation based on piezoelectric actuation. Biomed Microdevices 12:907–914
69. Lau AY, Lee LP, Chan JW (2008) An integrated optofluidic platform for Raman-activated cell sorting. Lab Chip 8:1116–1120
70. Ocvirk G, Salimi-Moosavi H, Szarka RJ, Arriaga EA, Andersson PE, Smith R, Dovichi NJ, Harrison DJ (2004) Beta-galactosidase assays of single-cell lysates on a microchip: a complementary method for enzymatic analysis of single cells. Proc IEEE 92:115–125
71. Niu XZ, Zhang MY, Peng SL, Wen WJ, Sheng P (2007) Real-time detection, control, and sorting of microfluidic droplets. Biomicrofluidics 1:044101
72. Tan YC, Fisher JS, Lee AI, Cristini V, Lee AP (2004) Design of microfluidic channel geometries for the control of droplet volume, chemical concentration, and sorting. Lab Chip 4:292–298
73. Mazutis L, Griffiths AD (2009) Preparation of monodisperse emulsions by hydrodynamic size fractionation. Appl Phys Lett 95:204103
74. Maenaka H, Yamada M, Yasuda M, Seki M (2008) Continuous and size-dependent sorting of emulsion droplets using hydrodynamics in pinched microchannels. Langmuir 24:4405–4410
75. Abate AR, Agresti JJ, Weitz DA (2010) Microfluidic sorting with high-speed single-layer membrane valves. Appl Phys Lett 96:203509
76. Shirasaki Y, Tanaka J, Makazu H, Tashiro K, Shoji S, Tsukita S, Funatsu T (2006) On-chip cell sorting system using laser-induced heating of a thermoreversible gelation polymer to control flow. Anal Chem 78:695–701
77. Saint Vincent MRD, Wunenburger R, Delville JP (2008) Laser switching and sorting for high speed digital microfluidics. Appl Phys Lett 92:154105
78. Yap YF, Tan SH, Nguyen NT, Murshed SMS, Wong TN, Yobas L (2009) Thermally mediated control of liquid microdroplets at a bifurcation. J Phys D: Appl Phys 42:065503
79. Zhang MY, Wu JB, Niu XZ, Wen WJ, Sheng P (2008) Manipulations of microfluidic droplets using electrorheological carrier fluid. Phys Rev E 78:066305
80. Franke T, Abate AR, Weitz DA, Wixforth A (2009) Surface acoustic wave (SAW) directed droplet flow in microfluidics for PDMS devices. Lab Chip 9:2625–2627
81. Ahn B, Lee K, Louge R, Oh KW (2009) Concurrent droplet charging and sorting by electrostatic actuation. Biomicrofluidics 3(4):44102
82. Baret JC, Miller OJ, Taly V, Ryckelynck M, El-Harrak A, Frenz L, Rick C, Samuels ML, Hutchison JB, Agresti JJ, Link DR, Weitz DA, Griffiths AD (2009) Fluorescence-activated

droplet sorting (FADS): efficient microfluidic cell sorting based on enzymatic activity. Lab Chip 9:1850–1858
83. Granieri L, Baret JC, Griffiths AD, Merten CA (2010) High-throughput screening of enzymes by retroviral display using droplet-based microfluidics. Chem Biol 17:229–235
84. Song H, Ismagilov RF (2003) Millisecond kinetics on a microfluidic chip using nanoliters of reagents. J Am Chem Soc 125:14613–14619
85. Holtze C, Rowat AC, Agresti JJ, Hutchison JB, Angile FE, Schmitz CHJ, Koster S, Duan H, Humphry KJ, Scanga RA, Johnson JS, Pisignano D, Weitz DA (2008) Biocompatible surfactants for water-in-fluorocarbon emulsions. Lab Chip 8:1632–1639
86. Frenz L, Blank K, Brouzes E, Griffiths AD (2009) Reliable microfluidic on-chip incubation of droplets in delay-lines. Lab Chip 9:1344–1348
87. Schmitz CHJ, Rowat AC, Koster S, Weitz DA (2009) Dropspots: a picoliter array in a microfluidic device. Lab Chip 9:44–49
88. Huebner A, Sharma S, Srisa-Art M, Hollfelder F, Edel JB, Demello AJ (2008) Microdroplets: a sea of applications? Lab Chip 8:1244–1254
89. Bai YP, He XM, Liu DS, Patil SN, Bratton D, Huebner A, Hollfelder F, Abell C, Huck WTS (2010) A double droplet trap system for studying mass transport across a droplet-droplet interface. Lab Chip 10:1281–1285
90. Mazutis L, Baret JC, Treacy P, Skhiri Y, Araghi AF, Ryckelynck M, Taly V, Griffiths AD (2009) Multi-step microfluidic droplet processing: kinetic analysis of an in vitro translated enzyme. Lab Chip 9:2902–2908
91. Malo N, Hanley JA, Cerquozzi S, Pelletier J, Nadon R (2006) Statistical practice in high-throughput screening data analysis. Nat Biotechnol 24:167–175
92. Dove A (1999) Drug screening—beyond the bottleneck. Nat Biotechnol 17:859–863
93. Theberge AB, Whyte G, Huck WTS (2010) Generation of picoliter droplets with defined contents and concentration gradients from the separation of chemical mixtures. Anal Chem 82:3449–3453
94. Churski K, Kamiński T, Jakiela S, Kamysz W, Barańska-Rybak W, Weibel D, Garstecki P (2012) Rapid screening of antibiotic toxicity in an automated microdroplet system: Lab Chip 12:1629–1637
95. Brouzes E, Medkova M, Savenelli N, Marran D, Twardowski M, Hutchison JB, Rothberg JM, Link DR, Perrimon N, Samuels ML (2009) Droplet microfluidic technology for single-cell high-throughput screening. Proc Natl Acad Sci U S A 106:14195–14200
96. Tawfik DS, Griffiths AD (1998) Man-made cell-like compartments for molecular evolution. Nat Biotechnol 16:652–656
97. Dittrich PS, Jahnz M, Schwille P (2005) A new embedded process for compartmentalized cell-free protein expression and on-line detection in microfluidic devices. Chembiochem 6:811–814
98. Courtois F, Olguin LF, Whyte G, Bratton D, Huck WTS, Abell C, Hollfelder F (2008) An integrated device for monitoring time-dependent in vitro expression from single genes in picolitre droplets. Chembiochem 9:439–446
99. Huebner A, Srisa-Art M, Holt D, Abell C, Hollfelder F, Demello AJ, Edel JB (2007) Quantitative detection of protein expression in single cells using droplet microfluidics. Chem Commun 12:1218–1220
100. Huebner A, Olguin LF, Bratton D, Whyte G, Huck WTS, de Mello AJ, Edel JB, Abell C, Hollfelder F (2008) Development of quantitative cell-based enzyme assays in microdroplets. Anal Chem 80:3890–3896
101. Boedicker JQ, Li L, Kline TR, Ismagilov RF (2008) Detecting bacteria and determining their susceptibility to antibiotics by stochastic confinement in nanoliter droplets using plug-based microfluidics. Lab Chip 8:1265–1272
102. He MY, Edgar JS, Jeffries GDM, Lorenz RM, Shelby JP, Chiu DT (2005) Selective encapsulation of single cells and subcellular organelles into picoliter- and femtoliter-volume droplets. Anal Chem 77:1539–1544

103. Raj A, van Oudenaarden A (2009) Single-molecule approaches to stochastic gene expression. Annu Rev Biophys 38:255–270
104. Cai L, Friedman N, Xie XS (2006) Stochastic protein expression in individual cells at the single molecule level. Nature 440:358–362
105. Chabert M, Viovy JL (2008) Microfluidic high-throughput encapsulation and hydrodynamic self-sorting of single cells. Proc Natl Acad Sci U S A 105:3191–3196
106. Edd JF, Di Carlo D, Humphry KJ, Koster S, Irimia D, Weitz DA, Toner M (2008) Controlled encapsulation of single-cells into monodisperse picolitre drops. Lab Chip 8:1262–1264
107. Shim JU, Olguin LF, Whyte G, Scott D, Babtie A, Abell C, Huck WTS, Hollfelder F (2009) Simultaneous determination of gene expression and enzymatic activity in individual bacterial cells in microdroplet compartments. J Am Chem Soc 131:15251–15256
108. Joensson HN, Samuels ML, Brouzes ER, Medkova M, Uhlen M, Link DR, Andersson-Svahn H (2009) Detection and analysis of low-abundance cell-surface biomarkers using enzymatic amplification in microfluidic droplets. Angew Chem Int Ed 48:2518–2521
109. Tewhey R, Warner JB, Nakano M, Libby B, Medkova M, David PH, Kotsopoulos SK, Samuels ML, Hutchison JB, Larson JW, Topol EJ, Weiner MP, Harismendy O, Olson J, Link DR, Frazer KA (2009) Microdroplet-based PCR enrichment for large-scale targeted sequencing. Nat Biotechnol 27:1025–1094
110. Beer NR, Hindson BJ, Wheeler EK, Hall SB, Rose KA, Kennedy IM, Colston BW (2007) On-chip, real-time, single-copy polymerase chain reaction in picoliter droplets. Anal Chem 79:8471–8475
111. Beer NR, Wheeler EK, Lee-Houghton L, Watkins N, Nasarabadi S, Hebert N, Leung P, Arnold DW, Bailey CG, Colston BW (2008) On-chip single-copy real-time reverse-transcription PCR in isolated picoliter droplets. Anal Chem 80:1854–1858
112. Kiss MM, Ortoleva-Donnelly L, Beer NR, Warner J, Bailey CG, Colston BW, Rothberg JM, Link DR, Leamon JH (2008) High-throughput quantitative polymerase chain reaction in picoliter droplets. Anal Chem 80:8975–8981
113. Schaerli Y, Wootton RC, Robinson T, Stein V, Dunsby C, Neil MAA, French PMW, deMello AJ, Abell C, Hollfelder F (2009) Continuous-flow polymerase chain reaction of single-copy DNA in microfluidic microdroplets. Anal Chem 81:302–306
114. Mazutis L, Araghi AF, Miller OJ, Baret JC, Frenz L, Janoshazi A, Taly V, Miller BJ, Hutchison JB, Link D, Griffiths AD, Ryckelynck M (2009) Droplet-based microfluidic systems for high-throughput single DNA molecule isothermal amplification and analysis. Anal Chem 81:4813–4821
115. Sykes PJ, Neoh SH, Brisco MJ, Hughes E, Condon J, Morley AA (1992) Quantitation of targets for PCR by use of limiting dilution. Biotechniques 13:444–449
116. Zeng Y, Novak R, Shuga J, Smith MT, Mathies RA (2010) High-performance single cell genetic analysis using microfluidic emulsion generator arrays. Anal Chem 82:3183–3190

Chapter 6
The Dropletisation of Bio-Reactions

Ehsan Karimiani, Amelia Markey, and Philip Day

6.1 Molecular Cancer Diagnostics: Future Possibilities with Current Technologies

Molecular diagnostics is a continually evolving scientific discipline, which is based on the study of medical symptoms and conditions, and is applied in every aspect of healthcare delivery [1] and is inextricably linked to prognosis and therapy. Increasingly the output from molecular diagnostics testing is related to specific therapy, and clinical medicine is being transformed by molecular pathology that will make predictive and personalised medicine possible. To maximise impact, modern molecular diagnostics is highly translational, sharing different aspects of clinical practice with disciplines such as point of care instrumentation developments and microfluidics, combined with biophysics and computational fluid dynamics [2].

Molecular techniques were developed for application in the clinic and research settings, and clearly long predate the Human Genome Project. In the current phase of post-genome research, synergy with molecular pathologic methods is being applied to explicate the genetic basis of many diseases, and these innovations have helped to develop the discipline of molecular diagnostics. In the longer term, medical pathology is expected to increase molecular distinction to provide high resolution classification of human cancers and the validation of predictive biomarkers for the personalised susceptibility of patients with dissimilar genetic clones [3]. Today, molecular diagnostics continues to improve in combination with medical imaging. The diagnostic sector is beginning to produce new kits, lab-on-a-chip integrated microfluidics, sensors and logic to provide more rapid genetic analyses [4]. But does microfluidics only resemble a means of packaging pre-existing bioassays?

E. Karimiani • A. Markey • P. Day (✉)
Manchester Institute of Biotechnology, University of Manchester,
131 Princess Road, Manchester M1 7ND, UK
e-mail: Philip.j.day@manchester.ac.uk

P. Day et al. (eds.), *Microdroplet Technology: Principles and Emerging Applications in Biology and Chemistry*, Integrated Analytical Systems,
DOI 10.1007/978-1-4614-3265-4_6,

Clinical testing is moving towards performing point of care and personalised medicine whilst molecular research endeavours to identify the genetic and proteomic biomarkers of disease. Mutations responsible for cancers are being discovered and routinely used in molecular diagnostic tests. An important goal of current miniaturised instruments, certainly in part, is to provide the packaging to facilitate present day methods so that clinicians have adequate information of the disease to enable point of care and rapid (multi-parallel) diagnosis of individual patients. So far, lab-on-a-chip advances have shed light on automated nucleic acid preparation, real-time polymerase chain reaction (PCR) and DNA sequencing [5]. However, clinical molecular diagnostic centres using miniaturised chips are currently limited to the more popular tests with a higher clinical utility. This is an understandably good starting point as investment and samples are available, and the microfluidic device has a better likelihood of achieving a high impact and commercial success. The case for developing microfluidics for point of care testing while packaging diagnostics tests (which for us is often nucleic acid based through the sensitivity offered by PCR) has been argued, however, there are other important drivers to improve on current molecular diagnostic analysis. Miniaturisation of bio-assays on the basis of cost saving is an insufficient rationale, and may indeed be inaccurate as there often exist associated high cost implications. A far higher impact value attributed to microfluidics is the partitioning of conventional bioassays to improve the resolution of data generation [6]. While detection of biomarkers is typically highly developed, the treatment of the raw clinical sample prior to the bioassay is rarely afforded any close attention. Another feature of many molecular analyses is their complexity and inability to offer high levels of inter-assay reproducibility. This paradox (of high molecular characterisation associated with poor reproducibility) can be addressed through ablating the highly heterogeneous clinical sample to produce a situation whereby a single cell can be analysed within a reaction. Such an approach will reveal the true molecular profile underpinning heterogeneity. As a consequence the *minimum* number of cells characterising a population will be revealed. A further and major benefit of this approach is that the common denominator across all bioassays becomes the cell, and the variables have units of molecules; numbers of molecules per cell. Therefore, while the packaging of (diagnostic) bioassays provide critical environments to perform analyses, a major role for microfluidics relates to the enhancement of conventional analyses through analysis of populations of single cells. Two-phase flow to produce aqueous droplets may provide the environment to generate absolute quantitative data. Figure 6.1 shows the formation of droplets for performing PCR and the Agilent traces produced to verify the occurrence of genes specific amplification.

Large scale studies aimed at unravelling the underlying genetic basis of complex (or network-based) diseases through statistical power gain is placing a near exponential increment in sample analysis to generate sufficient data to profile populations. The implementation of droplets has characteristics that are able to fulfill the criteria required for an analysis system capable of handling huge numbers of single cells, plus development of appropriate informatics

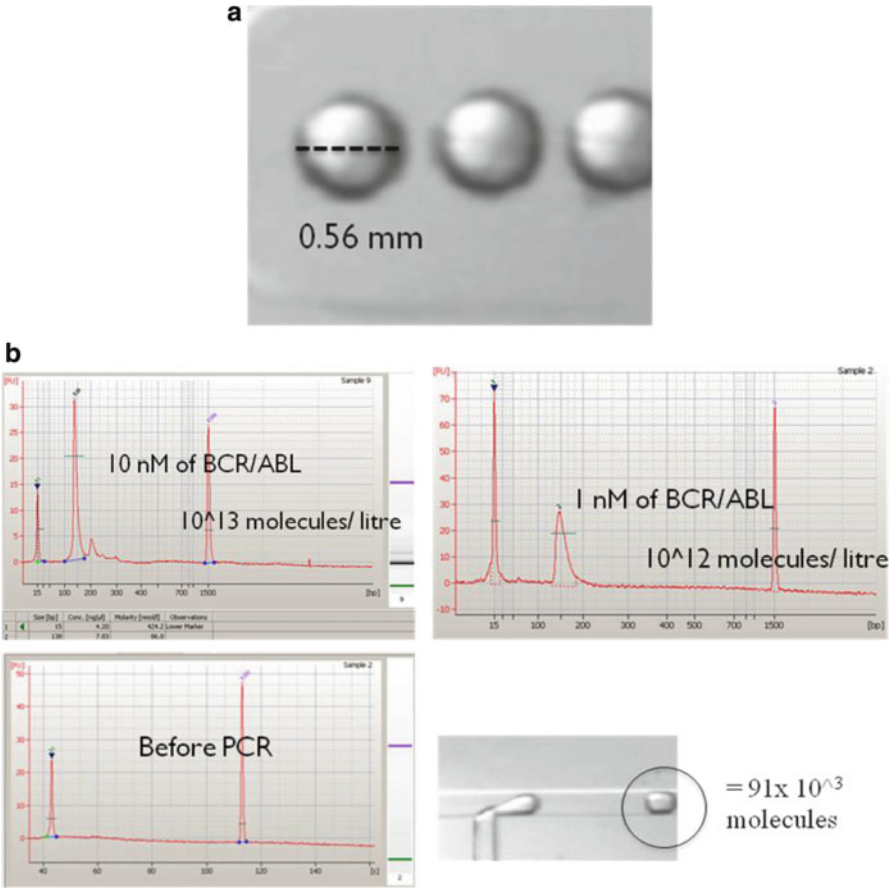

Fig. 6.1 (**a**) Shows the production of droplets for PCR. The droplets were produced by employing an oil flow rate of 2.8 μL/min in conjunction with a water flow rate of 0.7 μL/min. PCR thermo-cycling conditions comprised 30 s at 60 and 95°C. The volume of the droplet was 91 nL. (**b**) Shows the Agilent Bioanalyser 2100 trace signifying the level of amplification seen from the original 91×10^3 molecules per droplet

tools (see Fig. 6.2). This chapter explores this association and probes if droplets will also be able to deliver absolute and physiologically meaningful biomarker quantification.

6.2 Lab-on-a-Chip and Single Cell Analysis

Cell division is a fundamental developmental event; however, studies have shown that single cells can undergo an asymmetric cell division. Fluctuations in gene expression at the single cell level could be a key for generating developmental

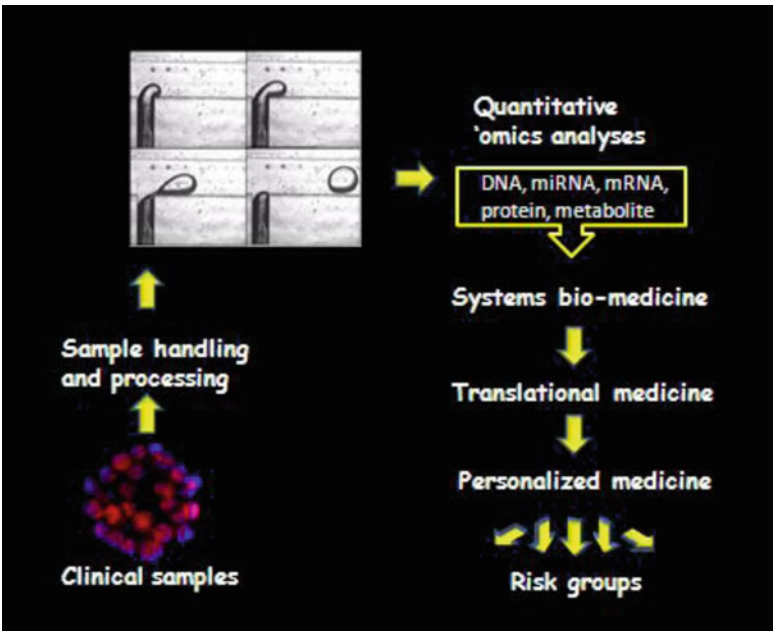

Fig. 6.2 This figure is a flow diagram representation of how a clinical sample can be treated to release its cellular content and permit analyses of numerous types of biological compounds to help characterise (by network modelling) the types, activities and inter-relationships of cells. The risk groups in turn will be associated with their own therapies

signals and therapeutic regimens [7]. Cells of a specific cell type can display a distribution of activities and this relates to their ability to synergise and cooperate within tissues in response to environmental cues. Current routine quantitative methodologies analyse the average expression level for a population of cells but disregard the variation between individual cells; current nucleic acid measurements are almost entirely bulk analyses. Some published studies report that the level of mRNA expression amongst individual cells is lognormal rather than symmetrically distributed. For that reason the average expression in a cell population does not represent the expression of a transcript in each cell within that population. The average data will be strongly biased by a minority population of individual active cells with a high level or indeed absence of a particular transcript [8]. Hence, it may not be valid to estimate values of gene expression studies at the single-cell level from data derived from a population of cells. This is an important reason why high-throughput means for single cell analysis are predicted to have a substantial role in the future of molecular diagnostics. Consequently, there is a fundamental need to improve molecular diagnostic techniques that can measure the heterogeneity of single cells in cancers and perhaps microfluidic platforms can assist. New developments have been made with a view to overcome the

challenges resulting from the analysis of the averages of a big population due to the inspection of cellular heterogeneity within a population of malignant cells [9]. In spite of the significant information that current methodologies provide on large cellular populations, this approach often leads to missing the rare events such as progenitor stem cells in cancers which can give rise to misleading interpretation in clinical trials and in diagnostics such as minimal residual disease investigations.

However, the present formulation of diagnostic testing, such as minimal residual disease in leukaemia, while subject to problems associated with measurement that compromises absolute sensitivity and quantification have been established and have gained much credibility following empirical testing. Single cell analyses as permitted by high-throughput droplets offer a distinct means to profiling cell based populations. However, basing present day diagnostics on single cell molecular signatures would be enshrined with incompatibilities, and an appropriate database would need to be established to enable the new point of care diagnostic approach to be evaluated and related to therapy [10].

Molecular techniques based on lab-on-a-chip know-how are gaining a foothold as an integral component of research in single cell analysis in cancers and stem cells [11]. Systems biology and systems bio-medicine are similarly addressing holistic approaches to understand biological function, with emphasis on the production and integration of quantitative markers for algorithm and model development, and biomedical control and function, respectively. The development of single cell studies at the proteomic and transcriptomic levels are starting to drive the advance of new risk classifications and related therapies to solid cancers, haematological malignancies and drug resistance clones.

6.2.1 Sample Handling

When considering all the virtues of microdroplet devices, both the capacity for seamless extraction and lysis of cells as well as the ability to quantitatively analyse biomarkers are key. Most other types of microfluidic handling use one of a finite array of reactor wells, or possess a format not lending themselves to very high throughput analysis, lack an ability to merge fluids, and chemistries are employed that require partitioning of waste from analyte.

In recent times the most impact within the world of nucleic acid discovery and analysis has been the capacity to sequence from single strands of DNA. This development is highly significant, bringing rapid and routine nucleic acid sequencing for biomarker analysis. An enabling feature of this sequencing technology (known as deep sequencing or next generation sequencing) is the fractionation of a biological sample using the random formation of aqueous droplets in an oil–water emulsion. While the procedure has been met with huge success, a problem of the method relates to the indiscriminate sequencing of all nucleic acids, including informative and uninformative, alike. A growing sector of deep

sequencing relating to sample enrichment has evolved to tackle this important issue. Droplet technologies could make an important impact in this sector whereby droplets are precisely produced to carry pre-selected strands of DNA.

6.3 Role of Microfluidic Devices in Molecular Pathology

The PCR has singularly been the most developed chemical amplifier within the field of miniaturisation, although a fully integrated micro total analysis system (μ-TAS) is far from in routine use. The PCR is one of the most practical molecular methods to amplify informative nucleic acid fragments especially from rare samples and single cells [12]. Stem cell and single cell research are gradually changing the clinical practice of stem cell therapy and molecular oncology. As our understanding of the physiological unit (molecules per cell) improves, more developments of microfluidic technologies capable of routine quantitative measurement of individual cells from small tissue samples will be necessary for the success of clinical trials and dynamic classification of patients into groups mostly benefited from personalised drugs [13].

So far, microfluidic technologies have presented intrinsic achievements in the detection of minimal samples, single cell analysis and precise control over sample delivery at nanoscale volumes. Some microscale platforms are capable of finding new applications for stem cell research, gene expression investigations [14] and proteomics. Some other studies have proposed single cell analyses; including the platforms that permit cultured single cells to interact and to initiate signalling pathways [15]. While deep sequencing offers crucial data on the building blocks of biological pathways, the technique is limited in terms of how it is applied to gain insight into the components of single cells and the subsequent stochastic behaviour that induces cellular heterogeneity. The noise in the quantification of nucleic acids and proteins at the level of individual cells ranges from noise induced from amplification signals to diversity of the biological mRNA expression.

New developments in the study of the response of single cells to therapeutic reagents, in relation to both cellular variability and the pathways involved, may support the application of various quantitative techniques. Different lab-on-a-chip platforms have been developed recently utilising droplet-based technologies that are potentially capable of analysing the expression level within single cells [16].

An increasing number of studies have utilised microfluidic platforms in order to selectively analyse single cells. This reflects the popularity and potential of this field. In future, modern molecular pathology will benefit from the high-throughput capability of droplet technology especially when combined with a sensitive detection technique. The isolation of individual cells will allow the detection of rare cells in a mixed population.

6.4 Advantages of Droplet-Based Microfluidics for Biological Assays

A wide variety of microfluidic design concepts have been implemented for the treatment and analysis of biological samples. These designs fall into three broad categories: well-based [17–19], single-phase continuous flow [20–24] and droplet-based devices [25–30]. Droplet-based designs possess several distinct advantages over other designs for the handling of biological samples, most notably for the case of single cell analysis (Fig. 6.3a). Both the advantages and disadvantages of each of these design types, with respect to the handling of bio-reactions, are shown in Table 6.1.

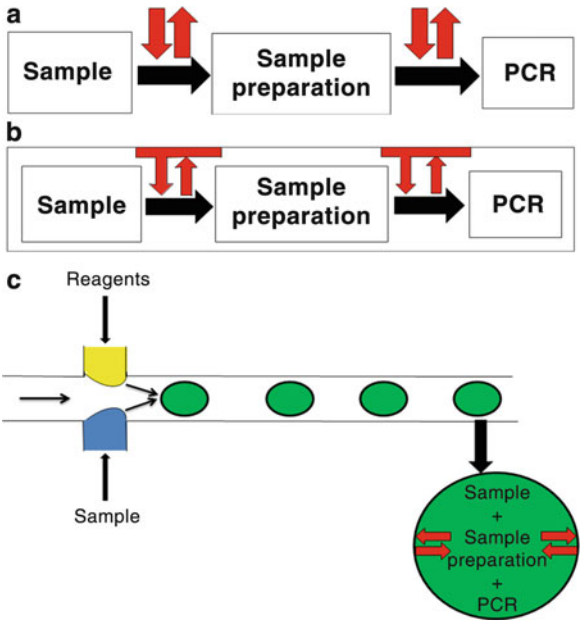

Fig. 6.3 Demonstration of the advantages of integrated sample preparation and analysis. (**a**) Demonstrates the conventional method of sample preparation whereby a sample is collected, prepared and analysed in separate steps. (**b**) Demonstrates a single phase μ-TAS format where sample loss to the internal walls of the device and the resulting contamination of subsequent samples still persists. (**c**) Shows a droplet-based μ-TAS format where the sample is contained and processed within a droplet eliminating sample loss and contamination

Table 6.1 Applicability of microfluidic designs to bioreactions

	Features					
Device design	High-throughput	Small volumes	Potential sample loss	Potential sample contamination	Isolate single cells	Applicable for μTAS
Well-based	X	✓	✓	✓	✓	X
Single-phase continuous	✓	✓	✓	✓	X	X
Droplet-based	✓	✓	X	X	✓	✓

First, the throughput of droplet-based devices is superior to that of well-based devices. Multiple wells would need to be manufactured in parallel in order to produce a high-throughput, well-based design. This has implications for the size of the device and has limited use over conventional 384- and 1536-well plates in terms of the number of samples processed in a given time. Some commercial manufacturers (such as Fluidigm) have increased the well density still further. However as both single-phase and droplet-based systems are continuous flow, as opposed to static wells, a much higher throughput can be achieved by allowing the sample to travel through the device, and the assay throughput becomes a function of time (see www.raindance-technologies.com) as opposed to the number of reactors available.

A limitation of both well-based and single-phase continuous flow designs is that the sample is in constant contact with the walls of the device [31]. Adsorption of the sample onto the walls of the device may not only hinder the analysis of the sample but may also present a potential source of contamination if this device is to be reused (Fig. 6.3b). Problems such as sample loss and contamination can be prevented to some extent by treating the internal walls of the device with a hydrophobic coating [24, 32–34]. However a more reliable prevention against sample loss and contamination is to encapsulate the sample within an aqueous droplet suspended in an immiscible oil carrier fluid (Fig. 6.3c). Optimised droplet generation, along with the use of surfactants, will avoid any interaction between neighbouring droplets whilst the immiscible oil carrier phase isolates the droplet contents from interaction with the walls of the device. In this way each droplet provides an isolated environment for a sub-micron scale bio-reaction.

Another feature of droplet-based microfluidic systems, which is particularly advantageous to molecular diagnostics, is that the contents of each individual droplet can be controlled with precise handling of the fluidics. This can be optimised to allow the isolation of a single cell within each droplet produced on the device [35, 36]. In this way multiple single cells can be processed and analysed in a high-throughput, contamination-free environment. The analysis of multiple single cells in isolation will not only allow the clinician to dissect the bulk cell population into more meaningful subpopulations of cells but will also heighten the detection of rare cells within the larger bulk population [21, 37, 38]. This means of analysis is currently available if cells are isolated from the bulk population by FACS prior to testing. However such a methodology will be inaccurate, prone to contamination and will not generate the throughput of analysis required to be feasibly implemented in a clinical setting.

A final requirement of microfluidics for bio-reactions is that the complete preparation and analysis of the crude sample can be integrated and carried out on a single microfluidic device. This μ-TAS should be able to prepare the sample from its crude, raw format to a state sufficient for the required biological assay, perform the assay without loss or contamination, and finally detect the output of this assay [39]. Such a goal requires the careful manipulation of both the sample and reagents on the device.

To achieve operations such as purification of the sample from its crude form, cell lysis, PCR and detection the sample must be transported through

multiple environments involving different buffer conditions, reagent additions and temperatures. For this to be achieved in a well-based or single-phase continuous flow format the sample would have to be transported between different regions of the device which would need to be separated with complex partitioning, gating or microvalve systems [17, 18, 40]. A droplet-based system provides the best format for true μ-TAS as droplets can be manipulated in a number of ways with ease. Through the use of electrodes the path of droplet travel can be directed allowing for the splitting [41–43], merging [44–48], sorting [42, 47, 49–51] and storage [52–56] of droplets on the device. For example, known quantities of reagents can be added to each sample through the precise merging of reagent-containing and sample-containing droplets [48].

The integration of all steps of sample preparation and analysis as well as having a known sample size, i.e. a single cell, are important features of a device required for the diagnosis of molecular pathologies in clinical samples. However to analyse each cell on an individual basis one must ensure that the cell is shielded from any source of contamination, that none of the limited sample is lost throughout the steps of preparation and analysis and that cells can be analysed in a high-throughput manner. As previously mentioned, clinical samples have a tertiary architecture and are often very heterogeneous in nature and as such require assessment of single cells to comprehend the level of tissue activities, and thus achieve an informative diagnosis. This is particularly important if the goal is to stratify patients into discrete risk groups for the basis of personalised medication. This type of targeted medication for specific risk groups of patients will help to curb the ever increasing drug attrition rate that has been caused by pursuing the "one-drug-fits-all" approach to drug development [57].

References

1. Molinaro RJ (2011) Cases on the rise: current diagnosis guidelines and research efforts for a cure. MLO Med Lab Obs 43(2):8, 10, 12 passim; quiz 16–17
2. Erickson D et al (2004) Electrokinetically controlled DNA hybridization microfluidic chip enabling rapid target analysis. Anal Chem 76(24):7269–7277
3. Ogino S et al (2011) Molecular pathological epidemiology of colorectal neoplasia: an emerging transdisciplinary and interdisciplinary field. Gut 60(3):397–411
4. Coupland P (2010) Microfluidics for the upstream pipeline of DNA sequencing—a worthy application? Lab Chip 10(5):544–547
5. Napoli M, Eijkel JC, Pennathur S (2010) Nanofluidic technology for biomolecule applications: a critical review. Lab Chip 10(8):957–985
6. Imaad SM et al (2011) Microparticle and cell counting with digital microfluidic compact disc using standard CD drive. Lab Chip 11(8):1448–1456
7. Tamburini BA et al (2010) Gene expression profiling identifies inflammation and angiogenesis as distinguishing features of canine hemangiosarcoma. BMC Cancer 10:619
8. Bengtsson M et al (2005) Gene expression profiling in single cells from the pancreatic islets of Langerhans reveals lognormal distribution of mRNA levels. Genome Res 15(10):1388–1392
9. Kamme F et al (2003) Single-cell microarray analysis in hippocampus CA1: demonstration and validation of cellular heterogeneity. J Neurosci 23(9):3607–3615

10. Abe T et al (2011) Point-of-care testing system enabling 30 min detection of influenza genes. Lab Chip 11(6):1166–1167
11. Li X, Chen Y, Li PC (2011) A simple and fast microfluidic approach of same-single-cell analysis (SASCA) for the study of multidrug resistance modulation in cancer cells. Lab Chip 11(7):1378–1384
12. Peham JR et al (2011) Long target droplet polymerase chain reaction with a microfluidic device for high-throughput detection of pathogenic bacteria at clinical sensitivity. Biomed Microdevices 13(3):463–473
13. Warren L et al (2006) Transcription factor profiling in individual hematopoietic progenitors by digital RT-PCR. Proc Natl Acad Sci U S A 103(47):17807–17812
14. Petriv OI et al (2010) Comprehensive microRNA expression profiling of the hematopoietic hierarchy. Proc Natl Acad Sci U S A 107(35):15443–15448
15. Frimat JP et al (2011) A microfluidic array with cellular valving for single cell co-culture. Lab Chip 11(2):231–237
16. Okochi M et al (2010) Droplet-based gene expression analysis using a device with magnetic force-based-droplet-handling system. J Biosci Bioeng 109(2):193–197
17. Marcy Y et al (2007) Nanoliter reactors improve multiple displacement amplification of genomes from single cells. PLoS Genet 3(9):1702–1708
18. Marcy Y et al (2007) Dissecting biological "dark matter" with single-cell genetic analysis of rare and uncultivated TM7 microbes from the human mouth. Proc Natl Acad Sci U S A 104(29):11889–11894
19. Wilding P, Shoffner MA, Kricka LJ (1994) PCR in a silicon microstructure. Clin Chem 40(9):1815–1818
20. Chien LJ et al (2009) A micro circulating PCR chip using a suction-type membrane for fluidic transport. Biomed Microdevices 11(2):359–367
21. Crews N, Wittwer C, Gale B (2008) Continuous-flow thermal gradient PCR. Biomed Microdevices 10(2):187–195
22. Frey O et al (2007) Autonomous microfluidic multi-channel chip for real-time PCR with integrated liquid handling. Biomed Microdevices 9(5):711–718
23. Sun Y, Kwok YC, Nguyen NT (2007) A circular ferrofluid driven microchip for rapid polymerase chain reaction. Lab Chip 7(8):1012–1017
24. Sugumar D et al (2010) Amplification of SPPS150 and Salmonella typhi DNA with a high throughput oscillating flow polymerase chain reaction device. Biomicrofluidics 4(2):024103
25. Markey AL, Mohr S, Day PJ (2010) High-throughput droplet PCR. Methods 50(4):277–281
26. Gonzalez A et al (2007) Gene transcript amplification from cell lysates in continuous-flow microfluidic devices. Biomed Microdevices 9(5):729–736
27. Kiss MM et al (2008) High-throughput quantitative polymerase chain reaction in picoliter droplets. Anal Chem 80(23):8975–8981
28. Mohr S et al (2007) Numerical and experimental study of a droplet-based PCR chip. Microfluid Nanofluid 3(5):611–621
29. Ohashi T et al (2007) A simple device using magnetic transportation for droplet-based PCR. Biomed Microdevices 9(5):695–702
30. Schaerli Y et al (2009) Continuous-flow polymerase chain reaction of single-copy DNA in microfluidic microdroplets. Anal Chem 81(1):302–306
31. Kuncova-Kallio J, Kallio PJ (2006) PDMS and its suitability for analytical microfluidic devices. Conf Proc IEEE Eng Med Biol Soc 1:2486–2489
32. Kricka LJ, Wilding P (2003) Microchip PCR. Anal Bioanal Chem 377(5):820–825
33. Shoffner MA et al (1996) Chip PCR. I. Surface passivation of microfabricated silicon-glass chips for PCR. Nucleic Acids Res 24(2):375–379
34. Wang W et al (2006) Silicon inhibition effects on the polymerase chain reaction: a real-time detection approach. J Biomed Mater Res A 77(1):28–34
35. Brouzes E et al (2009) Droplet microfluidic technology for single-cell high-throughput screening. Proc Natl Acad Sci U S A 106(34):14195–14200

36. Um E, Lee SG, Park JK (2010) Random breakup of microdroplets for single-cell encapsulation. Appl Phys Lett 97(15):153703
37. Zimmerlin L, Donnenberg VS, Donnenberg AD (2011) Rare event detection and analysis in flow cytometry: bone marrow mesenchymal stem cells, breast cancer stem/progenitor cells in malignant effusions, and pericytes in disaggregated adipose tissue. Methods Mol Biol 699:251–273
38. Chen CL et al (2011) Separation and detection of rare cells in a microfluidic disk via negative selection. Lab Chip 11(3):474–483
39. Manz A, Graber N, Widmer HM (1990) Miniaturized total chemical-analysis systems—a novel concept for chemical sensing. Sens Actuators B Chem 1(1–6):244–248
40. Brivio M, Verboom W, Reinhoudt DN (2006) Miniaturized continuous flow reaction vessels: influence on chemical reactions. Lab Chip 6(3):329–344
41. Link DR et al (2004) Geometrically mediated breakup of drops in microfluidic devices. Phys Rev Lett 92(5):054503
42. Link DR et al (2006) Electric control of droplets in microfluidic devices. Angew Chem Int Ed Engl 45(16):2556–2560
43. Song H, Tice JD, Ismagilov RF (2003) A microfluidic system for controlling reaction networks in time. Angew Chem Int Ed Engl 42(7):768–772
44. Chabert M, Dorfman KD, Viovy JL (2005) Droplet fusion by alternating current (AC) field electrocoalescence in microchannels. Electrophoresis 26(19):3706–3715
45. Christopher GF et al (2009) Coalescence and splitting of confined droplets at microfluidic junctions. Lab Chip 9(8):1102–1109
46. Mazutis L, Baret JC, Griffiths AD (2009) A fast and efficient microfluidic system for highly selective one-to-one droplet fusion. Lab Chip 9(18):2665–2672
47. Tan YC et al (2004) Design of microfluidic channel geometries for the control of droplet volume, chemical concentration, and sorting. Lab Chip 4(4):292–298
48. Tan WH, Takeuchi S (2006) Timing controllable electrofusion device for aqueous droplet-based microreactors. Lab Chip 6(6):757–763
49. Ahn K et al (2006) Dielectrophoretic manipulation of drops for high-speed microfluidic sorting devices. Appl Phys Lett 88(2):024104
50. Baret JC et al (2009) Fluorescence-activated droplet sorting (FADS): efficient microfluidic cell sorting based on enzymatic activity. Lab Chip 9(13):1850–1858
51. Kawano T et al (2005) On-chip sorting system using charged droplets. Micro Total Anal Syst 1(296):144–146
52. Beer NR, Rose KA, Kennedy IM (2009) Monodisperse droplet generation and rapid trapping for single molecule detection and reaction kinetics measurement. Lab Chip 9(6):841–844
53. Sgro AE, Allen PB, Chiu DT (2007) Thermoelectric manipulation of aqueous droplets in microfluidic devices. Anal Chem 79(13):4845–4851
54. Shi W et al (2008) Droplet-based microfluidic system for individual Caenorhabditis elegans assay. Lab Chip 8(9):1432–1435
55. Stan CA et al (2009) A microfluidic apparatus for the study of ice nucleation in supercooled water drops. Lab Chip 9(16):2293–2305
56. Wang W, Yang C, Li CM (2009) On-demand microfluidic droplet trapping and fusion for on-chip static droplet assays. Lab Chip 9(11):1504–1506
57. Myers S, Baker A (2001) Drug discovery—an operating model for a new era. Nat Biotechnol 19(8):727–730

Chapter 7
Droplet-Based Microfluidics as a Biomimetic Principle: From PCR-Based Virus Diagnostics to a General Concept for Handling of Biomolecular Information

J. Michael Köhler

7.1 Introduction

The ability of lithographic fabrication of microchannels for fluid transport on the one hand and the continuously decreasing critical dimensions during the development of microlithography over the last decades generated high expectations on the progress of automated processing of small amounts of substances. In particular, it was expected that large numbers of well distinguished chemical entities—atoms, molecules, nano particles—could become manipulated highly parallel and with high speed. This hope was fed by the imagination of an analogy between the electron transport in integrated circuits and the transport of chemical objects inside microfluidic networks. The experiences of the last both decades had shown that such ideas of a complete analogy are not realistic. The progress of handling of substance-coupled information is much slower as the progress of hard ware development in the electronic devices. But, beside this general disappointment, microfluidics is still promising the arise and growth-up of very important new strategies for organizing chemical systems at the microscale and for supplying functional interfaces between the complex information inside the world of molecules and particles on the one hand and electronic systems on the other hand.

Whereas clouds of electrons are manipulated in digital electronic devices, clouds of molecules are transported through microchannels by a convective flow. But, the special conditions in microfluidics cause low Reynolds numbers which reflect the small ratio of channel diameter and volume flow rate to the viscous forces. The microfluidic conditions cause always a laminary structure of flow with steep flow velocity gradients and results in to very high fluidic dispersion of concentration signals if homogeneous fluids are applied. So, the principle high potential of

J.M. Köhler (✉)
Institut für Mikro- und Nanotechnologien/Institut für Chemie und Biotechnik, Technische Universität Ilmenau, PF 10 05 65, D-98684, Ilmenau, Germany
e-mail: michael.koehler@tu-ilmenau.de

P. Day et al. (eds.), *Microdroplet Technology: Principles and Emerging Applications in Biology and Chemistry*, Integrated Analytical Systems,
DOI 10.1007/978-1-4614-3265-4_7,

microfluidics for handling of molecules and particles can only be exploited if the objects are processed individually or portions of manipulated objects can be defined and handled. This demand calls for a subdivision of continuous liquid phases and is in complete analogy to the microcompartimentation of living organisms by cells and subcellular structures.

The so-called method of microsegmented flow is a droplet-based microfluidic technique with a strictly controlled order of microfluidic compartments. The technique was originally introduced in analytical chemistry for the flow injection analysis [1–5]. The regular generation of small liquid portions which are transported with constant velocity was very efficient for this analytical method. In contrast to other droplet-based methods where more or less ordered emulsion are generated and processed, the segmented-flow technique works with a fixed temporal and spatial order of liquid portions and uses this order for keeping substance-related information through the whole process. The specific advantages of this method were rediscovered for applications in microfluidics whereby specific features of this technique are dominating the use in the different applications [6, 7]. Following points are particularly important for the application of micro segmented flow:

- Generation of large numbers of liquid portions with equal or well-controlled size and equal or well-controlled chemical composition
- Extreme narrow residence time distribution caused by the plug-flow transport and ensuring an extreme high homogeneity during chemical processes
- Addressability and strict order of generated and processed liquid portions
- Comparatively high concentrations of essential substances at comparatively low absolute amounts or number of molecules or particles due to small individual volumes
- Efficient mixing inside the fluidic compartments by the flow-induced circular convection
- Partial or complete decoupling between process liquid and wall and suppression of undesired surface processes as adhesion, nucleation, particle deposition, or biofouling
- Operability of fluid segments by keeping of the spatial or temporal order: switching, dosing, splitting, fusion, and sequence cloning

The main drawback of the technology is the enhanced complexity in cause of the required additional phase of the carrier liquid. In addition, pressure drops in microfluidic systems increase [8–11], so that very high flow rates applied for small channels cause a high energy loss and demand for powerful fluid actuation. But, these disadvantages are mostly accepted with respect to the unique advantages of the segmented-flow technique.

These advantages led to a lot of different fields of applications (Fig. 7.1). They reach from chemical synthesis [12–14] of organic and inorganic molecules over polymerization [15, 16] and synthesis of dielectric [17, 18], metal and semiconductor [19–21], nano and microparticles to a lot of biological applications including the controlled growth of protein crystals for structure analysis and biochemical operations [22, 23], the cultivation of bacteria [24, 25], human and

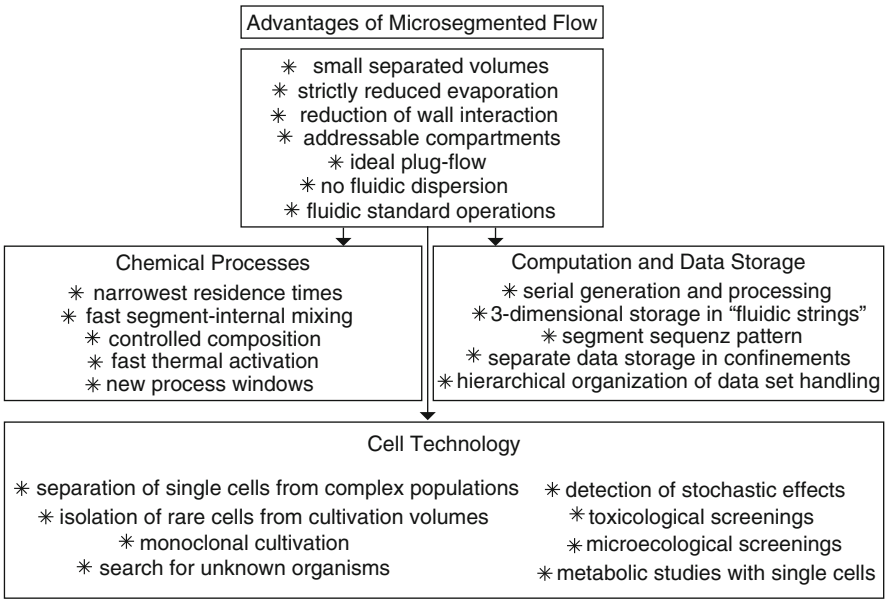

Fig. 7.1 Advantages and main application of micro-segmented flow

other mamalian cells [26, 27], and multicellular organisms [28–32] to the study of cellular interactions, for DNA analysis and for microtoxicological screenings [33].

The embedding of an aqueous phase into a liquid alkane, mineral oil, or liquid perfluorinated hydrocarbons is well suited for the application of microsegmented flow for cell cultivation and for biochemical processes. So, it can be applied, for example, for the implementation of PCR [34–36] and for the detection of virus transcripts by a RT-PCR [37]. In the following, principles of the handling and characterization of microfluid segments and the application of the technique for the detection of infective viruses will be explained and challenges for the future development of microsegmented flow devices to systems for handling of chemical and biological information will be discussed.

7.2 Ordered Handling of Fluidic Micro Compartments by Micro Segmented Flow

7.2.1 Liquid Compartimentation as a Fundamental Biomimetic Principle

The mobility of ions and molecules is one of the key features of each liquid. In contrast to solids as solid particles, liquid portions loss their individuality by

bringing them together with other liquids by the Brownian motion. The anonymity of parts of a liquid volume is overcome by spatial subdivision into separated volumes: The principle of compartimentation defines individuality in the liquid state.

The distinguishing of inner side and outside, the definition of an internal space in a liquid is the fundamental topological issue of a living cell and, therefore, for the whole life. All further development of intracellular structures and multi cellular morphologies, the phylogenetic evolution as well as the embryonic development are based on the liquid compartimentation. The basic operation in continuing of life and transferring of specific properties between generations is the topological operation of spatial liquid separation: one mother cell is splitting into two daughter cells representing two new individual liquid units.

The assembling of molecules on microspots in biochips as well as the assembling of substances inside small liquid volumes in micro- and nanotiterplates or arrays of droplets, the dispensing of liquid into flying droplets or the generation and manipulation of droplets on chip surfaces can be understood as technical counterparts to the liquid compartimentation by living cells. But, in all these cases the state of aggregation of the wall or, in general, the environment of the sample is different from the liquid.

In microfluid segments, the individual liquid portions are operated inside a carrier fluid. So, the whole system including all fluidic compartments is well separated but remains the mobility as usual in the liquid phase. The ordered chain of microfluidic segments inside an inert carrier liquid represents a fascinating compromise between mobility and operability at the one side and separation and well-defined individuality on the other side.

7.2.2 Constant Residence Times and Process Conditions

The individuality of liquid compartments is less important if continuous chemical processes should be implemented. In this case, the use of the microfluid segment technique is focused on the unique flow behavior, namely, the constant flow rates of all partial volumes, constant residence times, and fast heat and matter transfer mediated by the transport-induced segment-internal convection.

Beside chemical synthesis, the aspects of fast and homogeneous heat transfer, fast mixing, and other changing reaction conditions, are also of interest for biochemical or molecular biological operations and could also become interesting for future bioscreening processes under changing reaction conditions. The introduction of reagents or effectors, the thermal activation or inhibition of biomolecular interactions, or other biochemical processes as well as the control of whole cellular activity by changing chemical and thermal conditions will probably get increasing attractivity for automated analytical procedures and screenings in cell technology.

The strict ordered transport, the well reproducible conditions of segment transport and of the segment internal streaming patterns, and the equal conditions for the interaction of all liquid compartments with the environment contribute to an

excellent stability of reaction conditions and ensure highest reproducibility in all processes. In result, processes as well as products will be much more homogeneous as in use of alternative techniques.

7.2.3 Reproducible Detection Conditions

Both for the control of the formation and operation of the fluid segments itself and for the characterization of the segment content and ongoing processes, automated low-invasive or non-invasive monitoring conditions are required. A regular geometry of the conducting microchannel is important for the segment transport as well as for the characterization of the segments. A constant interface tension between the both liquid phases and constant conditions of the interaction between the liquid and the wall support constant conditions for characterization procedures. For analytic series, combinatorial investigations, and for screening runs with changing composition it has to be taken into account, that the interactions between the involved phases could shift and the interface geometries might become different. These influences are mainly effecting the geometry of the front and the back side of fluidic segments. Therefore in such cases, the central part of segments should be used for characterization purposes.

The homogeneity and reproducibility of the segment-internal convection pattern represents an important advantage of microfluidics and microfluid segments. In contrast to spatially more extend liquid systems, the convective structures including the formation of vortices is reproducible and predictable. So, all segments inside one sequence can be characterized under comparable conditions.

7.2.4 Generation of Fluidic Patterns

The existence of well-separated liquid compartments, the well-defined linear arrangement, and the constant transport conditions make the microsegmented flow for a perfect tool for generation and application of pattern. Such linear pattern can be defined by different features (Fig. 7.2): (1) the distance between segments, (2) the size of segments, (3) the concentration of one component, (4) composition types or all combinations of them. Figure 7.3 gives an example for a regular sequence of segments with constant size, constant distance, and constant composition. It was characterized by microflow-through photometry, each circle represents a single optical absorbance measurement. The equal width of peaks stands for the regular size, the distance of peaks proves the constant segment distance and the peak height reflects the constant concentration. A simple pattern of droplets with alternating size and composition is marked by differences in peak width and absorbance (example of microphotometric characterization in Fig. 7.4). The quality

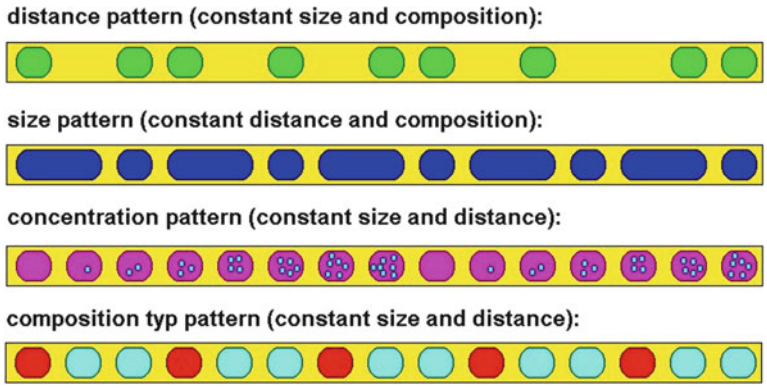

Fig. 7.2 Principle pattern types in microfluid segment sequences

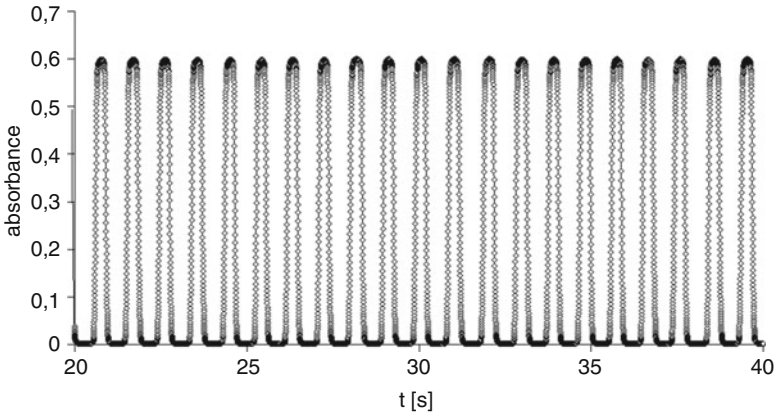

Fig. 7.3 Example of a microphotometric flow-through characterization of a regular sequence of fluid segments of equal size and content

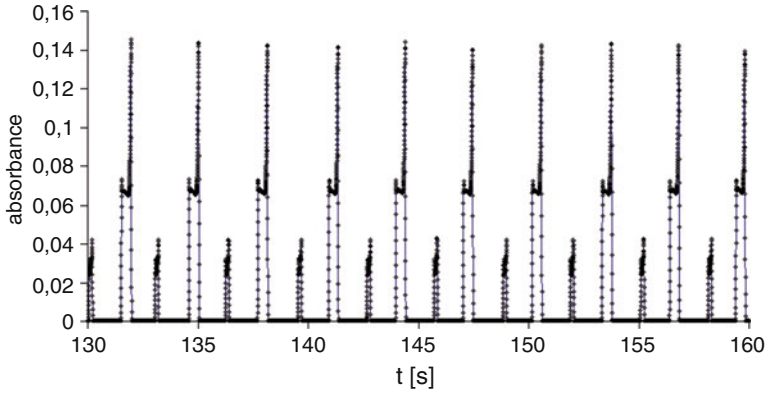

Fig. 7.4 Example of a microphotometric flow-through characterization of a regular sequence of fluid segments of alternating size and content after unification of two segment streams with a total flow rate of 60 µL/min (internal tube diameter: 0.5 mm)

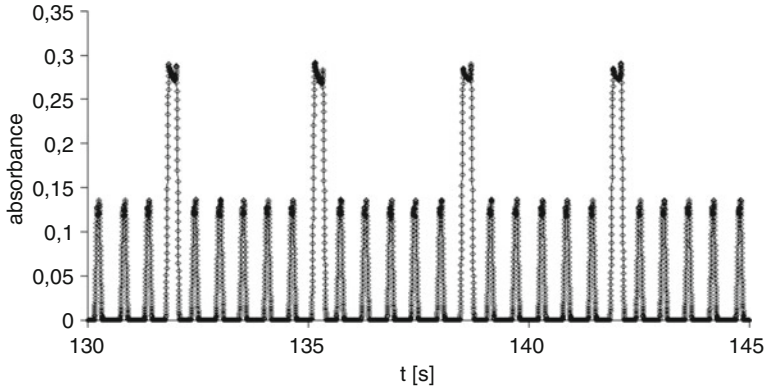

Fig. 7.5 Microphotometric flow-through characterization of a regular sequence of fluid segments of different size and content after unification of two segment streams with following flow rates: (1) carrier: 4 μL/min, aqueous solution: 1 μL/min, (2) carrier: 16 μL/min, aqueous solution: 4 μL/min (internal tube diameter: 0.5 mm)

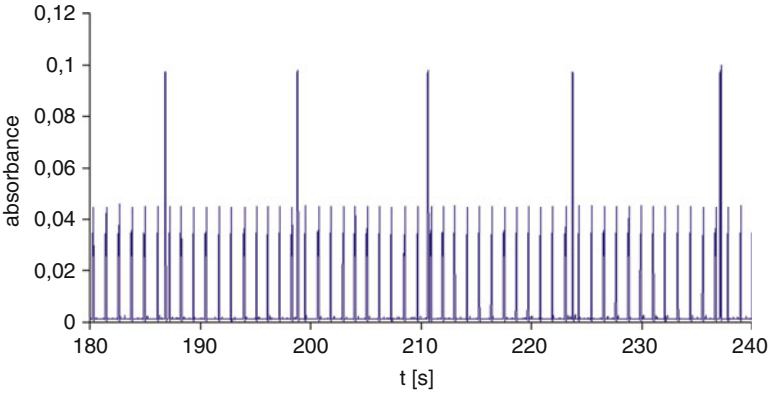

Fig. 7.6 Regular sequence of fluid segments in the case of higher flow rate ratios after unification of two segment streams with following flow rates: (1) carrier: 50 μL/min, aqueous solution: 1 μL/min, (2) carrier: 50 μL/min, aqueous solution: 10 μL/min (internal tube diameter: 0.5 mm)

of droplet pattern is dependent on the fluidic arrangement for generation. Different pattern types are obtained by a triple-T-arrangement and by a linear double-T-arrangement of injectors (Fig. 7.5). Beside the segment size and composition, fluidic sequences of two types of segments can also be distinguished by the ratio of segment numbers (Fig. 7.6). Size/Distance plots are well suited for the evaluation of the quality of segment populations. Frequently, the size homogeneity inside the population of one droplet type is high, but the distance between droplets can be varied significantly. An example for such a plot for a pattern consisting of two types of droplets is shown in Fig. 7.7.

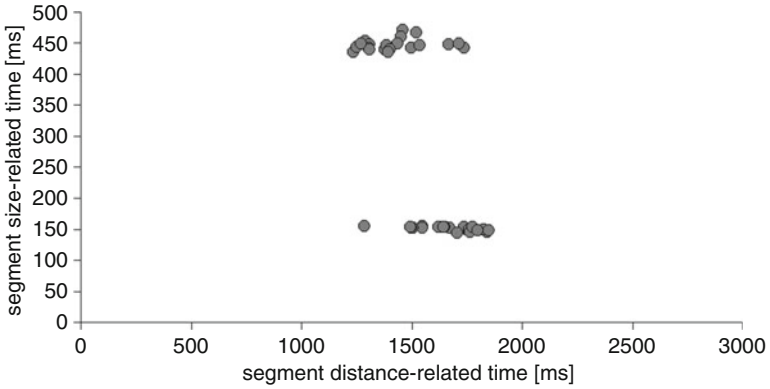

Fig. 7.7 Size-distance diagram for a sequence of two types of microfluid segments with same frequency but different size (total flow rate: 60 µL/min)

7.2.5 Operability

The possibility of manipulation of liquid portions is one of the big advantages of microsegmented flow in comparison with homogeneous liquid systems. This concerns not only the droplet motion and storage but also topological operations, namely, the splitting and fusion of droplets.

Figure 7.8 gives an example for a regular splitting of a droplet sequence by means of a symmetric Y-junction. The up streaming segment sequences were characterized by microflow-through photometers working in different spectral channels. So a different height of the absorbance signal was recorded in the both output channels. The splitting was performed with slug-like segments of about 0.5 µL volume in a 0.5-mm-tube. The input segment sequence was actuated by a syringe pump with a flow rate of 350 µL/min. Both of the outlet channels were actuated by sucking with two additional syringe pumps working by a flow rate of −175 µL/min each. A symmetric splitting resulting in equal size of optical signals was realized by this procedure.

Topological fluidic operations with unification or splitting of segments can be regarded as a simple model for topological processes in natural systems. So, they can be called as "Bioanalogous Fluidic Operations" (Fig. 7.9a). The splitting of droplets finds its analogy in the cell division, the fusion of droplets is a topological analogon to the unification of gametes. Segments can be grown by dosing material into the segment. The coalescence or the incorporation of a smaller droplet in a larger one finds its biological counterpart in an endocytosis. The asymmetrical splitting of microfluidic segments corresponds to an exocytosis.

Beside the equal manipulation of all segments in a sequence, the addressing of single segments is of particular interest for the realization of automated experimental programs. An "Operation on Demand" is challenged, therefore (Fig. 7.9b). The set of operation types includes the simple droplet generation on demand, the

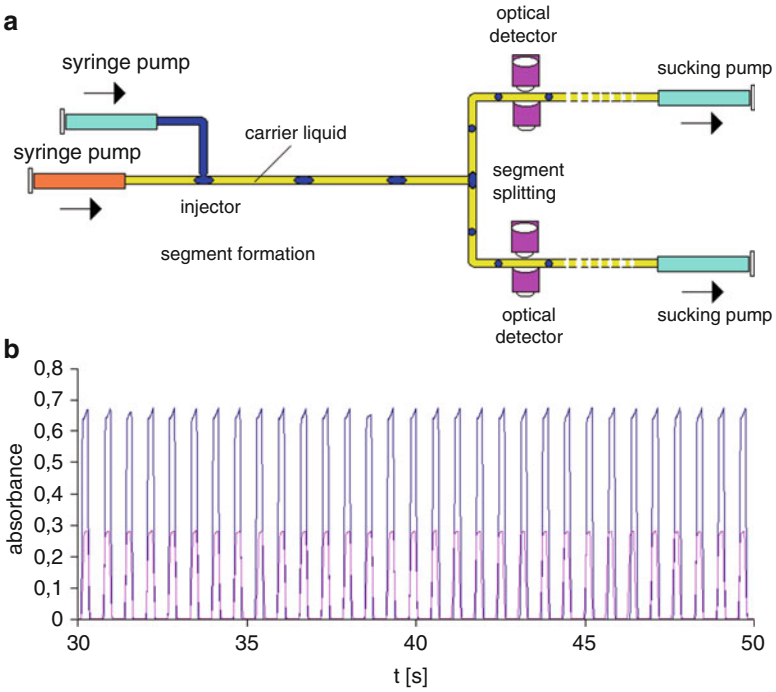

Fig. 7.8 Symmetrical splitting; (**a**): experimental arrangement, (**b**): photometric signal in both the outlet channels; the differences in the signal heights (absorbance) is due to different spectral sensitivity of the applied microphotometers

switching between two up streaming channels, the splitting or fusion of segments on demand, the shifting of segment volume, physical or chemical conversion of the segment content, the addressed initiation of biological processes as well the selection of single segments for storage and archivation.

7.3 Decoupling of Specific Molecular Processes and Contact-Free Information Transfer in Micro Segmented Flow Technique

7.3.1 Direct Electrical or Optical Read-Out

The read-out of information from microfluid segments can be realized by different transduction and signal transfer channels. Non-invasive and automatically working procedures are preferred. Therefore, the information transfer by electrical or electromagnetic fields is well suited.

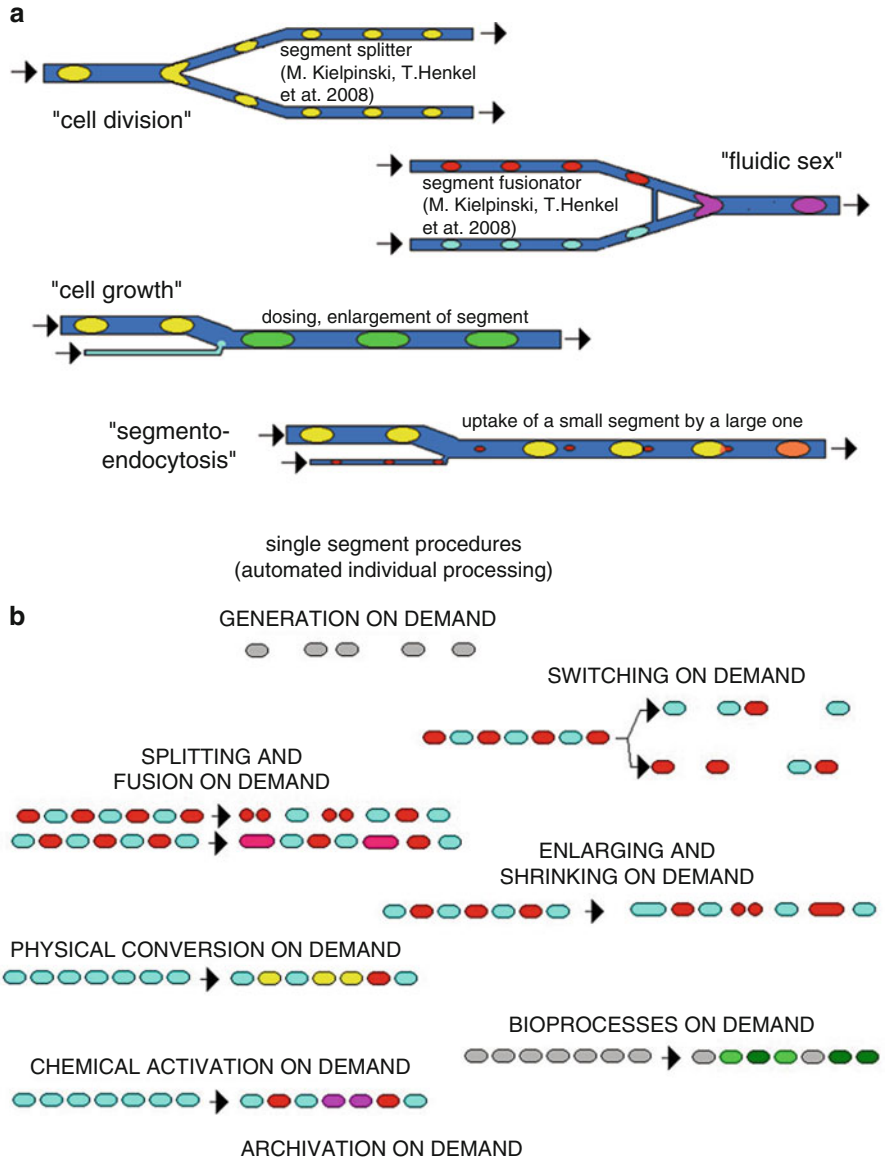

Fig. 7.9 Segment operations: (**a**) analogy to topological effects in cell biological processes, (**b**) challenges for individual segment switching and segment on demand techniques

The whole fluid segments can easily be distinguished from the carrier liquid by drastic differences in the electrical and optical properties. The large differences in the refractive index or in the electrical field constant make the detection of segments by an optical or electrical sensor simply.

Cells, particles and their motion inside microfluid segments can be detected by direct optical imaging, in principle. But, in many cases, the natural contrast given by observed objects is too small for a direct observation. In these cases, a labeling might be required. In other cases, the intensity of light scattering can be used for the measurement of cell or particle densities.

Concentrations of chemical species can easily be read-out if the substances can be measured by their own optical absorption or fluorescence. But, this strategy fails frequently due to low concentrations, low optical extinction coefficients, or high backgrounds for optical transmissive or fluorescence measurements.

Species without a significant own absorption or fluorescence can be detected if a indicator dye is used to mediate the information between the searched substances and the physical read-out system. Indicator dyes fulfill this demand and can be optically reported over shifts in their absorption of fluorescence.

The application of indicator dyes is not recommended if they disturb the biological processes inside microfluid segments which might be the target of screening. The molecular disperse distribution of dissolved indicator dyes supports a direct interaction with cells, can cause toxic effect and can be connected with a change in optical activities by metabolization.

7.3.2 Application of Sensor Particles

Microsensor particles are a very promising alternative to molecular disperse dyes. The chemical coupling of indicator dyes to the particle surface reduces the risk of direct toxic effects of the indicator dyes on cells and the risk of metabolization drastically.

So, pH-sensitive particles can be realized by coupling pH-indicator dyes with the polymer matrix, oxygen-sensitive fluorescence particles are made by coupling of fluorescence dyes with high sensitivity against fluorescence quenching by the triplet oxygen molecule [38, 39].

Sensor beads with a hydrophilic surface can be dispersed easily inside microfluid segments for cell cultivation. They can report about the changing pH or oxygen content by shifting or changing fluorescence which is caused by the physiological activity of cells [40]. This principle can be used for the monitoring of cell growth inside microfluid compartments as well as for the detection of toxicological responses of cell cultures in microfluid segments. The combination of different sensor beads can be used for the introduction of toxicological screenings with miniaturized multi-endpoint detection.

7.4 Micro Reverse Transcription PCR for Virus Diagnostics in Micro Tubes and Chip Devices

7.4.1 PCR in Micro Fluid Segments

The development of microdevices for the Polymerase Chain Reaction (PCR) started in the early 1990s [41–44]. The reduction of PCR volume and the use of highly heat conducting materials as silicon allowed to reduce the times for thermocycling considerably [45]. In addition, miniaturization opened the possibility of continuous flow PCR [46–49] and of realizing highly parallelized thermocycling processes. Meanwhile, a lot of different strategies reaching from micro- and nanotiterplates over chip arrays to emulsions and gel droplets is used for microscaled PCR in highly parallelized systems [50–52].

The PCR thermocycling represents a multi-step reaction which periodically changed thermal conditions. The chain of reaction steps can either be realized in a batch reactor by the periodic variation of temperature or it can be a continuous-flow process in which the process liquid passes periodically three different temperature zones. Such continuous working flow thermocyclers are realized in microreaction technology. In these devices, the PCR mix is conducted through a microchannel passing the different temperature zones.

The application of the PCR mix as homogeneous solution for flow-PCR suffers from the specific conditions of microfluidics. The low Reynolds number cause a laminar flow with strong velocity gradients. This effect causes a large residence time distribution. In result, single volume elements of the process liquid have different flow histories and, therefore, different conditions for heat transfer. So, the conditions for DNA denaturation, selective annealing and fast prolongation are not optimal. In addition, a fast serial processing of larger series of template is not possible due to cross-talk between the samples in cause of the fluidic dispersion.

These problems were overcome by the application of microsegmented flow for PCR. The transport of PCR mix in microfluid segments results in very narrow residence time distribution and very homogeneous process conditions over the whole thermocycling process. The flow-induced segment-internal convection supports a fast heat exchange between the channel walls and the process liquid. A cross-talk between samples in a sequence of droplets can be suppressed.

7.4.2 An Asymmetric Helical Tube Reactor for Virus Diagnostics

The development of chip devices for microflow-PCR was based firstly on a meandering microchannel passing three temperature zones. Such a three-zone reactor demanded always for back-flow channel sections. This disadvantage could be avoided by spiral-like arrangements [53]. An asymmetrical helical tube reactor was developed in order to realize optimal conditions of thermocycling with sufficient time for efficient elongation and a minimal thermal stress for the PCR mix

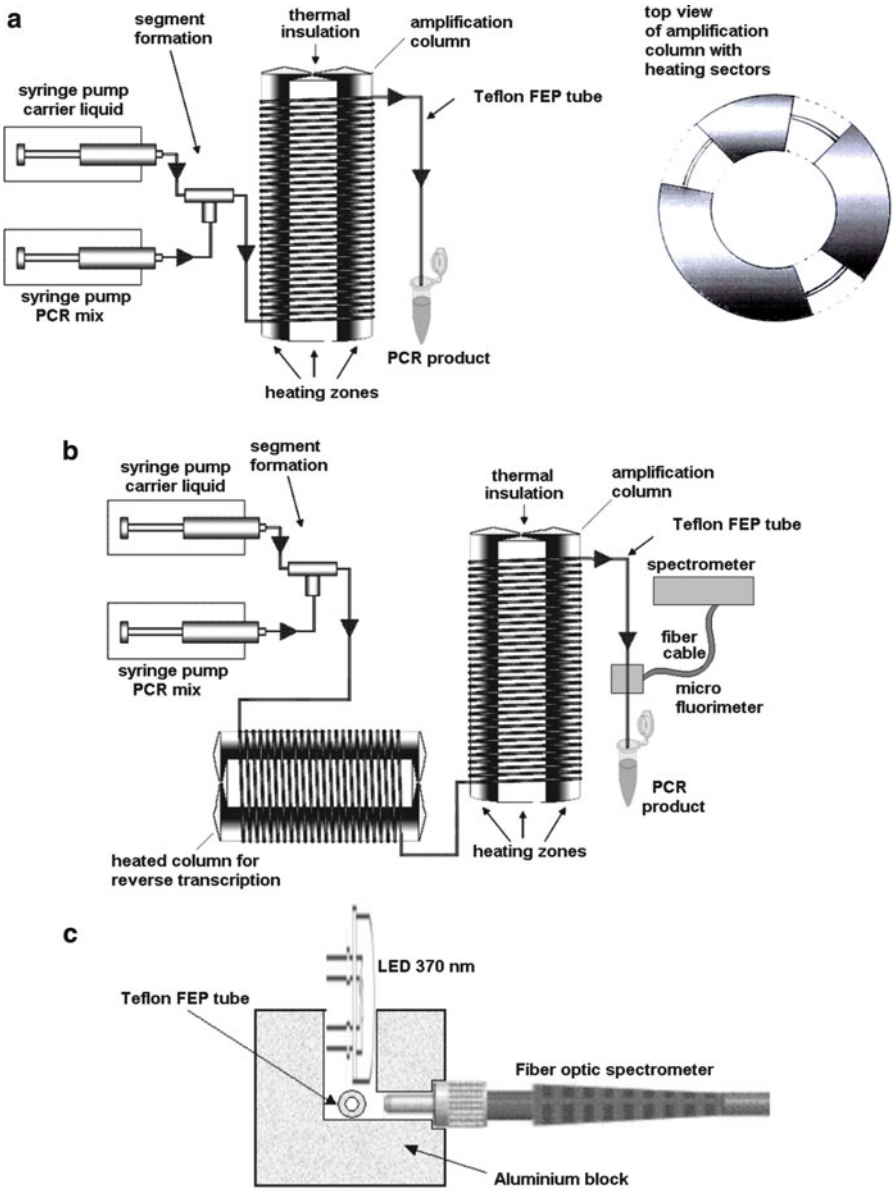

Fig. 7.10 Experimental arrangement for investigation of virus gene expression by a continuous-flow PCR using an asymmetrical helical tube reactor: (**a**) thermocycling module, (**b**) arrangement with integrated heated helical reactor for reverse transcription and helical flow-through thermocycler, (**c**) arrangement for in-tube fluorimetric monitoring [37]

during the denaturation phases [37]. The helical coiled microtube follows the periphery of a cylindric core and forms 42 loops of equal total length and constant length of the three temperature sections in each loop (Fig. 7.10a). The heating cylinder consists of three copper sections which are equipped with electrical heaters

and resistive temperature sensors for precise temperature control. The three sections can be heated individually in order to realize up to three different temperatures as required for denaturation, annealing, and primer extension. The size of the three segments is adapted to the required time ratio of the three process steps in the thermocycling. This is the reason for the asymmetric construction. The section for primer annealing is the largest one, the denaturation zone (highest temperature) forms the smallest section, and the annealing zone represents the section of mediate size.

The whole thermo stating cylinder has a diameter of 70 mm and a height of 80 mm. A tube for the realization of 42 temperature cycles has a length of 924 cm. An additional tube of a length of 15 cm was applied for the first denaturation step. For a simple PCR process, the PCR mix was injected by a syringe pump into a carrier stream of a perfluorinated hydrocarbon (PP9). The formed droplets were in the volume range of about 60 nL–0.1 μL (Fig. 7.10a, left). So, between 150 and 250 droplets were formed by 25 μL of the PCR solution. The PCR product was collected and characterized by gel electrophoresis.

A microcontinuous-flow expression analysis was performed by the integration of an additional tube reactor for the reverse-transcription process and a hot start tube. Therefore, a second columnar reactor (RT reactor) was applied in front of the amplification reactor (Fig. 7.10b). This reactor was also formed by a heated copper core and a helically coil tube. At first the microfluid segments of PCR mix containing hot start polymerase were formed at first. In a second step, these fluid segments were conducted through the RT-reactor. The fluid exit of this reactor was connected with a hot start region (94°C, 5 min residence time) and the fluid inlet port of the PCR-reactor. The RT reactor worked at a temperature of 50°C (for HPV viruses) and 60°C for the measles viruses.

Finally, a microflow-through fluorimetric arrangement (Fig. 7.10c) was used for the process monitoring and for the in situ determination of the concentration of amplificate. Therefore, the light of a UV-LED (Hero Electronics Limited, GB, 370 nm) was coupled into the center of the PCR outlet tube. The fluorescence light was collected by a optical fiber in a 90° arrangement and conducted to a compact spectrophotometer (Avantes, RB Eerbeck, Netherlands).

7.4.3 Micro Continuous RT-PCR for Detection of HPV 16 and Measles Viruses

The operation of PCR reactor was tested by the amplification of a sequence from lamda DNA (Fig. 7.11a). The complete microcontinuous-flow RT-PCR arrangement was applied for the detection of virus gene expression [37].

The application of micro-RT-PCR for the detection of transcripts of the human papilloma virus was investigated by use of SiHa cells (HTB-35). Each of the hosting cells contains two copies of the HPV16 genome which is integrated into

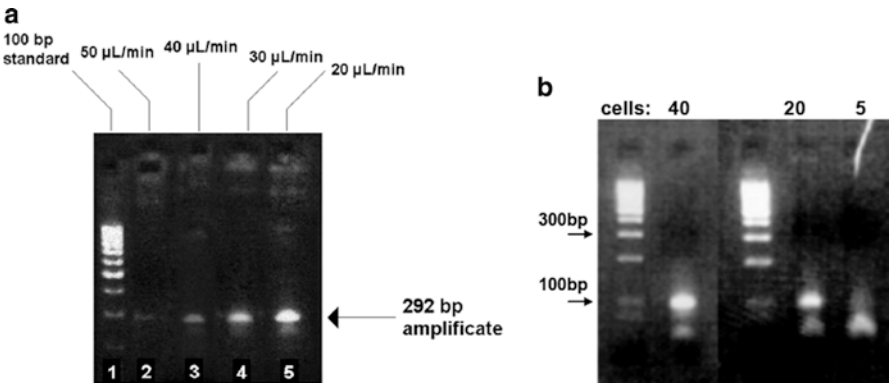

Fig. 7.11 (**a**) Evaluation of flow thermocycling: low rate dependence of PCR efficiency tested by a 292-bp DNA sequence of the lambda phage; PCR product could be found up to a flow rate of 50 µL/min (**b**) result of reverse transcription and amplification of viral transcripts in the RT-PCR process: HPV16 sequences: detection down to five cells/segment is possible [37]

the human chromatin. The amplification follows a protocol for rapid micro-PCR [54] for a so-called one step RT PCR (Invitrogen kit, Karlsruhe, Germany; Hot Start Taq polymerase, Genaxxon). SYBR Green was added for the microfluorimetric in situ detection of the formed double strand DNA.

The SiH cells were pretreated with paraformaldehyde for permeabilisation and fixation. The whole continuous-flow process consisted on the reverse transcription (30 min), the hot start (5 min), and the amplification (42 cycles of 2 min each). A residence time of 15 s was applied in the denaturation zone (94°C), of 22 s in the annealing zone (58°C), and of 38 s in the elongation zone (68°C). Additional 45 s was required for the intermediate time intervals between the three reaction zones. The successful amplification of the template (95 bp) could be proved by gel electrophoresis (Fig. 7.11b). It was possible to detect the HPV activity down to a concentration of ten cells per microliter corresponding to about 250 cells in the whole experimental run or of an approximate average of one cell per fluid segment.

The transcription and amplification of a sequence from measles viruses was chosen as a second example of a medically relevant investigation with the microcontinuous-flow PCR system. Therefore, persistently infected human glia cells (C6/SSPE) were applied [55]. The protocol was adapted from a rapid PCR process performed with a Light Cycler. A one-step RT-PCR kit (Qiagen, Hilden, Germany), Super Hot Start Taq polymerase (Genaxxon), and SYBR Green in a higher dilution were applied.

The expression activity of measles viruses in infected human cells was checked by the transcription and amplification of a 127 bp sequence. The cells were also treated with paraformaldehyde for permeabilisation and fixation. The whole continuous-flow process consisted on the reverse transcription (30 min at 60°C), the hot start (5 min at 94°C), and the amplification (32 cycles of 2 min each). A residence time of 15 s was applied in the denaturation zone (94°C), of 22 s in the

annealing zone (60°C), and of 38 s in the elongation zone (72°C). Additional 45 s was required for the intermediate time intervals between the three reaction zones. The successful amplification of the template (95 bp) could also be shown by gel electrophoresis. But, a much higher cell concentration (10^4 cells/μL) as in the case of HPV-infected cells was required.

Both of the examples described above illustrate the applicability of micro-segmented flow for the identification of pathogenic viruses and their activity by read-out of molecular information from the transcription process. So, this type of microfluidic processes supports the transfer of genotype and phenotype data from living cells into a technical information storage systems. As typical for analytical procedures, the process involves an analytical chain from the pretreatment of cells over a series of biomolecular processes up to the optical in situ measurement and conversion into electronic signals.

7.5 Tasks and Visions

7.5.1 Read-Out Tasks Beyond PCR

The Reverse Transcription PCR has meanwhile to be regarded as a classical process for read-out of biomolecular information on the physiological activity of cells. It is also promising for application as a biomolecular endpoint in miniaturized toxicological screenings (Fig. 7.12). But, the PCR process is connected with a destruction

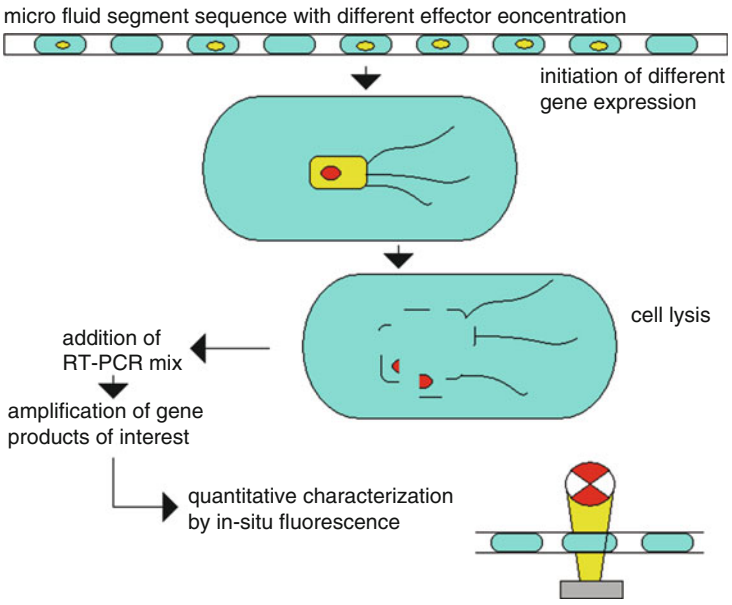

Fig. 7.12 Principle of application of serial PCR as end point in micro toxicological screenings

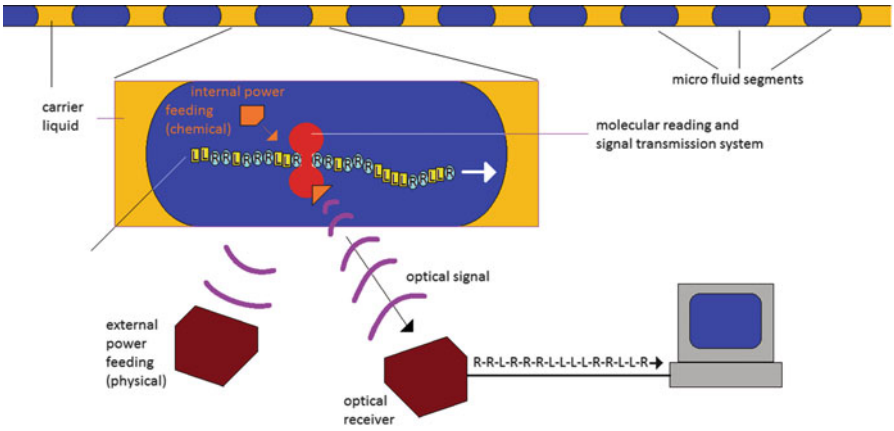

Fig. 7.13 Vision of a nano sequence reading and optical transduction from microfluid segments into an electronic system

of the investigated cell. So, it is a nonreversible analytical procedure. The extraction of a certain biomolecular information from the cell by PCR must be paid by the loss of the investigated object as whole. So, it is not suited for a molecular monitoring. In addition, beside DNA and RNA, a lot of other molecules carries information of interest and the read-out is much more complicated because the available molecular instruments for this read-out are not so convenient as in the case of the nucleic acid processing. So, there is the unsatisfied desire for a nondestructive instrument for transmitting information coded in sequence molecules.

Whereas the amplification and sequencing of nucleic acids is far developed and different microfluidic techniques are used for automation and parallelization, some principle challenges remain for the future development:

- Genotyping of living cells: read-out of DNA-sequence information without destruction of the cell
- Gene expression monitoring: read-out of m-RNA sequences without destruction of the cell
- Monitoring of the physiological state of a cell: read-out of a complete molecular set standing for certain types and intensities of physiological activities
- Monitoring of intercellular communication: read-out of transmitted molecular information

A read-out of information without any effect on the investigated object is principally impossible. But, the above formulated tasks demand for a minimization of interference between the information transfer process and the investigated cell. For this purpose, the whole process of information conversion and transmission should be decoupled from the normal cellular activity as far as possible. The ultimate primary transduction process would be a nano machine scanning the molecule of interest and convert the sequence information into a physical signal readable by an outer receiver system (Fig. 7.13). An alternative could be given by a

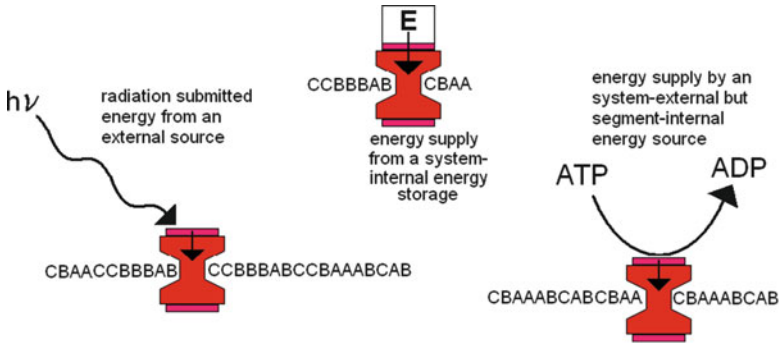

Fig. 7.14 Energy supply possibilities for autonomous nano sequence reading: pumping by radiation, feeding from an internal energy store, supply from a chemical energizer in the microenvironment

transcription of the desired biomolecular information by a molecular-sized machine into a molecule which is nearly no interfering with cellular activities and not metabolized in the process time of the information transfer. The further information transfer can either proceed by a direct physical readout by the transfer of the information-carrying transcript from the cell to the environment. It seems to be clear that the main challenge of this vision is directed to the development of synthetic molecular systems for transcription and transmission of biomolecular information.

The conversion of information by transcription, translation, and physical transmission is always connected with a consumption of energy and with the need of entropy export. The required energy and entropy flow must either be organized from outside or by use of the cell-internal energy supply and entropy export systems (Fig. 7.14). The coupling between the information conversion and cellular processes is unavoidable from the fundamental laws of thermodynamics. But the energetic interference should be kept as minimal as possible if a monitoring of life processes is intended. The consumption of cellular ATP for the information transfer is a principle possibility, but means a considerable molecular interaction between the monitoring process and the monitored living object. The introduction of micro- or nano-sized communication systems with an own energy reservoir into cells or small cell ensembles is a special variant of an outside energy supply. Such reporter systems act like a energy-autonomous microspion. The consumption of the energy in the reservoir is defining the life time of such a monitoring element. A prolongation of the life and action time of microspions is thinkable if energy reservoir can be fed by an energy transfer process from outside, for example, by physical fields or radiation which are not directly interacting with the biological system.

How could such information transfer systems work? A passive read-out could proceed by the conversion of a chemical information into a change in the interaction of a transducer with a field or radiation coming from outside. This principle is

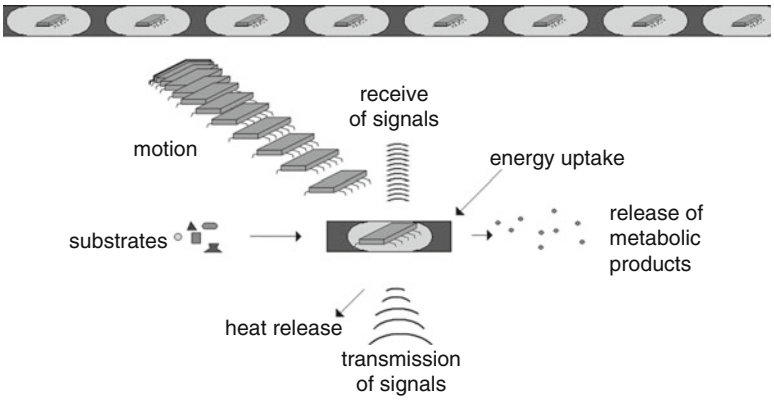

Fig. 7.15 Basic functions of an autonomous nano system for transduction of molecular information from fluidic microcompartments

realized, for example, in fluorescence detection. In these cases, the communication energy as well as the signal triggering are given from outside. An active signal generation could be based on a reservoir of chemoluminescent reagents. Their light signal is only formed if a certain event inside the monitored system takes place. So, the energy supply as well as the triggering of signal formation is controlled directly by the ongoing internal processes. Such systems could report, for example, about the concentration of substances of interest or the intensity of a monitored process. This active signal generation could also be applied for submitting of sequence information. The vision is a nano machine scanning a sequence molecule and generating a sequence of photons which report on the order of molecular units in the sequence molecule. The coding could be realized by the time pattern or an energy pattern (frequency) of emitted photons. The vision of such a machine is not far from the utopia of autonomous acting nano robots (Fig. 7.15).

The strategy for information transfer, signal transduction principles, and the final form of transmitted information must be adapted to the purpose of the information transfer. A conversion into electronically readable data sets is required, if the information has to be brought into an outside computer or into an other conventional technical system. But, it is imaginable, that this conversion of the biomolecular information is not required in many cases, because it can be feed directly into other molecules, biochemical, or cellular processes. For this purpose, a complete transduction chain from chemical to digital electronic information can be avoided and the technical task consists in an information management based on molecular translations, logic operations, and data processing alone.

The main demand for the realization of such molecular-based information processing systems is the control of single molecule interactions and synthesis by other molecular structures by nano scaled instruments. The objects of processing as well as the tools are completely under the restrictions of molecular dynamics involving Brownian motion, and therefore diffusion, internal oscillations, rotations, coiling, and entanglements. Well-defined spatial restrictions are necessary for

controlling these motions. The formation of two- and three-dimensional molecular net works, switchable gel-like states, formation of membranes, compartimentation and the organization of a hierarchy of spatial structures, and mobility are basic principles for the realization of the required spatial restrictions in the living nature. Probably, the same fundamental principles have to be used in nano scaled technical information processing systems based on chemical interactions.

7.5.2 Encapsulation, Droplet on Demand Techniques and Fluidic Hierarchies

The serial generation of fluidic compartments allows the automated separation of molecular or cellular components. So, the products of a stepwise decomposition of cells or macromolecules or the fractions of an analytical separation process can be fixed separately in small fluidic units [56]. Further treatments and characterization steps can occur individually after the aliquotation and encapsulation. The formation of small vesicles or capsules is supported by a microfluid segment approach [57–59].

The automated processing of larger series of droplets, segments, vesicles, or capsules [60] demand for reliable fluidic operations with single fluidic units. Switching [61, 62] and fusion [63, 64] are essential steps beside generation [65] and transport of the microliquid compartments.

Fluidic hierarchies include two principle aspects: one is the spatial structure, namely, the topological organization of objects at nested groups of objects with different linear scale. They are forming the structural hierarchies in fluidic systems. It is obvious that the organization levels can reach from the elementary particles and atoms over different nano and microlevels up to the level of macroscopic scale. The other is the hierarchy of mobility. Each object on a certain structural level is marked not only by its size, shape, and composition but is also marked by a specific mobility inside the whole system.

It is one of the most fascinating aspects of the nano cosmos that mobility can be very different and can be switched by changes in the molecular structures. In the upper and middle micrometer range, active transport is needed, but mechanisms of active transport are also available for smaller objects down to the molecular level. The liquid state—isotropic liquid, colloidal liquids, gel-like states, different types of liquid crystalline states—can be controlled and switched by physical and chemical meanings and can effect the transport behavior for larger and smaller objects. This controllability reaches down to electrons and excitons, which can be either strictly localized or movable over long ranges depending on the properties of the matrix.

These properties of matter give us the possibility to design hierarchically structured fluidic networks. These fluidic architectures must not be restricted to a planar arrangement but have to exploit the topological advantages of the

three-dimensional space. The most important aspect for spatial organization in three dimensions is the possibility of realization of different coherent net works, which are reaching through the same outer space but can be completely separated by phases. The superposition of different networks is not only of interest for the static spatial structure of hierarchic systems but also can be used at same time for the realization of different webs of trajectories of directed motions or transport tracks.

Microfluidics is challenged for the realization of these net works and fluidic hierarchies. The droplet-based systems are the first step into the direction of complex spatially organized liquids. They are realizing the general principle of compartimentation, but not more. The requirements of biomolecular and bio-analogous information processing demand for much more complex and intelligent liquid organization. This includes the keeping of spatial order, the controlled motion, and possible topological conversions beside the simple subdivision of space.

A rational information handling with a whole population of microfluidic compartments demands for a strategy of keeping the included information. Droplets have to be regarded as individual, which can be distinguished from each other by their properties as composition, size, or position inside a droplet arrangement. A release of droplets from a capillary or a tube into a larger volume with free mobility of droplets would destroy the spatial order and means a loss of information. Therefore, a guided transport, storage in well-defined arrangements and addressability are required. By these measures the knowledge about individual objects and their features can be kept.

The individual droplets can be recognized either by a characteristic label, which can be read-out by an interacting object or by their position inside a regular arrangement. The first has the advantage of a possible addressing without a conserved spatial order. But, the price of this independence of spatial order is the need of an individual labeling and recognition system. The second has the advantage of avoiding the need of labeling but demands for conservative handling strategies always keeping the droplets in a well-defined order. Labeling of phases and coding by position—these are complementary strategies of information storage inside liquid multiphase systems.

In case of labeling, the most promising solution would be a class of labels which are directly connected with a mechanism of micro- or nano-scaled hand-shaking (Fig. 7.16). This would allow an identification of individual compartments not only by an outside sensor system but also the identification by micro- or nano-scaled interaction partners. Hand-shaking labels would support the formation of permanent or temporal super-structures by self-organization.

Hierarchically structured liquid multiphase systems must be stabilized by rigid walls or at least molecular membranes. It was shown that double emulsions and multiple-phase systems can be regularly generated and transported by the application of suited surfactants [66, 67]. In contrast to a simple sequence of microfluid segments in a microchannel or tube, a packaging of segments is unavoidable if the segments should be moved in larger liquid volumes.

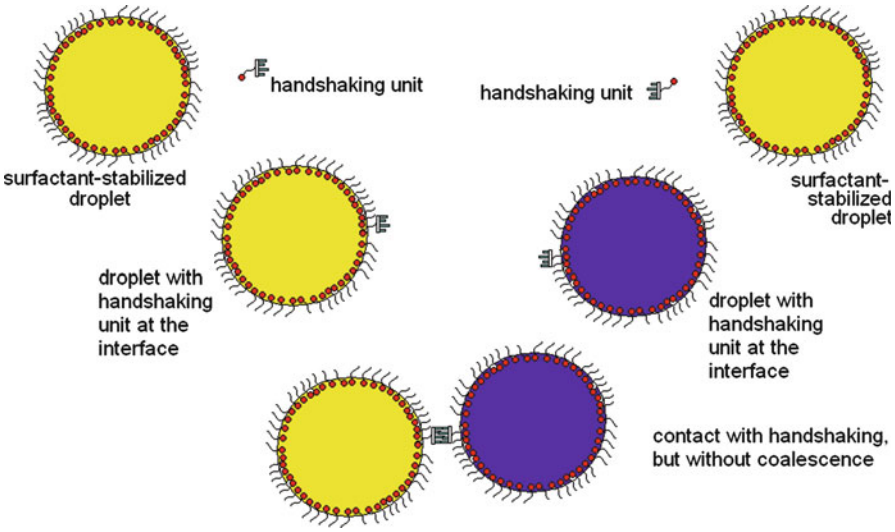

Fig. 7.16 Recognition of liquid compartments by molecular handshaking units incorporated in to a molecular interface layer

Probably, guided sequences of liquid droplets will normally form the highest level of hierarchical organization. At this level, the spatial order can easily be kept constant, droplet motion, other liquid operations and the interaction with outside systems were comparatively convenient to organize. With decreasing level in the hierarchical organization the mobility increases, the position of a single liquid object becomes less and the recognition by hand-shaking becomes more and more important.

A set of basic operations can be defined for the generation and manipulation of fluidic hierarchies. This set can be subdivided into four classes of operations:

1. External topological operations (creation, replication, and recombination of phases)
   - Segment/droplet formation
   - Deformation/spatial transformation
   - Spatial relaxation
   - Splitting
   - Fusion (coalescence)
   - Binding with other objects without fusion
2. Communication (information exchange)
   - Display label for interaction partners at surface
   - Recognize displayed information of interaction partners
   - Release of transmitter substances
   - Uptake or recognition of transmitter substances released by other objects
   - Conversion of signals

3. Internal conversion ("metabolisms")
   - Changes in internal fluidic topology
   - Changes in chemical composition by internal conversion
4. Volume changes (growth and shrinking)
   - Input of substances/objects
   - Output of substances/objects

7.5.3 Multiphase Architectures

The problem of information transfer from cellular and biomolecular objects into technical systems joins the problem of construction of micro- and nano-sized technical systems with cell-analogous meets properties and functions. Multiphase architectures have in this sense several different multiplicity aspects:

- From the microfluidic point of view: the multiplicity of separated phases
- From the material point of view: a multiplicity of physical phase types
- From the point of view of mechanical actuation: a multiplicity of mobility
- From a thermodynamic point of view: a multiplicity of energy forms and transport pathes
- From an information processing view: a multiplicity of information storage principles and communication channels
- From the point of view of construction: a multiplicity of arrangement types

Consequently, the goal of multiphase is no longer restricted to the separation of reaction spaces. As in biology, the compartimentation is accompanied with a differentiation in function, in stability, and dynamics including aspects of elastic and inelastic responses in mechanical as well as in a chemical sense. That is why future multiphase systems have not only to include droplets and surfactants. They have to be constructed under exploitation of the whole spectrum of available material states reaching from rigid solids over gels and liquid crystalline states, membranes, microemulsions, and colloidal solutions to microbubbles and foams. The intelligent exploitation of this multiplicity of phase types promises the realization of the required multiplicities of mobility, of energy and signal transport and conversion. In addition, it enables the different microobjects to become functional elements in a complex technical network. So, complex three dimensional hierarchies of ordered nested phases could be formed (Fig. 7.17).

The development and application of multi scale sensor particles for an optical read-out of cellular information gives a first example of a step into the direction of such systems. Rigid nano particles act as the primary transducers. Fluorescing nano particles—organic dyes or inorganic quantum dots—can work either by enhancement or reduction of fluorescence intensity or by shifting the fluorescence maximum, if certain surface interactions take place. Surface reactions and changes in the

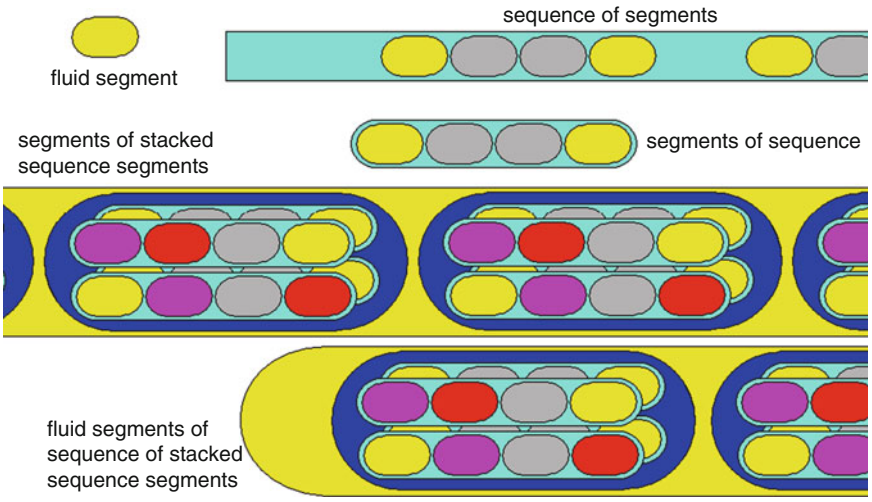

Fig. 7.17 Vision of systematic hierarchical stacking of liquid compartments by nested multiphases

charge density of metal nano particles cause also a shift of the plasmon absorption band of these particles which also can be used for sensing purposes. Both in case of fluorescence and plasmonic transduction the signal shift after a molecular interaction will be as larger as higher the surface-to-volume ratio of the involved nano particles is. So, small nano particles are desired from the point of view of primary signal formation. But, the total optical signal coming from one particle will increase with increasing particle size, and the probability and effect of undesired interactions of the transducing nano particles with the biological or chemical environment will also decrease with increasing particle size. This dilemma can be solved by multi scale particles consisting at least on a gel-like matrix and embedded nano particles. So, it becomes possible to bundle a lot of optically active nano particles in a small volume and to enhance the total of optical signal without reduction of the response of the single particle on a molecular interaction. In addition, the gel-like matrix support a partial decoupling of the nano particles from the monitored liquid because only molecules—between them the analyte species—can diffuse through the pores of the gel, but larger objects as cells, cell organelles, or viruses cannot interact directly with the chemically and optically active nano particles. It is thinkable that an additional level of hierarchical construction can be introduced into the gel-like sensor particles by combining several different sensor functions inside one larger sensor particle. The application of several label elements forming a label pattern is known from the microbar-codes. In analogy to this, labels sensor elements can also be arranged together in order to report on several parameters simultaneously. A coding of signal channel by color is needed if the different sensor particles are arranged randomly in an assembling multi sensor super particle. In case of a

bar-code-like particle arrangement the position of the single sensor functions can be used for the coding of the signal channels.

The formation or the reconfiguration of such micro- and nano-structured systems will neither be completely realized by outside-control nor by completely self-organizing mechanisms. It will be a form of controlled self organization with a partial autonomy for each entity and at each level of the hierarchic organization. The ability of recognition of special binding sites and other microcompartments or particles and specific interactions are an essential precondition for the self-organization of micro- and nano-phases and will become the most important challenge for the development of self-organized hierarchical architectures. In analogy to specifically functionalized nano particles, liquid nano phases must be equipped with recognition structures and molecular coupling functions at their surface. The interface between the nano phase and its environment must be stabilized by a membrane-like molecular layer or an interface film containing nano particles. The recognition and coupling functions must be anchored in the interface, either directly inside a molecular membrane or mediated by macromolecules or particles which are incorporated inside the membrane.

The self-organization concept for the formation of hierarchical liquid nano-structures asks for a system of interaction and specific bonding of liquid micro- and nano-phases. The synthesis and incorporation of sets of the required surface function elements represents a key issue for the realization of the concept. Therefore, the single liquid phases or nano particles need more than two surface functions. For construction of three-dimensional architectures at least three functions must be present in order to construct branched structures, cover areas, and fill complete spaces. Three or more specific recognition and binding sites are required for an addressing during the formation of liquid architectures.

7.5.4 From Information Read-out to Internal Processing: Short Feed-Back Loops and "Micro Techno Chimera"

The ability of construction of architectures from liquid nano- and micro-phases is only the first step into the direction of functional liquid multiphase systems. The goal of the nano architectures is the realization of new functions. Recently, all manipulations and analytical procedures with liquid micro- and nano-phases proceed by the control using outside measurement and control systems. That means that the microscopic objects are localized, characterized, and manipulated by a outside macroscopic machine. The microscope with an optical tweezer for cell manipulation or the manipulation of particles by a AFM probe are typical examples for this situation. The feed-back loop for the control of the system is always spanned over the macroscopic system.

A new quality of systemic organization would be achieved if the feed-back loops could be scaled down to micro- or even nanometer dimensions. This would allow to

construct autonomous working nano machines. It is to assume that a liquid multiphase approach with an internal hierarchical organization could take over the complete spectrum of functions for autonomous energy supply, motility, and chemical activity. Such a system would be a microorganism-analogue artificial nano system.

The formation of whole series of such micro- or nano-sized systems would give the opportunity of systematic variation of properties. This autonomous acting multiphase system could be handled like microorganisms. They can be brought into microfluidic screening systems in order to evaluate their properties and to optimize their functions and behavior. The small liquid multiphase system can be thought as able to form populations. It is imaginable that beside sheer technical functions also elements of natural molecular systems could be integrated in this artificial micro- or nano-systems. So, hybrid systems can be generated which unify technical and biological components. This could involve, for example, the local information processing with nucleic acids as well as with other technical data storage and processing systems. The variability of microorganisms can contribute significantly to the spectrum of artificial micromachines and can be applied for complete new microsystems with different numbers of biological and technical component which could be formed at the microscale and can be made available for evaluation and exploitation of new powerful devices. Finally, microecological systems including natural microorganisms, technical microsystems constructed by artificial liquid multi phases and chimeric individual consisting on biological and technical components ("techno chimera") could be evolved.

7.6 Conclusions

Microfluid segments can be reproducibly generated and processed in microtubes and microfluidic devices. The fluidic operations as well as the content of the segments can be controlled and characterized by fast working optical measurements. The specific labeling or the incorporation of microfluidic droplets in a well-defined sequence gives them an individuality which can be used for the read-out of biomolecular information and for other procedures in larger series of separated samples. The identification of genetic transcripts from pathogenic viruses is an example for such a bioanalytical application.

Whereas the application of droplet-base microfluidics in DNA-diagnostics and sequencing is already introduced, the further application of this microfluidic technique in other read-out procedures of molecular-encoded information or for the construction of nano molecular architectures is a desideratum of research. Beside the challenges for the biomolecular processes, an advanced liquid handling is challenged which allows the formation, monitoring, and automated handling of hierarchies of nested phases.

Acknowledgment I am very grateful for cooperation and for any support by A. Groß, M. Günther, S. Schneider, T. Henkel, M. Kielpinski, J. Metze and A. Grodrian in segmented flow technique in general, in microfluidic virus diagnostics by R. Hartung, G. Sczcepankiewicz and N. Häfner. The financial support of the federal ministry for education and research (BMBF, 16SV-3701) and the state of Thuringia (project Zellex) is gratefully acknowledged.

References

1. Skeggs LT (1957) Effect of ammonium chloride and urea infusions on ammonium levels and acidity of gastric juice. Am J Clin Pathol 28:311–322
2. Susic D, Scheibe P (1971) Neuer enzymatischer Farbtest zur Harnsäure-Bestimmung am Technicon-AutoAnalyzer. Z Anal Chem 257:130–132
3. Hsieh YS, Crouch SR (1995) Air-segmented flow injection: a hybrid technique for automated, low dispersion determinations. Anal Chim Acta 303:231–239
4. Ismagilov RF (2003) Integrierte Mikrofluidsysteme. Angew Chem 115:4262–4264
5. Huebner A, Sharma S, Sharma S, SrisArt M, Hollfelder F, Edel JB, DeMello AJ (2008) Microdroplets: a sea of applications? Lab Chip 8:1244–1254
6. Köhler JM, Henkel Th, Grodrian A, Kirner Th, Roth M, Martin K, Metze J (2004) Digital reaction technology by micro segmented flow – components, concepts and applications. Chem Eng J 101:201–216
7. Song H, Chen DL, Ismagilov RF (2006) Reactions in droplets in microfluidic channels. Angew Chem Int Ed 45:7336–7356
8. Adzima BJ, Velankar SS (2006) Pressure drops for droplet flows in microfluidic channels. J Micromech Miroeng 16:1504–1510
9. Gross GA, Thyagarajan V, Kielpinski M, Henkel Th, Köhler JM (2008) Viscosity-dependent enhancement of fluid resistance in water/glycerol micro fluid segments. Microfluid nanofluid 5:281–287
10. Malsch D, Gleichmann N, Kielpinski M, Mayer G, Henkel T (2008) Effects of fluid and interface interaction on droplet internal flow in all-glass microchannels. Proc. ICNM 2008, (Darmstadt 2008) No 62328
11. Vanapalli SA, Banpurkar AG, VandenEnde D, Duits MHG, Mugele F (2009) Hydrodynamic resistance of single confined moving droplets in rectangular microchannels. Lab Chip 9:982–990
12. Burns JR, Ramshaw C (2001) The intensification of rapid reactions in multiphase systems using slug flow in capillaries. Lab Chip 1:10–15
13. Günther A, Jensen KF (2006) Multiphase microfluidics: from flow characteristics to materials and chemical synthesis. Lab Chip 6:1487–1503
14. Poe SL, Cummings MA, Haaf MP, McQuade DT (2006) Solving the clogging problem: precipiate-forming reactions in flow. Angew Chem 118:1574–1578
15. Gross GA, Hamann C, Günther PM, Köhler JM (2007) Formation of polymer and nanoparticle droped polymer minirods by use of the microsegmented flow principle. Chem Eng Technol 3:341–346
16. Li W, Greener J, Voicu D, Kumacheva E (2009) Multiple modular microfluidic (M3) reactors for the synthesis of polymer particles. Lab Chip 9:2715–2721
17. Donnet M, Jongen N, Lemaitre J, Bowen P, Mat J (2000) New morphology of calcium oxalate trihydrate precipitated in a segmented flow tubular reactor. Science 19:749–750
18. Jongen N, Donnet M, Bowen P et al (2003) Development of a continuous segmented flow tubular reactor and the "scale-out" concept – in search of perfect powders. Chem Eng Technol 26:303–305

19. Shestopalov I, Tice JD, Ismagilov RF (2004) Multi-step synthesis of nanoparticles performed on milisecon time scale in a microfluidic droplet-based system. Lab Chip 4:316–321
20. Chan EM, Alivisatos PA, Mathies RA (2005) High-temperature microfluidic synthesis of CdSe nanocrystals in nanoliter droplets. J Am Chem Soc 127:13854–13861
21. Li S, Günther PM, Köhler JM (2009) Micro segmented flow technique for continuous synthesis of different kinds of ZnO nanoparticles in aqueous and DMSO solution. J Chem Eng Jpn 42:338–345
22. Um E, Lee D-S, Pyo H-B, Park J-K (2008) Continuous generation of hydrogel beads and encapsulation of biological materials using a microfluidic droplet-merging channel. Microfluid nanofluid 5:541–549
23. Joensson HN, Samuels ML, Brouzes ER, Medkova M, Uhlén M, Link DR, Andersson-Svahn H (2009) Detection and analysis of low-abundance cell-surface biomarkers using enzymatic amplification in microfluidc droplets. Angew Chem Int Ed 48:2518–2521
24. Martin K, Henkel T, Baier V et al (2003) Generation of larger numbers separated microbial populations by cultivation in segmented-flow microdevices. Lab Chip 3:202–207
25. Boedicker JQ, Li L, Kline TR, Ismagilov RF (2008) Detecting bacteria and determining their susceptibility to antibiotics by stochastic confinement in nanoliter droplets using plug-based microfluidics. Lab Chip 8:1265–1272
26. Clausell-Tornos J, Lieber D, Baret J-Ch et al (2008) Droplet-based microfluidic platforms for the encapsulation and screening of mammalian cells and multicellular organisms. Chem Biol 15:427–437
27. Hufnagel H, Huebner A, Gülch C, Güse K, Abel Ch, Hollfelder F (2009) An integrated cell culture lab on a chip: modular microdevices for cultivation of mammalian cells and delivery into microfluidic microdroplets. Lab Chip 9:1576–1582
28. Köhler JM, Henkel Th (2005) Chip devices for miniaturized biotechnology. Appl Micro and biotechnol 69:113–125
29. Funfak A, Brösing A, Brand M, Köhler JM (2007) Micro fluid segment technique for screening and development studies on Danio rerio embryos. Lab Chip 7:1132–1138
30. Shi W, Qin J, Ye N, Lin B (2008) Droplet-based microfluidic system for individual Caenorhabditis. Lab Chip 8:1432–1435
31. Chronis N (2010) Worm chips: microtools for C. elegans biology. Lab Chip 10:432–437
32. Crane MM, Chung K, Stirman J, Lu H (2010) Microfluidics-enabled phenotyping, imaging, and screening of multicellular organisms. Lab Chip 10:1509–1517
33. Funfak A, Hartung R, Cao J, Martin K, Wiesmüller K-H, Wolfbeis OS, Köhler JM (2009) Highly resolved dose-response functions for drug-modulated bacteria cultivation obtained by fluorometric and photometric flow-through sensing in microsegmented flow. Sensor Actuat B 142:66–72
34. Köhler JM, Dillner U, Mokansky A, Poser S, Schulz T (1998) Micro channel reactors for fast thermocycling. Proc. IMRET II, AIChE Spring Meeting, New Orleans, 1998, 9–12 March, pp 241–247
35. Curcio M, Roeraade J (2003) Continuous segmented-flow polymerase chain reaction for high-throughput miniaturized DNA amplification. Anal Chem 75:1–7
36. Reichert A, Felbel J, Kielpinski M, Urban M, Steinbrecht B, Henkel Th (2008) Micro flow-through thermocycler with simple meandering channel with symmetric temperature zones for disposable PCR-devices in microscope slide format. J Bionic Eng 5:291–298
37. Hartung R, Brösing A, Sczcepankiewisz G et al (2009) Application of an asymmetric helical tube reactor for fast indentification of gene transcripts of pathogenic viruses by micro flow-through PCR. J Biomed Microdev 11:685–692
38. Vasylevska GS, Borisov SM, Krause C, Wolfbeis OS (2006) Indicator-loaded permeation-selective microbeads for use in fiber optic simultaneous sensing of pH and dissolved oxygen. Chem Mater 18:4609–4616
39. Kocinova AS, Nagl S, Arain S et al (2008) Multiplex bacterial growth monitoring in 24-well microplates using a dual optical sensor for dissolved oxygen and pH. Biotechnol Bioeng 100:430–438

40. Funfak A, Cao J, Wolfbeis OS, Martin K, Köhler JM (2009) Monitoring cell cultivation in microfluidic segments by optical pH sensing with micro flow-through fluorometer using dye-doped polymer particles. Mikrochim Acta 164:279–286
41. Northrup MA, Ching MT, White RM, Watson RT (1993) DNA amplification in a microfabricated reaction chamber. Proc Transducers 93(7):924–926
42. Wooley AD, Hadley D, Landre P, DeMello AJ, Mathhies RA, Northrup MA (1996) Functional integration of PCR amplification and capillary electrophoresis in a microfabricated DNA analysis device. Anal Chem 24:380
43. Wilding P, Shoffner MA, Kricka LJ (1815) PCR in a silicon microstructure. Clin Chem 1994:40
44. Schneegaß I, Köhler JM (2001) Flow-through polymerase chain reaction in chip thermocyclers. Rev Mol Biotechnol 82:101–121
45. Poser S, Schulz T, Dillner U et al (1997) Chip elements for fast thermocycling. Sensor Actuat A 62:672
46. Kopp MU, DeMello AJ, Manz A (1998) Chemical amplification: continuous-flow PCR on a chip. Science 280:1046–1048
47. Auroux P-A, Koc Y, DeMello A, Manz A, Day PJR (2004) Miniaturised nucleic acid analysis. Lab Chip 4:534–546
48. Fukuba T, Yamamoto T, Naganuma T, Fujii T (2004) Microfabricated flow-through device for DNA amplification-towards in situ gene analysis. Chem Eng J 101:151–156
49. Felbel J, Reichert A, Kielpinski M et al (2008) Reverse transcription-polymerase chain reaction (RT-PCR) in flow-through micro-reactors: thermal and fluidic concepts. Chem Eng J 135S:298
50. Gulliksen A, Solli LA, Drese KS, Sörenson O, Karlsen F, Rogne H, Hoving E, Sirevag R (2005) Parallel nanoliter detection of cancer markers using polymer microchips. Lab Chip 5:416–420
51. Marcus JS, Anderson WF, Quake SR (2006) Parallel picoliter Pt_PCR assays using microfluidics. Anal Chem 78:956–958
52. Williams R, Peisajovich SG, Miller OJ, Magdassi S, Tawfik DS, Griffith AD (2006) Amplification of complex gene libraries by emulsion PCR. Nat Methods 3:545–550
53. Zhang C, Xing D, Xu J (2007) Continuous-Flow PCR microfluidics for rapid DNA amplification using thin film heater with low thermal mass. Anal Lett 40:1672–1685
54. Felbel J, Bieber I, Pipper J, Köhler JM (2004) Investigations on the compatibility of chemically oxidized dilicon (SiOx)-surfaces for applications towards chip-based polymerase chain reaction. Chem Eng J 101:333
55. Halbach M, Koschel K (1979) Impairment of hormone dependent signal transfer by chronic SSPE virus infection. J Gen Virol 42:615
56. Liu W, Kim HJ, Lucchetta EM, Du W, Ismagilov RF (2009) Isolation, incubation, and parallel functional testing and identification by FISH of rare microbial single-copy cells from multi-species mixtures using the combination of chemistrode and stochastic confinement. Lab Chip 9:2153–2162
57. Stachowiak J, Richmond DL, Li TH, Liu AP, Parekh SH, Fletcher DA (2008) Unilamellar vesicle formation and encapsulation by microfluidic jetting. Proc Natl Acad Sci U S A 105:4687–4702
58. Schemberg J, Grodrian A, Römer R, Cahill BP, Gastrock G, Lemke K (2010) Application of segmented flow for quality control of food using microfluidic tools. Phys Status Solidi A 207:904–912
59. Chokkalingam V, Weidenhof B, Krämer M, Maier WF, Herminghaus S, Seemann R (2010) Optimized droplet-based microfluidic for sol-gel reactions. Lab Chip 10:1700–1705
60. Mazutis L, Baret J-Ch, Treacy P et al (2009) Multi-step microfluidic droplet processing: kinetic analysis of an in vitro translated enzyme. Lab Chip 9:2902–2908
61. Henkel T, Bermig T, Kielpinski M, Grodrian A, Metze J, Köhler JM (2004) Chip modules for generation and manipulation of fluid segments for micro serial flow processes. Chem Eng J 101:439–445

62. Park S-Y, Teitell MA, Chou EPY (2010) Single-sided continuous optoelectrowetting (SCOEW) for droplet manipulation with light patterns. Lab Chip 10:1655–1661
63. Mazutis L, Baret J-Ch, Griffiths AD (2009) A fast and efficient microfluidic system for highly selective one to one droplet fusion. Lab Chip 9:2665–2672
64. Baret J-C, Taly V, Ryckelynck M, Merten ChA, Griffith AD (2009) Droplets and emulsions: very high-throughput screening in biology. Med Sci 25:627–632
65. Wang W, Yang Ch, Liu Y, Li ChM (2010) On-demand droplet release for droplet-based microfluidic system. Lab Chip 10:559–562
66. Nisisako T, Okushima S, Torii T (2005) Controlled formulation of monodisperse double emulsions in a multiple-phase microfluidic system. Soft Matter 1:23–27
67. Zhu J, Hayward RC (2008) Hierarchically structured microparticles formed by interfacial instabilities of emulsion droplets containing amphiphilic block copolymers. Angew Chem Int Ed 47:2113–2116

Chapter 8
Droplet Microreactors for Materials Synthesis

Nick J. Carroll, Suk Tai Chang, Dimiter N. Petsev, and Orlin D. Velev

8.1 Introduction

8.1.1 Microfluidics for Droplet Generation

The miniaturization of fluid flow and analytical systems has created exciting avenues of scientific and engineering research in materials synthesis. The conventional microfluidic devices have channels with widths in the tens of micrometer range. Fluidic behavior at the microscale may differ from that at larger scales in that interfacial tension, viscous effects, and energy dissipation can dominate the system. Microfluidics has received much attention in the scientific community and has been the topic of many excellent reviews [89, 100]. In some applications slow or minimal mixing is required, and the laminar flows obtained in microchannels become highly desirable. The conventional microfluidic channels can also process liquid in the form of microscopic droplets. Water-in-oil emulsions can be formed in microfluidic devices to form a steady stream of monodisperse aqueous droplets with volumes as small as picoliters [4]. The drops can be loaded with reactants to perform chemical reactions of interest [83, 85, 86].

N.J. Carroll • D.N. Petsev
Department of Chemical and Nuclear Engineering, Center for Biomedical Engineering, University of New Mexico, Albuquerque, NM 87131, USA

S.T. Chang
School of Chemical Engineering and Materials Science, Chung-Ang University, 221 Heukseok-dong, Dongjak-gu, Seoul 156-756, South Korea

O.D. Velev (✉)
Department of Chemical and Biomolecular Engineering, North Carolina State University, Raleigh, NC 27695-7905, USA
e-mail: odvelev@unity.ncsu.edu

P. Day et al. (eds.), *Microdroplet Technology: Principles and Emerging Applications in Biology and Chemistry*, Integrated Analytical Systems,
DOI 10.1007/978-1-4614-3265-4_8,

8.1.2 Scope of This Review

In this chapter we present an overview of the transport of fluids in microchannels with a focus on the formation and manipulation of emulsion droplets. We briefly present below the methods for fabrication of the devices used in similar work. The next section deals with defining the terminology and describing the physics of fluid flow in small channels. We briefly summarize approaches that are used to drive the fluid flow in the microchannels and dispersion of immiscible phases (oil and water) to create well-defined droplets. We then focus on material synthesis applications for droplet-based microfluidics. In particular, we review mesoporous microparticle formation in droplet reactors. Section 8.4 presents more unconventional dielectric liquid–liquid chip systems in which electric field manipulations of droplets have been utilized for material synthesis.

8.1.3 Fabrication of Microfluidic Devices

Various methods have been utilized to fabricate microfluidic devices. The most widely used research devices presently are those made from poly(dimethylsiloxane) (PDMS) elastomers [4, 102]. The materials for these devices are inexpensive and can be fabricated with facile soft lithography processes. This technique also has the potential to form channels with complicated and intricate flow patterns. The soft lithography process is robust and reproducible, which allows replicating flows in different devices that have the same design.

The first step in soft lithography is the production of a master mold, which is typically an Si wafer with epoxy structures. The epoxy structures are created with a high-resolution transparent printout as a photomask for generation of the master by photolithography. A negative photoresist is a type of epoxy in which the portion of the photoresist that is exposed to light becomes nearly insoluble to the photoresist developer. The unexposed portion of the photoresist is dissolved by the photoresist developer, leaving behind the desired channel features. Liquid PDMS precursor base along with a curing agent is then poured over the master mold. The liquid PDMS precursor conforms to the shape of the master mold, replicating the designed features. Vinyl groups present in the base react with silicon hydride groups in the curing agent to form a clear, cross-linked, elastomeric solid. The PDMS is then peeled away from the master mold; the master mold is not destroyed during the removal process, allowing it to be used again for subsequent devices. The PDMS channels are then sealed to a glass slide by exposing both the PDMS device and the glass slide to oxygen plasma and soon thereafter pressing both together to seal the bond.

The disadvantages are that PDMS devices typically can only handle low pressure drops before catastrophic rupture, and untreated PDMS can become swollen or chemically react with some solvents, thus limiting compatible fluids. Recent reports suggest that the walls of such channels can be coated with material that can improve the flow properties [51].

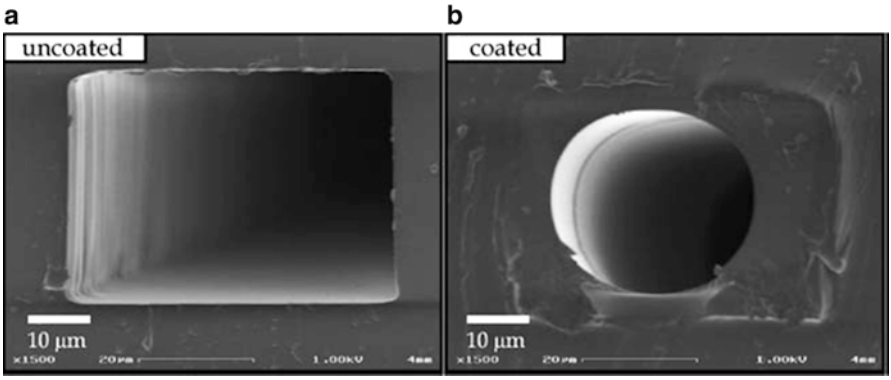

Fig. 8.1 Scanning electron micrographs of cross-sections of (**a**) uncoated and (**b**) coated PDMS channels. Rectangular PDMS channel dimensions are 50 × 35 µm. This fabrication method combines the ease of soft lithography processing with the benefits of a glass surface (reprinted with permission from Abate et al. [1])

Other popular fabrication methods involve etching glass, silicon or plastic substrates. The benefits of such devices are that these materials can be chemically inert and amenable to cleaning thereby making them reusable. Another advantage is that these substrates with etched channels can subsequently be well bonded to a working platform and allow for high pressure drops. Another microfluidic design that has shown promising applications utilizes very small diameter, commercially available, glass capillaries [45, 95]. The advantages for this system are that the geometry of the capillaries can be reconfigured with established glass molding techniques, and the inner glass walls can be chemically modified. Moreover, such concentric glass capillaries can be used to generate droplets composed of double emulsions [45]. However, there is limited complexity of flow patterns and the capillary pulling methods used to fabricate these devices may be hard to reproduce.

A method that combines the excellent wetting and surface property control of glass with the simplicity of PDMS-based photolithography fabrication was recently demonstrated [1]. This method involves the use of sol–gel chemistry to coat the channels of lithography-formed PDMS microfluidic devices with a glass layer (Fig. 8.1). The glass layer provides a chemical barrier to the PDMS walls, which are permeable to many liquids and gases. Additionally, the glass surface chemistry can be controlled allowing for manipulation of the hydrophilicity and wetting properties of the microchannels.

8.2 Transport in Microchannels

8.2.1 Pressure-Driven Flows

Microfluidic flow typically occurs at low Reynolds numbers ($Re < 1$). This results in laminar flow in which viscous forces dominate over inertial forces.

Simple tasks such as pumping and mixing become a challenge. Mixing is an important consideration when using the microfluidic channel as a chemical reactor or when dispersing two liquid phases into each other. Another practical consideration is the pressure drop across such channels. The pressure drop is inversely proportional to the square of the equivalent diameter, and small decreases of channel dimension scan result in large increases in pressure drops [5, 9, 88]. An alternative way to move fluids in microfluidic devices is through electroosmosis using externally applied electric fields [27, 38].

The equations of motion for an incompressible Newtonian fluid are [48]

$$\rho\left(\frac{\partial \boldsymbol{v}}{\partial t}+\boldsymbol{v}\nabla\boldsymbol{v}\right)=-\nabla p+\eta\nabla^2\boldsymbol{v}+\text{force terms},\quad \nabla\cdot\boldsymbol{v}=0 \tag{8.1}$$

where $\mathbf{v}$ is the velocity field, ρ is the fluid density, p is the pressure, and η is the dynamic viscosity. The momentum balance may also include other body force terms that are due to gravity and electric or magnetic fields (for charged or magnetic fluids). The relative importance of the acceleration and viscous terms is expressed by the Reynolds number: $\mathrm{Re}=\rho Ul/\eta$ where U and l are some characteristic velocity and length-scale for the problem. Scaling analysis of (8.1) leads to [48]

$$\begin{aligned}&\mathrm{Re}\left(\frac{\partial\tilde{\boldsymbol{v}}}{\partial\tilde{t}}+\tilde{\boldsymbol{v}}\tilde{\nabla}\tilde{\boldsymbol{v}}\right)=-\nabla\tilde{p}+\nabla^2\tilde{\boldsymbol{v}},\quad \nabla\cdot\tilde{\boldsymbol{v}}=0\\&\tilde{\boldsymbol{v}}=\boldsymbol{v}/U,\quad \tilde{t}=tU/l,\quad \tilde{p}=pl/\eta U,\quad \tilde{\nabla}=l\nabla\end{aligned} \tag{8.2}$$

For viscous-dominated low Re fluid flow the equations are [34, 48]

$$\eta\nabla^2\boldsymbol{v}-\nabla p=0,\ \nabla\cdot\boldsymbol{v}=0 \tag{8.3}$$

For slit-shaped channels the momentum balance for fluid flow in z-direction is

$$\eta\frac{\partial^2 v_x}{\partial y^2}=\frac{\partial p}{\partial x} \tag{8.4}$$

while for a circular capillary it is given by

$$\eta\frac{1}{r}\frac{\partial}{\partial r}\left(r\frac{\partial v_z}{\partial r}\right)=\frac{\partial p}{\partial z} \tag{8.5}$$

Integrating (8.5) leads to the well-known Hagen–Poiseuille expression for the flow velocity in cylindrical symmetry

$$v_z=\frac{1}{4\eta}\frac{\mathrm{d}p}{\mathrm{d}z}(r^2-R^2)=\frac{1}{4\eta}\frac{p_{\mathrm{in}}-p_{\mathrm{out}}}{L}(R^2-r^2) \tag{8.6}$$

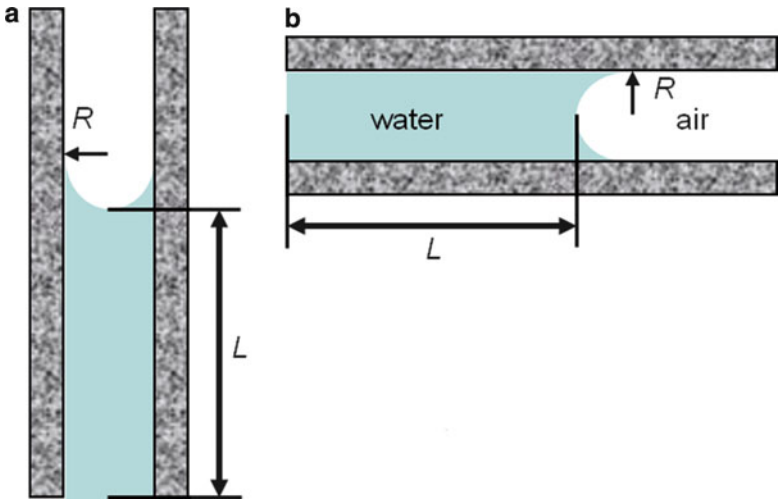

Fig. 8.2 Scheme of the fluid penetration in a vertical (**a**) and horizontal (**b**) capillaries

where p_{in} and p_{out} are the inlet and outlet pressures, L is the channel length, and R is the capillary radius. Similar expression exists for a slit-shaped channel where the flow profile also has a parabolic shape [48]. Equation (8.6) can be averaged over the circular cross-sectional area to give the mean fluid velocity

$$\langle v_z \rangle = \frac{p_{in} - p_{out}}{L} \frac{R^2}{8\eta} \tag{8.7}$$

8.2.2 Capillary Flows

Capillary flows are ones driven by surface tension in, e.g., parallel slit or cylindrical channels. The flow regime is viscous dominated (see above) with a possible exception at the very beginning of the flow [50]. The scaling length-scale is associated with the channel width or radius. Capillary flows are very convenient for initial loading of micro- and nanofluidic devices. The fluid must wet the surface forming a curved air/solution interface at the flow front (Fig. 8.2). The pressure drop in a perfectly wetted circular capillary with radius R is [76]

$$p_{in} - p_{out} = \frac{2\gamma}{R} - \rho g L \tag{8.8}$$

with γ being the interfacial tension. The second term accounts for the hydrostatic pressure due to gravity (see Fig. 8.2a). Inserting (8.8) into (8.7) leads to

$$\langle v_z \rangle = \frac{\gamma R}{4\eta L} - \frac{\rho g R^2}{8\eta} \tag{8.9}$$

For a horizontal capillary (Fig. 8.2b), the second term on the left hand side of (8.9) is zero. This equation also allows for tracing the position of the meniscus in time. Introducing $\langle v_z \rangle = \mathrm{d}L/\mathrm{d}t$ in (8.9) and integrating over time (in absence of gravitational effects) one obtains

$$L = \sqrt{\frac{\gamma R}{2\eta} t} \tag{8.10}$$

The boundary initial condition is $L = 0$ for $t = 0$. Equation (8.10) is known as Washburn equation. The time change in the average fluid velocity can be obtained by differentiating (8.10) with respect to time, which gives

$$\langle v_z(t) \rangle = \frac{1}{2} \sqrt{\frac{\gamma R}{2\eta t}} \tag{8.11}$$

Equations (8.9), (8.10), and (8.11) describe the interfacial tension-driven flow in narrow capillaries. They are also often used to describe flow in porous media, where all geometrical quantities such as capillary radii and lengths have the meaning of statistical averages that represent the actual structure.

8.2.3 *Electrokinetic Transport in Microchannels*

Electrokinetic phenomena present a powerful tool to control fluid and solute transport in microchannels. In most cases of practical importance the electric double layer (EDL) (Fig. 8.3) forms at the wall has much smaller thickness than the channel width. The electrokinetic motion of fluid, relative to a solid, was first analyzed by von Smoluchowski [82]. He used the similarity between the fluid velocity and electrostatic potential field in a thin EDL to obtain (see also [27, 38])

$$v_{\mathrm{eo}} = -\frac{\varepsilon \varepsilon_0 \zeta_{\mathrm{w}}}{\eta} E, \quad v_{\mathrm{ep}} = \frac{\varepsilon \varepsilon_0 \zeta_{\mathrm{p}}}{\eta} E. \tag{8.12}$$

In (8.12) $\varepsilon_0 = 8.854 \times 10^{-12}\ \mathrm{J^{-1}\ C^2\ m^{-1}}$ is the dielectric constant in vacuum, ε is the relative dielectric permittivity of the solvent ($\varepsilon = 78.5$ for water at room temperature 298°K), ζ_{w} and ζ_{p} are the electrokinetic zeta potential defined at the shear plane (see Fig. 8.3), η is the dynamic viscosity of the solvent ($\eta = 8.91 \times 10^{-3}\ \mathrm{kg\ m^{-1}\ s^{-1}}$ for water at room temperature 298°K), and E is the externally applied electric field. The first (8.12) represents the fluid motion in a stationary channel under the action of an externally applied electric field. The motion is called electroosmosis and the velocity is v_{eo}. The second (8.12) gives the velocity

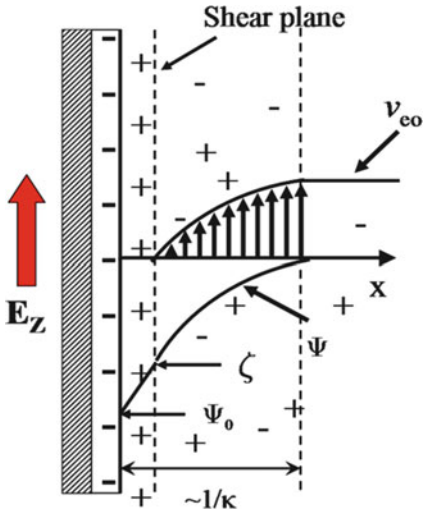

Fig. 8.3 Electric double layer (EDL) in the vicinity of solid wall (electroosmosis) or particle (electrophoresis). The electrokinetic ζ-potential is defined at the shear plane where the relative fluid velocity is zero. The EDL thickness is given by $1/\kappa$ and depends on the concentration of background electrolyte. The electrostatic potential decays with the distance from the wall into the fluid. At the same time the velocity increases until it reaches a constant value outside the EDL. For channels that are much wider than $1/\kappa$ the detailed velocity distribution in the EDL can be ignored and the velocity can be assumed to be constant and given by (8.12)

v_{ep} of filed-driven motion of charged suspended colloidal particle (or a dissolved molecule) driven by the same electric field. This motion is called electrophoresis. The EDL thickness of $1/\kappa$ depends on the concentration of background electrolyte [21, 27, 32, 38]

$$\kappa = \left(\frac{e^2}{\varepsilon \varepsilon_0 kT} \sum_i z_i^2 n_i^0 \right) \tag{8.13}$$

where e is the elementary charge, kT is the thermal energy, z_i is the charge of the i-th ionic species, and ${n_0}^i$ is its number concentration. Hence, the thickness of the EDL depends on the background electrolyte concentration. Aqueous solutions of monovalent electrolyte at room temperature with concentrations ranging between 0.1 and 10^{-6} M will lead to an EDL thickness from 1 to 300 nm. Microfluidic channels often have cross-sectional dimensions in the range of tens or even hundreds of micrometers; therefore, the EDL can be considered to be much thinner. The thin EDL approximation, used by von Smoluchowski [82], implies that the electric field effect on the fluid in a microchannel can be accounted for by means of boundary conditions at the wall instead of a body force term in the momentum balance, (8.1). These boundary conditions correspond to the electroosmotic velocity given by (8.12).

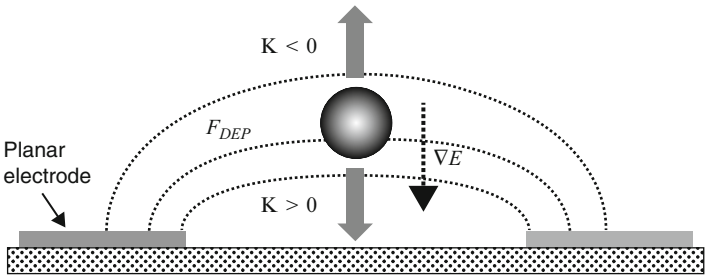

Fig. 8.4 Dielectrophoretic force moves the particle along the gradient of the electric field, ∇E. The particle is either attracted to or repelled from the high-field intensity region based on the sign of the relative polarizability, K

Electroosmosis can be used conveniently for pumping in microfluidic devices. The applied external electric field with magnitude E translates into a pressure gradient which for circular capillary with radius R is equal to [38]

$$\frac{\mathrm{d}p}{\mathrm{d}x} = \frac{8\varepsilon\varepsilon_0\zeta_w E}{R^2} \tag{8.14}$$

A number of different pump designs have been suggested [19, 57, 63–65, 69, 105] to achieve higher pressures and/or better flow rates.

8.2.4 Dielectrophoretic Particle and Droplet Transport

When a polarizable particle is subjected to an inhomogeneous electric field, a dipole is induced in the particle. The particle experiences attraction or repulsion from the high electric field region, depending on its polarizability compared with the surrounding medium as shown in Fig. 8.4. This electric field-driven motion of particles suspended in a medium under the nonuniform field is termed dielectrophoresis (DEP) [66]. In AC electric field, the DEP force leads to net particle displacement due to its nonzero time average [14, 41, 59, 71]. The usage of AC field in DEP, in particular, allows the use of high field strengths without electroosmotic flows and electrolysis [6, 97, 98]. The time average DEP force, F_{DEP}, is given by [66, 98, 101]

$$F_{\mathrm{DEP}} = 2\pi\varepsilon_m r^3 \mathrm{Re}|K(\omega)|\nabla E^2 \tag{8.15}$$

where r is the radius of the particle, ε_m is the dielectric permittivity of the medium, E is the electric field intensity, and $K(\omega)$ is the Clausius–Mossotti factor, i.e., the particle's effective polarizability in media. The direction of the force on the particle depends on the real part of $K(\omega)$,

$$\mathrm{Re}|K(\omega)| = \frac{\varepsilon_p - \varepsilon_m}{\varepsilon_p + 2\varepsilon_m} + \frac{3(\varepsilon_m\sigma_p - \varepsilon_p\sigma_m)}{\tau_{\mathrm{MW}}(\sigma_p + 2\sigma_m)^2(1 + \omega^2\tau_{\mathrm{MW}}^2)} \tag{8.16}$$

where σ_m is the conductivity of the medium, ε_p and σ_p are the dielectric permittivity and the conductivity of the particle, ω is the applied field frequency, and τ_{MW} is the Maxwell–Wagner charge relaxation time, $\tau_{\mathrm{MW}} = (\varepsilon_p + \varepsilon_m)/(\sigma_p + 2\sigma_m)$. Therefore, the direction in which the particle moves is not only determined by the properties of the particle and the medium but also the frequency of the applied field. For dielectric particles, the sign of the real part of $K(\omega)$ is changed at a cross-over frequency of $\omega_c = (\tau_{\mathrm{MW}})^{-1}$ [6, 41, 101]. When $\mathrm{Re}|K(\omega)|>0$, the particle is attracted toward the electric field maxima (positive DEP). Otherwise, the force on the particle is toward the lower field region (negative DEP). This particle control using DEP has been used in many fields of application such as assembly of microwires from metallic nanoparticle suspensions [6, 37, 98, 101], formation of colloidal crystals [55, 56], and separation of dielectric particles [18, 28, 47, 75]. Droplets flowing in a microchannel or floating on the surface of an immiscible liquid can be transported by DEP as explained further in the chapter. Microfluidic mixer was also developed using DEP actuation, which induced chaotic trajectories of suspended particles [24].

8.2.5 Droplet Formation in Microchannels

Emulsions are dispersions of droplets in immiscible liquid medium, which are extensively used in food, cosmetic, and pharmaceutical industries, just to name a few. The droplets are referred to as the dispersed or discontinuous phase, while the surrounding fluid is the continuous phase. The emulsions are thermodynamically unstable but the addition of surfactants or particles can provide significant kinetic stability. At constant volume and temperature, the Gibb's free energy for emulsification of two immiscible fluids is the difference in free energy between the mixed (or emulsified) state (G^{m}) and the unmixed state (G^{u})

$$\Delta G_{\mathrm{form}} = G^{\mathrm{m}} - G^{\mathrm{u}} = \gamma\Delta A - T\Delta S^{\mathrm{m}} \tag{8.17}$$

where γ is the interfacial tension, ΔA is the change in interfacial area, T is temperature, and ΔS^{m} is the positive change in entropy gained upon mixing (emulsification). The first term on the right hand side corresponds to the free energy, which is the work required to expand the interfacial area ($\Delta W = \gamma\Delta A$). Immiscible fluids in contact can have a large interfacial tension; therefore, the interfacial energy is generally much larger than the favorable entropic contribution, and the emulsification process is not spontaneous (positive free energy term). Because of the thermodynamic penalty, emulsion formation requires an energy input. In bulk systems this can be most easily achieved by vigorous stirring or shaking of the whole

oil/water/surfactant system. This approach leads to an emulsion with broad droplet size distribution. Microfluidics allows for the minimization of polydispersity and the creation of droplets that are virtually identical in size.

Given enough time, emulsified liquids would phase separate to lower the stored interfacial energy (by decreasing the interfacial area), with the less dense liquid making up the top layer because of gravity. However, when amphiphilic molecules, i.e., surfactants, are added to the mixture, the droplets might become meta-stable making the emulsion last for a much longer amount of time. Equation (8.17) makes clear that one reason for that effect is the lowering of the interfacial energy via surfactant adsorption at the interface.

Rupturing of a single spherical droplet is governed by the balance between interfacial (capillary) and shear forces. The proper conditions can be estimated from the dimensionless "capillary" number (Ca), which is the ratio of viscous stress over the restorative Laplace pressure (due to the interfacial tension, see (8.8))

$$\mathrm{Ca} = \frac{R_d \tau_{ij}}{2\gamma} \approx \frac{\eta U_\mathrm{d}}{\gamma} \tag{8.18}$$

where R_d is the droplet radius, η is the continuous phase viscosity, τ_{ij} is the relevant component of the viscous stress tensor, and U_d is the characteristic velocity. At $\mathrm{Ca} \approx 1$, the energy input is sufficient enough to rupture a droplet. The necessary viscous stress can be generated by applying pressure or electrically driven flow (see Sects. 8.2.1, 8.2.2 and 8.2.3 above).

Droplet-based microfluidic system is governed by the characteristics of the multiphase flow, interfacial tension, as well as the channel wall wetting and physical properties of the liquids. At different channel scales and fluid velocities, the system can be influenced by balancing inertial, viscous, or gravitational forces against the interfacial forces. In these cases other dimensionless numbers are relevant. For example the ratio of interfacial and gravitational force is given by the Bond number (Bo),

$$\mathrm{Bo} = \frac{\Delta\rho g d_\mathrm{h}^2}{\gamma} \tag{8.19}$$

where $\Delta\rho$ is the density difference between the two liquid phases, and d_h is the characteristic channel dimension. At the dimensions of most droplet forming microfluidic devices, interfacial tension typically dominates over the influence of gravity ($\mathrm{Bo} \ll 1$).

In the special cases when rapid acceleration (entrance effects, etc.) or inertia is present the important physics is given by the Weber number

$$\mathrm{We} = \frac{\rho U_\mathrm{d}^2 d_\mathrm{h}}{\gamma} \tag{8.20}$$

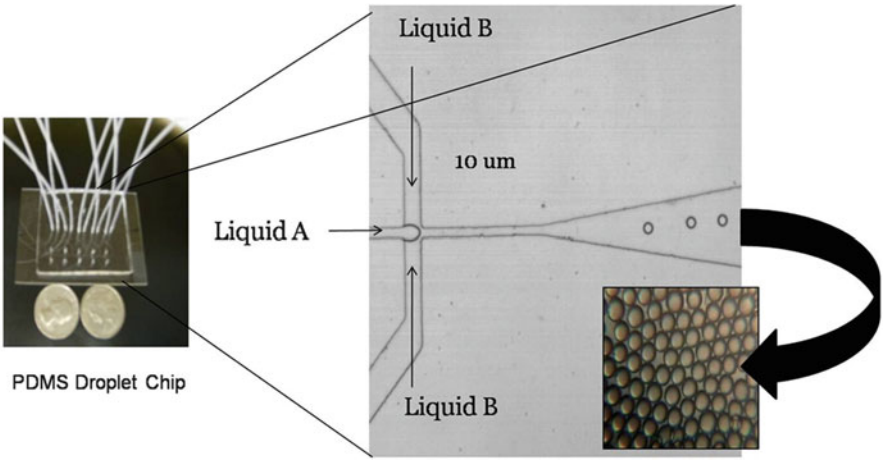

Fig. 8.5 Flow-focusing cross-junction configuration for droplet formation. The center fluid (liquid A) is hydrodynamically focused by the continuous phase (liquid B) within the small orifice. Viscous forces overcome interfacial tension with thread instability in the enclosed orifice producing monodisperse droplets as rapidly as kilohertz frequencies

By controlling fluid pressures, flow regimes, fluid viscosities, wetting properties, channel dimensions, and interfacial properties (i.e., surfactant concentration) it is possible to induce and control periodic break up of a liquid stream to produce microfluidic-generated emulsion drops.

The controlled formation of water-in-oil emulsion droplet stream in a T-junction microfluidic system was first demonstrated by Thorsen et al. [94]. Since then, there has been a plethora of articles published in this area. The analysis of the mechanism for droplet formation in a T-junction device was proposed by Garstecki et al. [31]. At low capillary numbers, it was demonstrated that breakup of drops or bubbles in a microfluidic T-junction is due to the pressure drop across the emerging bubble or drop and not dependent on shear stress. A few literature review articles discuss how these microfluidic systems can be exploited to study flow characteristics and for use as picoliter-sized chemical reactors [33, 81, 83, 85, 86, 93].

The design of a cross-junction microfluidic flow-focusing device (MFFD), with typical operation in the capillary regime where viscous forces are dominant, is shown in Fig. 8.5. A pressure gradient along the long axis of the device forces two immiscible liquids through the orifice. The continuous phase is infused from two sides. The liquid stream comprising the dispersed phase is supplied from the central channel. The continuous phase focuses the inner, immiscible, liquid so that the inner thread becomes unstable and breaks in the narrow orifice in a periodic manner. In some flow regimes the drop size is effectively established by the size of the orifice. In other cases the flow-focusing geometry produces threads that break into drops substantially smaller than the orifice. Droplet formation within the orifice is referred to as the dripping regime while droplet formation of the liquid thread further downstream of the orifice is known as jetting. In general, a liquid thread in the jetting

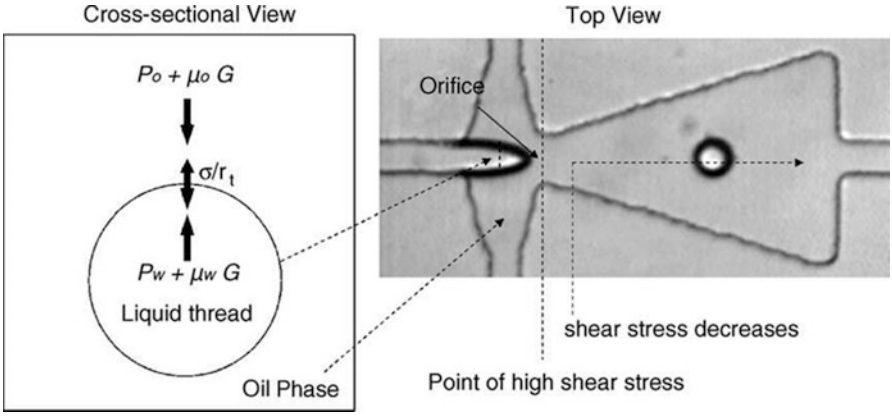

Fig. 8.6 Nozzle shape channel geometry. Droplet breakup occurs at a fixed point due to the focused velocity gradient created by the nozzle shape geometry. The radius of the liquid thread decreases due to the perturbation caused by the extension of the thread. Initial balance of the pressure and shear forces at the interface of the thread determines the initial radius of the thread. The device also produces monodisperse submicron satellite drops (reprinted with permission from Tan et al. [92])

regime experiences unbound flow capillary instabilities, and thus will typically produce less monodisperse drops than those formed in the dripping regime.

Another configuration shown in Fig. 8.6 combines flow-focusing cross-junction droplet formation with nozzle shape channel geometry [91, 92]. The droplet breakup occurs at a fixed point due to the focused velocity gradient created by the nozzle shape geometry. As illustrated in Fig. 8.6, the normal force balance on the surface of the liquid thread includes pressure and shear stresses differences against interfacial tension,

$$(p_{\mathrm{w}} + \eta_{\mathrm{w}} G) - (p_{\mathrm{o}} + \eta_{\mathrm{o}} G) = \frac{\gamma}{R_{\mathrm{t}}} \tag{8.21}$$

where G is the shear rate, p_{o}, η_{o}, p_{w}, and η_{w} are the pressures and viscosities of the continuous and dispersed phase, respectively, and R_{t} is the radius of the liquid thread. In the expanding nozzle geometry, the droplet always breaks at the orifice due to a designed focused shear gradient. The fluid flow accelerates before entering the nozzle and reaches the maximum velocity at the orifice before decreasing as it exits thus creating a focused velocity gradient (and therefore shear). Monodisperse submicron satellite drops were also observed with this system.

Link et al. [52] further modified cross-junction flow-focusing devices to incorporate forces that result from capacitance-like charging of the discontinuous aqueous phase in an applied electric field. This method produced smaller droplets at higher frequencies with more precise control over individual timing than in pressure gradient-driven systems which rely only on viscous forces to overcome surface tension. A voltage was applied to indium tin oxide electrodes incorporated

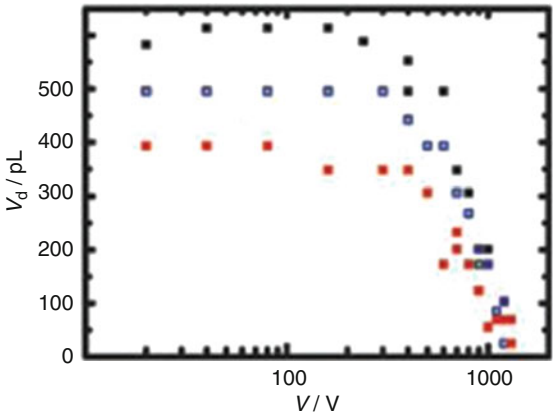

Fig. 8.7 Droplet size as a function of voltage. The crossover between flow-dominated and field-dominated droplet formation for three different flow rates (Qc) of the continuous phase oil (Qc increases from top to bottom: Qc = 80 nL/s; 110 nL/s; and 140 nL/s) (reprinted with permission from Link et al. [52])

into the device. The aqueous stream acts as a conductor whereas the oil acts as an insulator. Electrochemical reactions charge the fluid interface like a capacitor; thus the charge of the interface remains on the droplet. At high electric field strengths, there is an additional force F on the growing drop given by

$$F = qE \tag{8.22}$$

where q is the charge on the droplet and E is the electric field magnitude. Also the capacitance C is directly related to the applied voltage

$$C = q/\Phi \tag{8.23}$$

Therefore the charge on the droplet is dependent on the applied voltage Φ (see (8.22)). The additional force applied to the growing drop thus shows a dependence on Φ^2. The size and frequency of the droplets are determined by a simple mass (or volume) balance

$$Q_d = fV_d \tag{8.24}$$

where Q_d is dispersed phase flow rate, f is the frequency of droplet formation, and V_d is the droplet volume. The droplet size decreases with the field strength (Fig. 8.7) thereby increasing droplet formation frequency. Additionally, the authors demonstrated selective splitting, coalescence, and sorting using charged droplet-electric field manipulation.

8.2.6 Prospects for Droplet-Based Labs-on-a-Chip

Over the past decade there has been a broad effort in the scientific community to miniaturize chemical systems via microfluidic platforms. The concept is to construct compact devices with integrated modular functionalities [20]. These micrometer-sized modules can perform functions which are analogous to bench-scale laboratory processes, hence the name, "lab-on-a-chip." A droplet-based lab-on-a-chip microfluidic device could be envisioned to have the following modules: a built-in filter, a junction where the streams of immiscible fluids meet and where droplets are consequently formed, a tortuous channel where the contents within the droplets can be well mixed by the method of chaotic advection [84], a very long section of channel to allow time for chemical reactions to occur within the drops, and finally a detection/analytical feature to discriminate the resulting content inside the droplets. Such devices are overviewed in detail in other chapters of this book. Another emerging application for the droplet-based chips is materials synthesis inside the droplets, which offer both confined reaction or assembly space and the opportunity to move, manipulate, and collect the formed complex particles and structures. Two specific applications of such devices for materials synthesis and microbioassays developed by the authors are presented in the next two sections.

8.3 Droplet Microfluidics for Mesoporous Particle Synthesis

8.3.1 Overview of Materials Synthesis in Droplets

Microfluidic flow-focusing devices can be used as a means to synthesize solid particles. As mentioned earlier, by simply tuning flow rates or other system parameters, the morphology of the "drops" can be tuned to be spheres, spheroids, discs, or long rods. Not surprisingly, if a liquid-to-solid chemical reaction proceeds to completion within these drops, then the resultant solid particles could possess such shapes. Serra et al. performed a parametric study to demonstrate how various operating parameters of a microfluidic system affected the size of the synthesized polymer particles [79]. Production of particles with various shapes and morphologies via microfluidic reactors was reported by several research groups [22, 60, 103]. Moreover, by using clever double emulsion microfluidic schemes, Kim et al. formed spherical, hollow microparticles [45]. Further, Zhang et al. exploited this concept to make solid particles with multiple separate hollow compartments [106]. Another appealing feature to engineer into the particles is porosity, which allows encapsulating a material of interest within the pores. Such solute-loaded particles could be used for drug delivery: monodisperse particles with known porosity make possible strict control of the amount of drugs being delivered to a patient. Also, it has been envisioned that biological cells can be kept alive within the pores, and by tuning the porosity, one could control the

transport of nutrients and cell byproducts in and out of the particles and therefore optimize the cell's viability [16]. Finally, microfluidics has also been shown to be viable for making nanoparticles [80].

8.3.2 *Microfluidic Synthesis of Mesoporous Silica Microspheres*

Some of us have recently reported on the fabrication of monodisperse, nanostructured silica microspheres utilizing droplet-based microfluidics [11]. In this process, equally sized emulsion droplets with controlled diameter were produced at a frequency of ~100 Hz. The droplets contained the silica precursor/surfactant solution and were dispersed in hexadecane as the continuous oil phase. The solvent was then expelled from the droplets leading to concentration and micellization of the surfactant. At the same time the silica solidified around the surfactant self-assemblies forming equally sized mesoporous particles. The procedure could be tuned to produce individual particles or alternatively particles that are chemically bonded together allowing for the creation of 3-dimensional structures with hierarchical porosity.

The synthesis of mesoporous silicate solids using surfactant templating was developed over a decade ago [46]. An extension of that procedure, referred to as evaporation-induced self-assembly (EISA), involves confining all silica precursor and templating surfactant species within aerosol drops. The solvent progressively evaporates, which leads to an increase of the concentration of templating surfactant, which, upon surpassing the critical micelle concentration, assembles into spherical, cylindrical, or lamellar structures [8, 54]. After a certain reaction time, the silica solidifies around the surfactant self-assembled structures. This is followed by surfactant removal through high temperature calcination, resulting in the formation of well-ordered mesoporous silica. EISA has been successfully utilized to fabricate mesoporous silica thin films [8] and particles with diameters ~1 μm [8, 54] using a wide range of surfactants and block copolymers. However, such mesoporous silica particles obtained via aerosol spray EISA usually have substantial polydispersity.

Andersson et al. [3] recently demonstrated the synthesis of spherical, mesoporous silica particles using an approach which combines emulsion-based precipitation methods [39, 77] with the EISA process. This synthetic route, termed the emulsion and solvent evaporation method (ESE), produced well-ordered 2D hexagonal mesoporous silica microspheres. However, because the emulsions were prepared in bulk using vigorous stirring, the droplets, and therefore the resulting particles, were produced with a broad particle size distribution.

The production of monodisperse silica spheres containing highly ordered nanometer-scale pores (mesopores) of controllable size is of practical interest [70]. They can be used for drug delivery, biomolecular [53] and cellular [16] encapsulation. Monodisperse particles have been ordered into 2-dimensional ordered arrays [23, 26], which allows for the fabrication of catalytic structures

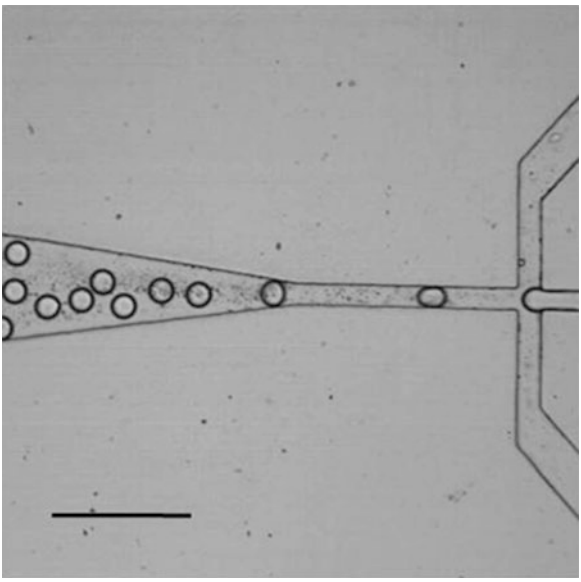

Fig. 8.8 Optical microscopy image of aqueous droplets formed at a cross-junction in a microfluidic device. The channel dimensions of the orifice are 25 μm (width) by 30 μm (height). The scale bar is 100 μm (reprinted with permission from Carroll et al. [11])

with controlled pore hierarchy. Mesoporous particles also have the potential for being used as chemical and biochemical sensors [10].

MFFDs provide a robust approach to form monodisperse emulsion drops [4]. Microfluidic-generated drops can function as both morphological templates and chemical reactors for the synthesis of monodisperse polymer [40, 79, 103] and biomolecular [106] microparticles. Below, we exemplify such processes by recent results from novel procedure for fabrication of well-defined monodisperse, mesoporous silica particles. It is based on MFFD emulsification of an aqueous-based sol [7] with subsequent EISA processing utilizing the aforementioned ESE method [3].

The details of the materials and methods are provided in the paper by Carroll et al. [11]. Briefly, the silica precursor solution was prepared by hydrolyzing tetraethyl orthosilicate (TEOS) in ethanol and hydrochloric acid under vigorous stirring at room temperature for 30 min. The amphiphilic, triblock copolymer templating agent (Pluronic P104) was dissolved in deionized water and then mixed with the hydrolyzed TEOS solution to complete the preparation of the aqueous sol. This allowed for the use of Pluronic surfactant as a templating reagent in the presence of a much lower concentration of ethanol than was used earlier [3].

Emulsification of the aqueous siliceous precursor was achieved by supplying the aqueous (sol–gel solution) phase and oil phase to the microfluidic device using two syringe pumps. The continuous phase was prepared by dissolving ABIL EM 90 surfactant in hexadecane which served as the emulsifier. The SU-8 photoresist-templated PDMS microfluidic device was fabricated using the soft-lithography method [102] described in the first section. The design of the microfluidic devices is shown in Fig. 8.8.

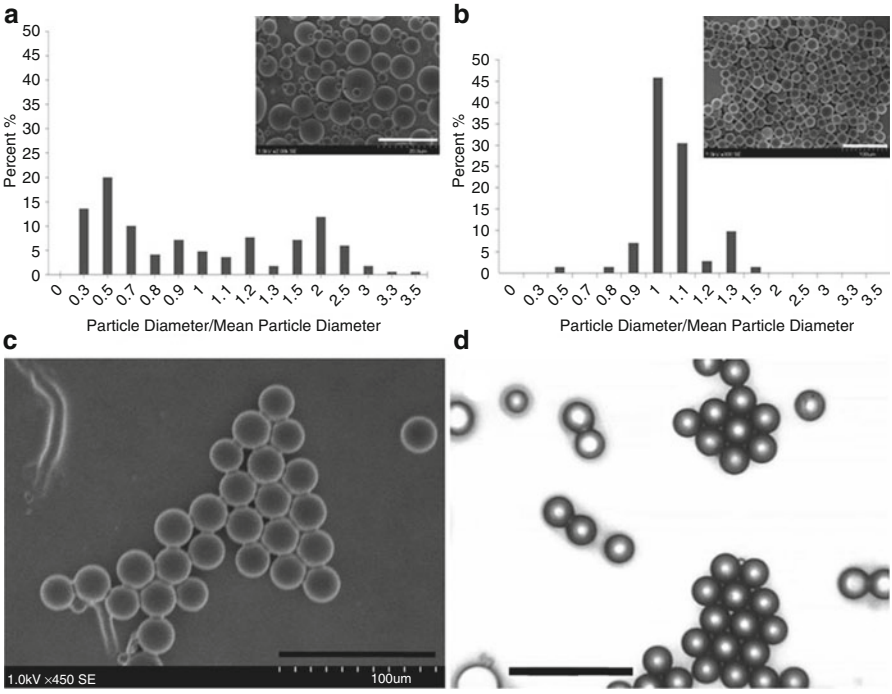

Fig. 8.9 (**a**) Polydisperse silica microspheres templated from shaken bulk emulsion. Scale bar is 20 μm. (**b**) Silica microspheres templated by monodisperse microfluidic device-generated droplets. Scale bar is 100 μm. (**c**) Scanning electron microscopy image and (**d**) optical photograph (scale bar is 40 μm) of particles that have fused together in a hexagonal array. The particles are connected by "bridges" which form when the particles come into contact before the completion of the gelation process (reprinted with permission from Carroll et al. [11])

The droplets, after being produced through the MFFD, were transferred to a flask, and heated to 80°C at reduced pressure for 2 h. To prevent droplet coalescence before the silica solidification was complete, the emulsion was mildly stirred. The particles were then separated from the oil phase followed by calcination at 500°C for 5 h to remove the surfactant template.

Silica particles obtained from droplets formed in a bulk shaken emulsion and the MFFD are shown in Fig. 8.9a, b respectively. The low ambient pressure allowed for the solvent (water and ethanol) to be transported out of the droplets and through the hexadecane phase, which led to micellization of the surfactant and subsequent gelation of the silica precursor. Due to loss of solvent, the solid particles are approximately half the size of the original liquid droplets. The particles obtained in a bulk shaken emulsion are spherical but very polydisperse. As mentioned earlier, it is difficult and impractical to narrow the size distribution because shaken emulsions, in general, produce polydisperse droplets, which result in a broad particle size distribution. Increasing the stirring intensity during the emulsion formation might reduce the average particle size and narrow the size

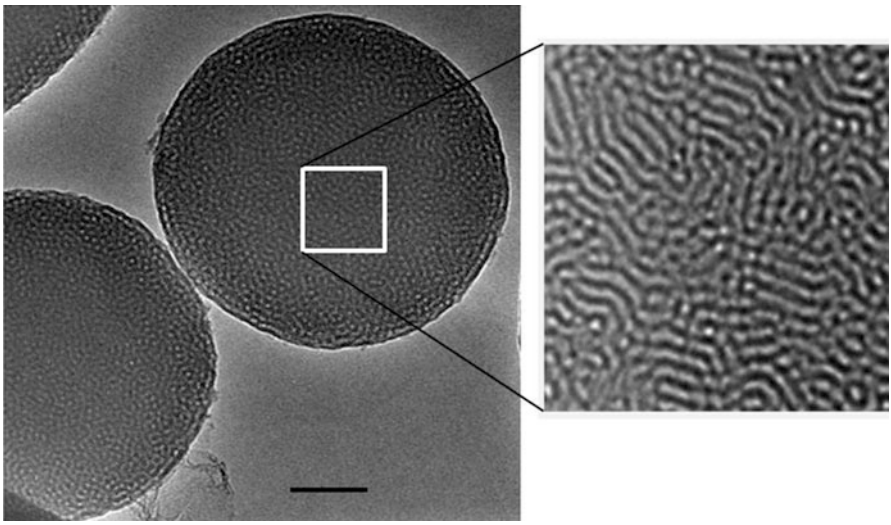

Fig. 8.10 Transmission electron image of silica microspheres containing well-ordered mesostructures templated by P104 surfactant. Scale bar is 100 nm (reprinted with permission from Carroll et al. [11])

distribution but cannot produce monodisperse droplets. Using the microfluidic device we formed monodisperse droplets, which is the necessary step to form monodisperse particles. The size of the droplets can depend on the dimensions of the droplet forming region, the flow rates of the oil and aqueous phases, the viscosity of the fluids (water/ethanol and oil) and the stabilizing surfactant. Hence a single device can produce monodisperse droplets (and particles) of different sizes by varying the relative magnitude of the viscous and interfacial forces that are involved [4].

The particles might stick together during the final stages of solvent evaporation unless some preventative operations are taken. The particles can become connected by silica "bridges," which form when the droplets come into contact before the completion of the gelation chemistry. This agglomeration could be exploited to obtain arrays of interconnected particles. Such bonding can result in robust layers of monodisperse mesoporous particles, which could then be deposited on other substrates to use in applications such as catalysis and sensing. Such multiparticle monolayers are shown in Fig. 8.9c, d. Figure 8.10 depicts a TEM image which clearly shows the presence of the nanostructured pores of diameter ~5–6 nm within the microparticles.

Varying the composition of the oil/water surfactant mixture leads for different morphologies of the obtained porous structure. A biporous structure formed in droplet microreactors using specific combination of surfactants is exemplified in Fig. 8.11 [12, 13]. The frame in Fig. 8.11a illustrates the results of a dynamic light-scattering characterization of the aqueous phase that forms the droplets. Two types

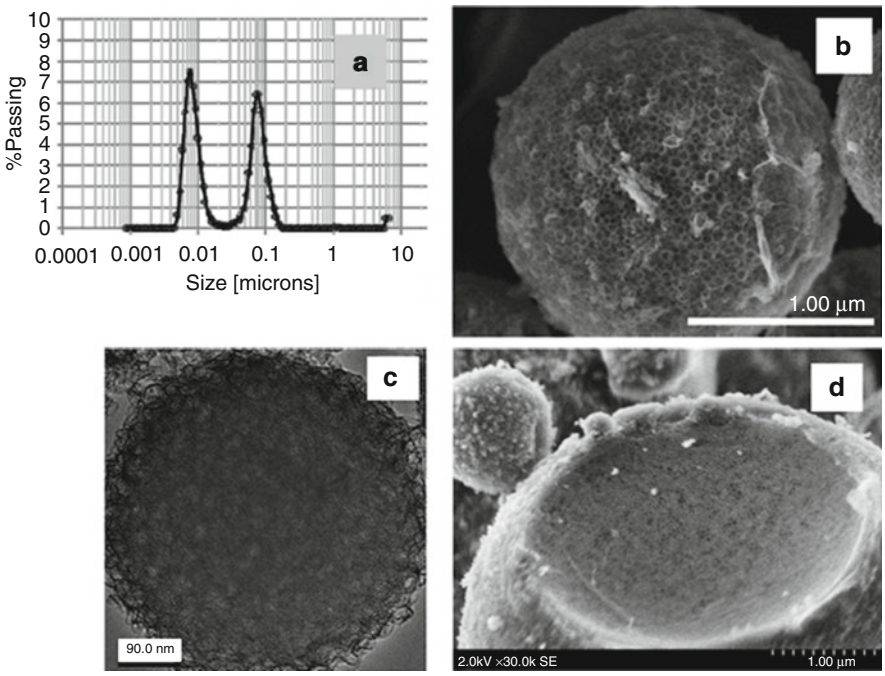

Fig. 8.11 Biporous silica particles obtained from oil/aqueous phase/surfactants. (**a**) DLS measurements of the aqueous phase indicate the presence of micelles (∼6 nm) and microemulsion droplets (tens of nm). (**b**) SEM image of silica particle surface with cavities (diameter ∼40 nm) arranged as honeycomb. (**c**) TEM images of silica particle showing open access to internal porous network. (**d**) SEM of broken particles showing the internal structure

of species are present. We hypothesized that these are micelles (smaller) and microemulsion droplets (larger), which then are templated to give pore in the nanometer and tens of nanometers range (as in Fig. 8.11b, c). Figure 8.12a–c demonstrates the effect of addition of salt in the aqueous phase. The effect is very strong, which is because one of the surfactants use dis cationic—cetyl trimethylamonium bromide (CTAB). The particle depicted in Fig. 8.12c is of particular interest. The large pores are uniformly monodisperse, but the smaller ones essentially collapsed. The surface is much smoother in comparison with a salt-free particle as the one in Fig. 8.12a. The effect of the oil to water relative ratio is shown in Fig. 8.12d, while the effect of the CTAB concentration is demonstrated in Fig. 8.12e, f. The latter suggest that increasing the concentration of the ionic CTAB increases the number of smaller pores while the larger ones disappear.

As mentioned above, there is great interest in encapsulating cells into porous monodisperse solid particles, thus turning them into biological microreactors of a kind [16]. Biopolymer capsules with diameters in the tens of microns with controlled morphology have been fabricated [106]. It has been demonstrated that droplet-based microfluidics can indeed be used to encapsulate single cells [29, 35].

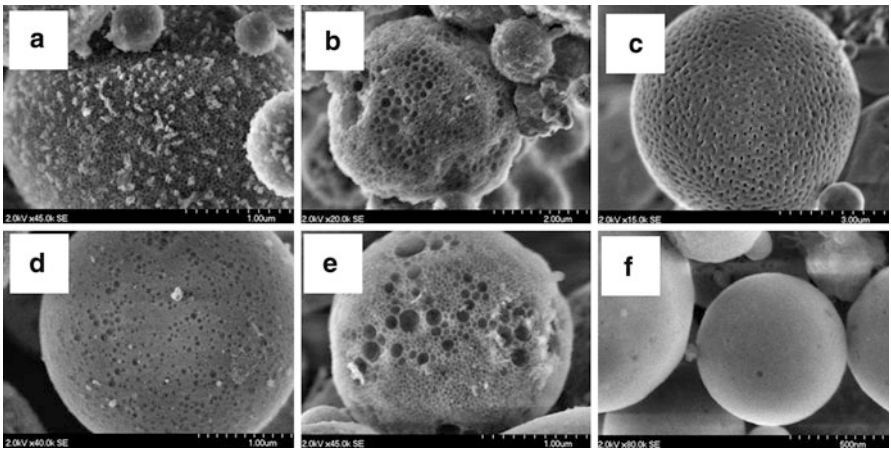

Fig. 8.12 Pore morphologies and particle surface areas created by varying microemulsion mixture components. Particles formed by: (**a**) standard microemulsion mixture, BET surface area 1,000 m^2/g. (**b**) Adding 0.075 M NaCl, BET surface area 650 m^2/g. (**c**) Adding 0.15 M NaCl, BET surface area 850 m^2/g. (**d**) 2:1 oil to water ratio, BET surface area 1,038 m^2/g. (**e**) Reducing mass of Abil EM90 surfactant by 25%, BET surface area 975 m^2/g. (**f**) Increasing mass of CTAB surfactant by 25%, BET surface area 1,250 m^2/g (reprinted with permission from Carroll et al. [13])

Tan et al. formed lipid vesicles within microfluidic channels with the aim of encapsulating and keeping cells viable [91, 92]. DNA amplification is another application that is well suited for such droplet microfluidics because of the requirement of small volumes, compartmentalization of chemical processes, and the capability of continuous ongoing in situ detection [25, 44].

8.4 Droplet Microreactors Manipulated by Electric Fields

8.4.1 Microfluidic Chips with Droplet Transport by Electrowetting

The droplets in the microfluidic chips described above are moved all together by the flow of the carrier fluid in the microchannels. An alternative approach is to apply electric fields in configurations that allow exerting forces and repositioning the droplets individually. In planar surface-based systems, discrete droplets are manipulated on two-dimensional (2D) arrays of electrodes. The electrodes can be designed and configured for the use of electrowetting on dielectric (EWOD) or DEP as the driving forces of the droplet motion. Such types of droplet-based microfluidic chips have the advantages of being compact and simple, while eliminating external pumps and channels. They allow for independent control of the position and

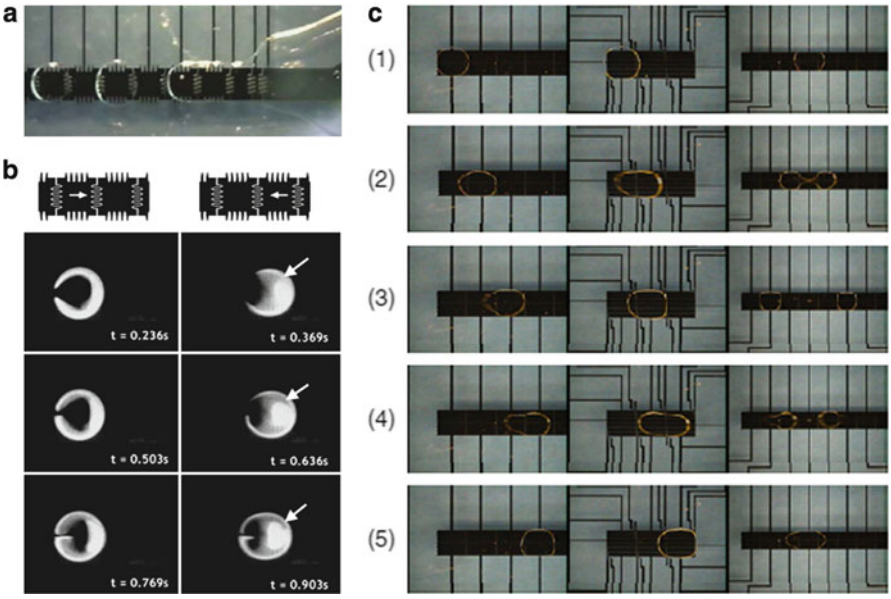

Fig. 8.13 Manipulation of droplets on planer surface-based systems. Droplets placed between two electrodes are controlled by means of electrowetting phenomenon. (**a**) Dispensing of uniform microdroplets from on-chip liquid reservoir (reprinted with permission from Pollack et al. [68]). (**b**) Time-lapsed images of mixing in oscillating droplets on two electrodes at 8 Hz of frequency (reprinted with permission from Paik et al. [61]). (**c**) Sequential images of transportation, breakup, and merging of droplets through surface electrodes (reprinted with permission from Yi and Kim [104])

trajectories of many droplets, and easy automation under software-driven electronic control. Droplet control using electrowetting is typically based on a configuration, where the water droplets are sandwiched between two planes and surrounded by dielectric oil phase [30, 68]. The bottom layer contains addressable electrode array and the top electrode is connected to ground. Insulating dielectric layers are covered on top of both electrodes to separate the droplets from the electrodes. The application of an electric field changes the interfacial energy between the liquid and the insulating layer. The contact angle of droplet at the energized electrode is lowered, causing the droplet to move along the activated electrodes. A wide variety of on-chip droplet operations, such as dispensing, merging, and fission, have been demonstrated using programmable electrowetting microdevices (Fig. 8.13a, c) ([17, 67, 68, 104]). Droplet mixing on the electrowetting-based microdevice has been accomplished by oscillating the droplet placed between two electrodes (Fig. 8.13b) [61, 62]. Such EWOD systems are very convenient for rapid chemical and biomedical analysis; however, the contact of the droplet with the solid surface limits their application in materials synthesis. An alternative configuration involving freely suspended droplets is described in the next section.

8.4.2 *On-Chip Dielectrophoretic Manipulation of Droplet Microreactors*

DEP is another electrically induced force that can be used for on-chip droplet manipulation. Jones et al. demonstrated uniform aqueous droplet dispensing in an open structure consisting of parallel, coplanar electrodes coated dielectric layer [2, 42, 99]. The DEP liquid actuation can be achieved without a second contact electrode as in the electrowetting-based devices, potentially completely avoiding the contact with solid surfaces. The surface contamination is reduced or eliminated. Velev et al. developed a new type of DEP-based lab-on-a-chip system for manipulating freely suspended droplets on the surface of dense perfluorinated hydrocarbon oil (F-oil) without any contact with solid surface [96]. Water or hydrocarbon droplets partially floating on the surface of dense fluorinated oil phase were captured and transported by AC fields originating from arrays of electrodes below the layer of F-oil (Fig. 8.14a). Because of the higher dielectric permittivity of the water droplet ($\varepsilon \approx 80$) rather than that of the F-oil ($\varepsilon \approx 2$) the floating droplets are always attracted to the area of higher field intensities as shown in the Fig. 8.14b. The dielectrophoretically trapped microdroplets move along computer-programmed paths synchronously in parallel or can be merged for rapid mixing by applying AC electric field consecutively through electrode arrays.

Within the partially floating droplets on the F-oil, microparticle separation and internal liquid circulation occurred as a result of a series of processes driven by mass and heat transfer due to the water evaporation from the droplet surface (Fig. 8.15). The process has been investigated and interpreted in detail by Chang and Velev [15]. During the evaporation from the droplet top protruding from the surface of the fluorinated oil, a surface tension gradient emerges by a nonuniform temperature distribution within the floating droplet on a chip. This interfacial gradient generates a Marangoni flow inside the evaporating droplet. The fluid inside the droplet eventually begins moving in a large vortex, rotating in an arbitrary direction (Fig. 8.15b). The process can be modeled well by numerical solution of the combined equations for heat and fluid transport. Partially as a result of the internal fluid rotation, the suspended particles moved by the flow are collected at the top of the droplets by the hydrodynamic flux compensating for the evaporation.

This DEP-driven droplet mixing and microseparation technique has potential in various on-chip materials synthesis processes involving particle assembly inside the shrinking droplets. When the droplets contain mixtures of microparticles and nanoparticles, the drying leads not only to the assembly of "supraballs" from aggregated ordered microspheres, but to separation of the nanoparticles in their own domain on the surface, as they can travel through the interstices of the structure formed by the larger particles [58] (Fig. 8.16a). The collection and assembly of the particles in layered domains can also result from sedimentation of magnetic field-driven separations. Overall, the microdroplets can serve as assembly sites and microreactors for the fabrication of "Janus," binary and ternary supraparticles, polymer capsules, and semiconducting microbeads (Fig. 8.16). Another application

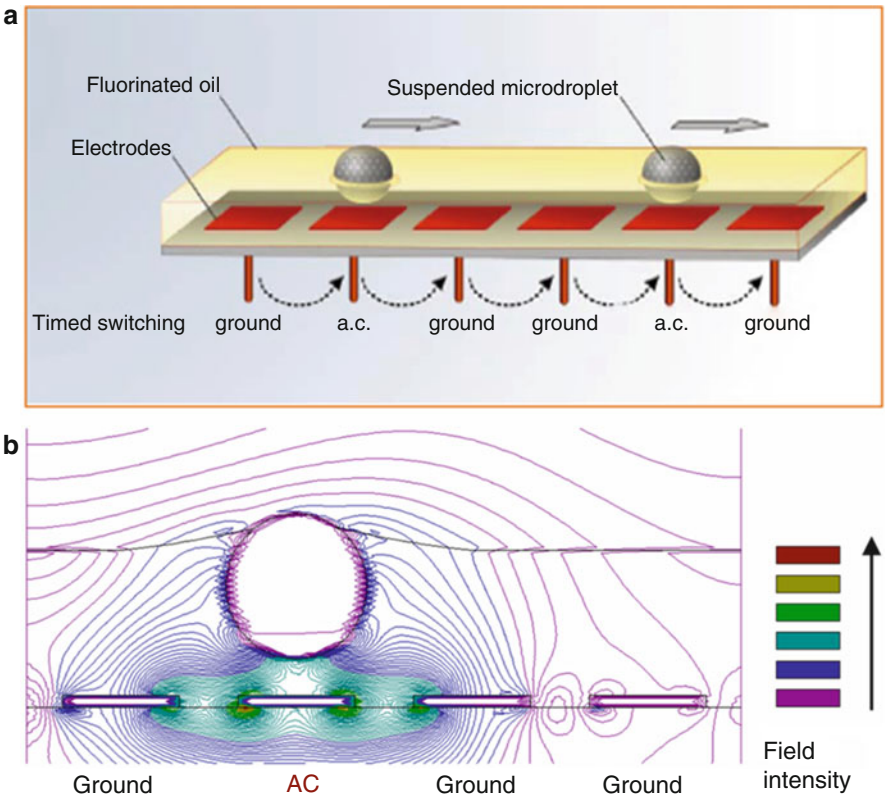

Fig. 8.14 On-chip manipulation of floating microdroplets using dielectrophoresis. (**a**) Schematic of the dielectrophoretic liquid–liquid microfluidic system with freely suspended droplets (reprinted with permission from Velev et al. [96]). AC electric field is applied by arrays of electrodes below the F-oil phase. (**b**) Simulation of the electric field intensity distribution in the vertical plane at the droplet equilibrium position in the DEP-based chip (reprinted with permission from Millman et al. [58])

of this platform has been the design of immuno-agglutination microbioassays, based on particle separation inside the droplets containing antibody-functionalized nanoparticles, microparticles, and molecules of interest [15, 72]. Overall, the DEP-driven droplet method can be potentially applicable in lab-on-a-chip devices for microsynthesis, microassays, high-throughput drug or toxin screening, manipulation and analysis of single cells, and other biotechnological processes on the microscale. A schematic illustration of some of the processes made possible by such "on-chip droplet engineering" is presented in Fig. 8.17. Recently, the authors have shown that the droplets used as microcontainers for complex particle assembly can be suspended on top of super hydrophobic surfaces, eliminating the need for perfluorinated oil as substrate and greatly simplifying the collection of the products [73, 74]. A variety of new configurations and automated materials synthesis platforms may be developed in the future.

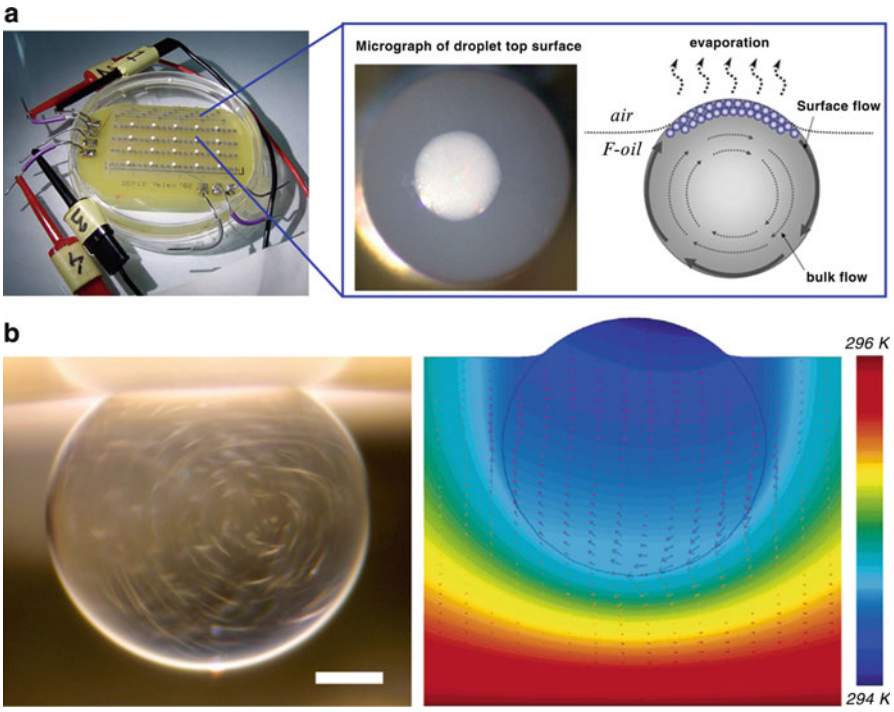

Fig. 8.15 Particle microseparation within the evaporating droplet floating on the DEP-based chip. (**a**) Multiple droplets of 1 μL containing polystyrene microspheres are trapped by DEP above electrode matrix in the F-oil layer (*left*) (reprinted with permission from Millman et al. [58]). Typical micrographs of particle separation on the top surface of an evaporating droplet (*right*) (reprinted with permission from Chang and Velev [15]). (**b**) Typical experimental images of the internal circular flow in the evaporating water droplets viewed from side (*left*) (reprinted with permission from Chang and Velev [15]). The tracers are microrod particles and the camera exposure time was 2 s. Scale bar = 200 μm. Simulation for the temperature distribution and velocity profile in the drying droplet using COMSOL multiphysics (*right*) (reprinted with permission from Chang and Velev [15]). Colors show the temperature and the velocity vector magnitudes are represented by the lengths of the *arrows*

8.5 Summary and Outlook

Droplet-based microfluidics has high potential for implementation in a variety of new technologies and applications. Researchers have successfully designed a variety of droplet-based microfluidic systems for the precise control of droplet formation, selective coalescence, sorting, and mixing to enable the manipulation of femto- to nanoliter droplet reactors. Particle synthesis in microfluidic-generated droplet reactors has the advantage of producing samples with high monodispersity. This brings another level of structural control in addition to well-defined internal mesostructures. Thus, opportunities are created for the design of new and better catalysts, drug delivery vehicles, coatings with fine-tuned optical, mechanical, and chemical properties.

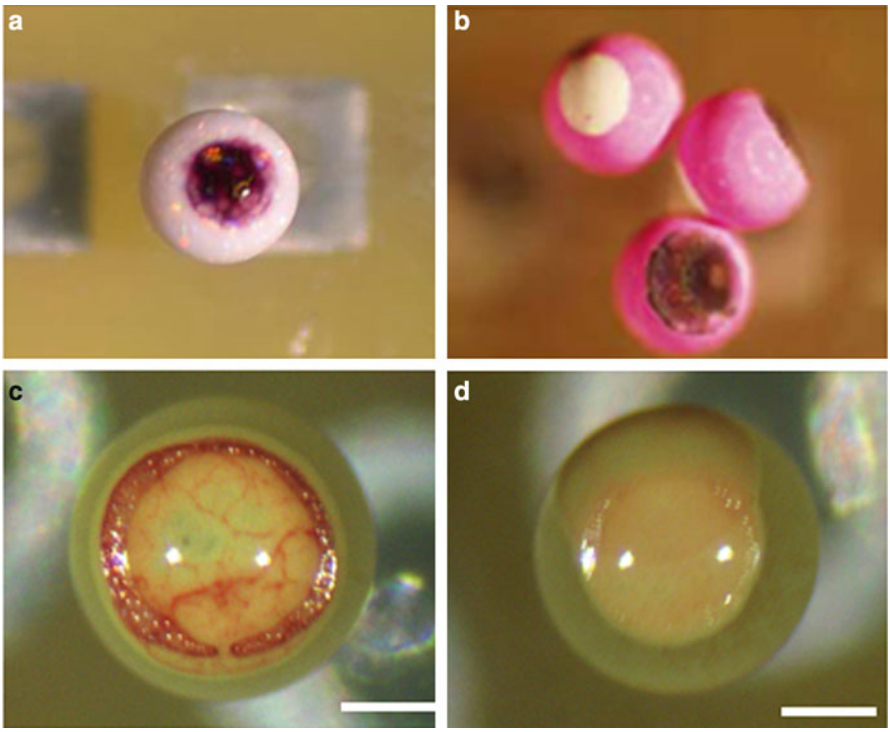

Fig. 8.16 Various applications of the floating droplets as microreactors. (**a**) Anisotropic supraparticle assembly by the evaporation of droplets from binary suspension of gold nanoparticles (*top layer*) and polystyrene latex above the energized electrode after a few hours drying (reprinted with permission from Millman et al. [58]). (**b**) Formation of multilayer particles by the evaporation of droplets from ternary particle mixtures of gold nanoparticles (*top layer*), fluorescent red latex beads (*middle*), and silica microspheres (*bottom*) (reprinted with permission from Millman et al. [58]). Negative control droplet after 30 min of drying (**c**) and test droplet where antibody (rabbit-IgG) is added after 30 min of drying (**d**) for the immuno-microbioassay on the basis of particle separation inside evaporating droplets on a chip (reprinted with permission from Chang and Velev [15]). Both droplets contain a binary suspension of 3 wt% 1 μm anti-rabbit IgG-coated latex particles and 0.02 wt% 40 nm anti-rabbit IgG-coated gold nanoparticles. Scale bars = 200 μm

The utilization of droplet microfluidics is not limited to the synthesis of microparticles. The novel and unique opportunities for processing minute solution samples within micron-sized droplets offer engineers, chemists, and biologists an innovative platform for molecular and biomolecular synthesis in addition to high-throughput analysis. Integration of heating elements into droplet-based microfluidic devices will make it possible to carry out in vitro single-molecule DNA amplification, protein expression, and a host of other biomolecular reactions. Another advantage of droplet-based fluidic systems over continuous flow ones is the sequestering of reagents into isolated droplet compartments surrounded by an immiscible oil phase. Thus each droplet presents a tiny test tube which allows for large-scale experiments using small amounts of reactants.

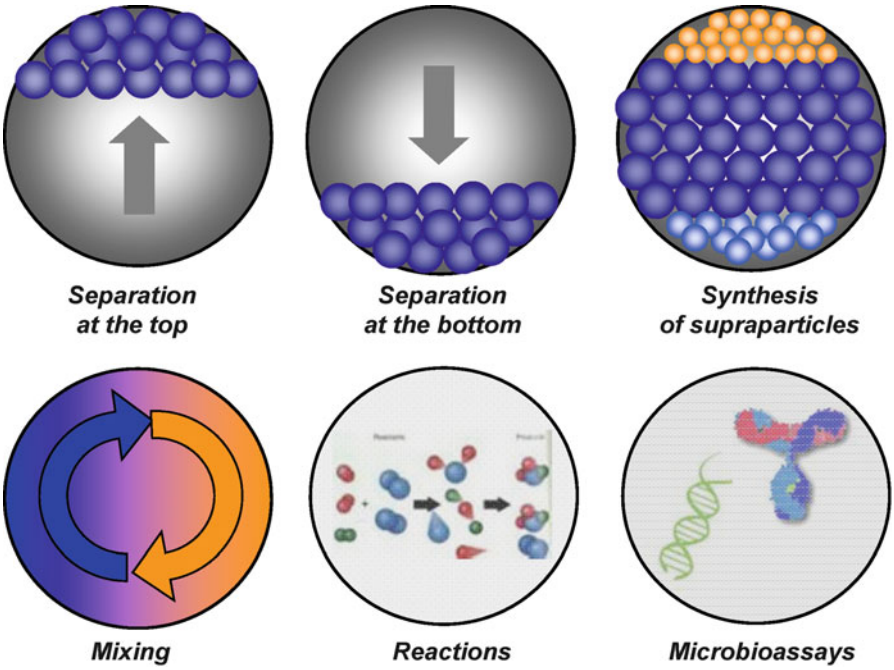

Fig. 8.17 Schematic of some of the processes that can be realized with the confines of freely suspended microdroplet reactors on a chip. The lack of contact with solid surfaces makes this system particularly suitable for the synthesis of complex anisotropic particles

Droplet-based microfluidics has also been employed for a number of unique chemical processes on a chip involving multiphase phenomena and crystallization including precipitation reactions [78, 87], synthesis of cobalt [83, 85, 86] and titania [90], titration of formic acid [36] and anticoagulants [83, 85, 86], and crystal growth [43]. Lau et al. examined 40 different conditions within a single device to crystallize catalase, glucose isomerase, thaumatin, and ferritin [49]. Such high-value multiphase processes, together with the materials aspects outlined in this chapter, hold promise that the present lab-on-a-chip systems will in the future be supplemented by "factory-on-a-chip" devices for making of high-value products and materials.

We believe that many or even the majority of these future microfabrication tools will operate on the basis of droplet confinement and manipulation. A better understanding of droplet microfluidic processes and the underlying physical laws is crucial for the further advancement of the research and development of the area. The fundamental challenges presented by these systems are fascinating and the potential afforded by multiphase droplet microfluidics for engineering, chemical, and biological applications is enormous.

Acknowledgments This work was supported by grants from the US National Science Foundation (CBET 0828900, PREM—DMR 0611616, and MRSEC DMR-1121107).

References

1. Abate AR, Lee D, Do T, Holtze C, Weitz DA (2008) Glass coating for PDMS microfluidic channels by sol–gel methods. Lab Chip 8:516–518
2. Ahmed R, Jones TB (2007) Optimized liquid DEP droplet dispensing. J Micromech Microeng 17:1052–1058
3. Andersson N, Kronberg B, Corkery R, Alberius P (2007) Combined emulsion and solvent evaporation (ESE) synthesis route to well-ordered mesoporous materials. Langmuir 23:1459–1464
4. Anna SL, Bontoux N, Stone HA (2003) Formation of dispersions using "flow focusing" in microchannels. Appl Phys Lett 82:364–366
5. Antencia J, Beebe DJ (2005) Controlled microfluidic interfaces. Nature 437:648–655
6. Bhatt KH, Velev OD (2004) Control and modeling of the dielectrophoretic assembly of on-chip nanoparticle wires. Langmuir 20:467–476
7. Bore MT, Rathod SB, Ward TL, Datye AK (2003) Hexagonal mesostructure in powders produced by evaporation-induced self-assembly of aerosols from aqueous tetraethoxysilane solutions. Langmuir 19:256
8. Brinker CJ, Lu YF, Sellinger A, Fan HY (1999) Evaporation-induced self-assembly: nanostructures made easy. Adv Mater 11:579–585
9. Brody JP, Yager P, Goldstein RE, Austin RH (1996) Biotechnology at low Reynolds numbers. Biophys J 71:3430–3441
10. Buranda T, Huang J, Rama Rao GV, Ista LK, Larson RS, Ward TL, Sklar LA, Lopez GP (2003) Biomimetic molecular assemblies on glass and mesoporous silica microbeads for biotechnology. Langmuir 19:1654–1663
11. Carroll N, Rathod SB, Derbins E, Mendez S, Weitz DA, Petsev DN (2008) Droplet-based microfluidics for emulsion and solvent evaporation synthesis of monodisperse mesoporous silica microspheres. Langmuir 24:658–661
12. Carroll NJ, Pylypenko S, Atanassov PB, Petsev DN (2009) Bidisperse nano-porous microparticles derived by microemulsion templating. Langmuir 25:13540
13. Carroll NJ, Pylypenko S, Ortiz A, Yonemoto BT, Lopez C, Atanassov P, Weitz DA, Petsev DN (2010) Droplet based microfluidics for synthesis of mesoporous silica microspheres. MRS Symp Proc 1272:KK08–KK02
14. Catellanos A, Ramos A, Gonzalez A, Green NG, Morgan H (2003) Eelectrohydrodynamics and dielectrophoresis in microsystems: scaling laws. J Phys D: Appl Phys 36:2584–2597
15. Chang ST, Velev OD (2006) Evaporation-induced particle microseparations inside droplets floating on a chip. Langmuir 22:1459–1468
16. Chia SY, Urano J, Tamanoi F, Dunn B, Zink JI (2000) Patterned hexagonal arrays of living cells in sol–gel silica films. J Am Chem Soc 122:6488–6489
17. Cho SK, Moon H, Kim C-J (2003) Creating, transporting, cutting, and merging liquid droplets by electrowetting-based actuation for digital microfluidic circuits. J Microelectromech Syst 12:70–80
18. Cui L, Holmes D, Morgan H (2001) The dielectrophoretic levitation and separation of latex beads in microchips. Electrophoresis 22:3893–3901
19. Culbertson CT, Ramsey RS et al (2000) Electroosmotically induced hydraulic pumping on microchips: differential ion transport. Anal Chem 72:2285
20. Daw R, Finkelstein J (2006) Lab on a chip. Nature 442:367
21. Debye P, Huckel E (1923) Zur Theorie der Elektrolyte. I. Gefrierpunktserniedrigung und verwandte Erscheinungen. Phys Ztschr 24:185
22. Dendukuri D, Tsoi K, Hatton TA, Doyle PS (2004) Controlled synthesis of nonspherical microparticles using microfluidics. Langmuir 21:2113–2116
23. Denkov ND, Velev OD, Kralchevsky PA, Ivanov IB, Yoshimura H, Nagayama K (1992) Mechanism of formation of 2-dimensional crystals from latex-particles on substrates. Langmuir 8:3183–3190

24. Deval J, Tabeling P, Ho C-M (2002) A dielectrophoretic chaotic mixer. Proc. IEEE MEMS 2002, Micro Electro Mechanical Systems, Las Vegas, USA, pp 36–39
25. Diehl F, Li M, He Y, Kinzler KW, Vogelstein B, Dressman D (2006) BEAMing: single-molecule PCR on microparticles in water-in-oil emulsions. Nat Methods 3:551–559
26. Dimitrov AS, Nagayama K (1996) Continuous convective assembling of fine particles into two-dimensional arrays on solid surfaces. Langmuir 12:1303–1311
27. Dukhin SS, Derjaguin BV (1974) Equilibrium double layer and electrokinetic phenomena. Surface and Colloid Science E. Matijevic. Wiley Interscience, New York
28. Dussaud AD, Khusid B, Acrivos A (2000) Particle segregation in suspensions subject to high-gradient ac electric fields. J Appl Phys 88:5463–5473
29. El-Ali J, Sorger PK, Jensen KF (2006) Cells on chips. Nature 442:403–411
30. Fair RB (2007) Digital microfluidics: is a true lab-on-a-chip possible? Microfluid Nanofluid 3:245–281
31. Garstecki P, Stone HA, Whitesides GM (2005) Mechanism for flow-rate controlled breakup in confined geometries: a route to monodisperse emulsions. Phys Rev Lett 94:164501-1-4
32. Gouy G (1910) Sur la constitution de la charge ´electrique ‘a la surface d’un electrolyte. J Physique 9:457–468
33. Gunther A, Jensen KF (2006) Multiphase microfluidics: from flow characteristics to chemical and materials synthesis. Lab Chip 6:1487–1503
34. Happel J, Brenner H (1983) Low Reynolds number hydrodynamics. Kluwer, Boston
35. He M, Edgar JS, Jeffries GDM, Lorenz RM, Shelby JP, Chiu DT (2005) Selective encapsulation of single cells and subcellular organelles into picoliter- and femtoliter-volume droplets. Anal Chem 77:1539–1544
36. Henkel T, Bermig T, Kielpinski M, Grodrian A, Metze J, Kohler JM (2004) Chip modules for generation and manipulation of fluid segments for micro serial flow processes. Chem Eng J 101:439–445
37. Hermanson KD, Lumsdon SO, Williams JP, Kaler EW, Velev OD (2001) Dielectrophoretic assembly of electrically functional microwires from nanoparticle suspensions. Science 294:1082–1086
38. Hunter RJ (1981) Zeta potential in colloid science. Academic, New York
39. Huo Q, Feng J, Schueth F, Stucky GD (1997) Preparation of hard mesoporous silica spheres. Chem Mater 9:14–17
40. Ikkai F, Iwamoto S, Adachi E, Nakajima M (2005) New method of producing monosized polymer gel particles using microchannel emulsification and UV irradiation. Colloid Polym Sci 283:1149–1153
41. Jones TB (1995) Electromechanics of particles. Cambridge Press, Cambridge
42. Jones TB, Gunji M, Washizu M, Feldman MJ (2001) Dielectrophoretic liquid actuation and nanodroplet formation. J Appl Phys 89:1441–1448
43. Ju JX, Zeng CF, Zhang LX, Xu NP (2006) Continuous synthesis of zeolite NaA in a microchannel reactor. Chem Eng J 116:115–121
44. Kelly TB, Baret J-C, Taly V, Griffiths AD (2007) Miniaturizing chemistry and biology in microdroplets. Chem Commun 18:1773–1788
45. Kim J-W, Utada AS, Fernandez-Nieves A, Hu Z, Weitz DA (2007) Fabrication of monodisperse gel shells and functional microgels in microfluidic devices. Angew Chem Int Ed 46:1819–1822
46. Kresge CT, Leonowicz ME, Roth WJ, Vartuli JC, Beck JS (1992) Ordered mesopourous molecular-sieves synthesized by a liquid-crystal template mechanism. Nature 359:710–712
47. Kumar A, Qiu Z, Acrivos A (2004) Combined negative dielectrophoresis and phase separation in nondilute suspensions subject to a high-gradient ac electric field. Phys Rev E 69:021402
48. Landau LD, Lifshitz EM (1988) Fluid mechanics. Pergamon Press, Moscow
49. Lau BTC, Baitz CA, Dong XP, Hansen CL (2007) A complete microfluidic screening platform for rational protein crystallization. J Am Chem Soc 129:454–455

50. Lavi B, Marmur A et al (2008) Porous media characterization by the two-liquid method: effect of dynamic contact angle and inertia. Langmuir 24:1918–1923
51. Li W, Nie Z, Paquet C, Seo M, Garstecki P, Kumacheva E (2007) Screening of the effect of surface energy on microchannels on microfluidic emulsification. Langmuir 23:8010–8014
52. Link DR, Grasland-Mongrain E, Duri A, Sarrazin F, Cheng Z, Cristobal G, Marquez M, Weitz DA (2006) Electric control of droplets in microfluidic devices. Angew Chem Int Ed 45:2556–2560
53. Lou T-JM, Soong R, Lan E, Dunn B, Montemagno B (2005) Photo-induced proton gradients and ATP biosynthesis produced by vesicles encapsulated in silica matrix. Nat Mater 4:220–224
54. Lu Y, Fan H, Stump A, Ward TL, Riker T, Brinker CJ (1999) Aerosol-assisted self-assembly of mesostructured spherical nanoparticles. Nature 398:223–226
55. Lumsdon SO, Kaler EW, Williams JP, Velev OD (2003) Dielectrophoretic assembly of oriented and switchable two-dimensional photonic crystals. Appl Phys Lett 82:949–951
56. Lumsdon SO, Kaler EW, Velev OD (2004) Two-dimensional crystallization of microspheres by a coplanar AC electric field. Langmuir 20:2108–2116
57. McKnight TE, Culbertson CT et al (2001) Electroosmotically induced hydraulic pumping with integrated electrodes on microfluidic devices. Anal Chem 73:4045
58. Millman JR, Bhatt KH, Prevo BG, Velev OD (2005) Anisotropic particle synthesis in dielectrophoretically controlled microdroplet reactors. Nat Mater 4:98–102
59. Morgan H, Green NG (2003) AC electrokinetics: colloids and nanoparticles. Research Studies Press Ltd., UK
60. Nie Z, Xu S, Seo M, Lewis PC, Kumacheva E (2005) Polymer particles with various shapes and morphologies produced in continuous microfluidic reactors. J Am Chem Soc 127:8058–8063
61. Paik P, Pamula VK, Pollack MG, Fair RB (2003) Electrowetting-based droplet mixers for microfluidic systems. Lab Chip 3:28–33
62. Paik P, Pamula VK, Fair RB (2003) Rapid droplet mixers for digital microfluidic systems. Lab Chip 3:253–259
63. Paul PH, Arnold DW et al (1998) Electrokinetic generation of high pressures using porous microstructures. Proceedings of the μ-TAS'98, Banff, Canada
64. Paul PH, Arnold DW et al (2000) Electrokinetic pump application in micro-total analysis systems; mechanical actuation to HPLC. Proceedings of the μ-TAS 2000, Enschede, The Netherlands
65. Piyasena ME, Lopez GP et al (2006) An electrokinetic cell model for analysis and optimization of electroosmotic microfluidic pumps. Sens Actuators B 113:461–467
66. Pohl HA (1951) The motion and precipitation of suspensoids in divergent electric fields. J Appl Phys 22:869–871
67. Pollack MG, Fair RB, Shenderov AD (2000) Electrowetting-based actuation of liquid droplets for microfluidic applications. Appl Phys Lett 77:1725–1726
68. Pollack MG, Shenderov AD, Fair RB (2002) Electrowetting-based actuation of droplets for integrated microfluidics. Lab Chip 2:96–101
69. Pretorius V, Hopkins BJ et al (1974) Electro-osmosis: a new concept for high-speed liquid chromatography. J Chromatogr 99:23–30
70. Rama Rao GV, Lopez GP, Bravo J, Pham H, Datye AK, Xu H, Ward TL (2002) Monodisperse mesoporous silica microspheres formed by evaporation-induced self assembly of surfactant templates in aerosols. Adv Mater 14:1301–1304
71. Ramos A, Morgan H, Green NG, Castellanos A (1998) AC electrokinetics: a review of forces in microelectrode structures. J Phys D: Appl Phys 31:2338–2353
72. Rastogi V, Velev OD (2007) Development and evaluation of realistic microbioassays in freely suspended droplets on a chip. Biomicrofluidics 1:14107
73. Rastogi V, Melle S, Calderón OG, García AA, Marquez M, Velev OD (2008) Synthesis of light-diffracting assemblies from microspheres and nanoparticles in droplets on a superhydrophobic surface. Adv Mater 20:4263–4268

74. Rastogi V, García AA, Marquez M, Velev OD (2010) Anisotropic particle synthesis inside droplet templates on superhydrophobic surfaces. Macromol Rapid Commun 31:190–195
75. Rodriguez NF, Markx GH (2004) Improved levitation and trapping of particles by negative dielectrophoresis by the addition of amphoteric molecules. J Phys D: Appl Phys 37:353–361
76. Rowlinson JS, Widom B (1982) Molecular theory of capillarity. Claredon Press, Oxford
77. Schacht S, Huo Q, Voigt-Martin IG, Stucky GD, Schueth F (1996) Oil–water interface templating of mesoporous macroscale structures. Science 273:768–771
78. Schonfeld F, Rensink D (2003) Simulation of droplet generation by mixing nozzles. Chem Eng Technol 26:585–591
79. Serra C, Berton N, Bouquey M, Prat L, Hadziioannou G (2007) A predictive approach of the influence of the operating parameters on the size of polymer particles synthesized in a simplified microfluidic system. Langmuir 23:7745–7750
80. Shestopalov I, Tice JD, Ismagilov R (2004) Multi-step synthesis of nanoparticles performed on millisecond time scale in a microfluidic droplet-based system. Lab Chip 4:316–321
81. Shui L, Eijkel JCT, van den Berg A (2007) Multiphase flow in microfluidic systems-control of droplets and interfaces. Adv Coll Int Sci 133:35–49
82. von Smoluchowski M (1903) Contribution a la theorie de l'endosmose electrique et de quelques phenomenes correlatifs. Bull Intern Acad Sci Cracovie Ser A 8:182–200
83. Song H, Chen DL, Ismagilov RF (2006) Reactions in droplets in microfluidic channels. Angew Chem Int Ed 45:7336–7356
84. Song H, Tice JD, Ismagilov RF (2003) A microfluidic system for controlling reaction networks in time. Angew Chem Int Ed 42:767–772
85. Song H, Li HW, Munson MS, Van Ha TG, Ismagilov RF (2006) On-chip titration of an anticoagulant argatroban and determination of the clotting time within whole blood or plasma using a plug-based microfluidic system. Anal Chem 78:4839–4849
86. Song YJ, Modrow H, Henry LL, Saw CK, Doomes EE, Palshin V, Hormes J, Kumar C (2006) Microfluidic synthesis of cobalt nanoparticles. Chem Mater 18:2817–2827
87. Sotowa KI, Irie K, Fukumori T, Kusakabe K, Sugiyama S (2007) Droplet formation by the collision of two aqueous solutions in a microchannel and application to particle synthesis. Chem Eng Technol 30:383–388
88. Squires TM, Quake SR (2005) Microfluidics: fluid physics at the nanoliter scale. Rev Mod Phys 77:978–1026
89. Stone HA, Kim S (2001) Microfluidics: basic issues, applications, and challenges. AIChE J 47:1250–1254
90. Takagi M, Maki T, Miyahara M, Mae K (2004) Production of titania nanoparticles by using a new microreactor assembled with same axle dual pipe. Chem Eng J 101:269–276
91. Tan Y-C, Hettiarachchi K, Siu M, Pan Y-R, Lee AP (2006) Controlled microfluidic encapsulation of cells, proteins, and microbeads in lipid vesicles. J Am Chem Soc 128:5656–5658
92. Tan Y-C, Cristini V, Lee AP (2006) Monodispersed microfluidic droplet generation by shear focusing microfluidic device. Sens Actuators B 114:350–356
93. Teh S-Y, Lin R, Hung L-H, Lee AP (2008) Droplet microfluidics. Lab Chip 8:198–220
94. Thorsen T, Roberts RW, Arnold FH, Quake SR (2001) Dynamic pattern formation in a vesicle-generating microfluidic device. Phys Rev Lett 86:4163–4166
95. Utada AS, Chu L-Y, Fernandez-Nieves A, Link DR, Holtz C, Weitz DA (2007) Dripping, jetting, drops, and wetting: the magic of microfluidics. MRS Bull 32:702–708
96. Velev OD, Prevo BG, Bhatt KH (2003) On-chip manipulation of free droplets. Nature 426:515–516
97. Velev OD (2003) Assembly of electrically functional microstructures from colloidal particles. In: Caruso F (ed) Colloids and colloid assemblies. Wiley-VCHPubl, Weinheim, pp 437–464
98. Velev OD, Bhatt KH (2006) On-chip micromanipulation and assembly of colloidal particles by electric fields. Soft Matter 2:738–750

99. Wang K-L, Jones TB, Raisanen A (2007) Dynamic control of DEP actuation and droplet dispensing. J Micromech Microeng 17:76–80
100. Whitesides GM (2006) The origins and the future of microfluidics. Nature 442:368–373
101. Wong PK, Wang T-H, Deval JH, Ho C-M (2004) Electrokinetics in micro devices for biotechnology applications. IEEE/ASME Trans Mechatron 9:366–376
102. Xia YN, Whitesides GM (1998) Soft lithography. Angew Chem Int Ed 37:550–575
103. Xu S, Nie Z, Seo M, Lewis P, Kumacheva E, Stone HA, Garstecki P, Weibel DB, Giglin I, Whitesides GM (2005) Generation of monodisperse particles by using microfluidics: control over size, shape, and composition. Angew Chem 117:734–738
104. Yi U-C, Kim C-J (2006) Characterization of electrowetting actuation on addressable single-side coplanar electrodes. J Micromech Microeng 16:2053–2059
105. Zeng S, Chen CH et al (2001) Fabrication and characterization of electroosmotic micropumps. Sens Actuators B 79:107–114
106. Zhang H, Tumarkin E, Peerani R, Nie Z, Sullan RMA, Walker GC, Kumacheva E (2006) Microfluidic production of biopolymer microcapsules with controlled morphology. J Am Chem Soc 128:12205–12210

Chapter 9
Single-Cell Analysis in Microdroplets

Michele Zagnoni and Jonathan M. Cooper

9.1 Introduction

The development of microfluidics has steadily increased in the past 20 years and has yielded integrated high-throughput analytical techniques at the microscale, providing novel lab-on-a-chip (LOC) systems to be used for biological and chemical applications [1–5].

Droplet microfluidics constitute a subset of microscale techniques also known as micro-emulsions, multiphase systems or segmented flow. These are characterised by using two or more immiscible fluids (e.g. oil and water), where each of the phases is considered to have a separately defined volume fraction and a distinct velocity field.

Microfluidic multiphase systems have been used to develop two technologies, known as "digital microfluidics" (DMF) and "droplet microfluidics" [6, 7]. DMF concerns the formation and transport of discrete liquid droplets (i.e. water-in-air droplets [W/A]) across the surface of an array of electrodes, where drops can be controlled individually by means of electromechanical actions exerted on the drops using electric fields. Differently, droplet microfluidics (DM) concerns the formation and transport of micro- and nano-sized emulsions, which are mainly obtained by hydrodynamic formation within microchannels. An emulsion is a mixture of two immiscible fluids, consisting of a liquid core (dispersed phase) suspended in a second immiscible liquid (continuous phase), as water-in-oil droplets (W/O) or in oil-in-water droplets (O/W). Both approaches have been widely used to address

M. Zagnoni (✉)
Centre for Microsystems and Photonics, University of Strathclyde, Glasgow G1 1XW, UK
e-mail: michele.zagnoni@eee.strath.ac.uk

J.M. Cooper
School of Engineering, University of Glasgow, Glasgow G12 8LT, UK
e-mail: jcooper@elec.gla.ac.uk

P. Day et al. (eds.), *Microdroplet Technology: Principles and Emerging Applications in Biology and Chemistry*, Integrated Analytical Systems,
DOI 10.1007/978-1-4614-3265-4_9,

cell-based applications, exploiting the ability to generate, transport, mix and analyse sub-μL droplet volumes.

Differently from DMF approaches, DM systems can produce highly monodisperse emulsions in the nanometre to micrometre diameter range. As an example, whilst DMF enables droplets to be formed and individually manipulated in the 1–10 Hz range, DM is characterised by a frequency of droplet formation that varies between 1 Hz and 10 kHz. To emphasise the capability of these systems, if one considers the productivity of W/O drops having a diameter of 50 μm, each of which constitutes a reactor, approximately 40,000 reactions can be simultaneously performed within a microchannel having an area of 1 cm^2 and a depth of 50 μm.

DM technology has been successfully used for the wealth of microfluidic applications. As example, for the formation of janus particles, colloidosomes, microcapsules and sol–gel beads. DM has also been used for enzymatic reactions, polymerase chain reaction (PCR) and cell screening, biomolecule synthesis, drug delivery and diagnostic testing [6, 8].

In this chapter, we focus solely onto analytical cell-based applications addressed using DM techniques. During the past decade, single-cell analysis has been increasingly investigated using microfluidic approaches. In this context, DM offers novel tools for the study of intracellular investigation, gene and protein content and expression, PCR, differentiation, lysis, cytotoxicity and fluorescence screening [9], providing powerful, analytical, droplet-based architectures to be developed.

We first describe the essential characteristics that these systems must fulfil to address single-cell applications, including droplet stabilisation, encapsulation techniques and droplet biocompatibility. After giving an account about DM analytical techniques, we present in more detail relevant protocols used in cell-based analytical applications. Finally, we discuss advantages and limitations of current DM examples, considering perspectives and advances that may provide novel future applications and capabilities of this technology. Throughout the chapter, the reader will be referred to the most relevant papers and classic reviews on droplet microfluidic methodologies.

9.2 Droplet Microfluidics Requirements for Cell-Based Applications

Cells can be considered as the basic units of life. Despite the different functions carried out by diverse cell types, similar features are shared. A mammalian single cell has a size that typically varies from 5 to 20 μm, weigh in the order of a few ng and have a volume of ca. 1–10 pL. They necessarily contain proteins, DNA and RNAs, which are the building blocks of life [10].

DM enables single cells to be addressed in large numbers using droplet volumes that are larger but comparable to those of cells, thus providing diffusion-limited mass transfer over the same length such as might be found in natural environments (Fig. 9.1). However, these DM systems need to satisfy some critical

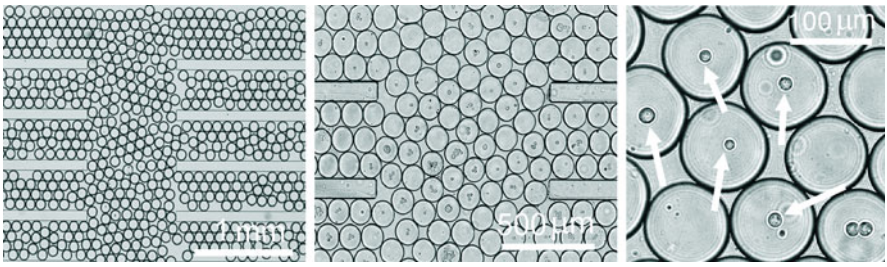

Fig. 9.1 Images showing single-cell encapsulated in on-chip W/O microdroplets. *White arrows* indicate single cells encapsulated within the surfactant-stabilised microdroplets

requirements to address cell-based applications. These include emulsion stability during drop storage and handling, droplet biocompatibility and particle encapsulation methods.

In microfluidic environments, the high surface area to volume ratio enhances the interfacial effects between the phases, which typically become dominant over inertial and viscous effects. Importantly, surface tension phenomena (both between the phases and between each phase and a solid surface) strongly influence the behaviour of the liquids in the microfluidic channels and also determine the stability of the emulsions during their transport and their storage. To form an emulsion, the inner phase must be completely surrounded by the outer phase. The implication is that the outer phase must have higher affinity to wet the solid surface of the channel wall than the inner phase. Also, the presence of surfactant molecules lowers the interfacial tension between the phases. Therefore, the hydrophobic and hydrophilic nature of a surface and the type of surfactants used are fundamental to determine the orientation and the stability of the emulsions. Emulsion stability in bulk and in microfluidic devices have been extensively reviewed elsewhere [11–18].

The materials used in the fabrication of microfluidic devices present different surface wettabilities. These include mouldable elastomeric polymers (i.e. poly (dimethyl)siloxane [PDMS]), hard polymers (i.e. poly(methylmethacrylate) [PMMA]), photocurable polymers, glass and silicon [19], with water static contact angles varying in a range 1–110°. Depending upon the application, emulsion stability and manipulation in LOC devices can be improved using surface treatments (such as silanisation, oxygen plasma treatment and film coating). These are used either to change the hydrophobic/hydrophilic properties of the overall channel surface or to create specific hydrophobic/hydrophilic patterns within the microfluidic devices [20–27].

T-junction and cross-flowing junctions are predominantly used in LOC devices. The phases are injected in the device either using syringe pumps (thus obtaining constant flow rates and variable hydrodynamic pressure in the microchannels) or by setting a constant pressure at the inlets (thus obtaining a constant pressure source and variable flow rates in the microchannels). Reviews of the current understanding of the drop formation mechanisms in microfluidic geometries can be found in the literature [12, 13].

A further feature offered by DM technology is that each drop serves as a microreactor. This characteristic, combined with droplet size, parallel analysis and biocompatibility, is highly valuable for biological particle encapsulation in droplets. In the next section, examples of microfluidic, high-throughput applications for the detection and analysis of biological particles are reported.

Usually, particle encapsulation in droplets is obtained by diluting a suspension of particles (i.e. cells, bacteria and other single-cell organisms) into the dispersed phase, resulting in an encapsulation process that follows a Poisson statistics. The Poisson distribution for particle insertion into droplets is given by

$$p(M;n) = \frac{M^n \mathrm{e}^{-M}}{n!}, \tag{9.1}$$

where n is the number of particles in a drop and M is the average number of cells per drop, where M is usually adjusted by controlling the cell suspension concentration. Therefore, if single-cell encapsulation is required, the methods are inefficient, leading to a large number of empty drops with a much smaller number of drops containing a single cell [28, 29]. This has led to the development of new microfluidic techniques to improve the efficiency of particle encapsulation in micro-emulsions [30–33]. In fact, to guarantee high throughput, inertial ordering has been proposed as an efficient particle encapsulation method [33]. As shown in Fig. 9.2, under appropriate flow conditions and channel geometries, regular spacing between flowing particles is achieved prior to encapsulation.

By matching the periodicity of the drop generation with that obtained for the particles, encapsulation efficiency as high as 80% has been achieved. By producing closely packed particles, two advantages can be gained over Poisson statistics: (1) increased encapsulation efficiency and (2) the particle periodicity can be controlled independently from drop formation, enabling controlled, multiple particle encapsulation [32]. Nonetheless, a disadvantage of inertial ordering is that of particle clogging in microchannel constrictions. A further disadvantage is also that of higher flow velocities, which require non-deformable microchannel walls due to build-up of high hydrodynamic pressures. Finally, as inertial ordering is obtained for higher Reynolds ($Re > 20$) [34] numbers than in conventional experiments, higher shear stresses will be generated during droplet formation, potentially resulting in damaged encapsulated cells.

Apart from the surface tension properties of the channel walls and hydrodynamic conditions, other important requirements must also be considered to guarantee that encapsulated cells and organisms are stored in a biocompatible environment. Some biological applications require, in fact, that droplets must be stored either on- or off-chip for long period of times (i.e. from hours to days) and retaining their initial character. Typically, due to the nature of the experiments when using cells and other living organisms, W/O droplets are used, and two factors play an important role in determining the above mentioned conditions: the choice of surfactant molecules and the gas permeability of the bulk material surrounding the microchannels.

Surface active agents or surfactants are amphiphilic molecules which contain both water-soluble and oil-soluble components. Their function is to lower the

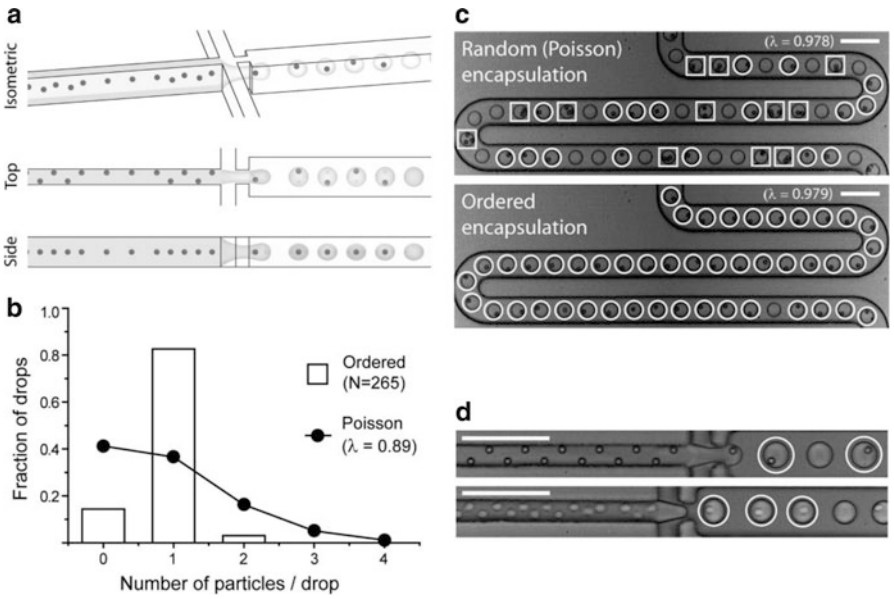

Fig. 9.2 An example of cross-flowing junction in a microfluidic device used for ordered cell and particle encapsulation in droplets. (**a**) Schematic representation of hydrodynamic interactions that cause particles to self-organise along one side of the microchannel or into a diagonal/alternating pattern; (**b**) comparison between particle encapsulation results obtained from inertial ordering and stochastic Poisson loading; (**c**) ordered encapsulation of particles generates more single-particle drops (*circles*) and fewer empty (not marked) or multiple-particle drops (*boxes*) than stochastic Poisson loading; (**d**) examples of self-organisation during particle (*top*) and cell (*bottom*) encapsulation in droplets. Scale bars are 100 μm (reproduced by permission of The Royal Society of Chemistry [33])

interfacial tension between two immiscible phases by self-orienting at the phases' interface due to energy minimisation effects [35, 36]. The choice of surfactants depends upon the nature of the continuous phase (i.e. hydrocarbon or fluorocarbon oil) and upon the experimental requirements.

Notwithstanding the use of surfactants both to improve the stability of the emulsions and the resistance to emulsion coalescence, an important feature is the regulation of the amount of small molecules that can diffuse through the surfactant layer between the inner and outer phase [37]. This property depends on the intermolecular forces between the surfactants molecules and the phases and is paramount in defining the droplet environmental conditions and their effects upon encapsulated cells. The nature of the hydrophilic head of the surfactant molecule has, in fact, an effect on the viability of encapsulated cells and on the rate of absorption of encapsulated molecules at the interface of the emulsion. Concerning these issues, it has been reported that the choice of surfactants is essential for prolonged emulsion stability, biocompatibility, for guaranteeing cell viability and also for handling emulsions off- and on-chip [29, 38]. More information on surfactant characteristics and their effects on emulsions in microfluidic devices can be found in the literature [8, 39–45].

As a final requirement, gas permeability (i.e. precise oxygen and carbon dioxide concentration within microchannels) constitutes another important parameter for maintaining encapsulated cells or other organisms alive within emulsions. For this, both the continuous phase and the material with which the microfluidic device is fabricated are important, as they must allow for the desired gas exchange between the inside and the outside of the device channels [46–48]. As examples, fluorocarbon oils improve gas permeability compared to hydrocarbon oils, whilst PDMS allows gas permeation through its porous structure relative to glass and other polymers.

9.3 Detection Techniques and Methodologies

In recent years, a library of microfluidic, droplet-based operations have been demonstrated for use in chemical and biological assays (Fig. 9.3) [49]. These include formation [12, 13, 25, 50–62], storage [28, 29, 48, 63–65], splitting [66, 67],

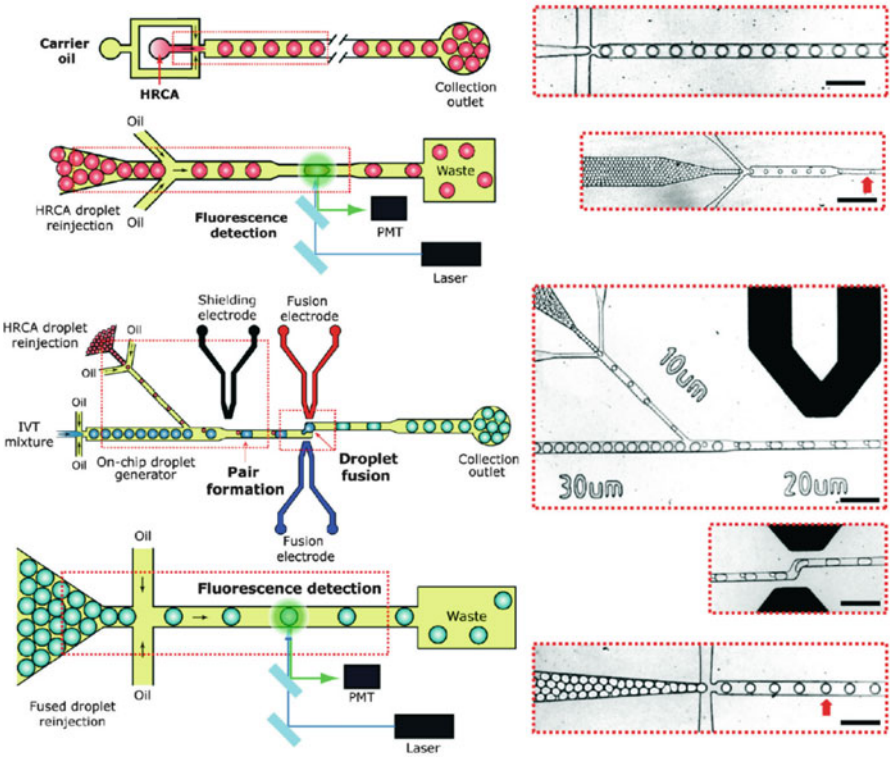

Fig. 9.3 Schematic representation and experimental results of droplet-based libraries implemented in microfluidic devices. Droplets can be produced and extracted from the microfluidic device for further processing and subsequently reinjected into the device. By combining droplet electrocoalescence with fluorescence spectroscopy, biological and chemical assays can be performed on a chip. Scale bars are 100 μm. Reprinted with permission from Mazutis et al. [49]. Copyright 2009 American Chemical Society

sorting [30, 68–70], passive [71–76] and active drop coalescence [66, 77–82], trapping and strategic emulsion positioning [37, 72, 83–85].

One important outcome obtained from microfluidic functionalities is to gain control over the transport of drops and particles in a passive manner, such as the residence time and velocity of a droplet inside a channel, as well as their packing and position. These parameters can be controlled by accurate design of the microfluidic channel geometries and also by the choice of the physical parameters of the phases. Alternatively, active components can be integrated within the microfluidic architectures to further improve functionality. To this extent, micro-heaters have been used to control the temperature of the phases [86]; electric fields have been employed either to coalesce droplets or to sort them in bifurcating channels [68]; surface acoustic waves [87, 88], magnetic fields [89], lasers [90, 91] and optical tweezers [31, 92, 93] have been used to manipulate droplets. These are all examples of the options available from a library of droplet-based operations that, when combined together, can offer enhanced means to perform analysis of cells in microdroplets, where emulsion compartmentalisation serves either as a carrier to transport cells or as a micro-chamber to perform a reaction. The ability to integrate these functionalities in miniaturised systems renders droplet microfluidics a powerful tool for biological and chemical research.

In the simplest case, because the species to be detected can be encapsulated within the emulsion, droplets can be stored on a chip, performing analysis in static conditions. For instance, microfluidic platforms suitable to store thousands of individual micron-sized droplets encapsulating single cells have been reported to monitor β-galactosidase activity [63]. Also, a detection procedure similar to fluorescent activated sorting systems (FACS) has been carried out using droplet microfluidics, exploiting the full potential of high-throughput analysis offered by the technology. Electric fields have also been used to demonstrate sorting of droplets based on the fluorescent readout due to enzymatic reactions from encapsulated bacteria in drops [70].

In other cases, emulsions have been stably extracted from the device for off-chip analytical steps. For instance, by destabilising emulsions containing cells or precipitates by inline fusion of droplets with a phase streams or using detergents, previously encapsulated cells in drops have been extracted from the emulsions and re-cultured to build experiments providing single-cell statistics [28]. Also, particle extraction has been shown by combining fluorescence intensity detection with selective emulsion fusion into a continuous aqueous stream using electric fields [94].

In conventional microbiology, cell-based fluorescence techniques have been successfully utilised to analyse the content of a droplet. However, when translating this into a DM system, a trade-off in sensitivity arises due to the transient time of a drop under the excitation beam and the exposure time required for detection. Due to this, fluorescence microscopy has been mostly used with DM systems for generating statistics and analysis for cell population studies in static conditions [48, 63, 95] or when detecting processes characterised by slow kinetics [96, 97]. Alternatively, laser-induced fluorescence spectroscopy has been used to enable high-throughput screening to be achieved using DM, providing higher sensitivity

and shorter detection times. Examples have been reported for cell-based assays [98] in microdroplets either using fluorescence lifetime imaging (FLIM) [99–101] or fluorescence resonance energy transfer (FRET) [102], resolving events at kHz frequencies.

9.4 High-Throughput Single-Cell Analysis

The encapsulation properties and the characteristic monodispersity of the generated emulsions are the main advantages offered by DM for cell analysis. Combined with classic microfluidic techniques, also the amount of substances enclosed within the droplets can be controlled with a high degree of accuracy, providing reagent delivery with femtolitre precision, providing excellent capabilities for single-cell studies. In addition, it is also possible to adjust the concentration of substances within droplets after encapsulation by fusing two or more droplets together.

Aqueous micro-compartments have been recently used as miniaturised vessels within which one can perform cell-based applications, developing biological assays using bacteria [103–105], yeast cells [106, 107], mammalian cells [29, 108] and vermiform organisms, such as *Caenorhabditis elegans* [29, 84], examples of which are shown in Fig. 9.4.

These examples offer a clear indication of the biocompatible nature of on-chip emulsions, allowing maintenance of encapsulated cells and multicellular organisms viable within the drops for several days. Other than cell growth and high-throughput viability tests of single-cells in drops [29, 63], analytical assays have also been developed, including the rapid laser photolysis of single cells in droplets [31]. This procedure enabled lysis of a single cell and confining of the lysate within the droplet volume, providing an analytical tool for detecting enzymatic activity at the single-cell level. Approximately 10^5 different proteins have been estimated to be contained in a cell [10] and the ability to selectively analyse single-cell contents is of great importance in biology to study signalling cell pathways, cell disease and protein expression.

Cell-based enzymatic assays are often used in cell biology for drug screening. Droplet compartmentalisation augments these techniques, enabling reliable measurements of low substance concentrations to be performed avoiding diffusion of the product outside of the discrete drop volume and using reduced number of cells [109].

Other enzymatic assays and particle analysis have been reported, including the investigation of phosphatise activity produced by *Escherichia coli* cells and providing time resolved kinetic measurements of wild type and mutant enzymes in picolitre droplets [110] and the detection and analysis of human cell surface protein biomarkers using enzymatic amplification inside microdroplets [111]. The latter method successfully demonstrated parallel analysis of a number of cell samples by encapsulating optical labels (i.e. quantum dots) within droplets, achieving higher optical sensitivity than standard FACS-like techniques together with

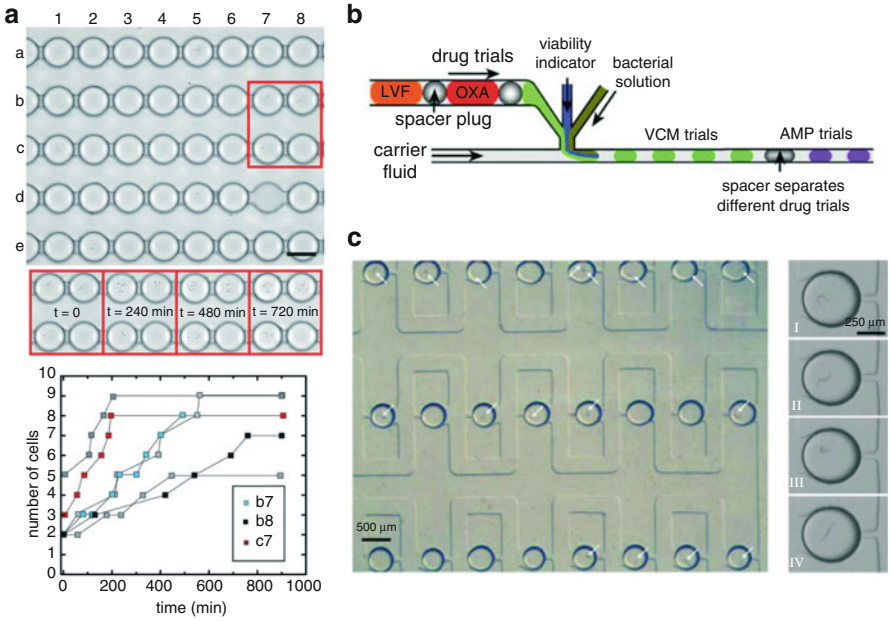

Fig. 9.4 Examples of single-cell and single-organisms encapsulated in W/O droplets. (**a**) Microdroplets containing yeast cells are stored in an array of chambers in a microfluidic device to monitor growth rates of single cells. Graph at the bottom shows the number of cells grown in individual drops over 15-h incubation period. Scale bar is 40 µm (reproduced by permission of The Royal Society of Chemistry [63]); (**b**) schematic drawing illustrating the formation of oblong droplets containing bacteria, viability indicator, and antibiotic from a pre-formed array of drops of different antibiotics (reproduced by permission of The Royal Society of Chemistry [104]); (**c**) image showing a 24-array device where *Caenorhabditis elegans* was mechanically trapped within the emulsion in the microchannels. The *white arrows* indicate the positions of the worms (reproduced by permission of The Royal Society of Chemistry [84])

high-throughput, droplet-based capabilities. In addition, microfluidic enzymatic assay, using bacteria encapsulated in droplets, has been developed in static conditions by simultaneously measuring the fluorescent readout obtained by time-dependent protein expression and cellular enzymatic activity [112].

Cell electroporation has also been demonstrated using droplet microfluidics [107, 113]. Electroporation or electropermeabilization is a technique which makes use of electric fields to control the level of permeability of cell membranes and is typically used in molecular biology to deliver molecules inside the cell. The method has been implemented in DM systems by flowing W/O droplets containing cells through a pair of microelectrodes to which a constant voltage was applied. By adjusting the drop velocity, encapsulated cells in droplets were exposed to the electric field for periods of a few ms whilst flowing past the electrodes (obtained by setting opportune volumetric flow rates). Cell electroporation has been demonstrated by delivering enhanced green fluorescent protein (EGFP) plasmid into Chinese hamster ovary (CHO) cells, obtaining cell viability levels up to 80%

after electroporation. However, this technique has not been extensively used in microfluidics and retains great potential for implementation into DM architectures for high-throughput functional genomics studies.

As previously stated, the characteristic small volumes of microdroplets, ranging from femtolitres to hundreds of picolitres, provide straightforward means of reducing the diffusion lengths within the volume. When mass transfer is limited by diffusion, then the time taken for reactions to come into equilibrium becomes greatly reduced.

By combining this feature with particle encapsulation, analytical processes that depend on volumetric particle concentration can be easily addressed. Examples of these have been given by a number of authors [103, 104, 114], including those investigating the response to antibiotics from bacteria in human blood plasma. By confining single cells into microdroplets of nanolitre volumes, the detection time is dramatically reduced with respect to standard laboratory procedures. Confinement also increases cell density and allows released molecules to accumulate around the cell in shorter times, eliminating pre-incubation steps. These results outline the potential of droplet microfluidics to develop new and faster functional assays for the detection of contaminated food or water, in clinical diagnostics and in monitoring industrial bioprocesses.

Cell experiments using DM have been carried out using both adherent and non-adherent cells within droplets, maintaining cells viability for up to 9 days and offering the option of recovering cells from drops for subsequent cell culture. However, open questions remain and further investigation is required to clarify particular biological issues. One of these not yet convincingly demonstrated concerns the response obtained from adherent cells within a droplet environment. This is in fact a non-adherent environment and far from representative of natural conditions.

While the advantages of single organisms or blood cells studies in drops obtained from the high-throughput characteristics of DM technology are evident, cell studies using microdroplets that target applications other than for detection and sorting (i.e. FACS-like applications) still have to be further improved to extract biologically relevant information. An important aspect to consider when developing cell-based procedures within droplets is to reproduce the complex cell-to-cell interactions and environmental stimuli, so as to mimic the "real" biological environment. These constitute important issues that necessitate attention in the immediate future.

A different approach to cell encapsulation in droplets that has been reported provides a possible solution to the non-adherent nature of liquid emulsions. By forming biocompatible, hydrogel particles or capsules through on-chip gelation [115, 116], cell adherence conditions can be improved. This microfluidic procedure has been used for the generation of monodisperse spherical alginate beads (either using photocurable or chemically curable gels). Gel micro-beads form a solid matrix that acts as a support for the encapsulated cell, also providing an environment for growth and diffusion of fuels and metabolites. In addition, the gelation process facilitates the extraction of the beads from the oil phase, for instance by

immersing the gellified drops in aqueous solutions. Several examples of such microfluidic techniques have been shown using embryonic carcinoma cells [117], yeast cells [106] and Jurkat cells in hydrogel alginate beads [118, 119].

Finally, notwithstanding the number of new biological assays that have been reported in recent years, droplet microfluidics also offers outstanding possibilities for emulsion-based PCR [120], where single or few copies of DNA molecules are amplified, able to generate millions to billions of desired DNA sequences. Performing this technique within LOC miniaturised emulsions enables fast and high-throughput results to be obtained, preventing inactivation of polymerase and cross-contamination between samples. As examples, this technique has been used in DM systems for quantification of rare events using encapsulated beads in droplets to capture the amplified DNA sequence, screening for mutated cancer cells [121] and transcription factor targets [122].

9.5 Discussion

Since the publication of what may be considered the first paper on droplet microfluidics in 2001 [123], this area of research has grown at a very fast pace, adding considerable value to emulsion-based science in terms of reproducibility and reliability. This progress has been driven by the constant development of new microfluidic techniques, including the fabrication of new platforms, improvement of surface treatments and synthesis of new surfactants.

Droplet microfluidics has great potential to develop highly sensitive LOC tools to be used for laboratory-based analysis and diagnostics. However, as for other microfluidic approaches, to date droplet microfluidics has not been demonstrated to be suitable for point-of-care applications and for use in the associated industry.

Other challenges to be faced, which are common to many areas of microfluidics, concern the multidisciplinary approach needed to address biological problems from a technological point of view. To solve these issues, more effort must be dedicated towards the development of LOC devices and procedures that use real biological samples, without requiring trained personal to interpret tissue architecture and without introducing artificial environments that do not represent the natural cellular conditions. The highly interdisciplinary approach required in biological applications when using droplet microfluidics (involving fluidic phenomena, electronic detection/control, chemistry/biochemistry and biology) has appeal, but also highlights the challenging nature of the field.

Because of the features of compartmentalisation within DM, the technique is also expected to be used to develop unconventional tools to mimic artificial cell environments. Protein transcription and translation processes can be performed in vitro within microdroplets, offering new means for evolutionary experiments. For instance, droplet microfluidics has been recently used for in vitro high-throughput expression of green fluorescent protein (GFP) [124] and for expression and detection of enzymes [38]. Future challenges will include developing

high-throughput systems based on microdroplet technology for in vitro expression of transmembrane proteins, using the emulsions as cellular frameworks. These characteristics will potentially lead to high-throughput analysis of membrane-based processes, assisting the realisation of artificial cell environments for drug screening.

Finally, specific problems related to droplet microfluidics concern automatic control and positioning of droplets maintaining high-throughput outcomes [37, 85, 125].

9.6 Conclusions

In the past 10 years, droplet microfluidics has steadily attracted the attention of diverse groups of researchers due to the range of multidisciplinary applications that can be addressed, from engineering to physics, biochemistry, chemistry and biology. Retaining all the well-known advantages offered by microfluidic techniques (including reduced sample volumes and faster analysis times), droplet microfluidics provides novel and attractive procedures that can be used to perform thousands of reactions in parallel for high-throughput, single-cell analysis. This allows a broad range of cell-based and biological applications to be addressed using this technology. Droplet microfluidics has great potential to develop microsystems characterised by improved robustness and reproducibility, enabling new applications in biology and at the single-cell level, creating a valuable interface between biomedicine and engineering.

References

1. Weibel DB, DiLuzio WR, Whitesides GM (2007) Microfabrication meets microbiology. Nat Rev Microbiol 5(3):209–218
2. Weibel DB, Whitesides GM (2006) Applications of microfluidics in chemical biology. Curr Opin Chem Biol 10(6):584–591
3. Mark D, Haeberle S, Roth G, von Stetten F, Zengerle R (2010) Microfluidic lab-on-a-chip platforms: requirements, characteristics and applications. Chem Soc Rev 39(3):1153–1182
4. Atencia J, Beebe DJ (2005) Controlled microfluidic interfaces. Nature 437(7059):648–655
5. Squires TM, Quake SR (2005) Microfluidics: fluid physics at the nanoliter scale. Rev Mod Phys 77(3):977–1026
6. Teh SY, Lin R, Hung LH, Lee AP (2008) Droplet microfluidics. Lab Chip 8(2):198–220
7. Fair RB (2007) Digital microfluidics: is a true lab-on-a-chip possible? Microfluid Nanofluid 3 (3):245–281
8. Theberge AB, Courtois F, Schaerli Y, Fischlechner M, Abell C, Hollfelder F, Huck WTS (2010) Microdroplets in microfluidics: an evolving platform for discoveries in chemistry and biology. Angew Chem Int Ed 49(34):5846–5868
9. Schmid A, Kortmann H, Dittrich PS, Blank LM (2010) Chemical and biological single cell analysis. Curr Opin Biotechnol 21(1):12–20

10. Alberts B (2008) Molecular biology of the cell, 5th edn. Garland Science, New York, p xxxiii, 1268, 40, 49, 1
11. Gunther A, Jensen KF (2006) Multiphase microfluidics: from flow characteristics to chemical and materials synthesis. Lab Chip 6(12):1487–1503
12. Baroud CN, Gallaire F, Dangla R (2010) Dynamics of microfluidic droplets. Lab Chip 10(16):2032–2045
13. Christopher GF, Anna SL (2007) Microfluidic methods for generating continuous droplet streams. J Phys D: Appl Phys 40(19):R319–R336
14. Boyd J, Sherman P, Parkinso C (1972) Factors affecting emulsion stability, and Hlb concept. J Colloid Interface Sci 41(2):359
15. Kabalnov A, Weers J (1996) Macroemulsion stability within the Winsor III region: theory versus experiment. Langmuir 12(8):1931–1935
16. Leal-Calderon F, Schmitt V, Bibette J. SpringerLink (online service) Emulsion science basic principles. http://dx.doi.org/10.1007/978-0-387-39683-5 Connect to e-book
17. Gelbart WM, Ben-Shaul A, Roux D (1994) Micelles, membranes, microemulsions, and monolayers. Springer, New York, p 608
18. Becher P (2001) Emulsions: theory and practice, 3rd edn. Oxford University Press, New York, p viii, 513
19. Becker H, Locascio LE (2002) Polymer microfluidic devices. Talanta 56(2):267–287
20. Seo M, Paquet C, Nie ZH, Xu SQ, Kumacheva E (2007) Microfluidic consecutive flow-focusing droplet generators. Soft Matter 3(8):986–992
21. Li W, Nie ZH, Zhang H, Paquet C, Seo M, Garstecki P, Kumacheva E (2007) Screening of the effect of surface energy of microchannels on microfluidic emulsification. Langmuir 23(15):8010–8014
22. Abate AR, Lee D, Do T, Holtze C, Weitz DA (2008) Glass coating for PDMS microfluidic channels by sol–gel methods. Lab Chip 8(4):516–518
23. Abate AR, Krummel AT, Lee D, Marquez M, Holtze C, Weitz DA (2008) Photoreactive coating for high-contrast spatial patterning of microfluidic device wettability. Lab Chip 8(12):2157–2160
24. Chae SK, Lee CH, Lee SH, Kim TS, Kang JY (2009) Oil droplet generation in PDMS microchannel using an amphiphilic continuous phase. Lab Chip 9(13):1957–1961
25. Bauer WAC, Fischlechner M, Abell C, Huck WTS (2010) Hydrophilic PDMS microchannels for high-throughput formation of oil-in-water microdroplets and water-in-oil-in-water double emulsions. Lab Chip 10(14):1814–1819
26. Darhuber AA, Troian SM (2005) Principles of microfluidic actuation by modulation of surface stresses. Ann Rev Fluid Mech 37:425–455
27. Lee GB, Lin CH, Lee KH, Lin YF (2005) On the surface modification of microchannels for microcapillary electrophoresis chips. Electrophoresis 26(24):4616–4624
28. Koster S, Angile FE, Duan H, Agresti JJ, Wintner A, Schmitz C, Rowat AC, Merten CA, Pisignano D, Griffiths AD, Weitz DA (2008) Drop-based microfluidic devices for encapsulation of single cells. Lab Chip 8(7):1110–1115
29. Clausell-Tormos J, Lieber D, Baret JC, El-Harrak A, Miller OJ, Frenz L, Blouwolff J, Humphry KJ, Koster S, Duan H, Holtze C, Weitz DA, Griffiths AD, Merten CA (2008) Droplet-based microfluidic platforms for the encapsulation and screening of mammalian cells and multicellular organisms. Chem Biol 15(5):427–437
30. Chabert M, Viovy JL (2008) Microfluidic high-throughput encapsulation and hydrodynamic self-sorting of single cells. Proc Natl Acad Sci U S A 105(9):3191–3196
31. He MY, Edgar JS, Jeffries GDM, Lorenz RM, Shelby JP, Chiu DT (2005) Selective encapsulation of single cells and subcellular organelles into picoliter- and femtoliter-volume droplets. Anal Chem 77(6):1539–1544
32. Abate AR, Chen CH, Agresti JJ, Weitz DA (2009) Beating Poisson encapsulation statistics using close-packed ordering. Lab Chip 9(18):2628–2631

33. Edd JF, Di Carlo D, Humphry KJ, Koster S, Irimia D, Weitz DA, Toner M (2008) Controlled encapsulation of single-cells into monodisperse picolitre drops. Lab Chip 8(8):1262–1264
34. Di Carlo D, Irimia D, Tompkins RG, Toner M (2007) Continuous inertial focusing, ordering, and separation of particles in microchannels. Proc Natl Acad Sci U S A 104(48):18892–18897
35. Tadros TF (1984) Surfactants. Academic, London, p xii, 342
36. Rosen MJ (1987) National Science Foundation (U.S.), Surfactants in emerging technologies. Dekker, New York, p x, 215
37. Bai YP, He XM, Liu DS, Patil SN, Bratton D, Huebner A, Hollfelder F, Abell C, Huck WTS (2010) A double droplet trap system for studying mass transport across a droplet-droplet interface. Lab Chip 10(10):1281–1285
38. Holtze C, Rowat AC, Agresti JJ, Hutchison JB, Angile FE, Schmitz CHJ, Koster S, Duan H, Humphry KJ, Scanga RA, Johnson JS, Pisignano D, Weitz DA (2008) Biocompatible surfactants for water-in-fluorocarbon emulsions. Lab Chip 8(10):1632–1639
39. Kreutz JE, Li L, Roach LS, Hatakeyama T, Ismagilov RF (2009) Laterally mobile, functionalized self-assembled monolayers at the fluorous-aqueous interface in a plug-based microfluidic system: characterization and testing with membrane protein crystallization. J Am Chem Soc 131(17):6042
40. Baret JC, Kleinschmidt F, El Harrak A, Griffiths AD (2009) Kinetic aspects of emulsion stabilization by surfactants: a microfluidic analysis. Langmuir 25(11):6088–6093
41. Roach LS, Song H, Ismagilov RF (2005) Controlling nonspecific protein adsorption in a plug-based microfluidic system by controlling interfacial chemistry using fluorous-phase surfactants. Anal Chem 77(3):785–796
42. Lee J, Pozrikidis C (2006) Effect of surfactants on the deformation of drops and bubbles in Navier–Stokes flow. Comput Fluids 35(1):43–60
43. Stone HA, Leal LG (1990) The effects of surfactants on drop deformation and breakup. J Fluid Mech 220:161–186
44. Wang K, Lu YC, Xu JH, Luo GS (2009) Determination of dynamic interfacial tension and its effect on droplet formation in the T-shaped microdispersion process. Langmuir 25(4):2153–2158
45. Liu Y, Jung SY, Collier CP (2009) Shear-driven redistribution of surfactant affects enzyme activity in well-mixed femtoliter droplets. Anal Chem 81(12):4922–4928
46. Lee JN, Park C, Whitesides GM (2003) Solvent compatibility of poly(dimethylsiloxane)-based microfluidic devices. Anal Chem 75(23):6544–6554
47. Shim JU, Cristobal G, Link DR, Thorsen T, Jia YW, Piattelli K, Fraden S (2007) Control and measurement of the phase behavior of aqueous solutions using microfluidics. J Am Chem Soc 129(28):8825–8835
48. Huebner A, Bratton D, Whyte G, Yang M, de Mello AJ, Abell C, Hollfelder F (2009) Static microdroplet arrays: a microfluidic device for droplet trapping, incubation and release for enzymatic and cell-based assays. Lab Chip 9(5):692–698
49. Mazutis L, Araghi AF, Miller OJ, Baret JC, Frenz L, Janoshazi A, Taly V, Miller BJ, Hutchison JB, Link D, Griffiths AD, Ryckelynck M (2009) Droplet-based microfluidic systems for high-throughput single DNA molecule isothermal amplification and analysis. Anal Chem 81(12):4813–4821
50. Hsiung SK, Chen CT, Lee GB (2006) Micro-droplet formation utilizing microfluidic flow focusing and controllable moving-wall chopping techniques. J Micromech Microeng 16(11):2403–2410
51. Cramer C, Fischer P, Windhab EJ (2004) Drop formation in a co-flowing ambient fluid. Chem Eng Sci 59(15):3045–3058
52. Abate AR, Poitzsch A, Hwang Y, Lee J, Czerwinska J, Weitz DA (2009) Impact of inlet channel geometry on microfluidic drop formation. Phys Rev E 80(2):026310
53. Abate AR, Romanowsky MB, Agresti JJ, Weitz DA (2009) Valve-based flow focusing for drop formation. Appl Phys Lett 94(2):23503

54. Zhang DF, Stone HA (1997) Drop formation in viscous flows at a vertical capillary tube. Phys Fluids 9(8):2234–2242
55. Stone HA (1994) Dynamics of drop deformation and breakup in viscous fluids. Ann Rev Fluid Mech 26:65–102
56. Gupta A, Murshed SMS, Kumar R (2009) Droplet formation and stability of flows in a microfluidic T-junction. Appl Phys Lett 94(16):164107
57. Lin YH, Lee CH, Lee GB (2008) Droplet formation utilizing controllable moving-wall structures for double-emulsion applications. J Microelectromech Syst 17(3):573–581
58. Wang W, Yang C, Li CM (2009) Efficient on-demand compound droplet formation: from microfluidics to microdroplets as miniaturized laboratories. Small 5(10):1149–1152
59. Zheng B, Tice JD, Ismagilov RF (2004) Formation of arrayed droplets of soft lithography and two-phase fluid flow, and application in protein crystallization. Adv Mater 16(15):1365–1368
60. Anna SL, Bontoux N, Stone HA (2003) Formation of dispersions using "flow focusing" in microchannels. Appl Phys Lett 82(3):364–366
61. Tice JD, Song H, Lyon AD, Ismagilov RF (2003) Formation of droplets and mixing in multiphase microfluidics at low values of the Reynolds and the capillary numbers. Langmuir 19(22):9127–9133
62. Ota S, Yoshizawa S, Takeuchi S (2009) Microfluidic formation of monodisperse, cell-sized, and unilamellar vesicles. Angew Chem Int Ed 48(35):6533–6537
63. Schmitz CHJ, Rowat AC, Koster S, Weitz DA (2009) Dropspots: a picoliter array in a microfluidic device. Lab Chip 9(1):44–49
64. Trivedi V, Doshi A, Kurup GK, Ereifej E, Vandevord PJ, Basu AS (2010) A modular approach for the generation, storage, mixing, and detection of droplet libraries for high throughput screening. Lab Chip 10(18):2433–2442
65. Boukellal H, Selimovic S, Jia YW, Cristobal G, Fraden S (2009) Simple, robust storage of drops and fluids in a microfluidic device. Lab Chip 9(2):331–338
66. Christopher GF, Bergstein J, End NB, Poon M, Nguyen C, Anna SL (2009) Coalescence and splitting of confined droplets at microfluidic junctions. Lab Chip 9(8):1102–1109
67. Link DR, Anna SL, Weitz DA, Stone HA (2004) Geometrically mediated breakup of drops in microfluidic devices. Phys Rev Lett 92(5):054503
68. Ahn K, Kerbage C, Hunt TP, Westervelt RM, Link DR, Weitz DA (2006) Dielectrophoretic manipulation of drops for high-speed microfluidic sorting devices. Appl Phys Lett 88(2):024104
69. Niu XZ, Zhang MY, Peng SL, Wen WJ, Sheng P (2007) Real-time detection, control, and sorting of microfluidic droplets. Biomicrofluidics 1(4):044107
70. Baret JC, Miller OJ, Taly V, Ryckelynck M, El-Harrak A, Frenz L, Rick C, Samuels ML, Hutchison JB, Agresti JJ, Link DR, Weitz DA, Griffiths AD (2009) Fluorescence-activated droplet sorting (FADS): efficient microfluidic cell sorting based on enzymatic activity. Lab Chip 9(13):1850–1858
71. Tan YC, Ho YL, Lee AP (2007) Droplet coalescence by geometrically mediated flow in microfluidic channels. Microfluid Nanofluid 3(4):495–499
72. Wang W, Yang C, Li CM (2009) On-demand microfluidic droplet trapping and fusion for on-chip static droplet assays. Lab Chip 9(11):1504–1506
73. Mazutis L, Baret JC, Griffiths AD (2009) A fast and efficient microfluidic system for highly selective one-to-one droplet fusion. Lab Chip 9(18):2665–2672
74. Hung LH, Choi KM, Tseng WY, Tan YC, Shea KJ, Lee AP (2006) Alternating droplet generation and controlled dynamic droplet fusion in microfluidic device for CdS nanoparticle synthesis. Lab Chip 6(2):174–178
75. Fidalgo LM, Abell C, Huck WTS (2007) Surface-induced droplet fusion in microfluidic devices. Lab Chip 7(8):984–986
76. Niu X, Gulati S, Edel JB, de Mello AJ (2008) Pillar-induced droplet merging in microfluidic circuits. Lab Chip 8(11):1837–1841

77. Zagnoni M, Baroud CN, Cooper JM (2009) Electrically initiated upstream coalescence cascade of droplets in a microfluidic flow. Phys Rev E 80(4):046303
78. Zagnoni M, Cooper JM (2009) On-chip electrocoalescence of microdroplets as a function of voltage, frequency and droplet size. Lab Chip 9(18):2652–2658
79. Priest C, Herminghaus S, Seemann R (2006) Controlled electrocoalescence in microfluidics: targeting a single lamella. Appl Phys Lett 89(13):134101
80. Ahn K, Agresti J, Chong H, Marquez M, Weitz DA (2006) Electrocoalescence of drops synchronized by size-dependent flow in microfluidic channels. Appl Phys Lett 88(26):264105
81. Bremond N, Thiam AR, Bibette J (2008) Decompressing emulsion droplets favors coalescence. Phys Rev Lett 100(2):024501
82. Zagnoni M, Le Lain G, Cooper JM (2010) Electrocoalescence mechanisms of microdroplets using localized electric fields in microfluidic channels. Langmuir 26(18):14443–14449
83. Tan WH, Takeuchi S (2007) A trap-and-release integrated microfluidic system for dynamic microarray applications. Proc Natl Acad Sci U S A 104(4):1146–1151
84. Shi WW, Qin JH, Ye NN, Lin BC (2008) Droplet-based microfluidic system for individual Caenorhabditis elegans assay. Lab Chip 8(9):1432–1435
85. Zagnoni M, Cooper JM (2010) A microdroplet-based shift register. Lab Chip. doi:10.1039/C0LC00219D
86. Yap YF, Tan SH, Nguyen NT, Murshed SMS, Wong TN, Yobas L (2009) Thermally mediated control of liquid microdroplets at a bifurcation. J Phys D: Appl Phys 42(6):065503
87. Franke T, Braunmuller S, Schmid L, Wixforth A, Weitz DA (2010) Surface acoustic wave actuated cell sorting (SAWACS). Lab Chip 10(6):789–794
88. Franke T, Abate AR, Weitz DA, Wixforth A (2009) Surface acoustic wave (SAW) directed droplet flow in microfluidics for PDMS devices. Lab Chip 9(18):2625–2627
89. Zhang K, Liang QL, Ma S, Mu XA, Hu P, Wang YM, Luo GA (2009) On-chip manipulation of continuous picoliter-volume superparamagnetic droplets using a magnetic force. Lab Chip 9(20):2992–2999
90. Baroud CN, de Saint Vincent MR, Delville JP (2007) An optical toolbox for total control of droplet microfluidics. Lab Chip 7(8):1029–1033
91. Baroud CN, Delville JP, Gallaire F, Wunenburger R (2007) Thermocapillary valve for droplet production and sorting. Phys Rev E 75(4):046302
92. Dixit SS, Kim H, Vasilyev A, Eid A, Faris GW (2010) Light-driven formation and rupture of droplet bilayers. Langmuir 26(9):6193–6200
93. Jeffries GDM, Kuo JS, Chiu DT (2007) Dynamic modulation of chemical concentration in an aqueous droplet. Angew Chem Int Ed 46(8):1326–1328
94. Fidalgo LM, Whyte G, Bratton D, Kaminski CF, Abell C, Huck WTS (2008) From microdroplets to microfluidics: selective emulsion separation in microfluidic devices. Angew Chem Int Ed 47(11):2042–2045
95. Courtois F, Olguin LF, Whyte G, Theberge AB, Huck WTS, Hollfelder F, Abell C (2009) Controlling the retention of small molecules in emulsion microdroplets for use in cell-based assays. Anal Chem 81(8):3008–3016
96. Liau A, Karnik R, Majumdar A, Cate JHD (2005) Mixing crowded biological solutions in milliseconds. Anal Chem 77(23):7618–7625
97. Damean N, Olguin LF, Hollfelder F, Abell C, Huck WTS (2009) Simultaneous measurement of reactions in microdroplets filled by concentration gradients. Lab Chip 9(12):1707–1713
98. Huebner A, Srisa-Art M, Holt D, Abell C, Hollfelder F, Demello AJ, Edel JB (2007) Quantitative detection of protein expression in single cells using droplet microfluidics. Chem Commun 12:1218–1220
99. Solvas XCI, Srisa-Art M, Demello AJ, Edel JB (2010) Mapping of fluidic mixing in microdroplets with 1 mu s time resolution using fluorescence lifetime imaging. Anal Chem 82(9):3950–3956
100. Srisa-Art M, Kang DK, Hong J, Park H, Leatherbarrow RJ, Edel JB, Chang SI, de Mello AJ (2009) Analysis of protein-protein interactions by using droplet-based microfluidics. Chembiochem 10(10):1605–1611

101. Srisa-Art M, deMello AJ, Edel JB (2008) Fluorescence lifetime imaging of mixing dynamics in continuous-flow microdroplet reactors. Phys Rev Lett 101(1):14502
102. Srisa-Art M, Dyson EC, Demello AJ, Edel JB (2008) Monitoring of real-time streptavidin-biotin binding kinetics using droplet microfluidics. Anal Chem 80(18):7063–7067
103. Boedicker JQ, Vincent ME, Ismagilov RF (2009) Microfluidic confinement of single cells of bacteria in small volumes initiates high-density behavior of quorum sensing and growth and reveals its variability. Angew Chem Int Ed 48(32):5908–5911
104. Boedicker JQ, Li L, Kline TR, Ismagilov RF (2008) Detecting bacteria and determining their susceptibility to antibiotics by stochastic confinement in nanoliter droplets using plug-based microfluidics. Lab Chip 8(8):1265–1272
105. Koster S, Evilevitch A, Jeembaeva M, Weitz DA (2009) Influence of internal capsid pressure on viral infection by phage lambda. Biophys J 97(6):1525–1529
106. Choi CH, Jung JH, Rhee YW, Kim DP, Shim SE, Lee CS (2007) Generation of monodisperse alginate microbeads and in situ encapsulation of cell in microfluidic device. Biomed Microdevices 9(6):855–862
107. Luo CX, Yang XJ, Fu O, Sun MH, Ouyang Q, Chen Y, Ji H (2006) Picoliter-volume aqueous droplets in oil: electrochemical detection and yeast electroporation. Electrophoresis 27(10):1977–1983
108. Tan WH, Takeuchi S (2007) Monodisperse alginate hydrogel microbeads for cell encapsulation. Adv Mater 19(18):2696
109. Martino C, Zagnoni M, Sandison ME, Chanasakulniyom M, Pitt AR, Cooper JM (2011) Intracellular protein determination using droplet-based immunoassays. Anal Chem 83(13):5361–5368
110. Huebner A, Olguin LF, Bratton D, Whyte G, Huck WTS, de Mello AJ, Edel JB, Abell C, Hollfelder F (2008) Development of quantitative cell-based enzyme assays in microdroplets. Anal Chem 80(10):3890–3896
111. Joensson HN, Samuels ML, Brouzes ER, Medkova M, Uhlen M, Link DR, Andersson-Svahn H (2009) Detection and analysis of low-abundance cell-surface biomarkers using enzymatic amplification in microfluidic droplets. Angew Chem Int Ed 48(14):2518–2521
112. Shim JU, Olguin LF, Whyte G, Scott D, Babtie A, Abell C, Huck WTS, Hollfelder F (2009) Simultaneous determination of gene expression and enzymatic activity in individual bacterial cells in microdroplet compartments. J Am Chem Soc 131(42):15251–15256
113. Zhan YH, Wang J, Bao N, Lu C (2009) Electroporation of cells in microfluidic droplets. Anal Chem 81(5):2027–2031
114. Kim HJ, Boedicker JQ, Choi JW, Ismagilov RF (2008) Defined spatial structure stabilizes a synthetic multispecies bacterial community. Proc Natl Acad Sci U S A 105(47):18188–18193
115. Shah RK, Kim JW, Agresti JJ, Weitz DA, Chu LY (2008) Fabrication of monodisperse thermosensitive microgels and gel capsules in microfluidic devices. Soft Matter 4(12):2303–2309
116. Shah RK, Kim JW, Weitz DA (2010) Monodisperse stimuli-responsive colloidosomes by self-assembly of microgels in droplets. Langmuir 26(3):1561–1565
117. Kim C, Lee KS, Kim YE, Lee KJ, Lee SH, Kim TS, Kang JY (2009) Rapid exchange of oil-phase in microencapsulation chip to enhance cell viability. Lab Chip 9(9):1294–1297
118. Workman VL, Dunnett SB, Kille P, Palmer DD (2008) On-chip alginate microencapsulation of functional cells. Macromol Rapid Commun 29(2):165–170
119. Workman VL, Dunnett SB, Kille P, Palmer DD (2007) Microfluidic chip-based synthesis of alginate microspheres for encapsulation of immortalized human cells. Biomicrofluidics 1(1):014105
120. Williams R, Peisajovich SG, Miller OJ, Magdassi S, Tawfik DS, Griffiths AD (2006) Amplification of complex gene libraries by emulsion PCR. Nat Methods 3(7):545–550
121. Kumaresan P, Yang CJ, Cronier SA, Blazei RG, Mathies RA (2008) High-throughput single copy DNA amplification and cell analysis in engineered nanoliter droplets. Anal Chem 80(10):3522–3529

122. Kojima T, Takei Y, Ohtsuka M, Kawarasaki Y, Yamane T, Nakano H (2005) PCR amplification from single DNA molecules on magnetic beads in emulsion: application for high-throughput screening of transcription factor targets. Nucleic Acids Res 33(17):e150
123. Thorsen T, Roberts RW, Arnold FH, Quake SR (2001) Dynamic pattern formation in a vesicle-generating microfluidic device. Phys Rev Lett 86(18):4163–4166
124. Dittrich PS, Jahnz M, Schwille P (2005) A new embedded process for compartmentalized cell-free protein expression and on-line detection in microfluidic devices. Chembiochem 6(5):811
125. Stanley CE, Elvira KS, Niu XZ, Gee AD, Ces O, Edel JB, de Mello AJ (2010) A microfluidic approach for high-throughput droplet interface bilayer (DIB) formation. Chem Commun 46(10):1620–1622

Chapter 10
Trends and Perspectives

Pavel Neužil, Ying Xu, and Andreas Manz

10.1 Summary of Chapters

Throughout the book chapters, researchers have highlighted the recent advancement in microfluidic areas, particularly those involving microdroplets.

Simon and Lee focused on microfluidics droplet manipulations and applications, including droplet fusion, droplet fission, mixing in droplets, and droplet sorting. By combining these operations, they have shown promising applications in executing chemical reactions and biological assays at the microscale.

Day and Karimiani discussed dropletisation of bio-reactions.

Zhang and Liu elaborated the physics involved in multiphase flows and microdroplets dynamics. They emphasized the important dimensionless parameters relating to droplet dynamics with droplet generation process as an example.

Barber and Emerson discussed the fundamental droplet handling operations and the recent advances in electrowetting microdroplet technologies. They also provided an overview of droplet-based electrowetting technologies in biological and chemical applications.

P. Neužil
Korea Institute for Science and Technology Europe, GmbH, Campus E71, Saarbrucken D66123, Germany

Y. Xu
Fraunhofer Institute for Biomedical Engineering, Ensheimer Str. 48, 66386 St. Ingbert, Germany
e-mail: ying.xu@ibmt.fraunhofer.de

A. Manz (✉)
Korea Institute of Science and Technology, GmbH, Campus E71, Saarbrucken D66123, Germany

Hwarangno 14-gil 5, Seongbuk-gu, Seoul 136-791, Korea
e-mail: manz@kist-europe.de

P. Day et al. (eds.), *Microdroplet Technology: Principles and Emerging Applications in Biology and Chemistry*, Integrated Analytical Systems,
DOI 10.1007/978-1-4614-3265-4_10,

Droplet-based microfluidics as a biomimetic principle in diagnostic and biomolecular information handling were highlighted by Köhler addressing potential of applying segmented fluid technique to answer to the challenges of information extraction from cellular and biomolecular systems.

Using the flow rates, applied pressures, and flow rate ratios in a closed feedback system, the active control of droplet size during formation process in microfluidics was achieved by Nguyen and Tan.

Velev, Petsev, and Chang discussed droplet microreactors for materials synthesis. They briefly described microfluidics for droplet generation as well as fabrication technology. They provided detail study of transport in microchannels and droplet microfluidics for mesoporous particle synthesis.

Kaminski, Churski, and Garstecki reviewed the recent advances in building modules for automation of handling of droplets in microfluidic channels, including the modules for generation of droplets on demand, aspiration of samples onto chips, splitting and merging of droplets, incubation of the content of the drops, and sorting.

Zagnoni and Cooper have demonstrated the use of on-chip biocompatible microdroplets both as a carrier to transport encapsulated particles and cells, and as microreactors to perform parallel single-cell analysis in tens of milliseconds.

10.2 General Situation

Here we try to explore the technology development cycle and market trend for microfluidics devices. Microfluidic systems were first pioneered by Stanford's research introducing a chromatography chip about 30 years ago [1]. It was probably too ahead of time, yet only 15 years later, an avalanche of microfluidics developments was triggered by Manz's group [2] introduction of on-chip capillary electrophoresis (CE). This technology went through a Gartner hype cycle as illustrated in Fig. 10.1. Manz's CE chip resulted in a technology trigger to lead to inflated expectations in the late nineties for microfluidics, mirroring the Silicon Valley Technology bubble hype. Since then, there have been thousands of researchers developing microfluidic systems for various applications and with different goals. [3] Some were interested in basic research, some in commercial applications. However, very few of them were commercially successful in finding the ground-breaking applications. Microfluidics failed to deliver the initial promises to provide a revolutionary technology platform for life sciences and hence disappointed investors. So far, the most successful droplet microfluidics device is the inkjet printer; the commercialization of other miniaturization technology remains highly attenuated even though some areas have made good progress, such as Caliper's LabChip. Why is it that with such tremendous effort there is so little outcome? Let's analyze the reasons for the slow adoption of this promising enabling platform technology. We will further discuss if this technology is close to finding the "holy-grail" of analytics despite the past disappointing track record.

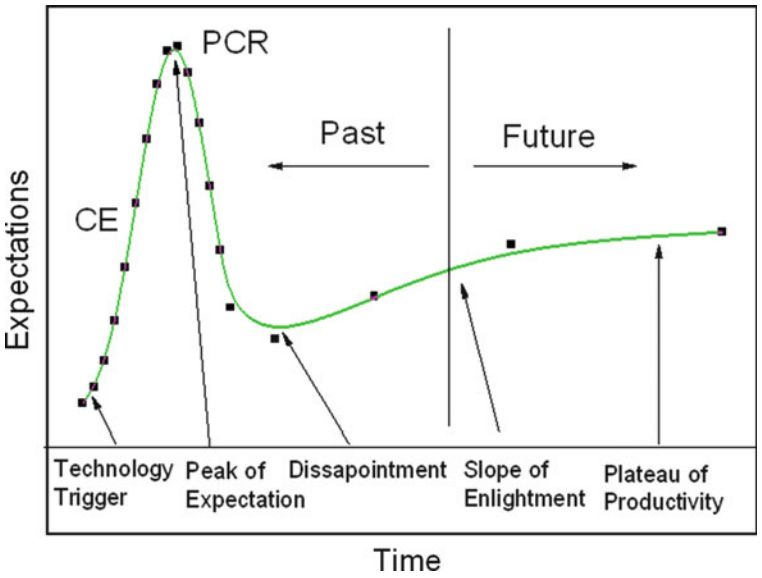

Fig. 10.1 Gartner Hype Cycle for Microfluidic Technology. The development of the capillary electrophoretic (CE) chip initially triggered the technology development. An example of a device produced during the peak expectation phase is exemplified by the micro polymerase chain reaction (PCR) system. After multiple disappointments currently the technology has now entered the slope of enlightenment

10.3 Scientific and Technology Origin

The chosen approach to demonstrate the value of microfludic applications contrary most likely is the major problem. Microfluidic systems have not been developed based on industrial or applications demand. These systems are mostly based on "leftover" manufacturing equipments and tools from the semiconductor industry. Using a push-pull analogy, microfluidics systems are "pushed" by manufacturers rather than "pulled" from market demand. The semiconductor industry follows the well known Moore's law, increasing wafer size, and shrinking device dimensions. The industry constantly needs to invest huge amounts of capital equipment with a short technology advancement cycle. In order not to obsolete the costly equipment, device manufacturers found microelectromechanical systems (MEMS) attractive. It is economical to convert the outdated integrated circuits (IC) production lines to produce MEMS devices such as pressure sensors, accelerometers etc. Meanwhile, integrated MEMS devices are also following Moore's law, although somewhat delayed in comparison to the ICs. Therefore, further converting such production lines to make microfluidic devices becomes the next natural option. The critical dimensions of these devices are well within the capability of existing semiconductor equipment and they are relatively simple to make. They need only a few fabrication

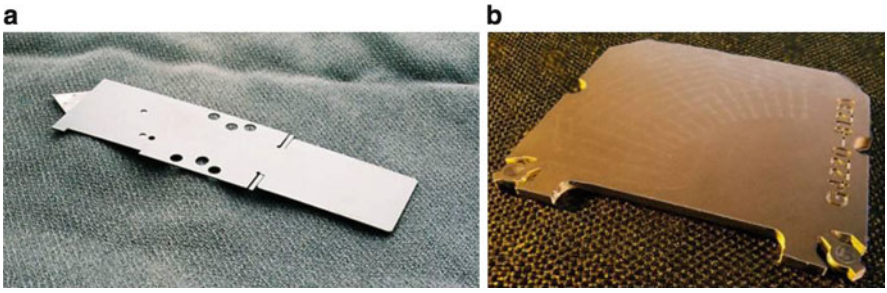

Fig. 10.2 Agilent chip device for (**a**) mixer from 6 layers of stainless steel and (**b**) LC-MS from Polyimide. Both devices are used in commercial products for proteomic mass spectrometry and for ultra high pressure liquid chromatography, respectively

steps, with contact printing for lithography often proving to perfectly suffice. The only special tool usually required is the wafer bonder, as well as the availability of etching method for glass. Next comes the basic question: who wants these devices and why? One of the fundamental problems of microfluidic devices not being commercially successful is rooted in the simple fact that they were NOT developed based on market demand, but quite contrarily. Such a starting point was risky as microfluidics development was often used to justify longer lifetime of leftover and aged IC facilities. Then the problem became how to find the applications and market demand for those devices. "Retrofitting" is well documented to rarely work.

Fortunately, there are now researchers who adopted the right approach. A new age of microfluidics devices for heat exchanging, mixing, and subsequent high performance liquid chromatographic (HPLC) separations are offered for example by Agilent based on the application demand for the device with specific performance in the market place, not to just redeplying old fabrication production line. These microfluidic devices are made of six layers of stainless steel cut by laser and glued together (see Fig. 10.2a). The devices are cheap, reliable, and able to withstand high pressure. To make them more user-friendly, the device extensions for connection can be bent to different angles based on application demand. Also previously a version of the HPLC chip that incorporated sample preparation was made from polyimide using printed circuit board (PCB) technology (see Fig. 10.2b). It enabled integration of heaters to locally control temperature.

Other fabrication techniques for microfluidics started to emerge, such as polymer-based microfluidics using polydimethylsiloxane (PDMS). The PDMS process is simple and it does not even require a well equipped cleanroom. Nevertheless the material itself is permeable to certain molecules which brings other problems making PDMS devices less competitive. Injection molding and hot embossing (imprinting) are other examples of different approaches compared to employing the silicon wafer processing facilities.

Are there any other problems with microfluidics? Firstly there is a scaling law which predicts problems for quantitative molecular detection limits at the nanometer scale. Every technique has a detection limit requiring a certain number of

molecules to be presented. This limit is not altered with the sample size, i.e., very small samples have to be highly concentrated to be exceed the limit of detection. This makes theses samples too concentrated to be of any interest. A restriction to pure compounds, or at the percentage level, seems to be interesting for more academic research only. Optimal fluidic dimensions for practical analytical chemistry look like to be from about 5–50 μm. That is a problem but still does not explain why the microfluidics devices are not flooding the market and why they have not "wiped out" conventional systems.

10.4 Example: PCR on Chip

Perhaps we can now analyze one popular microfluidics device as an example: miniaturized polymerase chain reaction system (microPCR). This process was first demonstrated by Northrup in 1993 and since then, hundreds of research groups have been designing their own systems in highly innovative approaches. However, none of them has been commercially introduced. The initial incentive seems very simple: the microPCR needs to be small so that it only requires the use of very small amount of reagents making the PCR economical. Surprisingly, in reality that is not always an advantage even though some researchers like to claim so. PCR is so sensitive that it can detect only a few molecules of DNA or RNA. Smaller amount of reagents indeed brings the cost down but the negative effect is that it decreases the risk of detection reliability through lowering the sample volume. Typically, a sample with volume from 5 μL to 10 μL can be used to detect one molecule of DNA. Using 10 μL for comparison, if the sample is split into 100 units with 100 nL each, then on the average the DNA concentration has to be increased 200 times to have a single DNA molecule in each sample. In reality that means that we are losing sensitivity by lowering sample volume making it unsuitable for direct diagnoses of infectious diseases. There are two exceptions, one is digital PCR [4] and the other one is PCR with sample pre-concentration [5]. Digital PCR divides one sample into into hundreds or thousands of tiny wells. It is based on exploiting use of sample dilution so extreme that a significant number of wells will intentionally receive no DNA while others gain a single DNA template to seed the PCR. The count of amplified wells determines the absolute number of DNA molecules in the original sample, making this PCR system intrinsically quantitative. That is an excellent approach and one that is specifically enabling through miniaturization. The only drawback is that for many applications quantitative PCR is not always required, and therefore the digital PCR is often overkill. However should quantitative PCR prove to be necessary, digital PCR could provide the answer.

A second case where the sample can be small is shown in Pipper's work as they run a pre-concentration step prior to PCR itself. His starting volume was only 40 μL compared to conventional Qiagen protocol requiring volume of 140 μL. Nevertheless he was able to run real-time RT-PCR with only a 100 nL sample volume while achieving two cycles smaller critical threshold, demonstrating that a small volume of PCR sample can be used for diagnostics without sacrificing the limit of detection.

This brings us to another problem which is working with clinical samples. These assays typically require binding of active component such as protein or DNA/RNA to achieve immobilization, washing off most of unwanted substances, and eventually release of the active component for further processing. A typical 140 μL volume of clinical sample as mentioned before is far too large to fit inside a micromachined microfluidic system. Also some reagents have to be stored separately from each other as well as outside the microfabricated device. If the sample as well as the reagents have to be stored separately (most likely in plastic devices), is there any justification of using the microfabricated device itself? Some researchers believe that the whole system can be produced by injection molding, such as GenExpert from Cepheid [6] which is one of the very few commercially available systems performing fully automated sample preparation followed by real-time PCR. A different approach was taken by Veredus Laboratories. They followed a previously described path of using outdated semiconductor process from ST Microelectronics to make advanced PCR systems with in situ hybridization [7]. The system is more labor intensive than sample-to-answer system such as GenExpert, but it is capable of identifying numerous genes simultaneously, offering advantage when screening for a few closely related pathogenic strains or detection of pathogens for homeland security applications.

10.5 Economical

From a technology development cycle perspective, there are other reasons why adoption of microfluidics technology is so slow.

Reason number one is the lack of economy-of-scale. In order for any technology to take off, it has to reach the tipping point in the market place to inflame the "viral effect" that triggers a high volume need; in economic terms, the economy-of-scale has to be in place. Without high volume it is hard to reduce manufacturing cost, and without an affordable price, it is hard for the new technology to be widely adopted. It is known as the "chasm" in the technology adoption cycle [8]. It becomes a "chicken-and-egg" dilemma. So what are the potential high volume markets? Over the years we have seen increasing rate of adoption of biological research helped by droplet microfluidic devices as tools. Examples of such significant progress are HPLC [9], "fluidic transistors" by Cytonix [10], and high throughput screening of biological reactions [11]. Digital microfluidics using "fluidic transistors" has potentially wide applications in diagnostic, chemical detection, bio-sequencing and synthesis as well as tissue engineering. The strong growing demand for fast, reliable, repeatable, and cost-effective biological analysis and diagnostic systems has driven the development of such systems. Microfluidic systems have been proven to be an enabling technology platform, benefitting through extensive research performed over years of exploration. However, currently, the devices were individually researched and prototyped by many academic research groups or small commercial groups. Each device has individual fabrication steps and choice of materials. It is lack of a "standard" manufacturing process which prevents

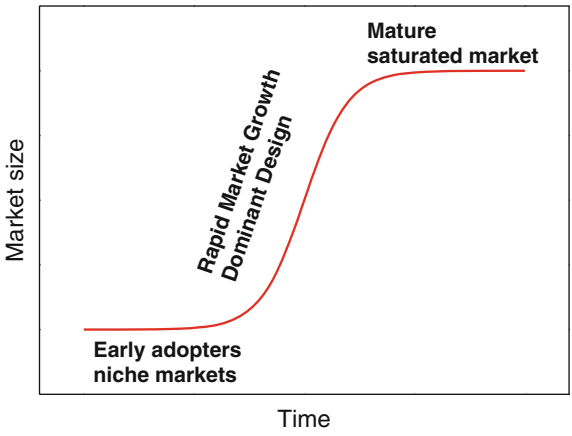

Fig. 10.3 Innovation life cycle

large scale repeatable production, therefore lack of the momentum of building critical mass towards the tipping point. High capital investment and low return on capital becomes the barrier. In our opinion, the commercialization community of microfluidic systems needs to converge on to adopting "standard" materials and manufacturing techniques. Interestingly with digital microfluidics we start to see the genesis of such a trend. Digital microfluidics has become a flexible platform for various bioprocessing and bioanalytical applications.

Reason number two is the co-development of supporting and companion technologies such as detection systems. Often, microfluidic devices are not stand alone as ready-to-use systems, they need to be integrated with other devices to form the complete system for given applications. If a technology platform is too ahead of its prime time, it will lack the associated supporting infrastructure, thus it would be suppressed until the companion technologies catch up. For example, in the case of microfluidic diagnostic devices such as micro real-time PCR, there is need for miniature reliable optical sensing devices and signal processing. In the past 10 years, CCD imaging and digital signal processing have made tremendous progress to make fast, reliable, and cost-effective diagnostic system possible.

Reason number three is the socio-economic environment. In the past 20 years, the bioscience community focused efforts on finding drugs for treating diseases. Now there is a political-social-economical shift towards early disease diagnoses and prevention to reduce the rapid increase in healthcare burden due to expensive treatment. Microfluidic systems have proven to be critical building blocks for bioanalysis and diagnostic instrumentation, and some of the devices have shown potential to be the consumer product for environmental monitoring and pandemic prevention diagnostic tools [5]. Also, for any technology platform, during the early development stage, there is need for enthusiasm from visionaries and investors. In the past 10 years, the venture capital community shifted investment strategy towards emerging markets, which reduced the early stage technology platform survival rate in

developed countries due to lack of funding to turn the corner on the s-curve of innovation life cycle (see Fig. 10.3). Nowadays, the situation starts to turn around.

Successful introduction of droplet microfluidics into the market requires scenario analysis in the early stage of the product development cycle, as would be expected for any other product development. The purpose is to identify the key drivers in the application market place and uncertainties, then to come up with several scenarios and corresponding technology trends so that the likelihood for commercial success can be more precisely recommended. Here the key drivers are cost effectiveness, high sensitivity, reliability, high-speed, and portability to perform bioanalysis. Cost effectiveness requires small sample volume and here the microfluidics has its place. The key uncertainties of the product development are convergence of repeatable large scale manufacturing techniques, macro-economic condition, and the emerging and development of competing technologies. As an example we can look at severe acute respiratory syndrome (SARS) [12] pandemic diagnostic market in 2003. At the time of the SARS pandemic the diagnoses was performed at specialized well equipped clinics and hospitals, e.g., in Singapore with its 4.5 million population all SARS testing was conducted only at Tan Tock Seng Hospital using laboratory-sized PCR systems. Luckily the early symptom of SARS is the onset of fever which could be detected by ultra fast infrared (IR) cameras. This mass testing practically eliminated the SARS virus spreading. This pandemic serves as a wakeup call. What would happen if technology such as offered by the IR camera is not effective for future pandemic? It is the perfect opportunity for microfludic technology to be implemented into a product that can penetrate consumer market. From this example we can see the importance of scenario analysis to spot the trend ahead of the market need and the necessary layout corresponding strategy for technology commercialization.

10.6 Outlook

Our previous discussion and overview may look pessimistic, but in fact we are just trying to identify the reasons why, in spite of a lot of efforts, the results are still evasive. So now comes the question: what kind of future awaits microfluidics? There are many examples of new technologies which looked so promising but soon were forgotten. Will microfluidics follow such a path? We believe that most likely this will not be happening. There are areas where microfluidics will eventually be the dominant if not the only technology. Obvious prime applications are anything with volume or weight limitations, for example, in space program applications [13] where weight limit is the dominate factor that filters out the conventional approaches. We can envision remotely controlled system for Moon or Mars exploration, that in microfluidics-based technology will be top candidate for any diagnostic and analytical tool due to its small volume and corresponding light weight. Besides these rather exotic systems, where else could microfluidics prevail? We have already mentioned digital PCR and surface-based virtual reaction chambers (VCRs). Their

advantages are obvious: digital PCR can be used to determine absolute number of DNA copies in the original sample and VCR-based systems cost only a few cents. What else? Of course, capillary electrophoreses is an example, liquid and gas chromatography and heat exchanger/mixers are also available and successfully marketed by Agilent. We can expect further development in these fields.

Further, we envision three major streams of future development apart from currently existing commercially successful devices.

A first stream could be massively parallel systems for drug or patient screening that are capable of competing with fully automated robotic systems used by big centralized hospital laboratories. Here the cost of the microfluidics is not critical because it is orders of magnitude cheaper than the current robotic approaches. An example of this approach is Steve Quake's massively parallel system [14]. Also Affymetrix's DNA chip [15] probably fits into this category.

A second stream could be simple microfluidic devices for point-of-care applications, where the cost of both capital investment and cost per test are of utmost importance. Here the microfluidics technology will compete with injection molding which naturally brings up a question, if there is even a chance that microfluidics can to win this contest. Injection molded parts are so cheap that their disposability is more economical than any attempt of cleaning the parts and reuse them. From a practical point of view, when it comes to clinical diagnostics, the doctors firmly insist on disposable devices to maintain an absolute sterile environment for the assay, and reduce ambiguity of determining results. This poses serious cost issue to microfluidics because currently they are just too expensive. Even channel free systems such as surface-based microfluidics relying on electrowetting is too costly. They are actually very interesting examples of versatile microfluidics systems due to the fact that they can be easily reprogrammed so that the layout of the microfluidics channel can be quickly changed. However, the reality is that for routine testing/diagnoses we do not need to change the microfluidics layout because there are simple techniques to achieve it so the versatility is not always needed. In this case, the technology can be considered overkill.

There are other competing techniques such as droplet-based PCR [16] which is based on single step lithography and simple heater. It can be probably further simplified to either use stamping (as shown schematically in Fig. 10.4) or eliminate requirement for lithography.

Another example is emulsion PCR [17]. Here the PCR is performed on beads each containing only single template molecule. Each bead is enclosed in a tiny sample droplet with PCR master mix and the thermal cycling is performed inside the droplet. The advantage of this system is that typically there is only a single DNA molecule and single bead within each droplet thus eliminating interference with other DNAs. Once the PCR is completed the emulsion is spread over a picowell plate reader. The size of each well is only 40 μm and beads 28 μm forming a system where there is only a single bead residing within each well which is enabling of single molecule sequencing.

A third stream of microfluidic devices is used for cell biology and tissue engineering research support [18]. Here the high cost of the microfluidic systems

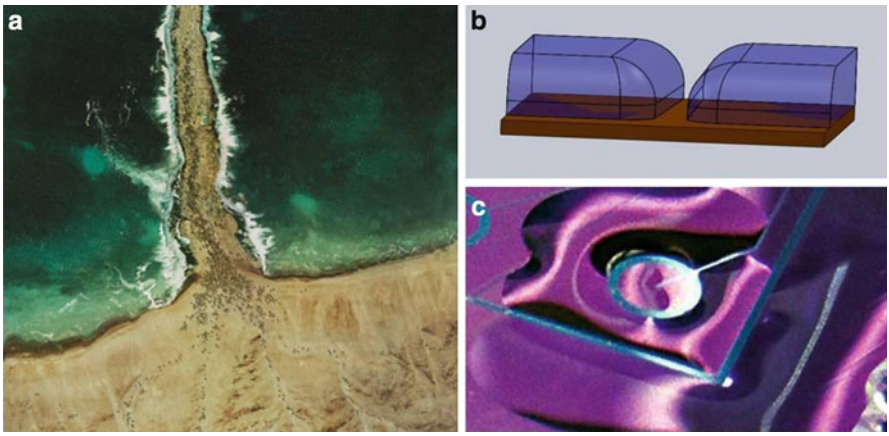

Fig. 10.4 (**a**) Satellite picture reconstruction of Moses leading his people across the Red Sea (copyright by The Glue Society, Australia, reprinted with permission), at this scale it is very unlikely, but nevertheless it is "an incredible story" showing that hydrostatic forces are dominated by surface tension. Inspired by earlier Takehiko Kitamori's presentation we show here schematically (**b**) device with two regions separated from each other by a hydrophilic/hydrophobic surface patterning. It can be relatively easily achieved at the micron scale where surface tension is much greater than hydrostatic forces. (**c**) Photograph of an actual device based on hydrophilic/hydrophobic concept

for research is tolerated as long as really novel effects or information can be achieved. So far cell biology is supported by microfluidics in areas of protein crystallization, stem cell sorting and differentiation, embryo handling [19] structured tissue engineering as well as regenerative medicine. One typical example is seeding stem cells on a scaffolding to form a bioartificial microreactor, such as kidney [20] or liver. Also potential patients would clearly benefit from bioartificial organs such as kidney which would eliminate their frequent visits of dialysis centers improving quality of their lives.

There will always be niche areas where microfluidics could play an important role, such as digital PCR for quantitative molecular testing for routine medical diagnostic.

Overall there is definitely light at the end of the tunnel but it will take some time to get there.

References

1. Terry SC, Jerman JH, Angell JB (1979) A gas chromatographic air analyzer fabricated on a silicon wafer. IEEE Trans Electron Devices ED-26:1880–1886
2. Manz A, Graber N, Widmer HM (1990) Miniaturized total chemical analysis systems: a novel concept for chemical sensing. Sensor Actuat B 1:244–248
3. Arora A, Simone G, Salieb-Beugelaar GB, Kim JT, Manz A (2010) Latest developments in micro total analysis systems. Anal Chem 82:4830–4847

4. Vogelstein B, Kinzler KW (1999) Digital PCR. Proc Natl Acad Sci U S A 96:9236–41
5. Pipper J, Inoue M, F-P Ng L, Neuzil P, Zhang Y, Novak L (2007) Catching bird flu in a droplet. Nat Med 13:1259–1263
6. Dority DB (2002) Fluid control and processing system. US patent number: 6374684
7. VereID^{TM} Biosystems: http://www.vereduslabs.com/products.html
8. Moore GA (1991) Crossing the chasm: marketing and selling high-tech products to mainstream Customers, ISBN 0060517123 published by Harper Business Essentials
9. Levkin PA, Eeltink S, Stratton TR, Brennen R, Robotti K, Yin H, Killeen K, Svec F, Fréchetad JMJ (2008) Monolithic porous polymer stationary phases in polyimide chips for the fast high-performance liquid chromatography separation of proteins and peptides. J Chromatogr A 1200:55–61
10. Brown J (1987) Capillary flow control, US patent number: 4676274
11. Churski K, Korczyk P, Garstecki P (2010) A droplet microfluidic device for high-throughput screening of reaction conditions. Lab Chip 10:816–818
12. http://www.ncbi.nlm.nih.gov/pubmedhealth/PMH0004460/
13. Pumera M (2007) Microfluidics in amino acid analysis. Electrophoresis 28:2113–2124
14. Hong JW, Studer V, Hang G, Anderson WF, Quake SR (2004) A nanoliter-scale nucleic acid processor with parallel architecture. Nat Biotechnol 22:435–439
15. Fodor SPA, Rava RP, Huang XHC, Pease AC, Holmes CP, Adams CL (1993) Multiplexed biochemical assays with biological chips. Nature 364:555–556
16. Zhang Y-X, Zhu Y, Yao B, Fang Q (2011) Nanolitre droplet array for real time reverse transcription polymerase chain reaction. Lab Chip 11:1545–1549
17. Binladen J, Gilbert MTP, Bollback JP, Panitz F, Bendixen C, Nielsen R, Willerslev E (2007) The use of coded PCR primers enables high-throughput sequencing of multiple homolog amplification products by 454 parallel sequencing. PLoS One 2:e197
18. Salieb-Beugelaar GB, Simone G, Arora A, Philippi A, Manz A (2010) Latest developments in microfluidic cell biology and analysis systems. Anal Chem 82:4848–4864
19. Zappe S, Fish M, Scott MP, Solgaard O (2006) Automated MEMS-based *Drosophila* embryo injection system for high-throughput RNAi screens. Lab Chip 6:1012–1019
20. Ananthanarayanan A, Narmada BC, Mo X, McMillian M, Yu H (2011) Purpose-driven biomaterials research in liver tissue engineering. Trends Biotechnol 29:110–118

Index

P. Day et al. (eds.), *Microdroplet Technology: Principles and Emerging Applications in Biology and Chemistry*, Integrated Analytical Systems,
DOI 10.1007/978-1-4614-3265-4,